Fatigue cracking of thermoplastic elastomers

Giorgia Scetta

PSL UNIVERSITÉ PARIS

lrccp

THÈSE DE DOCTORAT

DE L'UNIVERSITÉ PSL

Préparée à l'Ecole Supérieure de Physique et de Chimie Industrielles de la ville de Paris (ESPCI Paris)
Dans le cadre d'une cotutelle avec Laboratoire de recherches et de contrôle du caoutchouc et des plastiques (LRCCP)

Fatigue cracking of Thermoplastic Elastomers

Fissuration en fatigue des élastomères thermoplastiques

Soutenue par
Giorgia SCETTA
Le 16 décembre 2020

Ecole doctorale n° ED 397
Physique et chimie des matériaux

Spécialité
Chimie des Matériaux

Composition du jury :

Damien, VANDEMBROUCQ Directeur de recherche, ESPCI, Paris, CNRS	*Président*
Catherine, GAUTHIER Professeure, Michelin, LaDoux	*Rapportrice*
Yann, MARCO Professeur Associé, ENSTA, Bretagne	*Rapporteur*
Michelle, SEITZ Ingénieure de Recherche, DSM	*Examinatrice*
Costantino, CRETON Directeur de recherche, ESPCI, Paris, CNRS	*Directeur de thèse*
Matteo, CICCOTTI Professeur, ESPCI, Paris	Co-*Directeur*
Patrick, HEUILLET Ingénieur de Recherche,	*Invité*

ESPCI PARIS | PSL

Ai miei genitori,

da sempre custodi di sogni e creatori di speranza.

Acknowledgements

At the end of this journey, I really want to express my gratitude for the people who helped and supported me in the process of finding the story behind the data. Some of them contributed in a practical way, helping me with the experiments, data interpretation and fruitful discussion, others contributed in an emotional way. All of them feel to me equally important.

I want to thank my professors, Costantino and Matteo for having attempted to teach me (time will say if I learnt!) how to look into scientific problems and for their effort to constantly bring me back on track when I moved on the wrong road.

I want to thank Gabriel Sanoja for his wisdom in science and in life (and for the best homemade pesto I've tried!), my wonderful labmates: Juliette, Mehdi and Milena for their friendship and for cuddling me always as the "little-one" of the group.

My gratitude goes to Eric Eucheler, Jianzhu Ju, Bruno Bresson , Josh Yeh and Helen Minsky for their help with experiments and data interpretation.

A big thank also to Francisco, Yinjun, Louis, Pierre, Valentine and all colleagues from SIMM lab who added a great emotional value to these three years.

Last but not least, I want to thank my family for supporting me in every decision and my boyfriend Luca, for all the laughter, the discoveries and especially for understanding me and my unusual, but "happy-togetheeer", vision of life.

Thank you to all of those who contribute to this work.

,

Substantial summary in French

Les élastomères de polyuréthane thermoplastiques (TPU) sont une classe très versatile de polymères qui trouvent de nombreuses applications en raison d'une combinaison de propriétés thermiques et mécaniques. L'élevée extensibilité, l'élasticité réversible et une dureté réglable rendent les TPU comparables á les élastomères classiques à réticulation chimique et conviennent aux « applications de type caoutchouc» telles que les câbles, les ceintures et les chaussures pour n'en nommer que quelques-uns. Toutefois dans un certain nombre d'applications la facilité de mise en œuvre et les possibilités de recyclage des TPE les ont imposés comme une alternative aux élastomères traditionnels. Dans beaucoup de ces applications, la durabilité et la résistance à la fatigue jouent un rôle essentiel et sont considérées comme l'un des facteurs les plus importants pour éviter une défaillance inattendue du composant. La fatigue cyclique et la fracture ont été largement étudiées pour les caoutchoucs, mais c'est beaucoup moins le cas pour le TPU.

En effet si les élastomères vulcanisés sont très majoritairement des matériaux élastiques avec une déformation résiduelle quasi nulle, les élastomères thermoplastiques ont souvent :

- Un niveau d'extensibilité supérieur
- Une résistance au fluage nettement plus faible
- Une certaine déformation plastique en plus de la déformation élastique
- Modification de la structure locale avec la déformation

Dans cette thèse deux questions principaux ont été considéré :

1) Comment tenir compte du caractère anélastique des TPU pour évaluer leur résistance á la fatigue : Comment définir G (le taux de restitution d'énergie élastique) pour un matériau qui flue ? Comment tenir compte de la déformation plastic pendant les essais cyclique ?
2) Quel rôle est rôle joué par la morphologie à phases séparées : peut-il expliquer la remarquable résistance à la fatigue cyclique du TPU ? Quel est l'effet du gradient de déformation généré par la présence de la fissure sur la morphologie finale du TPU ?

Matériaux utilisés

Dans le cadre de cette thèse, on a utilisé trois TPU fourni par la société BASF. Les matériaux sont choisis en raison de leur aptitude à remplacer les élastomères chargés traditionnelles tous avec un module de Young <10MPa. Tous les TPU contiennent une fraction de segment dur et des modules linéaires similaires, mais des compositions des propriétés á grand déformation différentes. TPU_SOFT, que présent une petite quantité de polybutylène téréphtalate cristallisé (PBT), a un écrouissage sous contrainte considérablement moins intense avant la fracture, tandis que les deux autres (TPU_HARD et TPU_XTAL) ont un écrouissage remarquable que seulement pour TPU_XTAL est en partie attribué à la cristallisation sous contrainte (**Error! Reference source not found.**). Le comportement mécanique des TPU a été, dans le cadre de cette thèse, souvent compare avec celui des trois mélange styrène-butadiène (SBR) avec module de Young similaire (Figure 1(b)). Les donnes sur les SBR sont pris par le travail de recherche de Sami Mzabi(Mzabi, 2010).

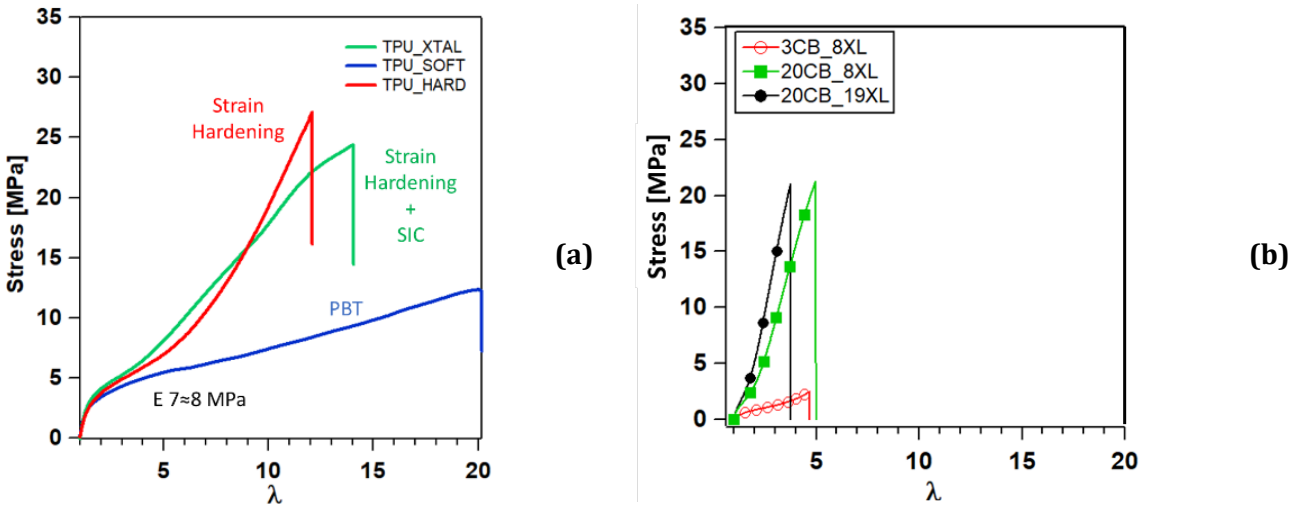

Figure 1 Réponse mécanique des trois TPU (a). Réponse mécanique des trois SBR(Mzabi, 2010)(b)

Les sujets principaux de cette thèse ont été abordé dans quatre chapitres expérimentaux organisés en articles scientifiques indépendants.

1. Caractérisation de la pointe d'une fissure lors de la propagation sous fatigue cyclique dans le caoutchouc styrène-butadiène (SBR).

Pour commencer il est logique, pour avoir un point de départ solide, de se demander ce qui contrôle la résistance à la fatigue dans les élastomères traditionnelles, mieux connu que les TPU. Dans ce chapitre nous avons caractérisé la région fortement déformée développée au fond de fissure pendant la fatigue cyclique de trois SBR renforcé avec du noir de carbone (CB). En particulier, nous nous sommes concentrés sur la forme et les processus qui se déroulent au fond de fissure pour compléter et enrichir l'analyse présentée dans notre précédent(Mzabi et al., 2011)

À l'aide d'une caméra infrarouge, nous avons démontré que la présence de charge contrôle principalement l'élévation de température dans le bulk tandis que la densité de réticulation contrôle l'étendue de la concentration de déformation au fond de fissure. Nous avons proposé que le taux de propagation de fissure dc / dn soit probablement contrôlé par une combinaison de dissipation en bulk (reliant le G appliqué à l'énergie locale disponible pour la croissance de la fissure et l'étirement maximal au fond de fissure λ_{max}) et le rapport entre λ_{max} et l'extensibilité limitante des chaînes polymères (contrôlée par la densité de réticulation et la teneur en charge grâce à l'effet d'amplification des déformations).

2.Definition de la méthode de fatigue pour les élastomères thermoplastiques souple.

Une des méthodes plus utilisées pour caractériser la résistance à la fatigue des élastomères classiques à réticulation chimique est la méthode de propagation de fissure qui suppose que des microfissures existent dans l'échantillon neuf et que la durée de vie est contrôlée par la vitesse de propagation de ces microfissures. L'avancement de cette fissure par cycle appliqué est caractérisé en fonction de taux de restitution d'énergie élastique G.

On a montré que, lorsque les TPU sont chargés cycliquement jusqu'à la même valeur d'étirement maximal, la courbe de tension-étirement (et donc G (λ_{max})) change avec le nombre de cycles appliqués, mais atteint finalement un état stationnaire après 10.000 cycles(Figure 2). Nous proposons une méthodologie appropriée pour évaluer la résistance à la fatigue cyclique dans les TPU, basée sur une approche de la mécanique de

la rupture avec des traitements supplémentaires pour tenir compte de la tendance plus élevée au fluage des TPU que les élastomères traditionnels. En comparant les résultats obtenus du TPU avec ceux des élastomères chargés classiques avec un module linéaire similaire, nous soulignons l'excellente ténacité et la résistance à la fatigue cyclique des TPU.

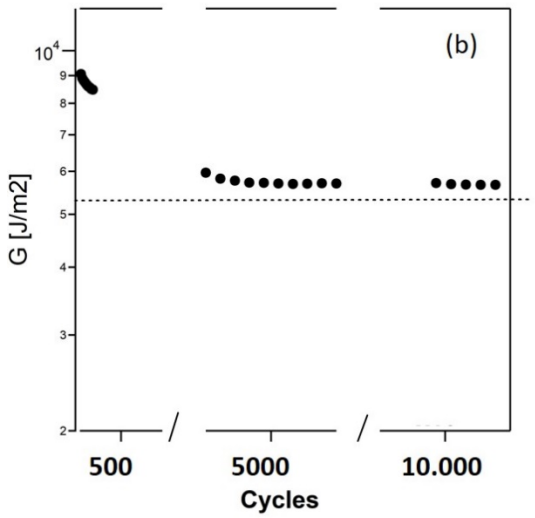

Figure 2 G en fonction du nombre de cycles pour la même valeur d'étirement maximal

3.Proprietés mécaniques des matériaux et rhéodurcissement local

Dans ce chapitre, on a étudié le comportement mécanique cyclique en tension uniaxiale des trois TPU. Malgré les différences á large déformation parmi les trois TPUs, les résultats des tests cycliques en traction uniaxiale montrent que les trois TPU présents des propriétés similaires :

- Grande hystérésis entre le premier cycle de chargement-déchargement (effet Mullins)
- Une déformation résiduelle marquée λ_{res} après déchargement.
- L'augmentation du module de Young a petite déformation après le chargement cyclique á des valeurs de déformation croissantes (Figure 3).

En particulier, le raidissement du TPU résultant d'un chargement cyclique est fondamentalement différent du ramollissement (également appelé dommage cyclique) typiquement observé dans les caoutchoucs chargés réticulés chimiquement et provient de la fragmentation du HD d'origine en sous-unités plus petites mais plus nombreuses

(Figure 4) qui peuvent elles-mêmes agir comme points de réticulation physiques supplémentaires.

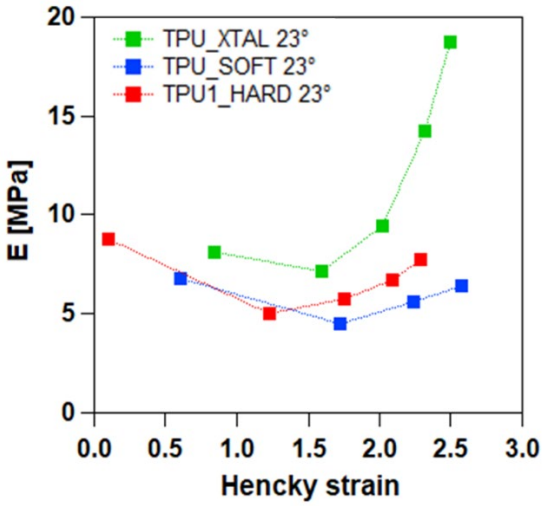

Figure 3 Young Modulus VS Hencky Strain pour les trois TPUs .

Nous proposons que ce renforcement causé par la déformation plastique, puisse jouer un rôle analogue à la cristallisation induite par déformation observée dans le caoutchouc naturel étiré, mais avec un caractère persistant. Il peut provoquer un renforcement local où un champ de déformation non homogène est présent, comme c'est le cas par exemple à la pointe d'une fissure se propageant en fatigue cyclique, fournissant une explication potentielle de la ténacité et de la résistance à l'usure bien connues du TPU.

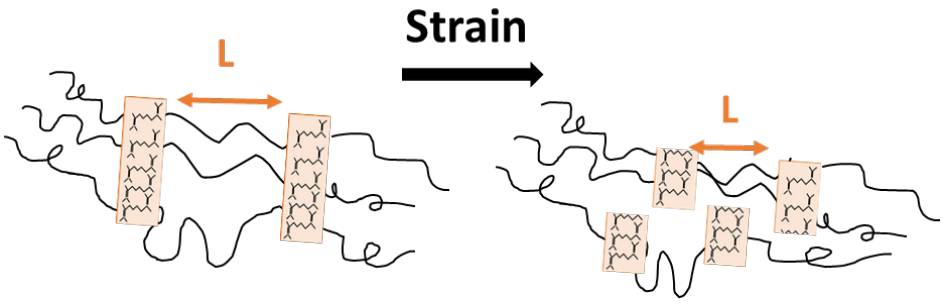

Figure 4 Représentation schématique de la fragmentation des HD avec le chargement.

4. Résistance á la fatigue des TPU et corrélation entre déformation et microstructure á l'échelle local

L'élevé résistance à la fatigue pour les trois TPU associé á l'absence de charges inorganiques et de réticulations chimiques (qui jouent un rôle dans la détermination de la résistance à la fatigue des élastomères) rend intéressant de réaliser une corrélation directe entre les propriétés mécaniques du caoutchouc et des TPU, et ouvre la question du rôle joué par la morphologie à phases séparées des TPU. En utilisant la corrélation d'image numérique (DIC) et la diffraction des rayons X in situ (SAXS et WAXD), nous avons caractérisé la région de forte déformation avant le fond de fissure dans les deux TPU, avant et après la fatigue cyclique. On a proposé que la localisation de la déformation et la structure anisotrope trouvée au fond de fissure dans les TPU après fatigue cyclique est liées à la restructuration locale des domaines durs qui, induit une rigidité plus élevée dans la région entourant la fissure. Nous proposons que cette variation spatiale des propriétés mécaniques réduit la concentration de déformation dans les cycles suivants, protégeant ainsi le fond de fissure des valeurs élevées de déformation et réduisant la probabilité de scission de la liaison à chaque cycle de chargement, expliquant ainsi la remarquable résistance à la fatigue cyclique des TPU.

TABLE OF CONTENT

PART I

1 INTRODUCTION AND CHAPTERS ORGANIZATION 1-3

1.1 INDUSTRIAL CONTEXT AND SCIENTIFIC QUESTION OF THE STUDY 1-3

1.2 ORGANIZATION OF THE STUDY 1-4

1.3 NOTE ON THE ADOPTED NOMENCLATURE 1-5

1.4 REFERENCES 1-7

2 ELASTOMERS 2-10

2.1 MAIN PROPERTIES OF ELASTOMER 2-10

2.2 DEFINITION OF ENTROPIC RUBBER ELASTICITY 2-11

2.3 STATISTICAL THEORY 2-11

2.4 VISCOELASTIC BEHAVIOUR OF ELASTOMERS 2-14

2.5 REFERENCES 2-16

3 FILLED RUBBERS 3-17

3.1 POLYMER MATRIX: SBR 3-18

3.2 VULCANIZATION 3-18

3.3 FILLER SYSTEM 3-19

3.4 DISSIPATIVE MECHANISMS IN FILLED RUBBERS 3-22

3.5 STRAIN INDUCED CRYSTALLIZATION 3-25

3.6 NANO-CAVITATION 3-26

3.7 CONCLUDING REMARKS 3-27

3.8 REFERENCES 3-28

4 THERMOPLASTIC ELASTOMERS 4-33

4.1 HISTORICAL SURVEY AND GENERIC CLASSIFICATION 4-34

4.2 MORPHOLOGY OF TPU 4-37

4.3 THERMODYNAMIC OF PHASE SEPARATION 4-38

4.4 STRENGTH OF TPU AND DEFORMATION MECHANISMS 4-40

4.5 Inelasticity of TPU 4-44
4.6 Concluding remarks 4-46
4.7 References 4-48

5 FRACTURE AND FATIGUE IN SOFT MATERIALS 5-53
5.1 Brief introduction to linear elastic fracture mechanic 5-53
5.2 From LEFM to fracture mechanic of soft materials 5-54
5.3 Cyclic fatigue 5-59
5.4 Strategy to improve fatigue resistance in soft materials 5-62
5.5 Concluding remarks 5-64
5.6 References 5-65

PART II

6 CYCLIC FATIGUE IN SBR: THE ROLE OF CRACK TIP 6-71
6.1 Abstract 6-72
6.2 Introduction 6-72
6.3 Materials and Methods 6-74
6.4 Results 6-76
6.5 Cyclic fatigue tests 6-78
6.6 Multi-scale crack tip observation 6-82
6.7 Extended Discussion 6-86
6.8 Conclusions 6-90
6.9 Supplementary information 6-90
6.10 Acknowledgements 6-91
6.11 References 6-91

7 CYCLIC FATIGUE FAILURE OF TPU 7-95
7.1 Abstract 7-96
7.2 Introduction 7-96
7.3 Materials and methods 7-102
7.4 Materials characterization 7-105

7.5 Discussion 7-114
7.6 Conclusion 7-115
7.7 Acknowledgements 7-116
7.8 References 7-117

8 MECHANICAL PROPERTIES OF SOFT TPU AND STRAIN INDUCED STRENGTHENING 8-121
8.1 Abstract 8-122
8.2 Introduction 8-123
8.3 Materials and methods 8-124
8.4 Mechanical testing and Structural Investigations 8-129
8.5 Damage analysis in cyclic loading 8-136
8.6 Discussion on the differences between TPU and SBR 8-141
8.7 Conclusions 8-142
8.8 Acknowledgements 8-143
8.9 References 8-144

9 SELF-ORGANIZATION AT THE CRACK TIP AND CYCLIC FATIGUE IN TPU 9-147
9.1 Abstract 9-148
9.2 Introduction 9-149
9.3 Materials and methods: 9-150
9.4 Results 9-155
9.5 Differences between microstructure at bulk and crack tip 9-162
9.6 Discussion 9-167
9.7 Conclusion 9-171
9.8 Acknowledgments 9-172
9.9 References 9-173

9 EXTENDED SUPPLEMENTARY INFORMATION.....9-177
9.1 X-RAY ANALYSIS.....9-177
9.2 STRAIN-INDUCED STRUCTURAL CHANGES.....9-180
9.3 RESIDUAL CRYSTALLINITY IN UNIAXIAL STRAINED TPU_XTAL.....9-181
9.4 CYCLIC FATIGUE METHOD B.....9-181

10 GENERAL CONCLUSION AND PROSPECTS.....10-185
10.1 FINAL REMARKS AND FUTURE PERSPECTIVES.....10-188
10.2 REFERENCES.....10-189

ANNEXES.....191
1. FTIR ANALYSIS.....191
2. TOUGHNESS: EFFECT OF TEMPERATURE AND STRAIN RATE.....193
1.1 EXPERIMENTAL CONDITIONS.....193
3. CRACK EXTENSION AND BLUNTING AT HIGH STRETCH RATE.....194
4. CREEP AND STRESS RELAXATION.....197
5. REFERENCES.....198

LIST of ABBREVIATION

CB Carbon Black

SBR Styrene-Butadiene Rubber

TPE Thermoplastic elastomer

TPU Thermoplastic polyurethane elastomer

PBT Polybutylene terephthalate

SIC Strain induced crystallization

HD Hard domain

SS Soft Domain

HS Hard segment

PS Pure Shear Geometry

DSC Differential scanning calorimetry

DIC Digital image correalation

SAXS Small Angle X-Ray Scattering

WAXD Wide Angle X-Ray Scattering

DMA Dynamic Mechanical Analysis

FTIR Fourier Transformed Infrared

Spectroscopy

Part I

Extended Introduction

1 INTRODUCTION AND CHAPTERS ORGANIZATION

1.1 Industrial context and scientific question of the study

Thermoplastic elastomers (TPE) made their appearance on the market “only” at the middle of last century and since then they saw a rapid development, especially because of their fast processability and adjustable mechanical properties. Among all TPE, the class of thermoplastic polyurethane elastomers (TPU) is very promising, especially because TPU can mimic some properties of common thermoset elastomers (such as high reversible stretchability and low Young modulus <10 MPa), coupled with an excellent abrasion resistance, and simultaneously offering the outstanding advantage of an easier processability and recyclability.

Sportwear industry (footwear, waterproof gloves, breathable socks), automotive (scratch bumper protection) and the medical sector (eco-friendly alternative to the commonly used polyvinyl chloride or PVC) are only some examples of TPU applications.

Figure 1-1 Example of TPU's applications

Coupled with the demand of TPU products has also grown the necessity of finding suitable testing procedures to implement safe design and predicting durability of this class of materials, especially in dynamic applications which often require to operate under repeated cyclic conditions.

Following the industrial trend, it is not surprising that the laboratory of research and control of caoutchouc and plastics (LRCCP) has witnessed an increasing demand for TPUs durability and fatigue characterization, which motivated the original objective of this work: the definition of a suitable methodology to assess cyclic fatigue resistance of TPUs.

At the same time, the limited understanding of TPU fracture mechanisms and the recurrent comparison between TPU and thermoset rubbers (despite their different molecular architecture), rapidly encouraged our interest toward the more fundamental research aspects of elucidating the crack propagation mechanisms operating in soft TPUs and how different they are compared to thermoset elastomers.

1.2 Organization of the study

This thesis was mainly structured in two parts. The first part is divided in four chapters and provides an extended introduction on the state of the art concerning the main topics treated in this work: elasticity and viscoelasticity, rubber and TPU, fracture mechanics and cyclic fatigue. The second part is divided in four chapters organised as independent scientific articles.

Part I: extended introduction

Chapter 1 deals with the general concept of entropic elasticity and introduces the concept of viscoelasticity that will be further discussed in the Part II.

Chapter 2 rapidly describes the filled rubber system that is the main subject of the Chapter 6 and is often used as a benchmark to compare the mechanical and fatigue behavior of TPU.

Chapter 3 starts with an extended introduction to the generic class of thermoplastic elastomers and then moves specifically to the sub-class of thermoplastic polyurethane elastomers. The second part of the chapter provides a summary of the state of the art for strain-induced structure modification of TPUs needed to address the issue of morphological changes near the crack tip in TPUs explained in Chapter 9.

Chapter 4 addresses the topic of fracture mechanics applied to elastomers. It briefly recalls the main methodologies adopted to evaluate cyclic fatigue resistance in elastomers and introduces some recent methodologies implemented to increase cyclic fatigue resistance in different soft materials.

Part II: four chapters in form of scientific articles

The first article (Chapter 6) focuses on the effect of heat dissipation in cyclic fatigue for different filled and crosslinked rubbers. This paper reanalyses some of the work carried out by Mzabi et. al on the characterization of the crack tip under cyclic loading for filled SBR. All the relevant data are taken from the PhD work of Mzabi [1,2].

The second article (Chapter 7) aims to define a suitable procedure to evaluate cyclic fatigue in TPU. We critically review some important aspects regarding the choice of methodology such as the achievement of steady state and definition of the cyclic loading conditions.

The third article (Chapter 8) represents a comprehensive mechanical characterization of the cyclic behaviour for three commercial TPU with similar linear properties but different large strain behaviours. We discuss the concept of cyclic strain-induced damage and energy dissipation.

The fourth article (Chapter 9) is focused on cyclic fatigue results in two commercial TPUs at different testing temperature. Using X-ray and digital image correlation (DIC), we discuss the effect of crack in structural modification on TPU that in turn, affects their fatigue resistance in cyclic conditions.

1.3 Note on the adopted nomenclature and materials

In the present work we used two kinds of material: styrene-butadiene rubber (SBR) and TPU.

All the data for SBR are taken from Mzabi[2]. The original samples were prepared moulded and cured by Michelin. All TPUs were provided by BASF and injected by LRCCP.

We decided to organize this work in four scientific articles thus, the specific composition will be separately reported in the “materials section” of each chapter (or article), consistently with the materials considered in the chapter.

To ensure an smooth readability of this manuscript, we briefly report here the basic nomenclature adopted for all materials.

The typical SBR will be label as: **20CB_8XL**

CB indicates the presence of carbon black preceded by the percentage of the filler volume fraction (20% in the example) . **XL** refers to the crosslinking density and is preceded by the crosslinking density expressed in [10^{-5} mol/cm^3] ($8 \cdot 10^{-5}$ mol/cm^3 in the example).

The three commercial TPUs on the other side, have been chosen based on their low Young modulus (<10MPa) which is very similar for all of them, and their large strain behaviour which is different one from another. To remark this aspect, we always report the commercial name of each TPU in the material section but we refer to them with the following names:

565 A 12P = **TPU_ XTAL**, where **XTAL** indicates the presence of strain hardening behaviour in the stress-stretch uniaxial curve with strain induced crystallization (SIC).

EC 60 A 10P= **TPU_HARD,** where **HARD** indicates the presence of strain hardening behaviour but without SIC. (Note that in Chapter 7 **TPU_HARD** will be simply referred as TPU to underline the differences with generic vulcanised rubbers)

LP 9277 10=**TPU_SOFT**, where **SOFT** indicates a softer behaviour at large strain compared to other two TPUs.

1.4 References

1. Mzabi S, Berghezan D, Roux S, Hild F, Creton C. A critical local energy release rate criterion for fatigue fracture of elastomers. *J Polym Sci Part B Polym Phys*. 2011;49(21):1518-1524. doi:10.1002/polb.22338

2. Mzabi S. Caractérisation et analyse des mécanismes de fracture en fatigue des élastomères chargés. 2010:1-310.

2 ELASTOMERS

Elastomers are polymeric materials which can be highly deformed by weak stress and return to their initial shape when the stress is removed. They generally are amorphous polymer composed by long and flexible macromolecules above their glass transition that in principle, makes elastomers analogous to a viscous liquid. Anyway, when these long molecules are sparsely chemically or physically bonded (crosslinked) together at relatively large distance they behave as a solid [1].

There are two main kinds of elastomers: thermoset and thermoplastic elastomers. Thermoset elastomers, often generically referred to as rubbers, are characterised by the presence of chemical bonds between polymer chains. They can be swollen into solvents but are generally insoluble. In thermoplastic elastomers, on the other hand, the spontaneous phase segregation and re-arrangement of hard domains generates physical (and reversible) crosslinking. They are generally soluble in solvents and have less temperature stability[2].

2.1 Main properties of elastomer

Elastomers are generally characterised by low tensile moduli (1-10MPa) , high extensibility , low permeability and electrical insulation [3]. They are used in several applications including sealant, tyres, vibration and corrosion protection, conveyor belts etc.

The main physical requirements for a polymer to show elastomeric properties are summarized by Treloar [4]:

- Long polymeric chains having a high degree of flexibility and mobility (glass transition temperature (T_g) must be below the operation temperature of the material).
- High molecular weight of the chains favouring the formation of entanglements among the molecules joining them together in a network structure.
- Random coil conformation in relaxed condition.

2.2 Definition of entropic rubber elasticity

In elastomeric polymers macro-molecules change their shape quickly and continuously at normal temperature by Brownian motion assuming random conformation[5]. When a perturbation is applied, as an external stress, polymer chains uncoil and begin to align into a more ordered state with correspondingly lower entropy. The driving force of the elastic recovery is therefore of entropic origin (not internal bond origin as enthalpic solid) since the material tends to return to its minimum free energy state by increasing the entropy level. An additional condition is that the polymer must be able to store deformation energy when strained without an excessive viscous flow of the chains. When chains flow the elastomers can retrieve its high entropy state of coiled conformation but it will not exhibit any elastic recovery after the application of the load (Figure 2-1). The introduction of chemical or physical reticulation points hinders viscous flow and ensure elastic behaviour.

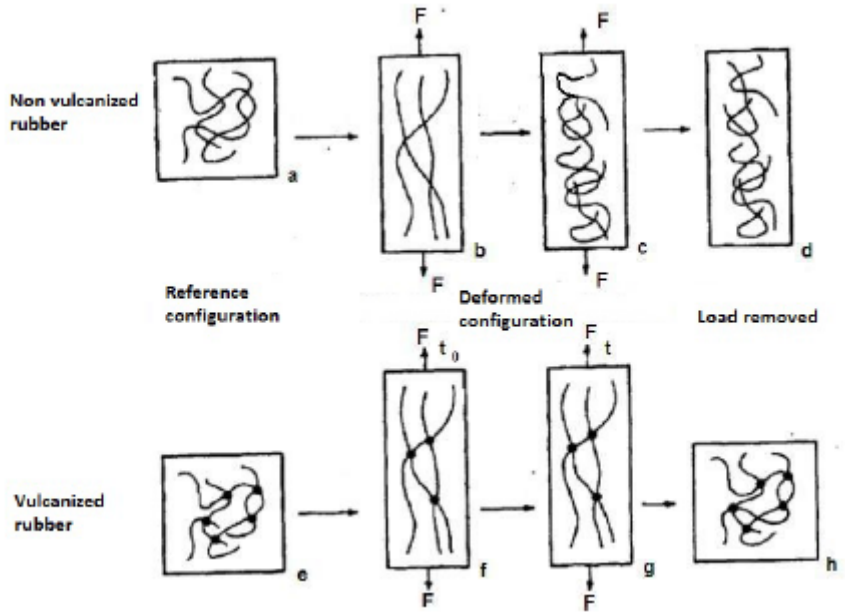

Figure 2-1 Schematic representation of application and removal of an external load in an un-crosslinked (up) and crosslinked elastomer (down)

2.3 Statistical theory

One of the simplest models to describe rubber elasticity of a polymer network is the affine model originally proposed by Kuhn and developed by Wall , Flory, James and Guth and accurately described by Treloar[4]. The two main assumptions are: the affine model and the Gaussian statistics of the polymer chains. The first implies that the deformation of each network strand is identical to the deformation of the macroscopic solid. The Gaussian assumption considers the entropy of the network as the sum of the entropies od individual chains and can be described by Gaussian statistics. Furthermore, the network is considered ideal so that enthalpic force are neglected (f_H=0) , the volume change is equal to zero, the chains are flexible ($T>T_g$) and there is no chain slip or strain induced crystallization. The entropy of a single chain with *n* links of equal length *l* with completely random orientation within the chain, can be expressed as

$$s = c - kb^2r^2 \qquad \textbf{Equation 2-1}$$

Where, c is an arbitrary constant with no physical meaning, $b^2 = \frac{3}{2}nl^2$ (function of chain length) and r is the end-to-end distance of the chain. Within the limit of the model assumption, given L_{i0} the polymer network dimension in the -i direction in the

undeformed state. If the network is deformed by the factor λ_i the dimension on the deformed network is described as:

$$L_i = \lambda_i * L_{i0} \qquad \textbf{Equation 2-2}$$

If each network strand is composed by N monomers and both end of the strands are deformed affinely to the macroscopic network, we can define the initial end-to-end vector R_0 and the projections along the -i direction of the deformed R as :

$$r_i = \lambda_i r_{i0} \qquad \textbf{Equation 2-3}$$

For an ideal network, in absence of any enthalpic contributions (which means that the presence of crosslinking is ignored), the total Helmholtz free energy of the system can be written as W=-T ΔS. Where ΔS is given by the sum of the N single chain entropy difference between the undeformed and deformed state: $\Delta S = \Sigma \Delta s$.

Combining Equation 2-3 and Equation 2-1 the total work of deformation or, elastically stored energy per unit volume W takes the form:

$$W = \frac{G}{2}(\lambda_x^2 + \lambda_y^2 + \lambda_z^2 - 3) \qquad \textbf{Equation 2-4}$$

And the shear modulus G can be expressed for as:

$$G = \frac{1}{2}NkT = \frac{\rho RT}{M_0 N_c} \qquad \textbf{Equation 2-5}$$

where ρ is the density of the rubber, R the gas constant , M_0 the molecular weight of the monomer and N_c the number of monomers per elastic strands, i.e. between crosslink points. Equation 2-4 is the fundamental expression defining the elastic properties of rubbers in the Gaussian approximation regime and has the huge advantage to enable the derivation of the stress-strain relationship for any type of applied strain. Additionally, it involves only a single physical parameter or elastic constant: G which contains the dependence of the materials structure. Equation 2-4 indicates that, as far as the Gaussian approach is valid, the elastic response of the rubber is independent of the chemistry of the polymer chains.

2.3.1 The case of uniaxial tension and limit of Gaussian theory

We can use the Gaussian theory to predict the stress strain behaviour in the specific case of uniaxial tension. According to incompressibility condition ($\lambda_x * \lambda_y * \lambda_z$ =1), the following holds:

$$\lambda_1 = \lambda; \qquad \lambda_2 = \lambda_3 = \lambda^{-\frac{1}{2}};$$

The strain energy density calculated with Equation 2-4 takes the form:

$$\boldsymbol{W = \frac{1}{2} G \left(\lambda^2 - \frac{1}{\lambda} - 3 \right)} \qquad \textbf{Equation 2-6}$$

And the force per unit cross-sectional area becomes:

$$\boldsymbol{\sigma = \frac{dW}{d\lambda} = G \left(\lambda - \frac{1}{\lambda^2} \right)} \qquad \textbf{Equation 2-7}$$

Experimental observations of stress-strain relationship in conventional elastomers anyway, reveal substantial deviations from the theoretical behaviour of Equation 2-7 . Figure 2-2 shows the comparison between stress-elongation behaviour predicted by statistical Gaussian theory (full line) with experimental behaviour observed for a vulcanized NR sample[4]. The model works quite well over a limited range of deformations below λ=1.5. The deviation at higher strain is due to the effect of limited chain extensibility that is not accounted in the Gaussian theory. Additionally, in NR and other stereo-regular elastomers strain induced crystallization effects will also increase the material stiffness and dominate at high strain. Unfortunately, the stiffening of crosslinked polymer chains cannot be predicted by simple considerations on the crosslinking density of the network. Several non-gaussian theories have been provided to describe the large strain behaviours of elastomers that can be mainly divided in: phenomenological models, invariant-based and physical models. Nevertheless, non-gaussian approaches are less general than the gaussian approach that, despite failing at large strain, maintains the advantage to provide an easy understanding of the relationship between the stress-strain curve for different type of loading (uniaxial, biaxial, pure shear, etc.)

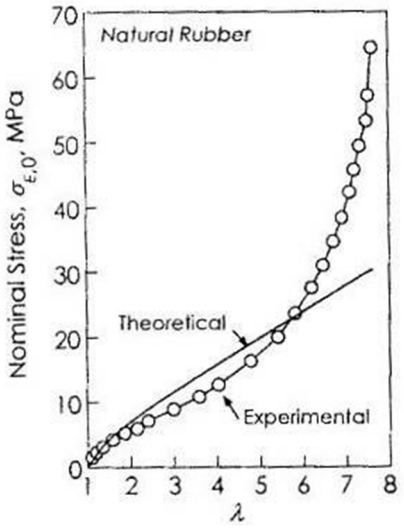

Figure 2-2 Comparison of statistical theory with experimental data for unfilled natural rubber from [4].

2.4 Viscoelastic behaviour of elastomers

In the previous sub-chapters, we mainly explored the ideal behaviour of an elastomer that is assumed to have a perfect reversible character. In practice, real elastomers are viscoelastic materials and exhibit time dependent and hysteretic behaviour. The viscoelastic behaviour of elastomers mainly originates from their own architecture made of several long macromolecules that can slide on each-other generating complex phenomena of friction and resistance to motion. As far as the energy of the system is above such energetic barrier the material is soft and the polymer chains have a high mobility. When the energy of the system is reduced (decreasing temperature for example) the polymer chains do not have enough thermal energy to overcome the molecular friction and the material behaves as a hard solid and becomes difficult to deform. A typical manifestation of the viscoelastic behaviour of elastomers is the variation of the complex modulus G* at low strain with applied temperature (or frequency). G* can be divided in an elastic component G' and in a viscous component G''. Figure 2-3 shows the typical variation of G' and loss modulus or $\tan\delta=\frac{G''}{G'}$ for a viscoelastic network where we can distinguish three regimes:

- T<Tg the material behaves as a hard solid and the elastic modulus is high ≈ GPa

- T≈Tg the material is in the transition state between a hard and soft solid where chain can move but are highly constrained. This generates a maximum in the dissipation indicated by the peak in tanδ (=G''/G')
- T>Tg the material is in a rubbery and soft state. Polymer chains can ideally flow unless they are kept together by some reticulation point as for vulcanised elastomers.

One typical difference between pristine and crosslinked elastomers is the Young's modulus dependence on temperature. Figure 2-3 shows that the drop in the modulus for the un-crosslinked elastomer is replaced by a plateau.

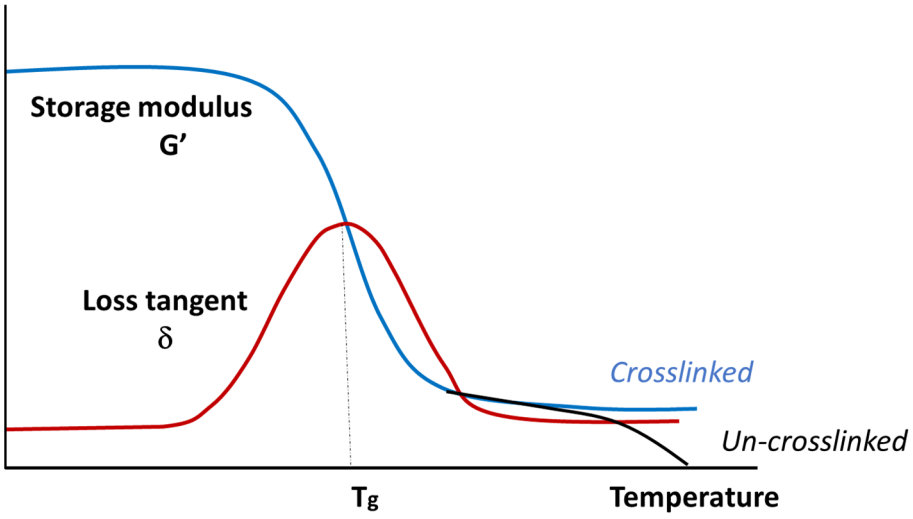

Figure 2-3 Schematic of elastic modulus and los tangent evolution with temperature

2.5 References

1. Gent AN. Elasticity. In: Gent AN, ed. *Engineering with Rubber*. ; 2012:37-88.
2. Holden G. *Understanding Thermoplastic Elastomer*.; 2000.
3. Morton. *Rubber Technology*. New York: Van Nonstrand Reinhold Co.; 1987.
4. Treloar LRG. The elasticity of a molecular network. In: Treloar LRG, ed. *The Physics of Rubber Elasticity*. third. OXFORD , Univeristy Press; 2009:59-77.
5. Gent AN. Rubber Elasticity: basic concepts and behvaior. In: Mark, J.E. ; Erman, B. ; Roloand CM, ed. *The Science and Technology of Rubber (Fourth Edition).* Academic press , Boston; 2013:1-26.

3 FILLED RUBBERS

The term “rubber” generally indicates a compound between an elastomeric matrix and several additives, fillers and crosslinking agents, whose structure has been modified into a permanent shape becoming essentially insoluble and not easy to re-shape using heat and moderate pressure. Commercial elastomers are generally divided into rubbers for general purpose and specialty elastomers. This classification is mainly based on suitability of elastomer for specific applications[1].

General purpose elastomers are probably the largest section and are characterised by: high extensibility, low Young modulus (within the range of some MPa) and good electrical insulation. Some common applications include: tyres, sealing, insulating and damping items, cable etc. (Figure 3-1).

Among rubbers for general purpose, we can distinguish between: natural and synthetic rubber. The first one can be isolated from hundreds of different species of plants and was historically the first material used for tyres. The advances in synthetic chemistry and the introduction of several cheaper elastomers limited the use of NR that is now only considered for its strength in specific and severe dynamic application (as truck and earthmover tyre tread).

Figure 3-1 Example of applications for rubbers

3.1 Polymer Matrix: SBR

In this work we used styrene-butadiene-rubber (SBR) that belongs to the class of general-purpose rubber. SBR is a statistical copolymer between butadiene and styrene. The presence of styrene contributes to increase abrasion resistance and strength reducing the overall price of the elastomer. The good mechanical properties, versatility and the low price of SBR contributed in its huge diffusion especially in the car industry (almost 50% of the production of car tyres are made on SBR [2]). Contrarily to natural rubber, the bulky styrene ring hinders the possibility of crystallization of polymers chain under strain.

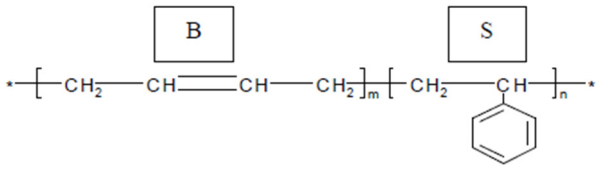

Figure 3-2 Chemical structure of SBR

3.2 Vulcanization

Vulcanization, is a commonly used procedure adopted in tyre industry to obtain items with typical rubber elasticity. The process was introduced in 1843 by Charles Goodyear to generate irreversible chemical junctions among polymer chains through the formation of sulphur bonds between polymer chains as sketched in Figure 3-3.

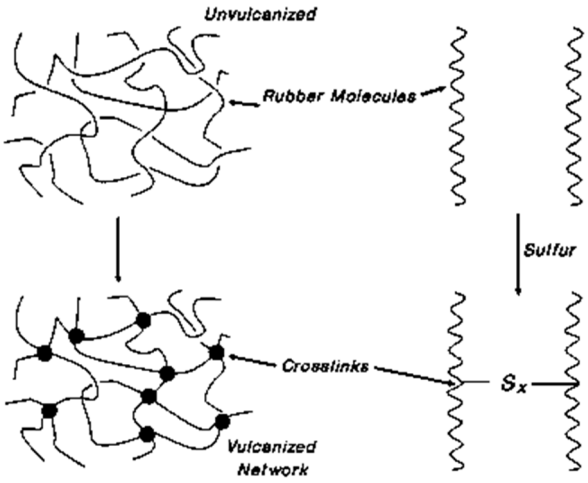

Figure 3-3 Introduction of crosslinking between chains using sulphur[3].

Differently from other crosslinking processes used in thermoset polymers, vulcanization is a mild crosslinking process and only a few amounts of crosslink points are generated. The crosslinked polymer maintains the random coil configuration with several degrees of freedom after vulcanization but at the same time viscous flow is suppressed. Once an elastomer has been vulcanized, it cannot be modelled anymore and the process is typically irreversible.

3.3 Filler system

The term “filler reinforced” can be used to identify the changes in stress-strain properties in a material compared to its unfilled state [4]. In rubbers, the addition of a suitable quantity of filler

(often nanoparticles of carbon black or silica) generally implies a marked increase in linear modulus, tensile strength, and maximum extensibility as shown in Figure 3-4 for two vulcanised SBR that only differ for the presence of 50Phr (parts by weight per hundred parts of rubber) of Carbon Black.

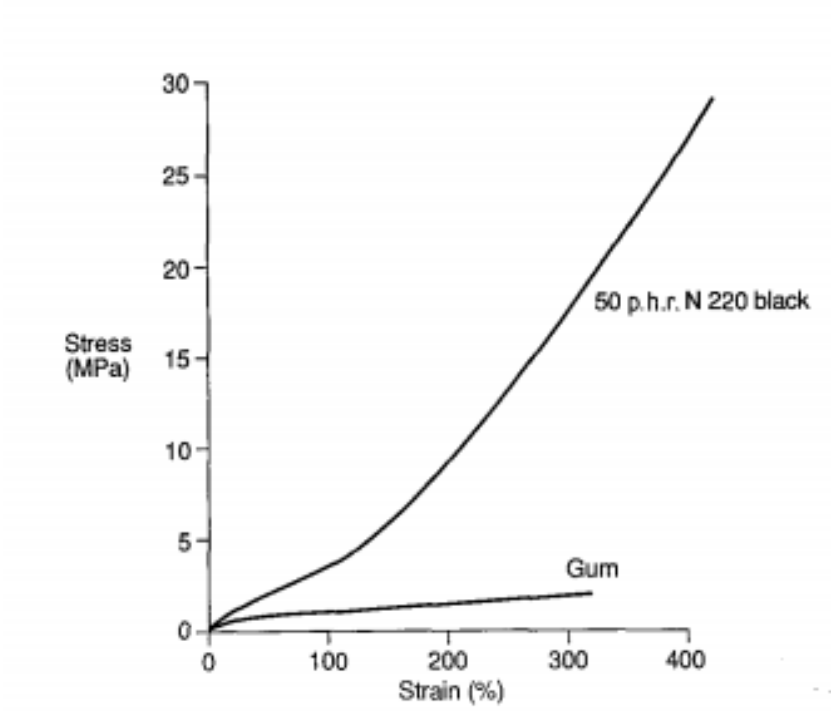

Figure 3-4 Stress-strain curve for filled and unfilled rubber taken from ([4])

Carbon black (CB) is one of the most common filler used to reinforce elastomers and is made by spherical particles which usually appear as fractal aggregates with average size ranging between 100nm -1mm (Figure 3-5). The reinforcing effect induced on the rubber by the addition of filler is not trivial and depends on several factors including filler composition, shape and dimensions. General conditions for filler reinforcement is the interaction between the filler particles and the polymer. The wide diffusion of the CB is justified not only by its low price but also by the good physical interactions that it can establish with the matrix. In particular, the surface of CB is made by graphitic layers with some high energy surface defects that are unstable absorption sites capable of strong interactions with unsaturated polymers (C=C). The phenomenon is referred as bound rubber and consist in a mobility reduction of rubber bounded on CB particle surfaces that in turn increases the reinforcing effect[5,6].

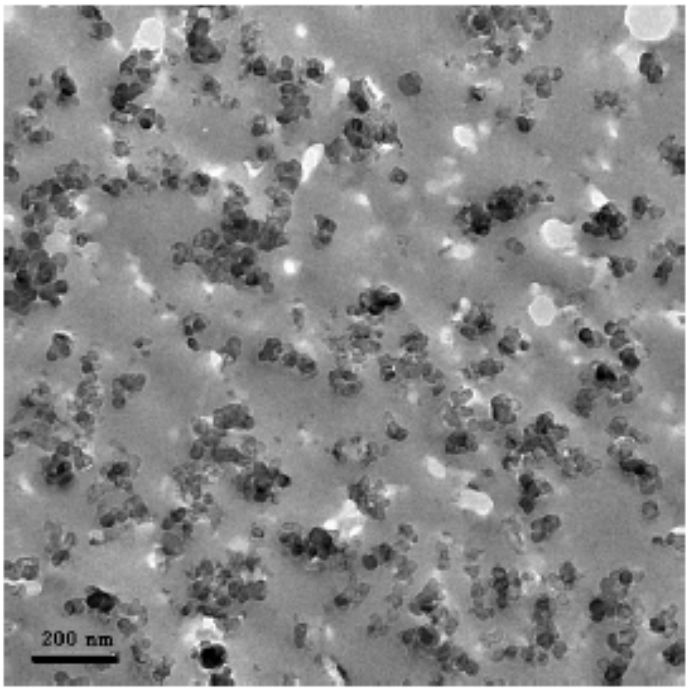

Figure 3-5 TEM images of CB aggregate in rubber. Re printed from[7]

3.3.1 Reinforcing effect on linear modulus

The most simple model, aiming to understand the increase on the modulus by the filler addition, is the Einstein-Smallwood [8] equation. Einstein equation was not originally meant for rubber but to model the effect of filler on the viscosity of dilute solution and Smallwood adapted his equation to explain the increase of the linear modulus of filled rubber using the concept of hydrodynamic effect. This derives from the fact that the filler is a rigid phase and unable to be deformed under the applied load. The Einstein-Smallwood equation consider only one filler-parameter that is its volume fraction $\boldsymbol{\phi}$.

$$\boldsymbol{E = E_0(1 + 2.5\phi)} \qquad \textbf{Equation 3-1}$$

Where, E is the modulus of suspension, E_0 is the modulus of the incompressible rubber. Equation 3-1 is valid for an infinitely dilute system and accounts for the individual contribution of the particles to the reinforcement but is not followed by rubber compounds where interaction between filler and matrix cannot be neglected. A modified version by Guth and Gold [9] who introduced a second-order term accounting for weak interactions.

$$\boldsymbol{E=E_0(1+2.5\phi+14.1\varphi_2)} \qquad \textbf{Equation 3-2}$$

Equation 3-2 is still excessively simplistic and must often be corrected taking in to account other additionally effects including the filler-polymer interactions (in-rubber structure) and elastic properties of the polymer after the vulcanization (polymer network contribution). Generally, the contribution to the modulus is divided in deformation-dependent and deformation-independent as will be discussed in 3.4.1.

3.4 Dissipative mechanisms in filled rubbers

Unfilled rubbers at low strain and far from T_g are mainly elastic and the most significant viscoelastic contribution is chain friction. Real rubbers anyway, are never used alone and always contain several additives and a certain amount of filler as previously explained. The addition of filler is irremediably related to an increase in viscous dissipation within the rubber system both at small and large strain.

3.4.1 Payne effect

Filled rubbers present a significant drop of the dynamic shear modulus under strain that is generally accompanied by a maximum in dissipation indicated by the peak in tan□. The maximum in tan□, generally occurs at some tenths of strain, a value that is likely to be close to the values of macroscopic deformation used in cyclic fatigue in filled elastomers. The reduction of modulus with strain was first studied by Payne [10,11] who interpreted it as the result of the breakage of physical bonds between filler particles, for example van der Waals or London forces, neglecting the role of the matrix itself. Actually, there are several parameters contributing to the Payne effect as: filler content, surface modification of the fillers and morphological characteristic (volume fraction, filler shape and aspect ratio) [12]. A more recent insight of Payne effect includes the presence of a glassy layer around the filler particles where polymer has reduced mobility. Such glassy layer forms a percolating structure that is responsible for the strain induced softening [13]. Generally, all the effects related to the structure of the material, that contribute to the strain amplitude dependency, are referred as “filler network” while polymer network, hydrodynamic effect and in-rubber structure are generally indicated as non-strain dependent as schematically shown in Figure 3-6.

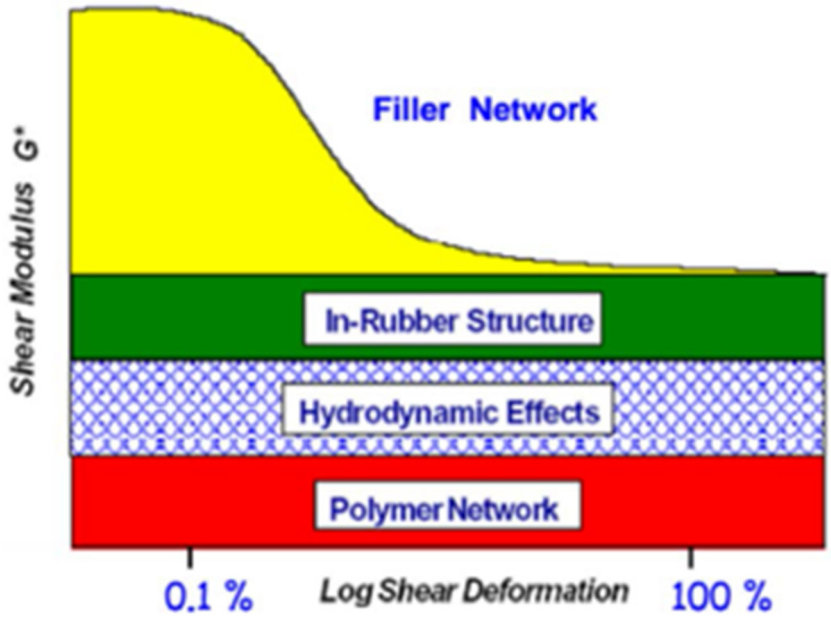

Figure 3-6 Schematic behaviour of the complex shear modulus versus dynamic shear deformation.

3.4.2 Mullins effect

Mullins effect was observed for the first time in filled vulcanised rubber around the beginning of the 1900[14] and later on, extensively studied by Mullins and co-workers for elastomeric systems when cyclically strained at high deformation [15]. Mullin's effect involves a remarkable stress softening between the first and the second cycle (at the same maximum strain) accompanied by a visible hysteresis between the loading and unloading path of the stress-strain curves. During the following cycles, within the same range of applied strain, the remaining hysteresis, is significantly smaller than in the first cycle and the stress-strain response tends to overlaps. When the maximum strain is further increased, the loading curve rapidly recovers the original behaviour of a single monotonic test as represented in Figure 3-7.

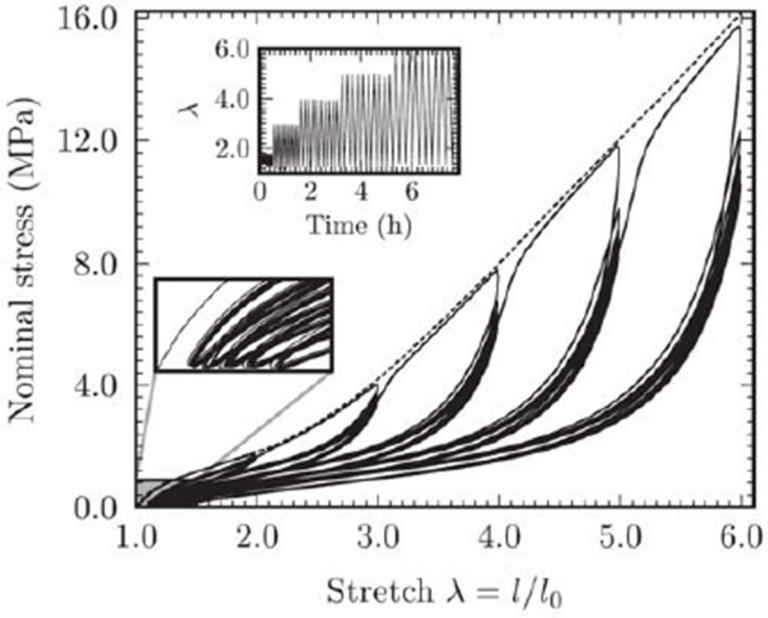

Figure 3-7 Illustration of Mullins effect on a filled SBR. Taken from [16]

Historically, the Mullins effect was observed in filled and crystallizing rubber when cyclically strained at high deformation but recently several authors reported the same phenomenon also for different systems such as thermoplastic elastomers [17] , hydrogels [18] and other living systems[19]. As reviewed by Diani et al. [20] several physical interpretations have been proposed to justify this dissipative behaviour but a complete agreement has not emerged yet. Some of them involve: microstructural modification of filler aggregates, bond ruptures or slippage of shorter chains between aggregates and network re-arrangement, chain disentanglements, network re-arrangement. Despite the absence of a unique explanation, Mullin's effect is generally considered as some form of permanent damage that is a-priori unknown and may cover for several phenomena as structural damage, chains rupture, nanovoids formation etc... Different models vary from each other in the definition of such damage parameter. In a recent paper, Merckel and co-workers [21] proposed an easy methodology to quantify the Mullin's contribution that allows comparison between different materials. They worked on styrene-butadiene-styrene rubber (SBR) cyclically strained at different, medium to large, strain levels and introduced two damage parameters: one to account for the reduction in linear modulus with applied strain and the other to account for the change in the onset of strain hardening with strain induced during loading at larger strain. They showed that, for filled elastomers these two parameters have the same dependence on strain and also have very similar values. This led

them to conclude that in filled elastomers, small and large strain damage are two manifestations of a single phenomenon.

3.4.3 Heat Generation

Energy dissipation is also related to the phenomenon of heat generation and temperature increase. As far as the generated heat has enough time to diffuse through the sample this is not really a problem and only leads to some degree of temperature increase within the sample (or heat build up). In other cases, especially for materials with low thermal conductivity and in cyclic conditions at high strain, the generated heat has not enough time to diffuse away and can cause a significant temperature increase in the whole sample or in localised highly stressed region, that can be detrimental [22–24]. The amount of dissipated heat per cycle depends on several factors such as: filler content, maximum strain amplitude, frequency[25]. Of great interest is the case of strained samples containing a crack. The crack in fact, creates a much higher local strain at the crack tip than in the bulk and as a consequence generates non uniform surface temperatures within the sample[26,27]. Persson and Carbone[22] used viscoelastic arguments, to show that, as long as the crack propagates slowly, the heat produced at the crack tip can diffuse away resulting in only small increases in surface temperature. On the other hand, a moderate crack velocity (>1cm/sec) may lead to a large temperature increase ($\approx 1000K$) in poorly conductive materials such as rubbers. In this case, the zone close to the propagating crack may be seriously damaged causing a degradation in mechanical resistance and unstable crack propagation. The first accurate measurement of heat sources and local temperature rise at the crack tip was provided by Martinez et al [27]. They used an infrared camera to evaluate the local heat generation at the crack tip in filled SBR and demonstrated the presence of a small zone close to the crack tip, smaller than the area of influence of the crack, where heat dissipation is remarkably higher than the bulk although the final surface temperature was only few degree higher. Their work highlighted the possibility of a local build-up of temperature only in the region at the crack tip that cannot be predicted only by surface measurements and must be considered to improve constitutive modelling of cyclic crack propagation in filled rubbers.

An interesting approach was proposed by Saux et al. [28] . They proposed an interesting correlation between heat build-up and cyclic fatigue in rubber using thermal measurements to deduce the fraction of dissipated energy related to cyclic induced damage.

3.5 Strain induced crystallization

Strain induced crystallization consists in alignment and further crystallization of polymer chains under tension. Historically, the phenomenon of SIC was firstly observed in NR and deeply studied by means of X-Ray analysis as reviewed by Huneau [29]. In case of NR, SIC appears above a certain threshold that depends on several factors such as filler content, temperature and strain rate. Despite the fact that SIC is completely reversible, the melting of crystallites is generally observed at lower stretch ratios than that required for their crystallization. The different kinetics between formation and melting of crystallites in loading-unloading has been often considered as a dissipative mechanism explaining the hysteresis loop in stress-strain curves of NR and identified as one of the major mechanisms responsible for high fatigue resistance of NR. Interesting, recent studies [30,31] used calorimetric analysis proving the absence of any mechanical dissipation over a cycle adducing the ability of NR to store mechanical energy without converting it in to heat as one of the principal cause of high crack propagation resistance of NR. The absence of any significant connection between energy dissipation induced by SIC and high fracture resistance of NR was also confirmed by the results of Demassieux et al [32,33]. They carried out a comprehensive X-ray investigation at the crack tip area of filled NR and identified the local stiffening induced by SIC, and the corresponding reduction in strain intensification as the major mechanism contributing to the remarkable cyclic fatigue resistance of NR .

3.6 Nano-cavitation

Another well-known source of dissipation in filled elastomers is the opening of nanocavities during extension[33–35]. Despite the phenomenon of cavitation in unfilled rubbers, was firstly proved by Gent and Lindley in 1958[36] (using specific sample geometry called “poker chip” which generates hydrostatic pressure in the bulk on the material) it took years before the observation of nanocavities in rubbers. Firsts observations on volume variation in filled rubbers were provided by Le Cam et al. [35] but only more recently, Zhang et al. proposed an accurate methodology to quantify the presence of nanocavities in filled elastomers. They used real time X-Ray scattering (and the analysis of SAXS scattering invariant) on two different rubbers: SBR and NR.[34,37] In particular, they found nanocavities of 20-40nm at the crack tip of filled SBR that were absent in unfilled rubber suggesting that nano-cavitation was the main cause of volume variation in filled rubber. Furthermore, the fibrillar structure, detected in the crack area

both in filled NR and SBR, suggested that nano-cavities could act as precursor of the observed ligaments in filled rubbers[26,38,39] .

3.7 Concluding remarks

This chapter introduces the topic of vulcanised rubbers and their main dissipative properties. In particular, two main concepts will be stressed in the Part II: the heat dissipation and the Mullins effect. The first topic will be explored in the Chapter 6 for SBR and related to the local conditions at the crack tip of fatigued samples. The second will be frequently recalled, especially in Chapter 3, to discuss and compare the concept of strain-induced damage during cyclic loading condition between TPU and filled thermoset rubbers.

3.8 References

1. Hamed GR. Materials and compounds. In: Gent AN, ed. *Engineering with Rubber*. III. Hanser Publishers, Munich; 2012:11-35.
2. Advanced rubbers. https://www.hexpol.com/rubber/resources/advanced-rubber-compounding/sbr/%0Ahttps://omnexus.specialchem.com/selection-guide/styrene-butadiene-rubber-sbr-guide%0A.
3. Coran AY. Vulcanization. In: *The Science and Technology of Rubber (Fourth Edition).* ; 2013:337-381.
4. Edwards DC. Polymer-filler interactions in rubber reinforcement. *J Mater Sci*. 1990;25(10):4175-4185. doi:10.1007/BF00581070
5. Leblanc JL. Rubber–filler interactions and rheological properties in filled compounds. *Prog Polym Sci*. 2002;27(4):627-687.
6. EM. D. Bound Rubber and Carbon Black Reinforcement. *Rubber Chem Technol*. 1986;59(3):512-524.
7. Jean A. Etude d'un élastomère chargé, de la nanostructure au macro-comportement. 2009.
8. Smallwood H. Limiting Law of the Reinforcement of Rubber. *J Appl Phys*. 1944;15(758).
9. Guth, E. Gold O. Theory of filler reinforcement. *Phys Rev E*. 1938;53:322.
10. Payne AR. Hysteresis in rubber vulcanizates. *J Polym Sci Polym Symp*. 1974;48(1):169-196. doi:10.1002/polc.5070480114
11. Payne AR. The dynamic properties of carbon black-loaded natural rubber vulcanizates. *J Appl Polym Sci*. 1962;Part I(6):57-63.
12. Bokobza L. The reinforcement of elastomeric networks by fillers. *Macromol Mater Eng*. 2004;289(7):607-621. doi:10.1002/mame.200400034
13. Berriot J, Montes H, Lequeux F LD. Gradient of glass transition temperature in filled elastomers. *Europhys Lett*. 2003;64:50-56.

14. Bouasse, H.; Carriére Z. Courbes de traction du caoutchouc vulcanisé. *nn Fac Sci Toulouse*. 1903;5:257-283.

15. Mullins L. Effect of stretchning in rubber. *J Rubber Res*. 1948;16:275-282.

16. Merckel Y, Brieu M, Diani J, Caillard J. A Mullins softening criterion for general loading conditions. *J Mech Phys Solids*. 2012;60(7):1257-1264. doi:10.1016/j.jmps.2012.04.001

17. Qi HJ, Boyce MC. Stress-strain behavior of thermoplastic polyurethanes. *Mech Mater*. 2005;37(8):817-839. doi:10.1016/j.mechmat.2004.08.001

18. Webber RE, Creton C, Brown HR, Gong JP. Large strain hysteresis and mullins effect of tough double-network hydrogels. *Macromolecules*. 2007;40(8):2919-2927. doi:10.1021/ma062924y

19. Munoz, M.J., Rodrigues, J.F. O et al. An experimental study of the mouse skin behaviour: Damage and inelastic aspects. *J Biomech*. 2008;41(1):93-99.

20. Diani J, Fayolle B, Gilormini P, Diani J, Fayolle B, Gilormini P. A review on the Mullins effect To cite this version : HAL Id : hal-00773015. 2013:601-612.

21. Merckel Y, Diani J, Brieu M, Gilormini P, Caillard J. Characterization of the mullins effect of carbon-black filled rubbers. *Rubber Chem Technol*. 2011;84(3):402-414. doi:10.5254/1.3592294

22. Carbone G, Persson BNJ. Crack motion in viscoelastic solids: The role of the flash temperature. *Eur Phys J E*. 2005;17(3):261-281. doi:10.1140/epje/i2005-10013-y

23. Medalia. Heat Generation in Elastomer Compounds Causes and Effects. *Rubber Chem Technol*. 1991.

24. Mars W V., Ellul MD. Fatigue Characterization of a Thermoplastic Elastomer. *Rubber Chem Technol*. 2017;90(2):367-380. doi:10.5254/rct.17.83780

25. Gent, A. N., Scott KW. Dynamic Mechanical Properties. In: Gent AN, ed. *Engineering with Rubber*. Hanser Publishers, Munich; 1992:89-117.

26. Mzabi S. Caractérisation et analyse des mécanismes de fracture en fatigue des élastomères chargés. 2010:1-310.

27. Martinez JRS, Toussaint E, Balandraud X, et al. Heat and strain measurements at the crack tip of filled rubber under cyclic loadings using full-field techniques To cite this version : HAL Id : hal-01148252 Heat and strain measurements at the crack tip of filled rubber under cyclic loadings using full-f. 2015.

28. Saux V Le, Marco Y, Calloch S, et al. Fast Evaluation of the Fatigue Lifetime of Elastomers Based on a Heat Build-up Protocol and Micro-tomography Measurements To cite this version : HAL Id : hal-00493227 Fast evaluation of the fatigue lifetime of rubber-like materials based on a heat build-u. 2011.

29. Huneau B. Strain-induced crystallization of natural rubber: a review of x-ray diffraction investigations. *Rubber Chem Technol*. 2011;83(4):425-452.

30. Samaca Martinez JR, Le Cam JB, Balandraud X, Toussaint E, Caillard J. Filler effects on the thermomechanical response of stretched rubbers. *Polym Test*. 2013;32(5):835-841. doi:10.1016/j.polymertesting.2013.04.003

31. Le Cam JB. Energy storage due to strain-induced crystallization in natural rubber: The physical origin of the mechanical hysteresis. *Polymer (Guildf)*. 2017;127:166-173. doi:10.1016/j.polymer.2017.08.059

32. Demassieux Q. These De Doctorat structural changes in the process zone of a cyclic fatigue crack in filled natural rubber. 2011.

33. Demassieux Q, Berghezan D, Cantournet S, Proudhon H, Creton C. Temperature and aging dependence of strain-induced crystallization and cavitation in highly crosslinked and filled natural rubber. *J Polym Sci Part B Polym Phys*. 2019;57(12):780-793. doi:10.1002/polb.24832

34. Zhang, H. ,Scholz, A. , Crevoisier J et al. Nanocavitation in Carbon Black Filled Styrene−butadiene rubber under tension detected by real time small angle X-ray scattering.pdf. 2012.

35. Le Cam JB, Toussaint E. Volume variation in stretched natural rubber: Competition between cavitation and stress-induced crystallization. *Macromolecules*. 2008;41(20):7579-7583. doi:10.1021/ma801290w

36. Gent, A. N.; Lindley PB. Internal rupture of bonded rubber cylinders in tension. *Proceedins R Soc L Ser - Math Phys Sci*. 1958;A249:195-205.

37. Zhang H, Scholz AK, Vion-Loisel F, et al. Opening and closing of nanocavities under cyclic loading in a soft nanocomposite probed by real-time small-angle X-ray scattering. *Macromolecules*. 2013;46(3):900-913. doi:10.1021/ma302325w

38. Le Cam, J. B. , Huneau B. , Verron E. , Gornet L. Mechanism of Fatigue Crack Growth in Carbon Black Filled Natural Rubber. *Macromolecules*. 2004:5011-5017.

39. Le Cam JB, Toussaint E. The mechanism of fatigue crack growth in rubbers under severe loading: The effect of stress-induced crystallization. *Macromolecules*. 2010;43(10):4708-4714. doi:10.1021/ma100042n

4 THERMOPLASTIC ELASTOMERS

Thermoplastic elastomers (TPE) are a widely diffused class of material and are present nearly everywhere in our daily life: toothbrush handles, mobile covers, sneakers soles are only some example of applications (Figure 4-1).

The reason behind the huge diffusion of TPU can thus be summarized in a single concept: *they allow rubberlike materials, that cannot be melted and reprocessed once moulded, to be produced and re-shaped as a thermoplastic*[1] *(e.g. injection moulding, extrusion).*

Rubbers are generally known for their characteristic elastic behaviour including the ability to be deformed several times their initial length, and to recover the original shape once the load is removed. The drawback is that classical rubbers are thermoset, that means that irreversible bonds are introduced between certain number of chains through an irreversible process called vulcanization as explained in Chapter 2. On the other side, thermoplastic elastomers have several properties of rubber such as softness and large strain elasticity but, can be rapidly and reversible shaped as a thermoplastic.

Figure 4-1 Example of TPE applications

4.1 Historical survey and generic classification

The history of TPE begins in 1930 when Goodrich scientists realised that adding plasticizers to PVC would convert hard PVC into a flexible product (Drobny n.d.; Holden 2000). Classic PVC is made by two different structures: syndiotactic and crystalline and amorphous atactic one. The use of plasticizers reduces the glass transition temperature of the amorphous atactic polymer and leads to a flexible polymer consisting in the combination of a rigid phase (that melts at high temperature) with a softer and amorphous one (above its glass transition temperature in usage condition). Despite the fact that plasticized PVC was still lacking many elastomeric properties, the higher flexibility provided by the coexistence of two different phases raised the interest toward a new class of flexible-thermoplastic polymers and opened the route for further development of soft and flexible thermoplastic elastomers. The second breakthrough in the history of the development of thermoplastic elastomers came in 1937 when Otto Bayer and his co-workers recognised the advantage of using a polyaddition reaction (noted since the middle of 1800) to produce useful plastics [1,2]. Bayer and co-workers originally produced polymer fibres consisting in semi-crystalline polyurethane rich domains (below their $T_{g,}$) and an amorphous phase (above its glass transition temperature) made of long polyols. Basically, using a diisocyanate, a short chain and a long chain glycol they reproduced the two-phase structure of PVC that nowadays we know to be the basis of the elastomeric behaviour of thermoplastic elastomers. This discovery received worldwide attention but, due to the constraints induced by the second World war, it was only in 1950 that the first production of commercial polyurethane based thermoplastic elastomers (TPU) started by the Goodrich

Company. The last and missing milestone that allowed a fast development and commercialization of thermoplastic elastomers was the emergence of the anionic polymerization in 1950 that opened an easy route for the production of block copolymers by alternating soft and hard blocks [1]. A new class of polymers, providing several properties of vulcanised rubber without any chemical vulcanization that could be shaped using thermoplastic techniques was finally discovered.

4.1.1 Classification of TPE

The development of the chemistry of TPE become suddenly extremely fast and creative. Different chemistries, respecting the basic requirement of the formation of the specific multi-phase structure, were explored to produce different TPEs with specific characteristics in terms of strength, elasticity, wear and oil resistance etc. Nowadays TPE can be classified in two major classes: segmented block copolymer and polymer blends [3] as represented in Figure 4-2.

- Segmented copolymers are characterized by alternating soft elastomers and hard thermoplastic block such as polyamide/elastomeric block copolymers (TPAs), polyether/elastomer block copolymers (TPEs), polyurethane/elastomers block copolymer (TPUs).
- Blends are essentially divided in polyolefin blends (TPOs) and dynamically vulcanized blends (TPV)

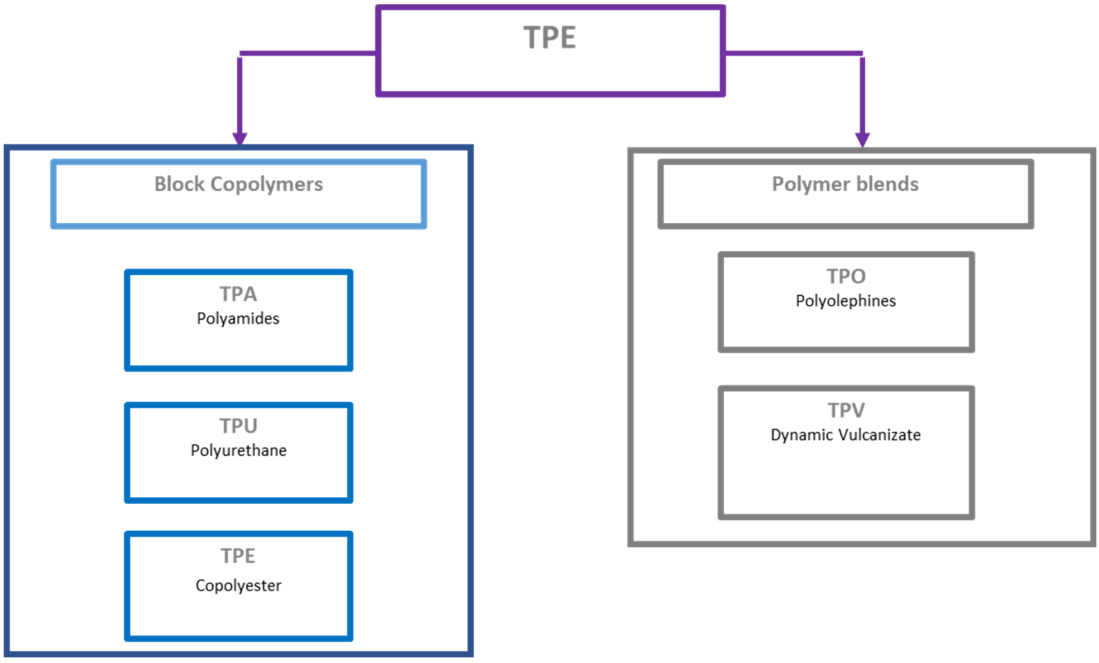

Figure 4-2 Example of classification of TPE.

Among all TPEs, the class of TPUs is one of the most versatile. The easy polyurethane chemistry allows to produce TPUs over a wide range of rigidity, with a modulus between 10 and 10.000 MPa [4]. As the majority of TPEs, TPUs do not require any curing operation and can be processed by a variety of techniques including: injection moulding, extrusion and solvent casting. Common properties of TPUs are: good elastic and flexible behaviour and an excellent resistance to abrasion. Additionally, TPU can be produced with low Young's moduli (<10 MPa) that makes them a possible sustainable alternative to commercial thermoset elastomers. Therefore, the importance of TPUs in the last years has grown because of their less expensive and faster production processes and the possibility of being recycled[5].

4.1.2 Chemistry and production of TPUs

TPUs are the product of polyaddition reactions involving three principal reactants: a difunctional linear diol (hydroxyl terminated polyether or polyester) also called soft segment; an aromatic or aliphatic diisocyanate and a chain extender (short chain diol) forming the hard segment. The typical structure of TPU is shown in Figure 4-3

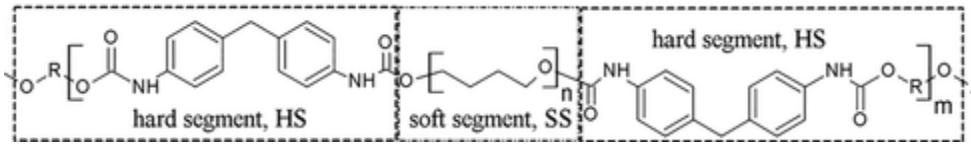

Figure 4-3 Schematic structure of TPU. Image from [6]

Among the most popular aromatic diisocyanates we find the aromatic 4,4'-methylene bisphenyl diisocyanate (MDI) (**Error! Reference source not found.**) The structural rigidity of the hard segments generally provides the TPU with a high tensile strength, modulus and thermal stability [7]. However the aromatic units are susceptible to ultraviolet attack and stabilizers are required to avoid excessive degradation and yellowing. A common aliphatic alternative is the 1,6-hexamethylene diisocyanate (HDI). TPU with aliphatic hard segments are generally characterised by higher flexibility and phase separation compared to aromatic one. [7–9]. There are two main procedures to produce TPU: one involves a single step where all reagents are mixed, the second requires the creation of a pre-polymer. Both processes have advantages and drawbacks in terms of timer and control of the final product.

A) Single step procedure: it implies that all reactants are mixed together and reacted in one step. This method is simple, however, the whole heat of reaction is released right away which suddenly increases the temperature of the reaction system considerably and makes it often incompatible with industrial procedures [10]. Low molecular weight chain extenders are often the most reactive elements having the tendency to react with the isocyanate faster and before the high molecular weight polyols.
B) Two steps procedure: the flexible block (either a polyether or polyester) reacts with the hard segment in the first step forming a pre-polymer containing both flexible and rigid block terminating with isocyanate groups. Then, the excess of diisocyanate reacts with the chain extender (usually a short chain diol or diamine) leading to the formation of the final TPU Generally, the single step procedure leads to the formation of more random copolymer while the two steps allows to obtain polymers with higher molecular weight (100.000 g/mol) and lower polydispersity index [11].

4.2 Morphology of TPU

As previously mentioned, the final structure of a TPU is a copolymer composed by the long macrodiol or soft segment (SS) and the diisocyanate & chain extender composing the hard segment (HS). The HS and SS are chemically incompatible and tend to phase separate. Moreover, HS gather together thanks to the favourable hydrogen bonding (red in Figure 4-4) between carbonyl and amine groups developing aggregation of small domains surrounded by a soft phase. Depending on a combination of chemical composition, molecular weight and steric hindrance, the phase separation can be more or less partial but is generally never complete. Hard domains occupy significant volume 5-30 nm and are stiffer than soft domains acting as nanoscale fillers and physical crosslinks at the same time [12,13].

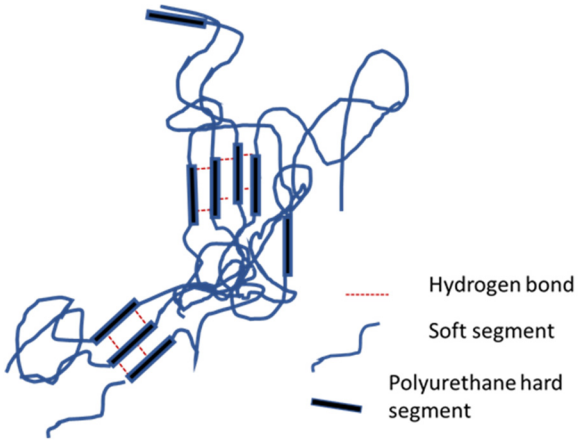

Figure 4-4 Schematic structure of TPU morphology.

4.3 Thermodynamic of phase separation

The tendency to segregate and forming phase-separated microdomains of HS is mainly driven by the chemical incompatibility between soft and hard segments but, as reported by Van Bogart, [11] the influence of temperature plays a key role in determining phase separation and usage limit of TPU. In a copolymer in fact, the most important variable controlling the phase separation is the free energy of mixing ΔG:

$$\Delta G = \Delta H - T\Delta S$$

Where ΔH is the enthalpy of mixing, ΔS the entropy of mixing and T the temperature of the system. The thermodynamic incompatibility between polar hard segment and less polar SS makes $\Delta G>0$ and force them to separate. The term $T\Delta S$ is generally small for high molecular weight polymer but if T increases the two-phase mixing is promoted. This simple argument demonstrates the importance of temperature in determining microstructure and properties of a segmented copolymer as TPUs and explain why thermoplastic elastomer have less thermal stability compared to thermoset rubbers. It is finally important to remark that, unlike the blending of two incompatible polymers, TPUs share covalent bonds between the HS and SS segments that prevents macroscopic separation of phase (as it the case of blends) resulting in the micro-phase separated morphology.

4.3.1 Role of hydrogen bonding in phase separation

The formation and stability of HD in TPU is promoted to the formation of extensively hydrogen bonding between urethane units. Hydrogen bond is one of the strongest intermolecular interaction (20-50KJ/mol) but weaker than a covalent or ionic bond. The NH group of the urethane linkage (-NHCO-O-) acts as a proton donator whereas the hydrogen bond acceptor can be found either in the carbonyl group of the hard segments or, to a lesser extent, in the soft segments. Figure 4-5 summarizes different possible kinds of hydrogen bonding in TPU. The first consequence of hydrogen bonding is the formation of physical crosslink points that can be compared with the chemical crosslinking taking place for classical vulcanized rubber. The extension of hydrogen bond interactions also affects the stability of hard-domains, that mainly derives from the self-assembly ability of urethane groups between inter-carbonyl and amino group [14]. Recently, Mc Kiernan et al. [15] compared to a series of conventional TPUs with analogous structures achieved without hydrogen bonding revealing the strong influence of hydrogen bonding in improving the crystallization ability and packing of HS in soft TPU. Nevertheless, the effective role of hydrogen bonding in TPUs is still discussed. Seymour and Cooper [16] found a good phase separation and similar mechanical properties in two series of TPUs with or without of hydrogen bonding concluding that the hydrogen bonding can be neither the principal reason responsible for phase separation nor the main reason of such excellent mechanical properties of TPU.

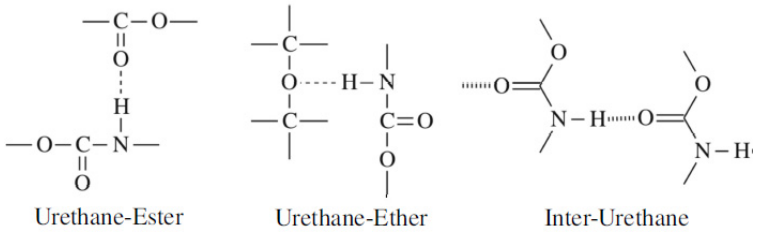

Figure 4-5 Possible hydrogen bonding in Polyurethane. Reprinted from [17]

4.3.2 Experimental evidence of the two phase morphology

According to He[10], Schollenberger [18] was the first to introduce the concept of "virtual" crosslinking in 1958 to underline the main difference between reversible physical interactions in TPUs and the irreversible crosslinking in classical rubbers. At the time anyway, there was no proof yet of the two-phase microstructure of TPU. The first evidence of the formation of a two phase morphology was provided by Cooper and Tobolsky [19] who suggested that the unusually high plateau modulus of TPUs was due to intermolecular associations between hard segments of TPU block copolymers. Some years later, Bonart and Clough et al[20] established that in TPUs, HS aggregate via hydrogen bonds form a physically crosslinked and reversible network. [13,21]. Some years later, Koutsky [22] confirmed the multiphase structure of TPU using a TEM analysis Figure 4-6. Later on, the effect of the micro-phase morphology on the final properties was investigated in depth by using several characterization techniques including scanning electron microscopy (SEM), atomic force microscopy (AFM), Fourier transform infrared (FTIR) An interesting review on the structure-composition relationship is provided by He et al. [10].

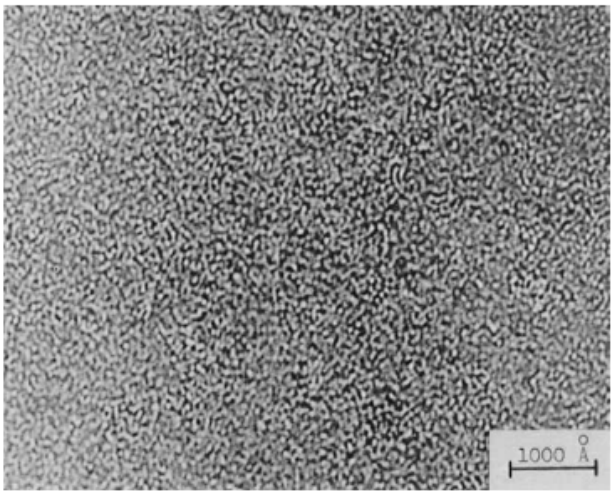

Figure 4-6 TEM image showing the 2-phase structure in polyester-urethane block copolymer. Reprinted from[22]

4.4 Strength of TPU and deformation mechanisms

As already pointed out, in phase separated TPUs the hard domains appear to behave as both crosslinking points and fillers. Early in 1974-76, Smith [23,24], proposed that the principal mechanisms explaining the reinforcing effect of hard domains in soft TPU elastomers are: increase in energy dissipation during strain, crack bifurcation, cavitation , and plastic deformation of domains. Additionally, comparing the tensile strength of TPU at different strain rates and temperatures, he highlighted that, for this class of materials, the time-temperature superposition does not work[23,25]. These results contributed to reinforce the idea that in segmented TPU, it is the specific hard-soft segment architecture (degree of phase separation, which is affected by the testing temperature and chemical composition of hard and soft segment, etc.) that governs the final strength and mechanical behaviour. This explains why, in the following years, investigating how the deformation mechanisms of TPUs were affected by their morphological features became an attractive topic and will be explored in 4.4.1.

4.4.1 Structural changes induced by deformation in TPU

In order to better understand the excellent mechanical strength of TPU the response of the microstructure to external deformation has been largely studied using different techniques. Bonart [21] was among the first investigating the deformation behaviour of TPU using small and

wide angle X-Ray scattering (SAXS and WAXD). He proposed that the hard segment reflections in the diffraction pattern were produced by lateral arrangement of HS via hydrogen bonding in a pseudo-crystalline formation. According to his analysis, for strains below 200-300%, the progressive tensile alignment of strained SS exerts a torque on the HD that, as a result, tend to orient transversal to the direction of the applied load as schematically represented in Figure 4-7. A further elongation was associated with breaking and restructuring of HD along the loading direction. Nevertheless, further studies suggested that for high value of strain the nature of the hard segments greatly affects the deformation behaviour. Crystalline HD with a high diisocyanate content (>40%), never become completely aligned and mainly act as inert filler and [26].

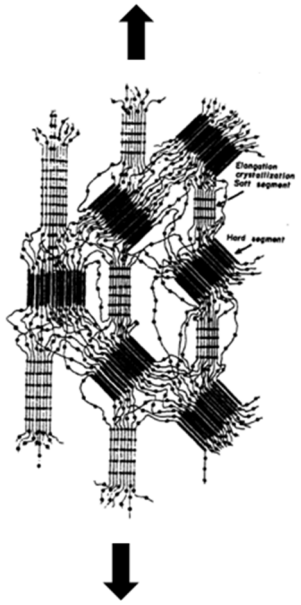

Figure 4-7 Schematic structure of TPU at 200% of strain (From Bonart 1968). The loading direction is indicated by the arrows.

The process of "cross-linking restructuration" as defined by Ishihara [27], consists in breaking and re-forming of hydrogen bonding to allow the hard segment to be re-aligned. An excellent summary on X-ray investigations in deformed TPU with a low hard segment content (<12%) was provided by Yeh and co-workers[28] and schematically represented in Figure 4-8 . Moreover, they also proposed that the disrupted hard domain lamellae and elongated or strain induced SS contribute to the equatorial scattering often visible in soft TPU that should arise from electron density contrast between restructured and aligned hard blocks and aligned soft chains. Lee[29] and co-workers also proposed that the initial orientation of HS, that may be induced during the

processing of TPU, affect the final mechanisms favouring or not the fragmentation of the hard domains.

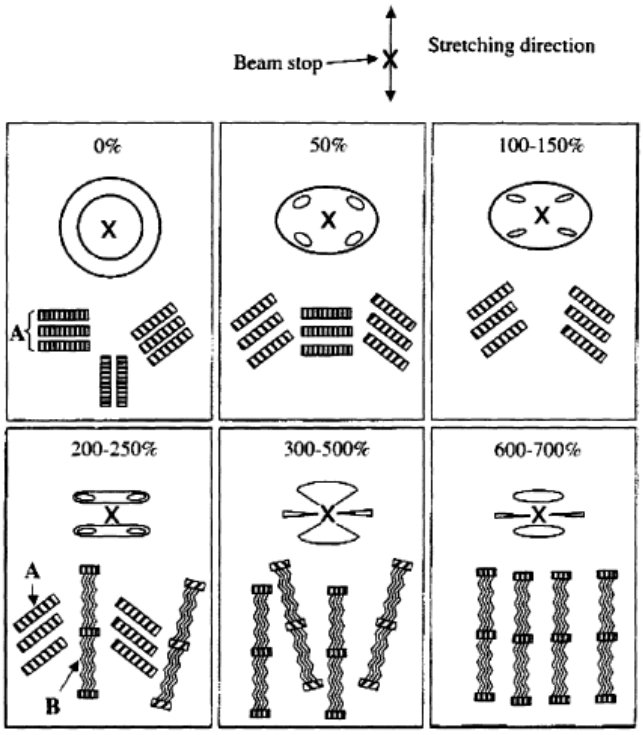

Figure 4.5: Summary of Deformation-Induced Structural Development in Segmented Polyurethaneureas for Soft Segment Continuous Morphologies[10]

Figure 4-8 Schematic of strain-induced structural modification in TPU with low HD content. Reprinted from [28]

Further studies[30–33] used Fourier-transform infrared (FT-IR) dichroism to confirm Bonart model. Cooper and al[32]. proved that orientation of hard segments is mainly affected by HS length while SS orientation that progressively evolves parallel to the load, do not depend on the composition. Kimura et al[27,31] further proposed that the elongation mechanism can involve a complete re-organization of the hard domains through the progressive rotation of the principal axis of the HD from a relaxed to a strained condition as reported in Figure 4-9. In the relaxed condition, the principal axis lies in the direction perpendicular to the lamellae stack of HS while upon deformation and restructuration of HD, it changes to orient along the parallel direction of the applied load inducing a fibrillar structure.

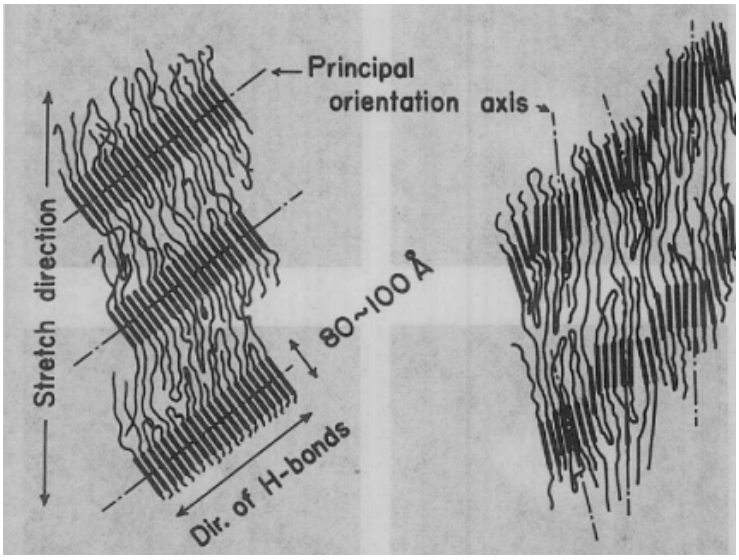

Figure 4-9 Schematic illustration of HD rotation and principal axis direction during TPU rotation (from Kimura)

4.4.2 Effect of composition and modelling of mechanical behaviour

Mechanical properties of TPU where extensively studied in the past. The effect of temperature, strain rate, hard/soft segment ratio and composition was often investigated mainly with the aim to better understand how they affect the mechanical strength in TPU. [12,34–37].

Russo et al. [35] studied mechanical properties at low strain rate of a series of TPUs with different content of hard segments. They correlated the increase in hard segment content with the increase of the initial modulus and ultimate strength and the decrease in elongation at break.

O'sickey [37] and others analyzed the effect of changing hard segment content and molecular weight of soft segments in polyurethane-urea. They concluded that the molecular weight of SS had considerable influence on the morphology of TPUs while the hard segment content mainly affects the reversible elasticity (TPU with E <10MPa).

More recently, Buckley and al [38] analyzed the large strain mechanical properties of TPUs by varying the crystallinity and composition of hard and soft segments. They found that the linear modulus of TPU significantly increased with increasing hard domain content and crystallinity, but was almost independent of the degree of phase separation. Moreover, a remarkable uniformity in dissipated energy was revealed by TPUs with linear moduli ranging from 40-300MPa during the second and following loading cycles.

An interesting review on the correlation between mechanical properties and morphology is reported by Qi and Boyce[34] who proposed a constitutive model for the observed elastic

behavior treating hard domains as reinforcing particles in an elastomeric matrix. Although the model captures the time dependent behavior and strain induced softening in cyclic loading, it fails in predicting the unloading path and only takes into account the evolution of the volume fraction of soft domains with deformation without accounting for time dependent and anisotropic response. The latter reinforces the importance of the microstructure evolution with applied strain. The developing anisotropic behavior (both in hard and soft segments) cannot be neglected in order to predict the cyclic response in TPU.

4.5 Inelasticity of TPU

When cyclically loaded, TPU generally present a certain residual plastic deformation (that in some case can be partially recovered) and cyclic hysteresis (or Mullin's effect). An example of TPU stress-strain curve is reported in in Figure 4-10.

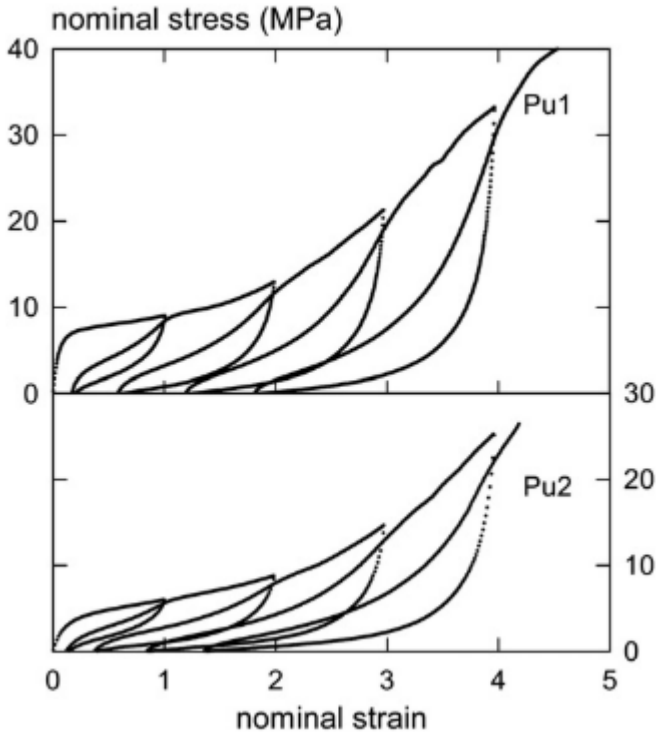

Figure 4-10 Example of Cyclic stress-strain curve for two TPUs with different chain extender and crystallinity. Re-printed from [38]

These inelastic phenomena are a common feature of several TPUs irrespectively of the specific hard/soft segment ratio and chemistry. Buckley et al[38]. tested the cyclic response of fourteen TPUs differing in hard and soft segment chemistry (MDI or DBDI) content and molecular

weight, and found similar qualitative behaviours in terms of hysteresis and residual deformation. Regardless of their origin, both residual strain and large hysteresis can be detrimental in several applications especially those requiring several loading-unloading cycles and must be carefully evaluated.

4.5.1.1 Microscopic interpretation of Mullins effect

We already presented the Mullins effect in classical thermoset rubber. In the case of TPU this has been less extensively investigated but, an interesting interpretation at the microscopic scale of the Mullins effect in TPU was proposed by Sui et al[39] who investigated the phenomenon by exploring deformation at the micro- and nano-scales of DBDI/PEA TPU using in-situ x-Ray analysis. They evaluated the apparent modulus of the hard and soft phase and of the in-between interface and associated the Mullins effect to the strongest change of apparent modulus at the interface. They argued that, for strain lower than 50% this interface is the first to be deformed and accommodates the strain gradient between hard and soft phase. On the other hand, for higher strain values the large hysteresis is more likely to be attributed to larger structural changes. This result mainly refutes the general consideration that HD restructuring is the sole phenomenon accountable of hysteresis in TPU.

4.5.1.2 SIC in Thermoplastic elastomers

SIC was found both in TPE [40] and TPU [8,41,42] containing either polytetrahydrofuran (PTHF) or Poly(oxytetramethylene) glycol (PTMG). One of the main differences between SIC in TPE and NR is that in the case of NR, SIC is completely reversible and no crystalline structure is generally observed after the removal of the load, while in TPE the presence of a residual crystalline phase was often found after the removal of the stress using both X-Ray and calorimetric analysis[40,42,43].

4.5.2 Fracture and fatigue behaviour

Despite the growing interest toward the class of TPU, their fracture and fatigue behaviour has been only poor investigated. Major et al[44]. evaluated cyclic fatigue in two classes of TPU filled and unfilled at the frequency of 2 and 10Hz. They highlighted the dependence of energy release rate on the number of cycles and the slightly better crack resistance at 10Hz for the unfilled TPU. Additionally, they noted the formation of a whitening layer close to the crack tip that they associated to the process zone. More recently Mars and Ellul[45] ,evaluated the cyclic crack propagation for a commercial TPE known as Santoprene™ consisting in a blend of vulcanized

EPDM (Ethylene propylene diene monomer) and polypropylene. This class of material is generally harder than the soft TPU considered in this study (E =∼400 MPa) and presents evident yielding. Mars and Ellul [45] inferred that, the fracture mechanic framework can still be adopted in this class of materials presenting high inelastic behaviour provided that, only the fraction of recovered energy is considered in the calculation of G. Thus, they proposed an experimental routine to account only for the fraction of the stored energy (associated to the elastic part of the strain) in the calculation of G.

4.6 Concluding remarks

This extended introduction on thermoplastic elastomers (and in particular on TPU) was aimed to recall some theoretical tools which will be adopted the Part II. In particular, the key messages of this part can be summarized as follows:

- Soft TPUs present high extensibility and elastic behaviour, comparable to that of vulcanised elastomers, coupled with the outstanding advantage to be processed as a thermoplastic with less time-consuming processes than those conventionally adopted in rubbers.
- The excellent mechanical properties of unfilled and un-crosslinked TPU, derive from the presence phase-separated morphology (HD and SS). The HDs (formed by aggregation of HS through hydrogen bonds) play the role of both filler and crosslinking points.
- TPU generally present inelastic phenomena. Some of them: SIC, Mullins effect and residual deformation, are qualitatively similar to those found in filled rubbers. Other, as the re-orientation of HDs with applied strain and plastic deformation, are characteristic of this class of materials. In particular, the lack of experimental works on cyclic and fracture behaviour of TPU leaves several open questions about the effect that their strain-dependent microstructure can have on fracture and fatigue properties of TPU.

4.7 References

1. Holden G. *Understanding Thermoplastic Elastomer*.; 2000.
2. Holden, G. ; Bishop, E. T.; Legge NR. Thermoplastic Elastomers. *J Polym Sci Part C Polym Symp*. 1970;26(1):35-57. http://www.scopus.com/inward/record.url?eid=2-s2.0-0014954923&partnerID=40&md5=26204daeba729373c80f6b26d755735b.
3. Legge NR. Thermoplastic Elastomers. *Rubber Chem Technol*. 1987;60(3):83-117. doi:10.5254/1.3536141
4. BASF. Elastollan Material Properties. http://199.83.243.175/img/pdf/Elastollan_Material_PropertiesR1.pdf.
5. Research and Markets: Global Production of Thermoplastic Polyurethane Market (TPU) will Increase by 5.0% CAGR Up Until 2017. https://www.businesswire.com/news/home/20130730006152/en/Research-and-Markets-Global-Production-of-Thermoplastic-Polyurethane-Market-TPU-will-Increase-by-5.0-CAGR-Up-Until-2017. Published 2013.
6. Datta, Janusz; Kasprzy P. Thermoplastic polyurethanes derived from petrochemical or renewable resources: A comprehensive review. *Polym Eng Sci*. 2017;58(S1):E14-E35. doi:https://doi.org/10.1002/pen.24633
7. Prisacariu C. *Thermoplastic Elastomers Handbook*.; 2011.
8. Koberstein JT, Stein RS. Small-Angle X-Ray Scattering Studies of Microdomain Structure in Segmented Polyurethane Elastomers. *J Polym Sci Part A-2, Polym Phys*. 1983;21(8):1439-1472. doi:10.1002/pol.1983.180210814
9. Prisacariu C, Olley RH, Caraculacu AA, Bassett DC, Martin C. The effect of hard segment ordering in copolyurethane elastomers obtained by using simultaneously two types of diisocyanates. *Polymer (Guildf)*. 2003;44(18):5407-5421. doi:10.1016/S0032-3861(03)00489-0
10. He Y, Xie D, Zhang X. The structure, microphase-separated morphology, and property of polyurethanes and polyureas. *J Mater Sci*. 2014;49(21):7339-7352. doi:10.1007/s10853-014-8458-y
11. J.W.C Van Bogart, A. Lilaonitkul SLC. Morphology and properties of segmented

polyether poly(urethaneureas). *Am Chem Soc*. 1979. doi:10.1295/polymj.17.969

12. Z. S.Petrovic JF. POLYURETHANE ELASTOMERS. *Prog Polym Sci*. 1991;16:695-836.

13. Bonart R. Thermoplastic Elastomers. *Brydson's Plast Mater Eighth Ed*. 1979;20(July):653-703. doi:10.1016/B978-0-323-35824-8.00024-4

14. Mattia J, Painter P. A comparison of hydrogen bonding and order in a polyurethane and poly(urethane-urea) and their blends with poly(ethylene glycol). *Macromolecules*. 2007;40(5):1546-1554. doi:10.1021/ma0626362

15. Mc Kiernan, R. L. , Heintz, A.L., Hsu, S.L. et al. Influence of hydrogen bonding on the crystallization behavior of semicrystalline polyurethane. *Macromolecules*. 2002;35:6970-6974.

16. Seymour, LW; Cooper S. Thermal analysis of polyure- thane block polymers. *Macromolecules1*. 1973;6:48-53.

17. Prisacariu Cristina. *Polyurethane Elastomers- From Morphology to Mechanical Aspects*. Springer, New York, USA; 2011.

18. Schollenberger, C. S.; Scott, H.; Moore GR. Polyurethane VC, a Virtually Cross-linked Elastomer. *Rubber World*. 1958:137-549.

19. Cooper SL, Tobolsky A V. Properties of Linear Elastomeric Polyurethanes. 1966;10:1837-1844.

20. Clough, B. ; Schneider N. et al. Small-angle X-ray scattering from polyurethane elastomers. *J Macromol Sci Part B*. 1968;B2(4):641.

21. Bonart R. X-ray investigations concerning the physical structure of cross-linking in segmented urethane elastomers. *J Macromol Sci Part B*. 1968;2(1):115-138. doi:10.1080/00222346808212867

22. Koutsky, JA ; Hien, NV; Cooper S. Some results on electron microscope investigations of polyether- urethane and polyester- urethane block copolymers. *Polym Lett*. 1970;8(5):353-359. doi:10.1002/pol.1970.110080508

23. Smith TL. Tensile Strength of Polyurethane and Other Elastomeric Block Copolymers.

J Polym Sci Polym Phys Ed. 1974;12:1825-1848. doi:10.5254/1.3534952

24. Smith. Tensile Strength of Polyurethane And Other Elastomeric Block Copolymers.pdf. 1976.

25. Smith TL. Strength of elastomers—A Perspective. *Polym Eng Sci*. 1977;17(3):129-143. doi:10.1002/pen.760170302

26. Waletzko RS, James Korley LST, Pate BD, Thomas EL, Hammond PT. Role of increased crystallinity in deformation-induced structure of segmented thermoplastic polyurethane elastomers with PEO and PEO-PPO-PEO soft segments and HDI hard segments. *Macromolecules*. 2009;42(6):2041-2053. doi:10.1021/ma8022052

27. Ishihara H, Kimura I, Yoshihara N. Studies on Segmented Polyurethane-Urea Elastomers: Structure of Segmented Polyurethane-Urea Based on Poly(tetramethylene glycol), 4,4′-Diphenylmethane Diisocyanate, and 4,4′-Diaminodiphenylmethane. *J Macromol Sci Part B*. 1983;22(5-6):713-733. doi:10.1080/00222348308245751

28. Yeh F, Hsiao BS, Sauer BB, Michel S, Siesler HW. In-situ studies of structure development during deformation of a segmented poly(urethane-urea) elastomer. *Macromolecules*. 2003;36(6):1940-1954. doi:10.1021/ma0214456

29. Lee HS, Yoo SR, Seo SW. Domain and segmental deformation behavior of thermoplastic elastomers using synchrotron SAXS and FTIR methods. *J Polym Sci Part B Polym Phys*. 1999;37(22):3233-3245. doi:10.1002/(sici)1099-0488(19991115)37:22<3233::aid-polb8>3.0.co;2-j

30. Seymour, R. W.; Allegrezza, A. E., Jr; Cooper SL. Segmental orientation studies of block polymers. I. Hydrogen-bonded polyur- ethanes. *Macromolecules*. 1973;6:896-902.

31. Kimura I, Ishihara H, Ono H, Yoshihara N, Nomura S, Kawai H. Morphology and Deformation Mechanism of Segmented Poly(urethaneureas) in Relation to Spherulitic Crystalline Textures. *Macromolecules*. 1974;7(3):355-363. doi:10.1021/ma60039a018

32. Cooper, G M; Estes, R W Seymour SL. Infrared Studies of Segmented Polyurethane Elastomers. II. Infrared Dichroism. 1971;248(3):452-457. doi:10.1021/ma60022a018

33. Hu, C S P, Sung CB. Orientation Studies of Segmented Polyether Poly (urethaneurea)

Elastomers by Infrared. 1981:212-215. doi:10.1021/ma50002a047

34. Qi HJ, Boyce MC. Stress-strain behavior of thermoplastic polyurethanes. *Mech Mater*. 2005;37(8):817-839. doi:10.1016/j.mechmat.2004.08.001

35. Russo R, Thomas EL. Phase Separation in Linear and Cross-Linked Polyurethanes. *J Macromol Sci Part B*. 1983;22(4):553-575. doi:10.1080/00222348308224776

36. Yi J, Boyce MC, Lee GF, Balizer E. Large deformation rate-dependent stress-strain behavior of polyurea and polyurethanes. *Polymer (Guildf)*. 2006;47(1):319-329. doi:10.1016/j.polymer.2005.10.107

37. Sickey MJO, Lawrey BD, Wilkes GL. Structure – Property Relationships of Poly (urethane urea) s with Ultra-low Monol Content Poly (propylene glycol) Soft Segments . I . Influence of Soft Segment Molecular Weight and Hard Segment Content. 2002:229-243.

38. Buckley CP, Prisacariu C, Martin C. Elasticity and inelasticity of thermoplastic polyurethane elastomers: Sensitivity to chemical and physical structure. *Polymer (Guildf)*. 2010;51(14):3213-3224. doi:10.1016/j.polymer.2010.04.069

39. Sui T, Salvati E, Ying S, et al. Strain softening of nano-scale fuzzy interfaces causes Mullins effect in thermoplastic polyurethane. *Sci Rep*. 2017;7(1):1-9. doi:10.1038/s41598-017-00904-3

40. Toki S, Hsiao BS, Kohjiya S, Tosaka M, Tsou AH, Datta S. Synchrotron X-Ray Studies of Vulcanized Rubbers and Thermoplastic Elastomers. *Rubber Chem Technol*. 2011;79(3):460-488. doi:10.5254/1.3547946

41. Koerner H, Kelley JJ, Vaia RA. Transient microstructure of low hard segment thermoplastic polyurethane under uniaxial deformation. *Macromolecules*. 2008;41(13):4709-4716. doi:10.1021/ma800306z

42. Zhu P, Zhou C, Dong X, Sauer BB, Lai Y, Wang D. The segmental responses to orientation and relaxation of thermoplastic poly(ether-ester) elastomer during cyclic deformation: An in-situ WAXD/SAXS study. *Polymer (Guildf)*. 2020;188:122120. doi:10.1016/j.polymer.2019.122120

43. Chen Y, Sijbesma RP. Dioxetanes as mechanoluminescent probes in thermoplastic

elastomers. *Macromolecules*. 2014;47(12):3797-3805. doi:10.1021/ma500598t

44. Major Z, Isasi M, Schwarz T. Characterization of the fracture and fatigue behavior of thermoplastic elastomer materials. *Key Eng Mater*. 2010;417-418:789-792. doi:10.4028/www.scientific.net/KEM.417-418.789

45. Mars W V., Ellul MD. Fatigue Characterization of a Thermoplastic Elastomer. *Rubber Chem Technol*. 2017;90(2):367-380. doi:10.5254/rct.17.83780

46. Demassieux Q. These De Doctorat structural changes in the process zone of a cyclic fatigue crack in filled natural rubber. 2011.

47. Mzabi S. Caractérisation et analyse des mécanismes de fracture en fatigue des élastomères chargés. 2010:1-310.

5 FRACTURE AND FATIGUE IN SOFT MATERIALS

5.1 Brief introduction to linear elastic fracture mechanic

The theory that studies the crack propagation in an elastic solid is known as LEFM and originated around 1921 with Griffith's work on fracture of glass fibres. At the time, the effect of stress amplification played by a crack subjected to a static load was already known thanks to the work of Inglis [1]. Griffith's intuition was to apply the concept of stress intensification factor to microscopic flaws, naturally present in all materials, to explain the reduction of the strength to rupture of a glass fibre when increasing its diameter. Based on this assumption, he proposed an energy based approach for crack propagation comparing the work required to break atomic bonds with the strain energy released as a crack grows concluding that, the crack propagation is due to the conversion of the elastic energy (stored within the deformed elastic material) into the energy required to separate the crack surfaces $\Gamma = 2\gamma$, where γ represents the material surface energy. In other words, the condition for crack propagation can be expressed as

$$\boldsymbol{G = \frac{dU_w}{dA} - \frac{dU_{el}}{dA} \geq \Gamma} \qquad \textbf{Equation 5-1}$$

An equivalent description of LEFM in terms of singular stress field was provided by IRWIN in 1957 who calculated the singular stress field produced around a loaded crack. He found a

square root dependence of the stress on the distance from the crack tip expressed as: $\sigma \sim \frac{K}{\sqrt{r}}$. Where K is a loading parameter. Using this approach, an equivalent condition for crack propagation in terms of stress can be then expressed as $K>K_c$. It can be demonstrated that for linear elastic material, the two approaches (energetic-local stress) are equivalent and, indicating with E the linear elastic modulus of the material the following holds:

$$K \sim \sqrt{EG} \qquad \textbf{Equation 5-2}$$

In other words, in LEFM both energy criterion and stress criterion are equivalent and the maximum stress achieved at the crack tip is essentially defined by the external work or input energy provided to the entire sample.

5.2 From LEFM to fracture mechanic of soft materials

One of the main differences between fracture in hard (see glass) and soft materials (see elastomers) is the localization of the bond breakage process. In the first case, fracture is directly associated to bond breakage that takes place in a small region around the crack tip. Namely, there is a clear separation of scale between the bulk of the sample, that is macroscopically deformed, and the stress conditions achieved at the crack tip.

As carefully reviewed by Creton and Ciccotti[2], in case of soft materials, this sharp separation between the sample scale and the local bond breakage disappears. The whole process of fracture in soft materials involves bonds breakage at the molecular level, bulk dissipation associated to linear viscoelasticity and a transition region (or zone of influence ≈ 100nm-100μm) where several processes as irreversible deformation, nonlinear elastic effect, damage etc. take place. A generalised model of main process involving fracture in soft material can be schematically described as follows (see Figure 5-1):

- Bulk: far away from the crack tip the material may dissipate energy through different irreversible phenomena such as viscoelastic or plastic energy losses. For an ideal elastic material no dissipation occurs in this region.

- Zone of crack influence or process zone: the crack tip region (100nm-100μm), where the singularity generates a complex and non-linear strain field is fundamentally important for soft materials. When the Young's modulus of the sample is sufficiently

low the crack blunts reducing the strain concentration and retarding crack propagation in soft materials[3].

- Local damage zone: at the molecular scale chains friction and bonds breakage are among the main dissipation mechanisms.

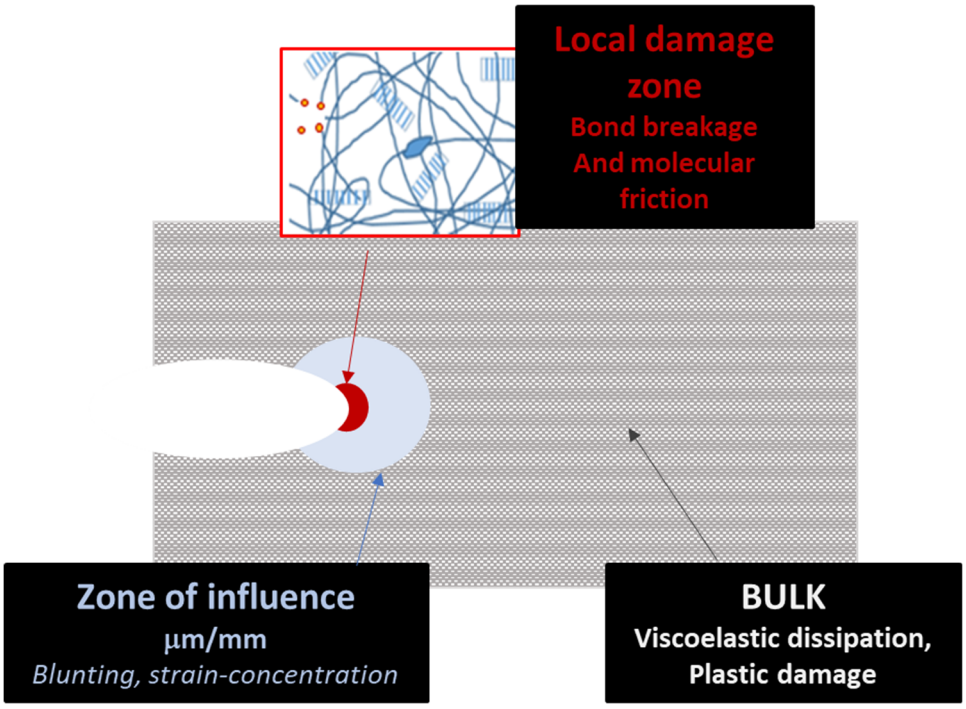

Figure 5-1 Schematic of the different length-scales involved in a crack propagating in soft material. Re-arranged from ([2])

It is clear thus that several energy dissipation sinks, acting at different length-scales, must play a significant role in crack propagation of soft materials and the equivalence $\Gamma = 2\gamma$ in principle is not valid anymore. Despite the difficulty in separating the single contribution coming from each length-scale, a generalised form for the fracture energy Γ that accounts for all sources of dissipation can still be adopted as will be described in the next sub-chapter.

5.2.1 A criterion for crack propagation on elastomers

Around 1953, Rivlin and Thomas started to study the problem of crack growth in rubbers translating the Griffith criterion from a brittle material to vulcanised rubber. They extended the concept of fracture energy to rubber under the following assumption:

- The elastic energy is not only converted in free surface energy but it is also dissipated in other forms as irreversible process in the bulk and at the crack tip.

- Dissipative phenomena are limited to a relatively small volume of the material compared with the overall dimensions of the body.

Under these assumptions, the energy release rate to propagate a crack historically defined as tearing energy in rubber (T or G) is a material characteristic and defined as :

$$G = -\frac{dU}{dA} \qquad \textbf{Equation 5-3}$$

Where U is change in the total mechanical energy and A the crack surface. The criterion for crack propagation can still be expressed as $G > \Gamma$. Γ also defined as fracture toughness, indicates the energy required to propagate the crack and, unlike the case of an elastic material, contains all non-linear dissipative effects associated to the crack propagation. It is worth to remember that G and Γ are two distinct variables. G is a loading parameter while Γ is a characteristic of the material measuring the energy dissipation associated with the propagation of the crack.

5.2.2 Analytical form of G, the easy case of pure shear geometry

The exact calculation of G (**Equation 5-3**) may be critical in elastomers where stress and strain at the crack tip are not infinitesimal and would require the complex resolution of the local field at the crack tip. Rivlin and Thomas derived simple analytical forms of G for different test pieces [4], some of them are shown in Figure 5-2

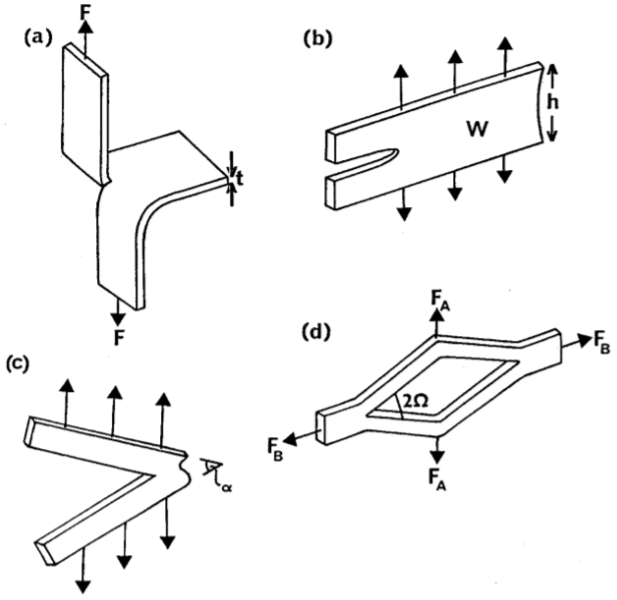

Figure 5-2 : Some geometries used in fracture experiment for rubber (a) "trousers"; (b) pure shear; (c) "angled" ; (d) "split" tear. Reprinted from[5].

In particular, the so-called pure shear geometry (b) (in Figure 5-2) consists in a long and thin rectangular sheet with width/height ratio are between 6 and 15 [6]. This particular geometry, is often used to evaluate the fracture resistance in monotonic and cyclic condition because of the easy calculation of G independent from the crack length. The term "pure shear" refers to the strain condition generated in the transversal side of the sample that is clamped along the long side and strained in the vertical direction. When the two extremities are pulled apart the lateral contraction along the long side is prevented by the clamps (except for the two edges that can contract towards the centre) while the sample may contract in its thickness generating a pure shear state indicated by the arrows in the lateral section of the sample Figure 5-3.

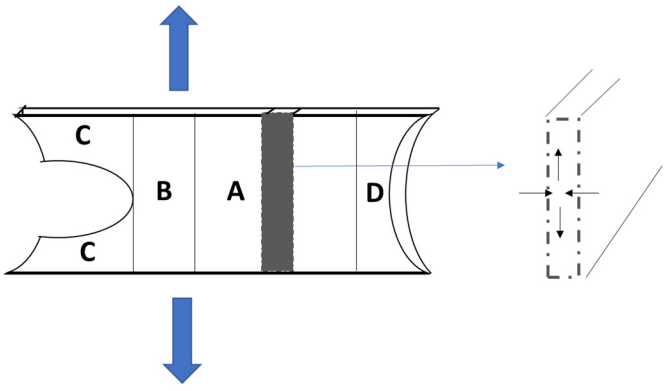

Figure 5-3 Schematic of pure shear geometry and different loaded areas according to lake and Thomas(a). Section of the pure shear sample showing the principal strain acting on the sample(b).

As reported by Thomas, in the presence of a long crack the sample can be divided in four regions as depicted in Figure 5-3:

- A is homogenously loaded in pure shear condition
- B is affected by the complex crack tip field, but according to Saint Venant's principle this area remains localized to a lateral dimension close to the sample height h_0[6].
- C is fully relaxed
- D differs from PS because of the vicinity with free edges.

When the crack advances by a small amount δc, the area B is merely translated forward, increasing the size of C at the expenses of A. Thus, the energy variation associated with crack growth is simply: $\delta U = W(\lambda) h_0 t \delta c$ where $W(\lambda)$ is the strain energy in the region A at the constant applied stretch λ, h_0 and t the height and the thickness of the unstrained sample. The energy release rate for a selected value of stretch λ is thus independent from crack length and can be calculated as:

$$G(\lambda) = -\frac{dU}{dA} = -\frac{dU}{tdc} = W(\lambda) h_0 \qquad \textbf{Equation 5-4}$$

5.2.3 Condition at the crack tip

At first glance it may be surprising that an approach that is derived from consideration far from the crack tip may be related to the local process of a propagating crack. However, the relationship between strain energy density and local conditions at the crack tip was proved by Thomas in 1955[7] who found the following equation for G closely related to the strain energy density at the crack tip.

$$G = W_t d \qquad \textbf{Equation 5-5}$$

Where W_t is a suitable averaged strain energy density at the crack tip and d is the effective crack diameter. This result was further confirmed by Andrews with direct photoelastic measurements [8] and compared with the values of G obtained using the external applied forces

Equation 5-3 showing a general good agreement . This result confirms the close relationship between G and the local strain condition at the crack tip. Additionally, because the value of G is independent of the geometry of the specimen Equation 5-5 indicates that also the crack tip diameter d should be independent of the test piece geometry.

5.3 Cyclic fatigue

When rubber components are used in applications that involve repeated loading cycles, they can undergo fatigue failure even if the level of deformation is well below the maximum extensibility of the material. Cyclic fatigue is a specific case of fracture, that involves the nucleation of microscopic flaws in regions where they were not-observable before, followed by nucleation and finally propagation of dangerous macrocracks. This form of mechanical damage is of superior importance for several applications such as tyres, damping objects, gaskets etc, and must be carefully assessed to avoid unpredictable catastrophic failure during usage.

5.3.1 Two approaches for cyclic fatigue

Fatigue life prediction is fundamentally important for engineering applications as witnessed by the great amount of work that was devoted to the subject as reviewed by Mars and Fatemi in 2002 [9] and most recently by Tee et al.[10].

There are two main approaches used to study cyclic fatigue in rubber: crack nucleation and crack growth.

The first approach is based on the detection of a spontaneous crack nucleation within a material for a specific stress/strain history. This approach considers the material's lifetime as the number of cycles requires to create a crack of a specific size. This crack nucleation method was used for the first time by Wöhler (to determine the lifetime of locomotive axles in 1860) and modified for rubber by Cadwell around 1940[11]. The control parameter used in this approach can be either strain, energy density (generally estimated from an hyperelastic function) or stress (barely used for rubber).

The second is an extension of the fracture mechanics approach developed for monotonic crack propagation[4] and explicitly considers the introduction of a macroscopic crack and evaluates its extension as function of the ability of materials to store elastic energy when deformed.

Considering that the pre-cut is typically much longer than any other defect or imperfection within the material, the fracture typically starts from the crack. This method is suitable for applications where lifetime is controlled crack growth before failure.

5.3.2 Extension of the fracture mechanics approach in cyclic fatigue

In their early works on rupture of rubbers, Rivlin and Thomas [4] established that the strain energy G required to extend a crack does depend only on the material, not on the sample shape or loading conditions. Similarly, they observed that in cyclic conditions, the crack propagation rate was mainly determined by the value of the maximum energy release rate G achieved in the cycle regardless of the specific manner to achieve it [12,13]. Therefore, the crack propagation per cycle is typically a function of the strain energy release rate and can be expressed as: $\frac{dc}{dn} = f(G)$. Where c is the crack length and n the number of cycles. In their investigation on dynamic crack growth in vulcanized rubbers, Lake and Lindley [14] identified the presence of a threshold energy G_0 below which the crack propagation was not activated by mechanical loading. They used a log-log plot to express dc/dn VS G and proposed four distinct regimes of propagating crack for rubber as follows:

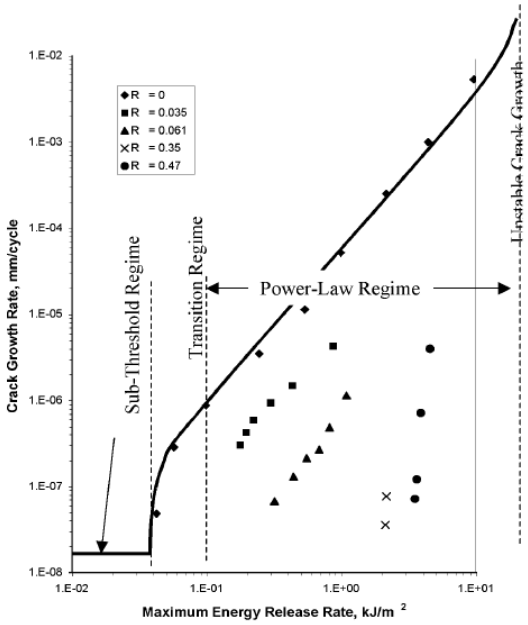

Figure 5-4 Typical regimes of crack propagation dc/dn of natural rubber. Reprinted from Mars[15]

- For values of $G < G_0$ the crack can only propagate only for external chemical attack as ozone degradation.

- Above this critical level and before the threshold energy for cyclic fatigue a transitional regime occurs and the crack increases almost linearly with applied G.

- As G achieves the fatigue threshold and $G_t<G<G_c$ the crack rate and the applied G follow a power law. Interestingly, in this regime the power exponent was found to vary between 2 and 6 for several elastomers and to depend mainly on the rubber network and to a lesser extent on specific compounding ingredients such as filler, additives and crosslinking agent.

- Finally, at highest value of $G \geq G_c$ the crack propagates catastrophically after only a few cycles. A fatigue resistant material generally possesses a high fatigue threshold and low α exponent.

The different regimes evidenced in cyclic fatigue are summarized in Table 5-1

Table 5-1 Summary of the different regimes in cyclic fatigue

Sub threshold regime	**Transition regime**	**Power law regime**	**Failure regime**
$G<G_0$	$G_0<G<G_t$	$G_t<G<G_c$	$G=G_c$
Stationary	Transition regime	Power law	Catastrophic failure
$\frac{dc}{dN} = V_0$	$\frac{dc}{dN} = A(G - G_0)$	$\frac{dc}{dN} = BG^{\alpha}$	$\frac{dc}{dN} = Vc$

5.3.3 Threshold energy G_0

From several works on fracture of vulcanised rubber, [4,16–18] carried on different sample's geometry and types of vulcanised rubbers, emerged a very similar threshold value G_0 (50-100J/m2) defining the limit below which, under repeated stresses no propagation occurs. This value was very similar for several different elastomers. The observation that G_0 was uncorrelated to the viscoelastic properties of the material and was weakly dependent on the

chemical structure of the rubber, suggested that G_0 is a property determined by the failure of the primary C-C bonds of the network. In parallel Lake and Thomas[19], proposed that, in the absence of any energy dissipation (at high temperature far from Tg or with oil swollen rubber), a value of G_0 in monotonic loading could be predicted from molecular assumptions. They proposed that, when a crack advances, only the chains lying across the fracture planes are broken and the total energy stored in each bond of the stretched strands (portion of the chain between two crosslinks) is consumed during the process (Figure 5-5). Under these assumption G_0 in monotonic loading can be estimated as follows:

$$G_0 = N_x U_b \Sigma \qquad \textbf{Equation 5-6}$$

Where N_x is the number of C-C bonds between crosslinks, U_b is the bond energy for C-C bond and S is the areal density of chains crosslink the crack plane. For an homogeneous network, S and N_x are not independent and, using the hypothesis of affine deformation it can be demonstrated that :

$$G_0 \propto \frac{\rho\, l\, U_b N^{\frac{1}{2}}}{M_0} \qquad \textbf{Equation 5-7}$$

Where r is the monomer density, M_0 the molar mass of the monomer and *l* the length of the monomer. Equation 5-7 is fundamentally important because reveals that there is a trade-off between stiffness and G_0. Its validity was demonstrated experimentally for several rubbery systems and more recently also for hydrogels[20–24].Although it was never proven experimentally for fatigue, it is generally assumed that for conventional rubbers the fatigue threshold and the monotonous loading threshold at high T are both scaling as as $G_0 \propto N^{\frac{1}{2}}$.

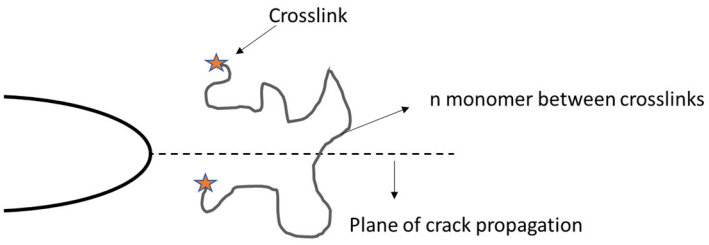

Figure 5-5 Schematic of a polymer chain crossing the fracture plane according to Lake and Thomas theory[19]

5.4 Strategy to improve fatigue resistance in soft materials

As previously described, the average fatigue threshold for a generic elastomer is between 50-100 J/m^2, considerably lower than its toughness or G_0 (10^3-10^5 J/m^2)[25]. Nevertheless, a high cyclic fatigue threshold is a fundamental property for materials such as elastomers, that are often required to be deformed several times in their lifetime. This is why several studies focused on finding solutions for improving cyclic fatigue resistance of elastomers and soft materials without changing their stiffness. Here we propose some of the most recent approaches that used induced anisotropy to increase cyclic fatigue resistance in soft materials.

5.4.1 Composite networks

In a recent work, Li et al. [25] reported a threshold energy G_0 (above 500J/m2) for a new class of composite elastomer. Their idea was to use a reinforcing net made of hard elastomer microscopically aligned in the direction parallel to the applied load. This hard structure deflects the crack and increases the threshold energy without having a significant effect on the modulus of the softer matrix. Other similar strategies have been implemented to reinforce different soft materials such as hydrogels that generally suffer from a low fatigue threshold [26,27].

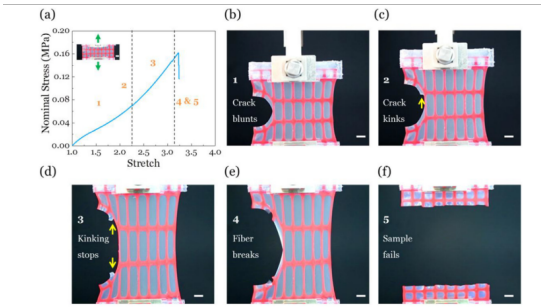

Figure 5-6 Example of composite elastomers. The crack is deflected by the hard network fibres.

5.4.2 Bio-inspired hydrogels

Load-bearing biological tissues (as skeletal muscles) are an excellent example of bio-engineering that takes advantage of aligned nanofibrils to produce an excellent combination of high fatigue resistance and strength. Lin et al.[27] produced muscle-inspired hydrogels which can be mechanically trained to increase their fatigue threshold (>1200J/m2). The mechanical training uses repeated pre-stretches of the chain to induce high density of nanocrystalline domains with aligned nanofibrillar microstructure that deflects the crack and strongly increases the fatigue threshold.

Another example of bio-inspired anti-fatigue hydrogels was produced by Li et al. [28]. In this case, the ability to stop the crack propagation is linked to the hierarchical structure of a continuous bi-phase network. The critical energy to crack propagation (G_0) is determined by the soft network at the smallest scale (10nm) but the crack advance is slowed down by the hard/soft bi-phase structure. This anti-fatigue behaviour is maintained until a critical value of $G_t > G_0$, determined by the rupture of the hard-phase network at larger scale, when the crack will propagate rapidly.

5.5 Concluding remarks

To conclude, the reinforcing mechanisms of soft crosslinked networks have been studied in depth in the past years and different strategies have been proposed to improve their fatigue resistance. Nevertheless, this field of research is relatively new and is still confined to the lab-scale. Therefore, an accessible and implementable engineering alternative to classical reinforced rubbers to improve fatigue threshold is still missing. Within the field of soft materials, the family of TPU has demonstrated a very high strength and toughness even in their

unfilled state [29,30]. The possibility for TPU to achieve a high toughness in their unfilled state coupled with a peculiar multi-phase structure, ignited a scientific interest towards the possible use of TPU in cyclic applications. Soft TPU in fact, can be produced with low modulus >10MPa very comparable to conventional filled rubbers and possess a multi-phase architecture with a strain-induced aligned morphology that recalls some characteristics of the reinforcing strategy implemented in muscle-like hydrogel and seems to be promising for cyclic application. Nevertheless, to fully exploit the nature of cyclic resistance of TPU a better understanding of the effect of cyclic deformation of TPU multi-phase structure is necessary.

5.6 References

1. Inglis CE. Stresses in a plate due to the presence of cracks and sharp corners. *Trans R Titute Nav Arch*. 1913;60:219-241.

2. Creton C, Ciccotti M. Fracture and adhesion of soft materials: a review. *Reports Prog Phys*. 2016;79(4):046601. doi:10.1088/0034-4885/79/4/046601

3. Hui CY, Jagota A, Bennison SJ, Londono JD. Crack blunting and the strength of soft elastic solids. *Proc R Soc A Math Phys Eng Sci*. 2003;459(2034):1489-1516. doi:10.1098/rspa.2002.1057

4. Rivlin RS, Thomas AG. Rupture of rubber. I. Characteristic energy for tearing. *J Polym Sci*. 1953;10(3):291-318. doi:10.1002/pol.1953.120100303

5. Lake GJ. Fracture mechanics and its application to failure in rubber articles. *Rubber Chem Technol*. 2003;76(3):567-591. doi:10.5254/1.3547761

6. Yeoh OH. Analysis of deformation and fracture of "pure shear" rubber testpiece. *Plast Rubber Compos Process Appl*. 2001;30(8):389-397. doi:10.1179/146580101101541787

7. Thomas a. G. Rupture of rubber. II. The strain concentration at an incision. *J Polym Sci*. 1955;18(88):177-188. doi:10.1002/pol.1955.120188802

8. Andrews EH. Stresses at a crack in an elastomer. *Proc Phys Soc*. 1961;77(2):483-498. doi:10.1088/0370-1328/77/2/333

9. Mars W, Fatemi a. A literature survey on fatigue analysis approaches for rubber. *Int J Fatigue*. 2002;24(9):949-961. doi:10.1016/S0142-1123(02)00008-7

10. Tee YL, Loo MS, Andriyana A. Recent advances on fatigue of rubber after the literature survey by Mars and Fatemi in 2002 and 2004. *Int J Fatigue*. 2018;110:115-129. doi:10.1016/j.ijfatigue.2018.01.007

11. Cadwell SM, Merrill RA, Sloman CM, Yost FL. Dynamic Fatigue Life of Rubber. *Ind Eng Chem - Anal Ed*. 1940;12(1):19-23. doi:10.1021/ac50141a006

12. Gent AN, Lindley PB, Thomas AG. Cut growth and fatigue of rubbers. I. The relationship between cut growth and fatigue. *J Appl Polym Sci*. 1964;8(1):455-466. doi:10.1002/app.1964.070080129

13. Thomas a. G. Rupture of Rubber V Cut Growth in Natural Rubber Vulcanizates. *Rubber Chem Technol*. 1958;32(2):477-489. doi:10.5254/1.3542412

14. Lake GJ, Lindley PB. Mechanical Fatigue Limit for Rubber. *J Appl Polym Sci*. 1965;9:1233-1251. doi:10.5254/1.3544847

15. Mars, W. V., Fatemi A. Factors That Affect the Fatigue Life of Rubber. *History*. 2004;77(3):419-423. doi:10.5254/1.3547831

16. Greensmith HW, Thomas AG. Rupture of rubber. III. Determination of tear properties. *J Polym Sci*. 1955;18(88):189-200. doi:10.1002/pol.1955.120188803

17. Thomas AG. Rupture of rubber. VI. Further experiments on the tear criterion. *J Appl Polym Sci*. 1960;3(8):168-174. doi:10.1002/app.1960.070030805

18. Gent , A.N., Thomas AG. forms for the stored energy function for vulcanized rubber. 1957;(3):1-4.

19. Lake GJ, Thomas AG. The Strength of Highly Elastic Materials. *Proc R Soc A Math Phys Eng Sci*. 1967;300(1460):108-119. doi:10.1098/rspa.1967.0160

20. Bhowmick AK. Threshold Fracture of Elastomers. *J Macromol Sci Part C*. 1988;28(3-4):339-370. doi:10.1080/15583728808085379

21. Bhowmick A, Gent AN, Pulford CTR. Tear Strength of Elastomers Under Threshold Conditions. *Rubber Chem Technol*. 1983;56(1):226-232. doi:10.5254/1.3538115

22. Mazich KA, Samus MA, Smith CA, Rossi G. Threshold Fracture of Lightly Cross-Linked Networks. *Macromolecules*. 1991;24(10):2766-2769. doi:10.1021/ma00010a020

23. Ahagon A, Gent AN. Threshold fracture energies for elastomers. *J Polym Sci Polym Phys Ed*. 1975;13(10):1903-1911. doi:10.1002/pol.1975.180131005

24. Akagi Y, Sakurai H, Gong JP, Chung U Il, Sakai T. Fracture energy of polymer gels with controlled network structures. *J Chem Phys*. 2013;139(14):1-7. doi:10.1063/1.4823834

25. Li C, Yang H, Suo Z, Tang J. Fatigue-Resistant elastomers. *J Mech Phys Solids*. 2020;134:1-12. doi:10.1016/j.jmps.2019.103751

26. Lin S, Liu X, Liu J, et al. Anti-fatigue-fracture hydrogels. 2019;(MARCH):1-10.

27. Lin S, Liu J, Liu X, Zhao X. Muscle-like fatigue-resistant hydrogels by mechanical training. *Proc Natl Acad Sci U S A*. 2019;116(21):10244-10249. doi:10.1073/pnas.1903019116

28. Li X, Cui K, Lin T, et al. Mesoscale bicontinuous networks in self-healing hydrogels delay fatigue fracture. 2020;117(14). doi:10.1073/pnas.2000189117

29. Yi J, Boyce MC, Lee GF, Balizer E. Large deformation rate-dependent stress-strain behavior of polyurea and polyurethanes. *Polymer (Guildf)*. 2006;47(1):319-329. doi:10.1016/j.polymer.2005.10.107

30. Qi HJ, Boyce MC. Stress-strain behavior of thermoplastic polyurethanes. *Mech Mater*. 2005;37(8):817-839. doi:10.1016/j.mechmat.2004.08.001

Part II

Experimental Section

Important note:

Each chapter is presented in the form of finished scientific paper: title, authors and affiliation, abstract and body of paper. Nevertheless, the articles are still under improvement and some changes are likely to be done before the official submission of the papers.

6 CYCLIC FATIGUE IN SBR: THE ROLE OF CRACK TIP

Characterization of the tip of a crack during propagation under cyclic fatigue in Styrene-Butadiene Rubber.

Giorgia Scetta[1], Matteo Ciccotti[1] and Costantino Creton[1*]*

[1]Sciences et Ingénierie de la Matière Molle, ESPCI Paris, Université PSL, CNRS, Sorbonne Université, 75005, Paris, France.

matteo.ciccotti@espci.psl.eu, Costantino.creton@espci.psl.eu

6.1 Abstract

We characterized the highly strained region developed at the crack tip during cyclic fatigue of three different carbon-black (CB) filled SBRs with the aim to discuss the different effect of filler content and crosslinking density. Using an infrared camera, we demonstrated that the presence of filler mainly controls the temperature rise in the bulk while, the crosslinking density controls the extent of strain concentration at the crack tip. Additionally, optical imaging reveals that the addition of CB contributes to strongly modify the crack shape (from blunted to sharp) and the fracture surfaces from chaotic and delocalized front (composed by thick fibrils) to localized and thin fibrillar crack front in highly filled SBR only visible at the microscopic scale. Surprisingly, similar observations are valid both in monotonic and cyclic fracture. Using the results of the present work, we completed the information of our previous article and we propose a better defined interpretation of the fracture mechanisms acting at the local scale.

6.2 Introduction

Carbon black filled elastomers based on natural rubber or styrene-butadiene rubber are well known for their reversible elasticity and remarkable toughness. They can be reversibly deformed several times without visible permanent damage up to relatively large strains. Nevertheless, when such elastomers are cyclically loaded over hundreds of thousands of cycles, they can still fail at strain values much lower than their maximum extensibility often due to the propagation of pre-existent cracks [1]. Such a crack propagation process under low amplitude cyclic loading, named cyclic fatigue, has been extensively characterized in the literature for a variety of elastomers and macroscopic loading conditions [2–9]. Nevertheless, the relationship

between cyclic fracture resistance in elastomers and their composition and molecular structure is still a highly empirical endeavor. A common misconception concerning the fatigue resistance of elastomers is that, increasing the level of dissipation in the material upon deformation will necessarily reduce crack propagation velocity in fatigue. This notion, that has been clearly validated in monotonic condition [10–12], is mainly related to the tendency of neglecting the small scale damage mechanisms present at the crack tip such as localized hysteresis, large strain deformation and finally bond breakages. This has been recently point out in a review on fatigue of hydrogels[13]. Resistance to crack propagation in fatigue is commonly characterized in terms of crack propagation per cycle (dc/dn) as function of applied energy release rate (G). Generally, the crack propagation rate, in relevant fatigue conditions, is of the order of a few nm/cycle, meaning that most of the energy input during each loading/unloading cycle is either dissipated by heat or reversibly released back to the system during the unloading of the sample, while only a small fraction contributes effectively to the breakage of bonds leading to crack propagation. In order to better understand the problem of cyclic fatigue some authors concentrated on the smaller microscopic scale using different techniques. A significant body of work has been done in particular for natural rubber that presents the interesting ability to crystallize under strain [14–17]. On the other hand, much less has been done for non-crystallizing elastomers such as filled SBR [18–20]. In our previous paper [5], we used digital image correlation to explore the microscopic area around the tip of a fatigue crack for filled SBR elastomers revealing directly, for the first time, the existence of a steady-state process zone in front of the crack, where the elastomer is highly stretched. At the same maximum stretch λ_{max}, applied to pure shear samples, the local steady-state strain-field was quite different for different elastomers and mainly controlled by the material composition. We evaluated a local energetic parameter g_{loc} representing the only fraction of the overall released elastic energy that reaches the crack tip (net of dissipation). Remarkably, all the data of crack propagation rate dc/dn as function of g_{loc} of four different SBR based materials collapsed on a single master-curve, while their crack propagation velocity differed by more than two orders magnitude if plotted as a function of the applied macroscopic G. We concluded that, the fatigue behavior in filled SBR was only controlled by the local condition at the crack tip while the relationship between the macroscopic energy input (G) and that locally available g_{loc} was mainly determined by the crosslinking density and, to a lesser extent by the filler content .

This paper aims to complete the work of Mzabi et al.[5] explaining more in detail the role played by filler and crosslinking density in controlling different aspects of cyclic fatigue behavior in

filled elastomers. We divided this work into three parts. The first part is dedicated to mechanical properties and fatigue resistance of selected SBRs. In the second part, we present thermal measurements on notched and un-notched samples and investigate the effect of composition on the occurrence of a temperature gradient between the crack tip region and the bulk. The last part focuses on the optical imaging of the crack shape and surface morphology under monotonous and dynamic loading conditions at different magnifications.

6.3 Materials and Methods

We investigated three non-crystallizing random copolymers of styrene and butadiene (SBR) with different fractions of carbon black (CB) and crosslinking densities [21]as indicated in Table 6-1 . The uncrosslinked SBR used has a weight M_n of 120 kg/mol and a polydispersity of 1.94. Its styrene content is 15 wt % and the glass transition temperature measured by differential scanning calorimetry (DSC) is T_g =-48°. Two of the SBR are representative of what is used in classical tyre applications, but the third one containing only 5 phr (or ϕ = 0.03) of CB (3CB_8XL) has essentially the properties of an unfilled SBR and will be often referred as "unfilled" in the following.

All samples were prepared molded and cured by Michelin. For tensile tests, samples were cut with dog-bone shape and cross section of 2x4mm. For crack propagation experiments we used samples with the "pure shear" geometry (PS) that is commonly used to study fatigue in elastomers [22]. The sample dimensions are: length l_o = 157 mm, height h_0 = 13 mm and thickness t_0 = 2 mm. The crack propagation rate is expressed as crack propagation per cycle (dc/dn) as a function of the the maximum applied energy release rate G_{max}. Each value of G_{max} is evaluated using Equation 6-1 as proposed by Rivlin [23]. $W_{PS}(\lambda)$ is conventionally defined as the integral under the loading curve from λ_{min}=1 to λ for an identical PS sample without notch previously strained for 1000 cycles at λ_{pre}=3.7 higher than those used during fatigue test. This pre-conditioning is used to avoid Mullin's effect that generally lasts for a number of cycles in filled rubber[24].

$$G_{max}=W_{PS}(\lambda)h_{0PS} \qquad \textbf{Equation 6-1}$$

All the fatigue fracture tests were carried out using the same cycling frequency of 10 Hz. Two edge cracks and one center crack were cut with a fresh razor blade. Each pre-conditioned

sample was cycled between $\lambda = 1$ and the maximum stretch λ corresponding to the desired value of G_{max}. The sample was illuminated with a cold source in order to avoid extrinsic heating and imaged at regular time intervals with a digital camera. The crack length *c(n)* at the n^{th} cycle was measured by identifying the most advanced point of the crack cavity in the open configuration. After a poorly reproducible transitory that typically lasted less than 5.000 cycles, the crack propagation per cycle (dc/dn) achieved a stable steady-state regime.

Table 6-1 Chemical composition in Phr. Filler content and crosslinking density are reported in volumetric fraction. Data from[21]. Note that N347 is a type of carbon black, Sulfur is a crosslinking agent, Struktol™ and N-Cyclohexyl-2-benzothiazole sulfenamide (CBS) are accelerators to vulcanize the rubber, and N-(1,3-dimethylbutyl)-N'-phenyl-p-phenylenediamine (6PPD) is an anti-oxidant.

	3CB_8XL	**20CB_8XL**	**20CB_19XL**
SBR	100	100	100
N347	5	50	50
6PPD	1	1	1
Struktol	3	3	3
CBS	1.5	1.5	1.5
Sulfur	1.5	1.5	3
ϕ	0.03	0.2	0.2
ν	8.1*10-5	7.1*10-5	19*10-5

The surface temperature was imaged during cyclic fatigue experiments for all samples using an IR camera (CEDIP JADE MWIR InSb) with a resolution of 320x256 pixels, a sensitivity of 20 mK and a spectral band ranging from 3 to 5.1 μμ. The acquisition frequency was set between 25Hz and 100Hz.

To explore the morphology of the crack front region within the crack cavity, a second set of optical images were taken with a high-speed camera fixed on a tripod. The camera resolution

was 0.31 Megapixel. The objective allowed a field of view of 2 mm and focus distance of 10 mm. Two sets of pictures were taken during static and cyclic fatigue experiments. For static tests, the sample was notched and slowly strained up to the threshold value of ε (specific of each material) that allows slow crack propagation in order to expose fresh crack surfaces. The displacement was then kept constant leaving the sample under stress relaxation and slow crack propagation conditions. For cyclic fatigue pictures we used the procedure detailed above, but we pivoted the sample's clamps so that the crack front could face the camera. The crack front region was also imaged by scanning electron microscopy (SEM Hitachi 3600) in crack propagation conditions. The presence of carbon black allowed a good resolution without any metallization. The SEM chamber was equipped with a DEBEN (Microtest, Woolpit, UK) micro tensile machine. The sample was vertically mounted allowing the primary electron beam to scan the propagating crack surface while the sample was strained under constant applied displacement.

6.4 Results

6.4.1 Uniaxial tensile tests

The uniaxial stress-strain curves of the three materials are reported in Figure 6-1. Both filled SBRs (20CB) are stiffer than 3CB_8XL and increasing crosslinking density in 20CB_19XL results in a reduction of the maximum extensibility.

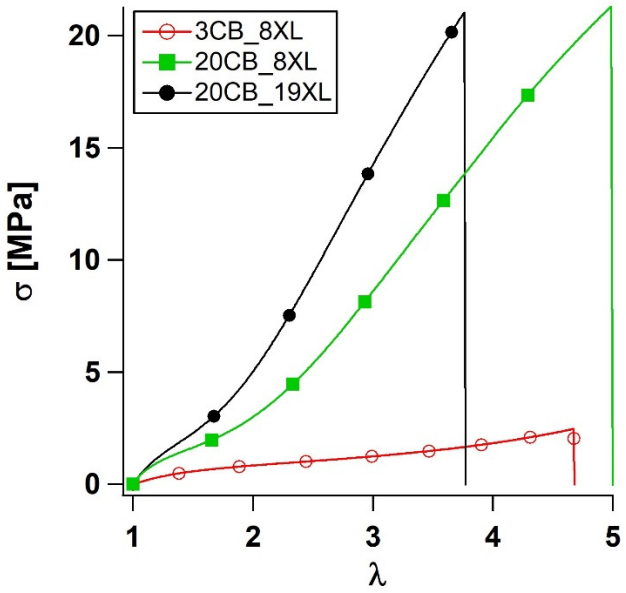

Figure 6-1 Nominal stress-strain curves in uniaxial tension of the three materials. Data from Mzabi(Mzabi, 2010)

It is well known that the presence of filler, while stiffening the matrix, induces additional mechanical dissipation generating a larger hysteresis loop than the unfilled matrix. Figure 6-2 (a) reports the loading-unloading curves in a step-cycling test done in uniaxial extension for all three samples. The unfilled SBR 3CB_8XL has a predominantly elastic character with very low or negligible energy dissipation. Both filled SBRs display a typical Mullin's effect [24,25] and the energy dissipated in the first cycle is considerably higher than in all the following ones. Figure 6-2 (b) reports the energy dissipated in the second cycle vs. applied maximum stretch. We remark that the dissipated energy in the second cycle is a good approximation of the asymptotic regime.

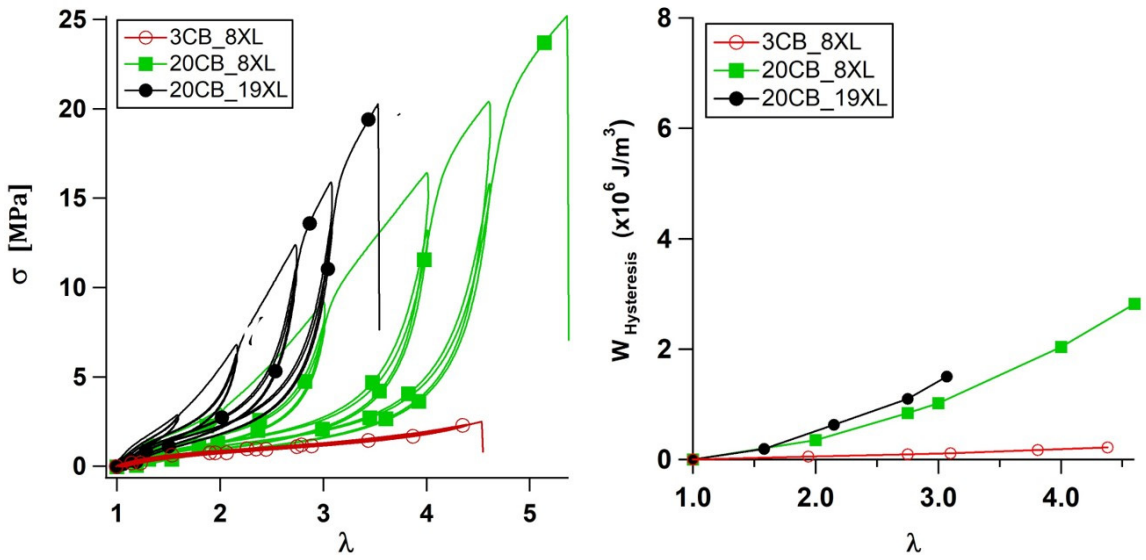

Figure 6-2 Cyclic stress strain curve for the three materials (a) Values of energy dissipated in the second cycle (b). Data from Mzabi[21]

6.5 Cyclic fatigue tests

Figure 6-3 reports the values of the crack propagation rate (dc/dn) as function of the applied $\mathcal{G}$ for all tested materials. As reported in the literature [1], for several different elastomers the value of dc/dn increases with the power of $\mathcal{G}$. For the same applied $\mathcal{G}$, the unfilled 3CB_8XL is the least resistant to crack propagation (higher dc/dn). For the two filled materials reducing the crosslink density leads to a significantly lower crack propagation rate.

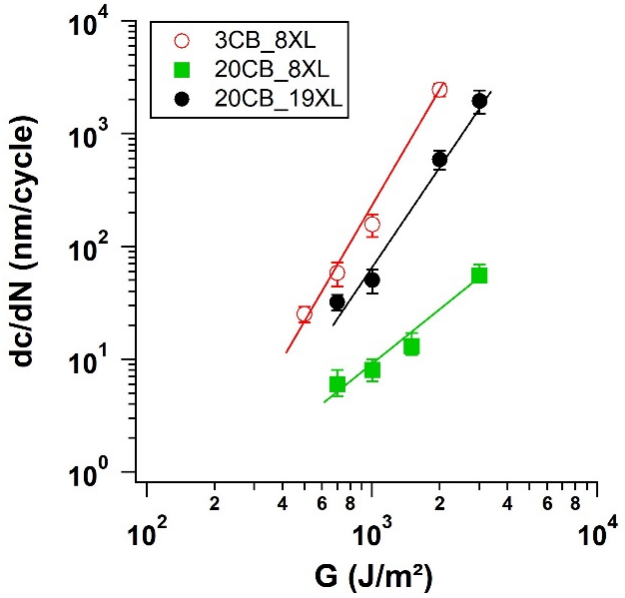

Figure 6-3 Crack propagation rate dc/dn as function of $\mathcal{G}$ for all tested materials. Data from Mzabi [21]

6.5.1 Heat generation

During cyclic loading, several hysteretical phenomena such as internal friction at the monomer level and network rearrangements can lead to a temperature rise due to the low thermal conductivity of the rubber. Using the IR camera, we mapped the evolution of the surface temperature during cycles for notched and un-notched PS samples (the same as that used for fatigue experiments). The data were collected after a short transient lasting some hundreds of cycles during which surface temperature stabilizes to a steady-state. In all un-notched samples, the maximum temperature (T_{max}) is achieved in the center and symmetrically decreases when moving towards the edges of the sample as shown in Figure 6-4(a). Notched samples mainly differ for the occurrence of a hotter area close to the crack tip (Figure 6-4(b)) with a higher local maximum temperature T_{CT}, while the temperature T_{bulk}, evaluated in the middle line far from the crack, is comparable with the maximum value T_{max} found for un-notched samples at the same value of stretch.

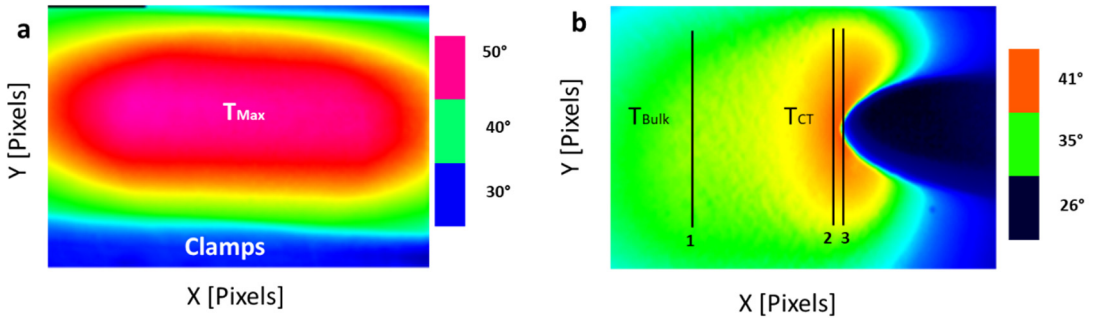

Figure 6-4 Example of temperature map for the un-notched 20CB_8XL strained at λ= 1.28% (a) and the notched 20CB_19XL strained at λ=1.23. Data from Mzabi [21]

Since T_{bulk} and T_{max} can be considered the same, in Figure 6-5(a) we report only the values of T_{max} , plotted as function of applied strain for all un-notched samples. As expected, T_{max} increases with applied strain for all materials and, at the same value of λ, the increase in temperature is governed by the filler content. Surprisingly, if we plot the same data of T_{max} as function of $\mathcal{G}$ (instead of λ) all points tend to collapse on a single curve as shown in Figure 6-5(b). The latter indicates that, regardless of the maximum applied strain, at iso-$\mathcal{G}$ the combination of heat produced and diffused leads all materials to achieve approximately the same surface temperature in the steady-state far from the notch localization. One should be careful however, since the measured temperature is a balance between heat generated and thermal conductivity. Introducing filler does increase the heat generation, but also the thermal conductivity.

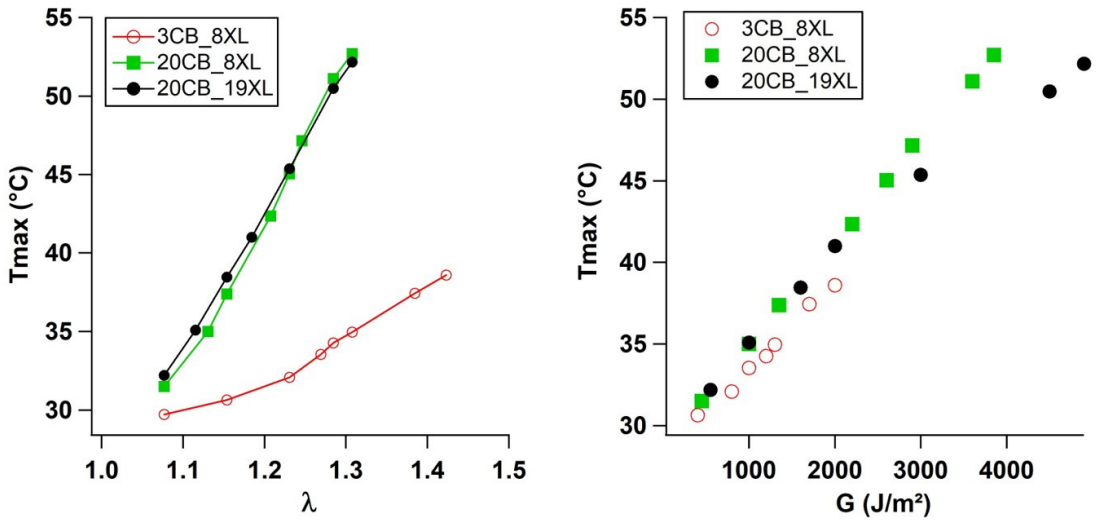

Figure 6-5 Maximum value of surface temperature as function of applied deformation (a) and energy release rate $\mathcal{G}$ (b). Data from Mzabi [21]

The enhanced temperature rise at the crack tip with respect to the bulk in steady-state conditions is expressed as $\Delta T = T_{CT} - T_{max}$ and is reported in Figure 6-6 as function of the applied strain. When deformed less than λ=1.25, all materials present a negligible temperature difference ($\Delta T \approx 0°C$) between crack tip and bulk. On the other hand, for higher values of maximum strain, all samples show a $\Delta T > 0$. The temperature difference between crack tip and bulk is related to the higher deformation experienced in the crack tip region [5] as will be discussed in the following section.

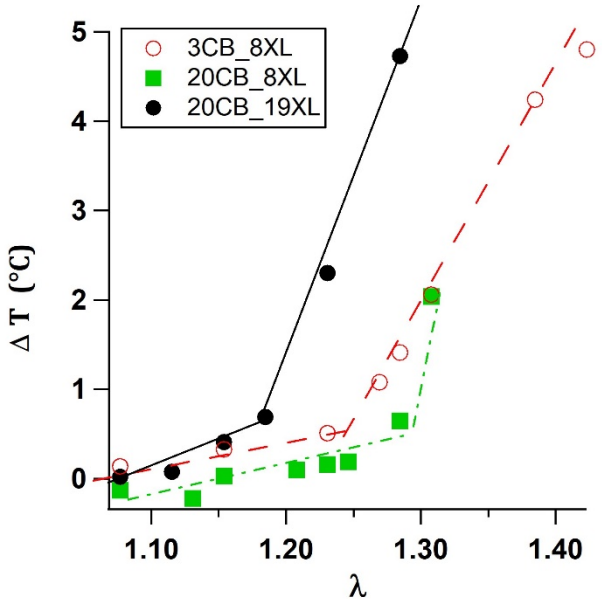

Figure 6-6 Temperature difference between bulk and crack tip (ΔT) as function of applied strain. Data from Mzabi [21]

The maximum ΔT is around 5 °C but, for the same class of materials, the maximum strain near the crack tip was found to be between 10 and 14 times higher than far from the crack[5]. However, the instantaneous temperature increase in the first cycles (before the achievement of steady state) reported in Figure 6-7, shows that the surface temperature increases faster at the crack tip than in the bulk as visible in Movie_1. This suggests that the source of heat generation is initially larger at the crack tip and eventually leads to similar value of surface temperature after stabilization.

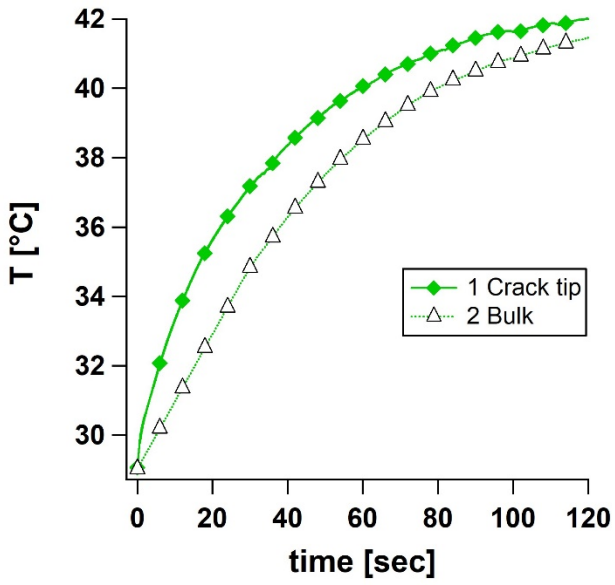

Figure 6-7 Surface temperature measured at the beginning of the first load. Close (1) and far away (2) from the crack for the sample 20CB_8Xl at λ= 1.23.

6.6 Multi-scale crack tip observation

During cyclic experiments, we observed that the shape of the crack tip for the unfilled SBR was much more blunted (less pointy) compared to filled samples as qualitatively visible in Figure 6-8*(a)*. To quantify the difference in shape between all materials, we performed a parabolic fitting on the profile of all fatigued samples. The resulting crack radius, reported in Figure 6-8*(b),* confirms the more highly blunted profile for 3CB_8XL for all value of λ adopted in cyclic fatigue experiment.

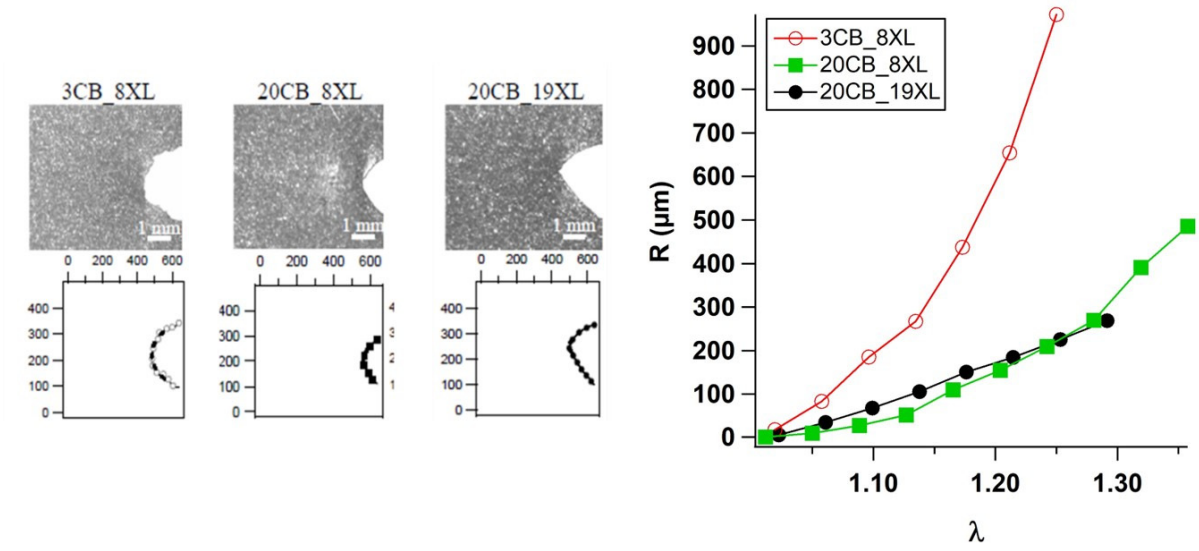

Figure 6-8 Example of open crack profile during a fatigue experiment for all SBR at λ_{max}=1.27 (a). Fitted crack radius VS λ for al SBR in cyclic fatigue experiment (b).

In order to further confirm that the major differences in crack profile are mostly governed by the presence of filler, we investigated the morphology of the crack front surfaces by moving the camera in front of the crack (instead of its side). This point of view also had the advantage to reveal a pronounced 3D structure of the crack, that is best appreciable in the movies in the supplementary material(Movie_2 and Movie_3). Using this camera configuration, we took high resolution images of the crack tip under both static (monotonic load up to the onset of crack propagation) and dynamic loading conditions as shown in Figure 6-9(a-b) for 3CB_8XL. Interestingly, while the applied strain required to propagate the crack in monotonic loading conditions is considerably higher than that used in cyclic fatigue, both images of the fibrillar structure look quite similar. This indicates that the morphology developed at the crack front is the same whether the crack propagates at fixed strain or in cyclic dynamic conditions. The only difference is the time spent by the material at single values of deformation and thus the applied deformation required to propagate the fracture. Furthermore, the images taken during crack propagation from this point of view confirmed obvious differences between the crack surface of the weakly filled 3CB_8XL and the other two highly filled SBR irrespectively of the crosslinking density. The 3CB_8XL presents a very chaotic aspect of the fracture front with elongated rubber strands extremely strained over a region larger than 500-700µm. From the supplementary movie (Movie_2) we can also appreciate that these rubber strands break in

a highly delocalized fracture area of ≈200µm. The chaotic scenario is completely in contrast with the more localized and well-defined crack surface for both filled SBR Figure 6-9(c-d).

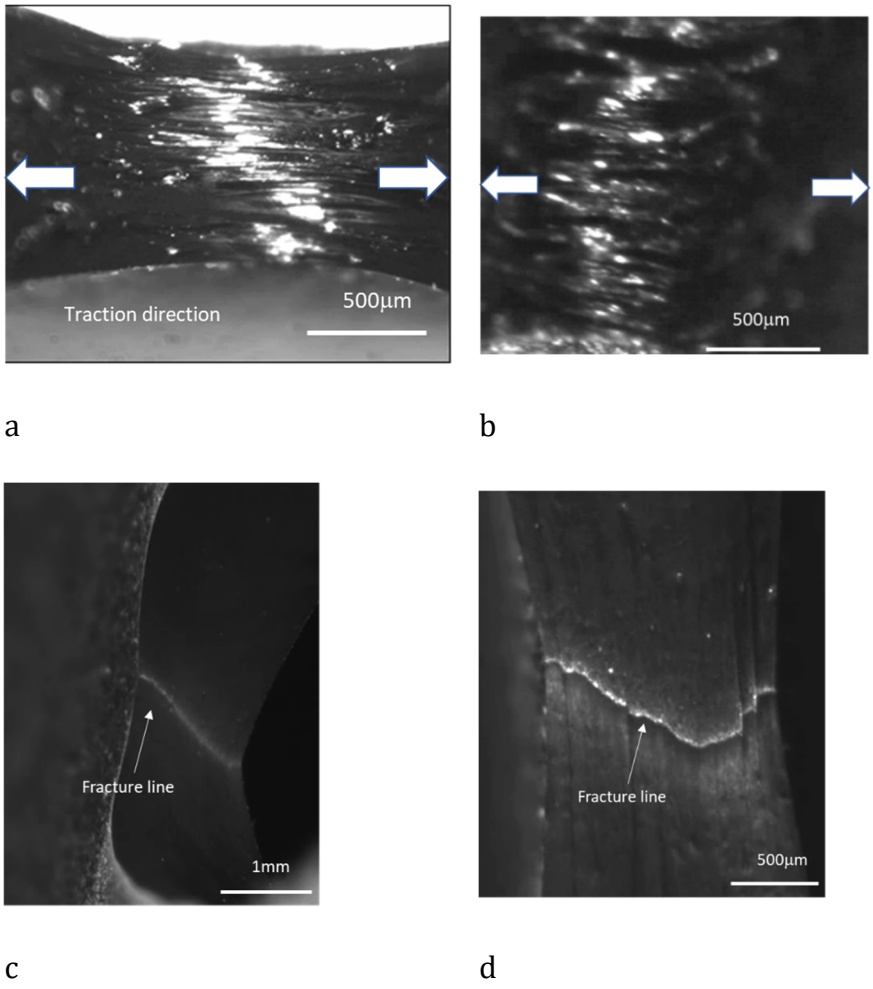

Figure 6-9 Optical images of crack front for the sample 3CB_8XL strained at λ =1.18 in cyclic (a) and at λ=1.67 in static (b) conditions. 20CB_19XL at λ= 1.30 (c) and 20CB_8XL at λ =1.80 in static conditions.

Intrigued by these differences, we decided to perform a microscopic investigation (SEM) to further investigate the difference between unfilled and filled SBR. Since no differences were observed in optical images between cyclic and static loading, we performed SEM observations on notched samples with a crack propagating under static conditions. The pre-notched samples were stretched allowing the crack to slowly propagate, in order to expose fresh cracked surfaces, and then the displacement was kept constant. At this magnification the sole significative difference in crack surface is again between unfilled and filled SBR as visible in

Figure 6-10(a-b) confirming the chaotic VS highly localized front for 3CB_ 8XL and 20CB 8XL and 19XL. In both filled SBR, we additionally found out that the crack front line, as identified from the optical images, actually consists in several thin fibrils with an average diameter of 2-5µm Figure 6-10(c-d). Table 2 presents a summary of the main features of the fracture surfaces for unfilled and filled SBRs obtained by optical imaging. The fracture zone, corresponds to the area where breaking of fibrils take place as highlighted in Figure 6-10 .

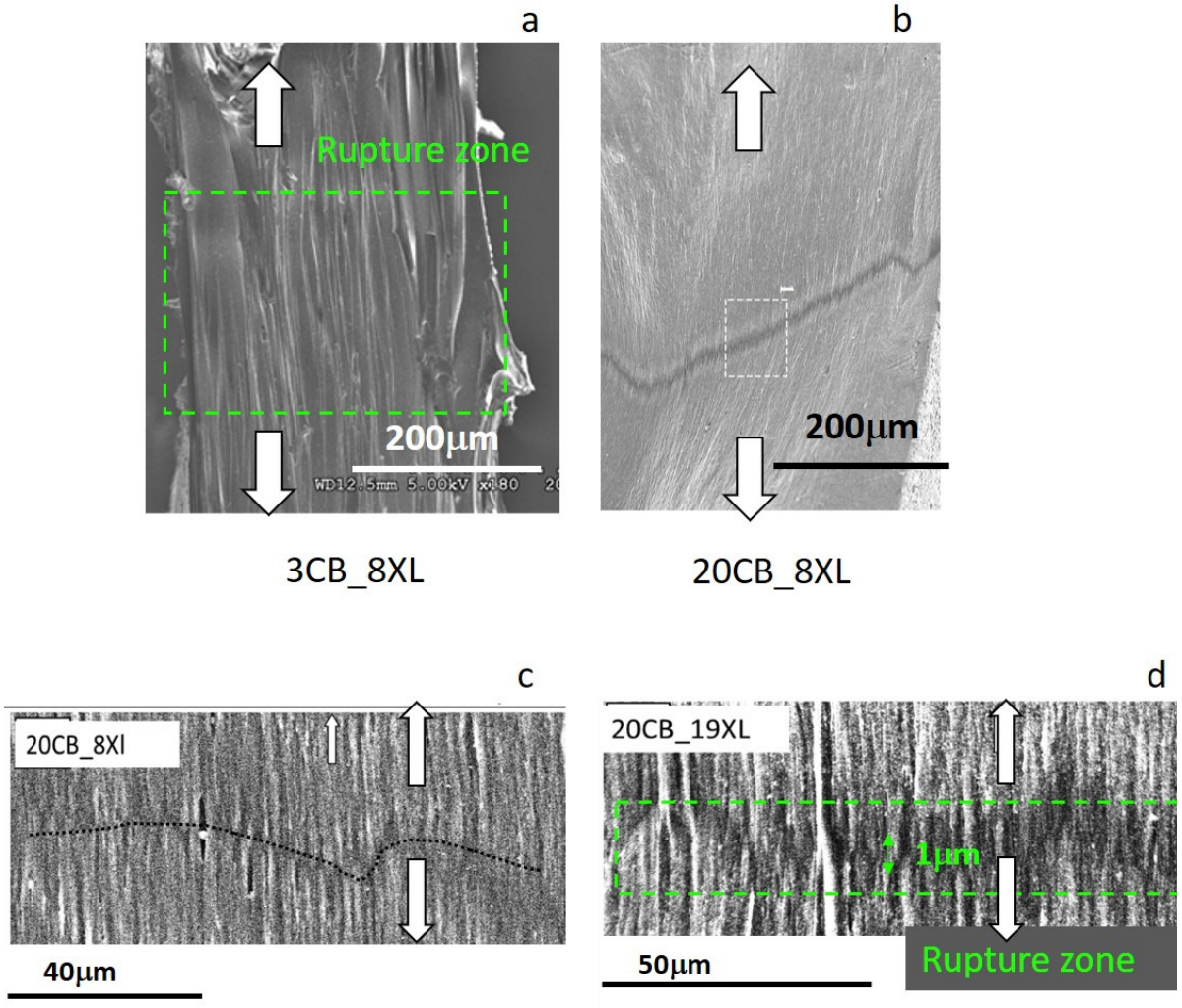

Figure 6-10 SEM images of the crack front for 3CB_8XL at λ =1.67, and 20CB_8XL at λ =2.33. The white rectangle indicated the are magnified in picture c) for 20CB_8XL and d) 20CB_19XL . Arrows indicate the traction direction.

Table 6-2 Overview of the principal characteristic dimensions of the fibrilla region observed near the crack tip as a function of the filler content.

Sample	**20CB (both)**	**3CB**
Rupture zone	<1 μm	≈200 μm
Fibril diameter	2-5 μm	10-15 μm

6.7 Extended Discussion

The characterization of the crack tip in fatigued sample was divided in two main parts: thermal analysis and optical imaging.

Monitoring the surface temperature in the bulk and at the crack tip in steady-state conditions we demonstrate that the increase in surface temperature is mainly driven by two factors: filler-induced dissipation and local level of strain. In particular, we showed that the surface temperature is higher for both highly filled SBR but the more crosslinked 20CB_19XL has the highest ΔT (Figure 6-6). This can be explained considering that, increasing the crosslinking density does not affect the amount of dissipation at fixed λ, as shown in Figure 6-5(a), but does increase the local strain field established in steady state at the crack tip (λ_{max}) generating different ΔT for the same macroscopic λ in SBR with same filler content.

We also pointed out that, despite the high value of local strain present at the crack tip, the maximum increase in ΔT relative to the bulk value is surprisingly low. Such a small increase in crack tip temperature can be explained considering that our measurements were taken under non-adiabatic conditions. The value of surface temperature is then the result of complex phenomena of heat diffusion including conduction due to the temperature gradient and convection of the surrounding air. In 2D, the heat diffusion takes the form:

$$\frac{dT}{dt} - D_0 \Delta T = \frac{S}{\rho C} \qquad \textbf{Equation 6-2}$$

where D_0 is the thermal diffusivity, ρ the density, C the specific heat and S the heat source produced by the material. The right term has the dimension of °C/sec. In the case of a strong strain localization, as for a loaded crack tip, the heat source is not homogeneous and, as demonstrated by Martinez et. al [26], the main part of the generated heat at the crack tip is transferred by diffusion through the sample justifying the relatively low temperature rise at the crack tip. A detailed analysis of the heat source at the crack tip is beyond the scope of this study but the faster temperature increase at the crack tip before the achievement of steady (Figure 6-7) state confirms the higher thermal activity at the crack tip even for negligible ΔT.

By performing comprehensive optical imaging analysis of both the lateral and the frontal view of the crack tip and different magnifications, we revealed that the filler strongly modifies the crack front while doubling the crosslinking density does not have any visible effect. For the unfilled 3CB_8XL the images of a very chaotic crack front, composed of thick fibrils breaking very randomly and independently in a delocalised way, contrast with the well-defined fracture front, composed by thinner fibrils (only visible at the SEM microscopic scale) in both filled SBR. This different picture can be explained by considering that the addition of filler particles suppresses the instability at a larger scale, that is responsible for the generation of thick rubber strands in 3CB_8XL. This hypothesis is supported by the work of Zhang et al. [20,27] who used a highly collimated X-ray beam to investigate the structure of the region near the crack tip of different SBR. They detected nano-cavities with average dimensions between 20-40 nm, only at the crack-tip of filled samples previously fatigued. Such kind of nanocavities weren't detectable in unfilled elastomers.

These results are in line with the idea already discussed in our previous work [5], that in cyclic fatigue the effect of dissipation is not the predominant one but other effects including strain localization and delocalization of the fracture area should be considered. In particular, the lower crack propagation rates per cycle, demonstrated by the less crosslinked SBR at the same filler content, must be related to a lower probability of chain breakage in this material. We previously found [5] that the less crosslinked SBR presents both a lower level of local strain λ_{max} at the crack tip and less elastic energy available at the crack tip (g_{loc}) for the same value of applied $\mathcal{G}$. Furthermore, reducing the crosslink density, while decreasing the stiffness of the rubber, also increases the maximum chain extensibility, that determines the maximum strain at which the polymeric chains can be stretched before breaking (λ_{lim}). All these three parameters: the maximum deformation at the crack tip, the chain extensibility and the local energy release

rate, play a specific role in determining the probability that the crack will propagate for a certain value of applied $\mathcal{G}$ and when it does, at which dc/dn the fracture will move. Each parameter depends on the material composition and or on the external loading conditions as follow:

- λ_{lim}: the distribution of maximum chain extensibility depends on to the crosslinking density and network homogeneity. This is a characteristic of the polymer network chemistry and it does not depend on the applied strain.
- λ_{max}: the maximum strain achieved at the crack tip, depends on both the specific ability of the material to reduce strain concentration at the crack tip (that will probably depend on different factors including non-linear viscoelastic dissipation) and on the maximum applied strain. Figure 6-11(a) reports λ_{max} (at ~30-50μm from the crack tip) as a function of the macroscopic applied stretch as evaluated by DIC. It shows that for the same value of applied macroscopic stretch λ, the unfilled SBR achieves the highest value of λ_{max} while among the filled samples the less crosslinked has the lowest λ_{max}. This observation suggests that λ_{max} depends on both the filler content and crosslinking density.
- g_{loc}: the energy per unit area consumed during the crack propagation (evaluated on the basis of the maximum strain achieved at the crack tip λ_{max}) mainly depends on the network architecture, as predicted by the original Lake and Thomas approach for monotonic fracture[28], rather than on the specific composition as suggested by the existence of a master curve of dc/dn vs. g_{loc} for different SBRs found by Mzabi et al.[5]. It is worth to note that, in the original calculation of g_{loc} we neglected the role of the increased temperature at the crack tip, that is different between all samples (Figure 6-6) . g_{loc} in fact, was calculated using the cyclic stress-strain curve that simulates the maximum strain experienced at the crack tip at 23°. In a more accurate evaluation, this calculation should be refined by using the material behavior at the evaluated T_{CT} to account for the effective viscoelastic contribution.

The probability for crack propagation could be expressed thus as a function of the difference $\Delta\lambda = \lambda_{lim} - \lambda_{max}$. The smaller the value of $\Delta\lambda$ and the higher is the probability that chains are broken during each loading up to a specific applied $\mathcal{G}_{max}$, resulting in an increased value of dc/dn.

This concept is expressed in Figure 6-11 (b) that represents dc/dn VS λ_{max} for all three materials. Regardless of the applied macroscopic strain, for the same value of λ_{max} the unfilled and weakly crosslinked SBR has the lower dc/dn, followed by the filled but weakly crosslinked 20CB_8XL. This ranking can be rationalized by differences in λ_{lim}. $\lambda_{lim}$is the highest for 3CB_8XL unfilled and less crosslinked. 20CB_8XL is filled and hence the stretch seen by the chains is amplified by the presence of filler [29,30]. Finally, the 20CB_19XL has both a lower λ_{lim} and amplification of the stretch which makes it the closest to the finite extensibility of the chains.

To summarize, the specific composition of the material, in particular the crosslinking density, determines the ratio between the macroscopic strain (or $\mathcal{G}$) and λ_{max}. Nevertheless, for the same value of λ_{max} , the more extensible SBR (less crosslinked) and less filled material must have less probability to propagate (to break a smaller number of chains per cycle) resulting in an enhanced fatigue resistance. Interestingly these two parameters may go in opposite directions. 3CB_8XL may have a large extensibility (favorable) but it also has by far the highest λ_{max} for a given applied $\mathcal{G}$ (very unfavorable).

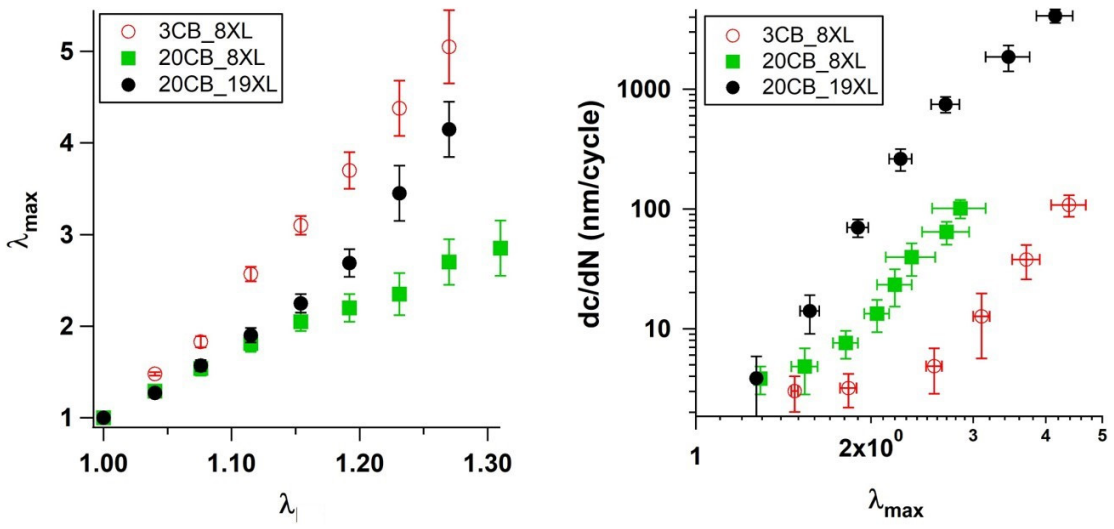

Figure 6-11 Maximum λ_{max} at the crack tip as function of applied macroscopic λ (a) and dc/dn as function of λ_{max} (b) for all SBR.

6.8 Conclusions

In this work, we completed the analysis of crack propagation in fatigue in non-crystallizing filled and unfilled SBR elastomers. In particular, we focused on the shape and processes taking place at the crack tip to complete and enrich the analysis presented in our previous paper[5]. We provide additional insights concerning the role of the filler and crosslink density in the mechanisms involved at the crack tip including heat dissipation and fracture localization. As expected, the presence of filler improves the material resistance to crack propagation in fatigue, but the predominant effect is played by the crosslinking density. By measuring with an IR camera the increase of surface temperature due to self-heating during cyclical loading of un-notched samples, we identified the filler content as the major factor responsible for energy dissipation in the bulk of the material, while the crosslinking density mainly controls the maximum strain achieved at the crack tip. Interestingly, we found that the crack front presents the same fibrillar morphology for a given material when propagation occurs under cyclic loading or under static loading. However, the presence of filler influences not only the dissipation but also the crack shape (that is sharper in filled SBR), the localization of the fracture area and the length-scale of the fibrils that are in fact thicker and more randomly broken in 3CB_8XL compared to both highly filled SBR. We also show that the crack propagation rate dc/dn is probably controlled by a combination of bulk dissipation (relating the applied $\mathcal{G}$ to the local energy g_{local} available for crack growth and maximum stretch at the crack tip λ_{max}) and the ration between λ_{max} and the limiting extensibility of the polymer chains (controlled by the crosslink density and filler content through the strain amplification effect).

6.9 Supplementary information

Supplementary information includes three movies:

The video obtained by the infrared camera of the lateral profile of 20CB_8XL at the beginning of a typical fatigue experiment before achieving the steady state (Movie_1). It shows the not-uniform heating of the whole sample, with the hottest area the area surrounding the crack.

Optical movies of the front crack for 3CB_8XL (Movie_2) and 20_CB_8XL (Movie_3) during monotonic extension. In Movie_2 we can distinguish the very chaotic crack front with several thick fibrils breaking in a random and delocalised way. This scenario is very different from the smoother crack front in Movie_3 where is clearly visible a thin fracture line which maintains its shape as the crack propagates.

6.10 Acknowledgements

We are in debt with Samy Mzabi who did all the experiments and kindly allowed us to use the data for this paper.

6.11 References

1. Mars, W. V., Fatemi A. Factors That Affect the Fatigue Life of Rubber. *History*. 2004;77(3):419-423. doi:10.5254/1.3547831

2. Tee YL, Loo MS, Andriyana A. Recent advances on fatigue of rubber after the literature survey by Mars and Fatemi in 2002 and 2004. *Int J Fatigue*. 2018;110:115-129. doi:10.1016/j.ijfatigue.2018.01.007

3. Lake GJ, Lindley PB. Mechanical Fatigue Limit for Rubber. *J Appl Polym Sci*. 1965;9:1233-1251. doi:10.5254/1.3544847

4. Lake GJ, Lindley PB. Fatigue of rubber at low strains. *J Appl Polym Sci*. 1966;10(2):343-351. doi:10.1002/app.1966.070100214

5. Mzabi S, Berghezan D, Roux S, Hild F, Creton C. A critical local energy release rate criterion for fatigue fracture of elastomers. *J Polym Sci Part B Polym Phys*. 2011;49(21):1518-1524. doi:10.1002/polb.22338

6. Saintier, N.; Cailletaud, G.; Piques R. Cyclic loadings and crystallization of natural rubber: An explanation of fatigue crack propagation reinforcement under a positive loading ratio. *Mater Sci Eng*. 2011;528 (3)(1078-1086).

7. Rublon, P.; Huneau, B.; Saintier, N.; Beurrot, S.; Leygue, A.; Verron, E.; Mocuta, C.; Thiaudière, D.; Berghezan D. In situ synchrotron wide-angle X-ray diffraction investigation of fatigue cracks in natural rubber. J Synchrotron Radiat 2013, 20 (1), 105-109. *J Synchrotron Radiat*. 2013;20(1):105-109.

8. Munoz, L.; Vanel, L.; Sanseau, O.; Sotta, P.; Long, D.; Odoni, L.; Guy L. Fatigue crack growth dynamics in filled natural rubber. *Plast Rubber Compos Process Appl*. 2012;41(7):273.

9. Stadlbauer F, Koch T, Archodoulaki VM, Planitzer F, Fidi W, Holzner A. Influence of experimental parameters on fatigue crack growth and heat build-up in rubber. *Materials (Basel)*. 2013;6(12):5502-5516. doi:10.3390/ma6125502

10. Lake, G. J., Thomas AG. Strength. In: Gent AN, ed. *Engineering with Rubber*. Hanser Publishers, Munich; 1992:95-128.

11. Smith TL. Strength of elastomers—A Perspective. *Polym Eng Sci*. 1977;17(3):129-143. doi:10.1002/pen.760170302

12. Smith TL. Tensile Strength of Polyurethane and Other Elastomeric Block Copolymers. *J Polym Sci Polym Phys Ed*. 1974;12:1825-1848. doi:10.5254/1.3534952

13. Bai R, Yang J, Suo Z. Fatigue of hydrogels. *Eur J Mech A/Solids*. 2019;74:337-370. doi:10.1016/j.euromechsol.2018.12.001

14. Albouy PA, Vieyres A, Pérez-Aparicio R, Sanséau O, Sotta P. The impact of strain-induced crystallization on strain during mechanical cycling of cross-linked natural rubber. *Polymer (Guildf)*. 2014;55(16):4022-4031. doi:10.1016/j.polymer.2014.06.034

15. Le Gac PY, Albouy PA, Sotta P. Strain-induced crystallization in a carbon-black filled polychloroprene rubber: Kinetics and mechanical cycling. *Polymer (Guildf)*. 2019;173(April):158-165. doi:10.1016/j.polymer.2019.04.019

16. Demassieux Q, Berghezan D, Cantournet S, Proudhon H, Creton C. Temperature and aging dependence of strain-induced crystallization and cavitation in highly crosslinked and filled natural rubber. *J Polym Sci Part B Polym Phys*. 2019;57(12):780-793. doi:10.1002/polb.24832

17. Le Cam, J. B. , Huneau B. , Verron E. , Gornet L. Mechanism of Fatigue Crack Growth in Carbon Black Filled Natural Rubber. *Macromolecules*. 2004:5011-5017.

18. Samaca Martinez JR, Le Cam JB, Balandraud X, Toussaint E, Caillard J. Filler effects on the thermomechanical response of stretched rubbers. *Polym Test*. 2013;32(5):835-841. doi:10.1016/j.polymertesting.2013.04.003

19. Zhang H, Scholz AK, Vion-Loisel F, et al. Opening and closing of nanocavities under cyclic loading in a soft nanocomposite probed by real-time small-angle X-ray scattering. *Macromolecules*. 2013;46(3):900-913. doi:10.1021/ma302325w

20. Zhang H, Scholz AK, De Crevoisier J, et al. Nanocavitation around a crack tip in a soft nanocomposite: A scanning microbeam small angle X-ray scattering study. *J Polym Sci Part B Polym Phys*. 2015;53(6):422-429. doi:10.1002/polb.23651

21. Mzabi S. Caractérisation et analyse des mécanismes de fracture en fatigue des élastomères chargés. 2010:1-310.

22. Lake GJ. Fatigue and Fracture of Elastomers. *Rubber Chem Technol*. 1995;68(3):435-460. doi:10.5254/1.3538750

23. Rivlin RS. Large Elastic Deformations of Isotropic Materials 4. Further Developments of the General Theory. *Philos Trans R Soc London Ser a-Mathematical Phys Sci*. 1948;241(835):379-397.

24. Merckel Y, Diani J, Brieu M, Berghezan D. Experimental characterization and modelling of the cyclic softening of carbon-black filled rubbers. *Mater Sci Eng A*. 2011;528(29-30):8651-8659. doi:10.1016/j.msea.2011.08.023

25. Diani J, Fayolle B, Gilormini P, Diani J, Fayolle B, Gilormini P. A review on the Mullins effect To cite this version : HAL Id : hal-00773015. 2013:601-612.

26. Martinez JRS, Toussaint E, Balandraud X, et al. Heat and strain measurements at the crack tip of filled rubber under cyclic loadings using full-field techniques To cite this version : HAL Id : hal-01148252 Heat and strain measurements at the crack tip of filled rubber under cyclic loadings using full-f. 2015.

27. Zhang H, Scholz AK, De Crevoisier J, et al. Nanocavitation in carbon black filled styrene-butadiene rubber under tension detected by real time small angle X-ray scattering. *Macromolecules*. 2012;45(3):1529-1543. doi:10.1021/ma2023606

28. Lake GJ, Thomas AG. The Strength of Highly Elastic Materials. *Proc R Soc A Math Phys Eng Sci*. 1967;300(1460):108-119. doi:10.1098/rspa.1967.0160

29. Nielsen LE. Simple Theory of Stress-Strain Properties of Filled Polymers. *J Appl Polym Sci*. 1966;10:97-103.

30. Bueche F. Molecular Basis for the Mullins Effect. *J Appl Polym Sci*. 1960;IV(10):107-114.

7 CYCLIC FATIGUE FAILURE OF TPU

Cyclic fatigue failure of TPU using a crack propagation approach

Giorgia Scetta[1], Nathan Selles[2], Patrick Heuillet[2] Matteo Ciccotti[1*] and Costantino Creton[1*]

[1]Sciences et Ingénierie de la Matière Molle, ESPCI Paris, Université PSL, CNRS, Sorbonne Université, 75005, Paris, France

[2]Laboratoire de Recherches et de Contrôle du Caoutchouc et des Plastiques , 60, Rue Auber 94408 Vitry-sur-Seine, France

matteo.ciccotti@espci.psl.eu, Costantino.creton@espci.psl.eu

7.1 Abstract

Thermoplastic polyurethane elastomers (TPU) are stretchable, tough, wear resistant and easily processable soft materials. Especially because of their recyclability, TPUs can be suitable candidates to replace rubbers in several applications such as damping, footwear and cable coatings. However, their capacity to operate under cyclic loads over many cycles was rarely investigated, mainly due to their complex strain-dependent morphology and viscoplastic character. Additionally, the absence of chemical crosslinks results in a certain degree of creep and plastic deformation when TPUs are cyclically strained, questioning how to unambiguously define fracture mechanics variables such as the energy release rate G, typically used to evaluate fatigue crack growth in chemically crosslinked elastomers. We show that when TPUs are cyclically loaded up to the same value of maximum strain, their stress-stretch curve changes with the number of applied cycles, but eventually achieves a steady-state. We propose a suitable methodology to evaluate the cyclic fatigue resistance in TPUs, based on a fracture mechanics approach with some additional treatments to account for the higher tendency to creep of TPUs than thermoset rubbers. Comparing the obtained results of TPU with those for classical filled rubbers with a similar linear modulus, we underline the excellent toughness and cyclic fatigue resistance of TPUs, opening new opportunities in their use for applications requiring to resist to crack propagation under cyclic loading at large strains.

7.2 Introduction

Thermoplastic polyurethanes (TPU) are an interesting class of thermoplastic materials that appeared on the market around 1950. Soft TPU display a rubberlike behavior at ambient temperature without

any need for chemical crosslinking. They are typically composed of long polyether or aliphatic polyester flexible chains called soft segment (SS) and short sequences containing an isocyanate linked with a short chain extender called hard segments (HS). Because of their chemical incompatibility SS and HS tend to separate in a two-phase system, while the presence of inter-hydrogen bonding between urethane units causes the HS to aggregate in small and hard domains (HD) of nanometric dimensions. These HS clusters connect the polymer chains with physical links and prevents them to flow at working temperature. When the softening temperature of the hard phase is reached, the polymer flows and can be easily and reversibly shaped with conventional thermoplastic processing techniques such as extrusion and injection moulding. Classical elastomers need to be chemically crosslinked and filled (with carbon black and/or silica) to show the combination of reversible elasticity and toughness typical of commercial rubber. On the other hand, the properties of TPU can be tuned to achieve specific strength and elasticity by changing the chemical nature and relative proportion of either the hard polyurethane group or the long soft segment. The HS microdomains are generally sufficient to reinforce the materials without any additional filler. Figure 7-1 reports a sketch of the network organisation for vulcanized rubbers and TPUs. This peculiar microstructure provides TPU with some advantages compared with conventional rubbers such as the possibility to be easily processed and reprocessed through injection moulding and extrusion. Moreover, they also possess an excellent abrasion resistance as well as blood and tissue compatibility, so that they have been rapidly used in numerous applications such as footwear, medical cables, wheels or dampers. Nevertheless, the suitability of TPUs in applications requiring the material to sustain cyclical loads and to prevent sudden failure or fatigue crack growth requires a robust characterization method in cyclic fatigue. Opposite to rubbers, where cyclic fatigue resistance has been thoroughly studied[1,2], only few investigations have been carried out on fatigue fracture in TPUs[3–5]. This shortcoming mainly comes from the complex visco-plastic character of TPUs at large strains. The mechanical properties of TPUs are indeed deeply related to their complex strain-dependent morphology. Size and orientation of the hard domains were shown to change under the application of a load[6–8], inducing mechanical hysteresis in cyclic loading and a permanent modification of the elastic modulus and extensibility of the material. Additionally, the absence of chemical crosslinking induces a significant residual plastic strain (and stress softening) that increases with cyclic sample deformation. Such complex change in structure and strain dependent properties[6,9] are not straightforward to include in the common framework of fracture mechanics used to assess cyclic fatigue in rubbers that are mostly elastic.

In this work, we use a pure shear geometry to investigate how a crack propagates in a typical commercial soft TPU. submitted to a cyclic loading. We used two different testing protocols and

assessed their suitability and the effect on the crack propagation rate. Finally in order to highlight key differences between TPU and conventional elastomers, we also compared our results with those obtained on a filled SBR having a similar Young's modulus.

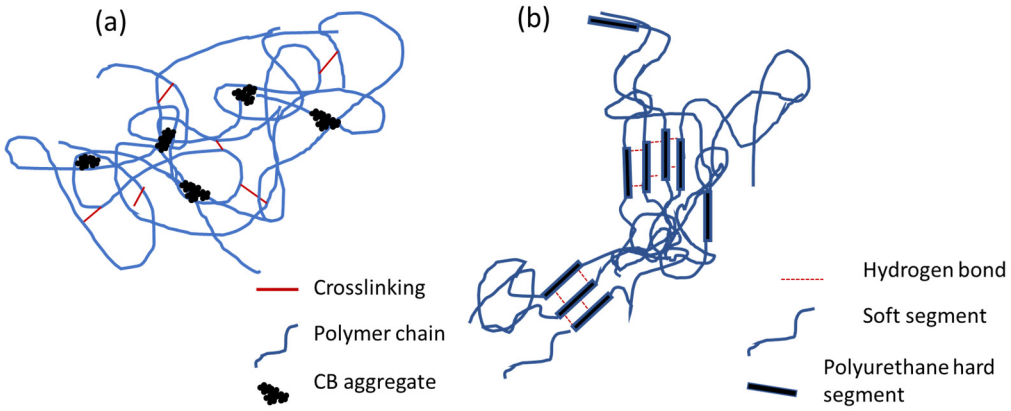

Figure 7-1 Example of network organization for filled crosslinked rubbers (a) and TPUs where the hard domains act as physical crosslinks (b).

7.2.1 The classic fracture mechanics approach for cyclic fatigue in rubbers

Since the last century, the field of cyclic fatigue resistance was largely developed for crosslinked elastomers[2,10] and two main approaches have been used to define their cyclic fatigue resistance: onset of crack nucleation[11,12] and crack propagation rate[13,14]. The first method defines fatigue resistance as the maximum number of cycles at a given strain or stress to achieve a definite loss in strength or end of life of the material. The second one seeks to evaluate the crack growth rate of a pre-existing crack per cycle as a function of applied energy release rate G [15]. We focused on the second approach that has in our view several advantages:

- The use of the energy release rate G (instead of strain or stress) allows to compare samples of different sizes tested under different loading conditions.
- Opposite to crack nucleation, where small defects (that are potentially precursors of the macroscopic failure) are randomly distributed in the sample, in notched samples the macroscopic cut dominates over all the pre-existent defects leading to more reproducible results.
- It is suitable for applications where cracks are nucleated from the start, but lifetime is limited by propagation.

Following the crack propagation approach, fatigue resistance in rubbers is typically carried out using samples in the pure shear geometry[16] (PS) which corresponds to a wide and thin rectangular strips with width(w) and height (h) >> thickness (t) as schematically showed in Figure 7-2 . Fatigue

resistance is expressed in terms of crack propagation per cycle *dc/dn* vs maximum applied energy release rate G. For filled elastomers this characteristic curve provides a convenient assessment of fatigue resistance as a material property and has the advantage to allow an easy comparison of fatigue data among different materials.

As reported in the literature[14,17], irrespectively of their composition elastomers typically show similar trends of *dc/dn* vs. G, which can be summarized as follows:

- For values of G lower than a critical threshold G_t, in the absence of any chemical attack, the crack does not propagate.
- For $G > G_t$, *dc/dn* can be described by a monotonically growing function of G, which presents a linear region for small G, followed by a a power law for larger G.
- Finally, for G larger than a critical value G_c, generally named "toughness" in the literature of filled rubbers, a catastrophic propagation is observed and the material ruptures in a few cycles.

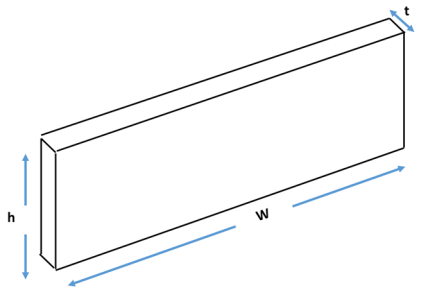

Figure 7-2 Example of PS geometry.

7.2.2 Evaluation of G in conventional elastomers and thermoset rubbers.

One of the main advantages of using the PS geometry is that it allows an easy evaluation of the energy release rate $G(\lambda)$ as a function of the applied stretch λ, which is independent of crack length as shown by the seminal work of Rivlin and Thomas[15] and can be calculated as:

$$G(\lambda) = -\frac{dU}{dA} = -\frac{dU}{tdc} = W(\lambda)h_0 \qquad \textbf{Equation 7-1}$$

Where $W(\lambda)$ is the integral under the stress-strain curve of an unnotched sample with the same geometry.For an elastic material the typical stress-stretch curve during cycles is stable in time, and takes the form of Figure 7-3(a). All the curves mainly overlap and the strain energy $W(\lambda)$ is well defined and is calculated as the area under the loading stress-strain curve up to λ.

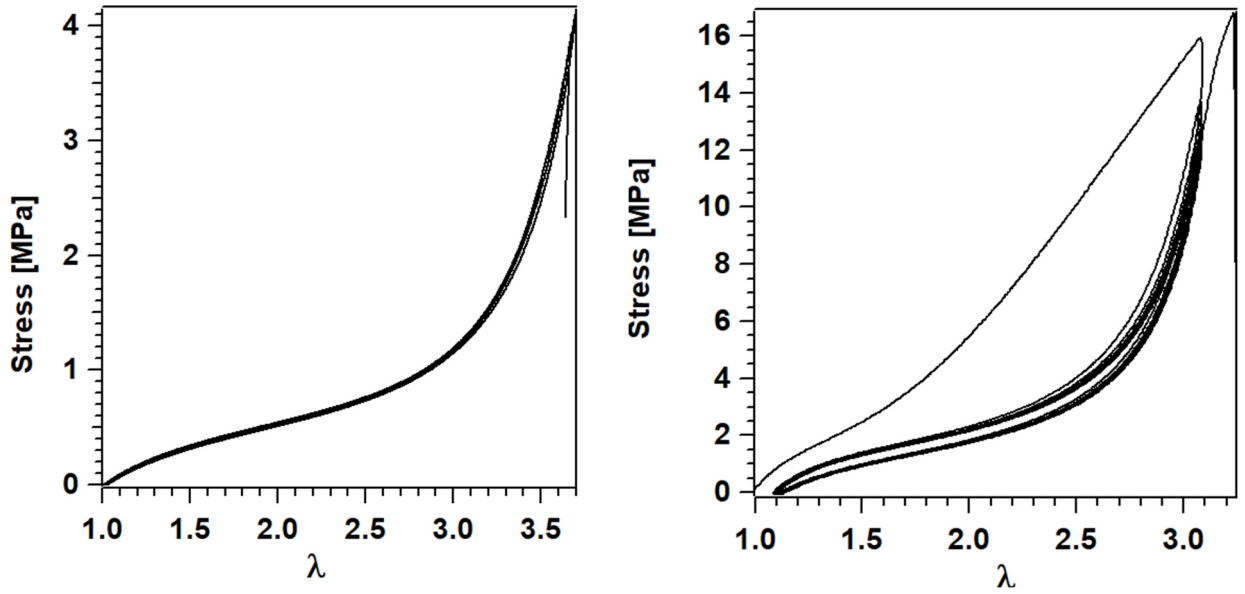

Figure 7-3 Example of stress-stretch curve for a nearly elastic material (data from Gabriel E. Sanoja) (a) and a filled thermoset rubber (data from Mzabi[18]) (b)

Figure 7-3(b) reports an example of typical filled elastomers that are generally not fully elastic. Hysteresis during the first cycle (also called Mullin's effect) and cyclic hysteresis are typical manifestations of the damage and viscoelastic character of common filled rubbers. The damage in the rubber network is more evident in the first cycle and it gradually decreases in the following ones. A common approach to calculate $G(\lambda)$ in filled rubbers is to pre-strain (or precondition) the unnotched sample for some thousands of cycles at higher values of λ than those used in fatigue testing and then to evaluate $G(\lambda)$ by cyclically straining the accommodated sample at different values of increasing stretch. In this way most of transient effects related to Mullin's damage in the first cycles are avoided in the calculation of the relevant G for long term cyclic fatigue. The pre-conditioned sample can still present residual hysteresis between the loading and unloading curves associated to viscoelasticity. Figure 7-4 shows a typical stress-stretch curve for a PS sample (taken from Mzabi[18]). The area indicated as W_1 corresponds to the energy dissipated per cycle, W_2 to the energy recovered, the total work done on the material during the loading phase of each cycle is W_1+W_2. Since the evaluation of the energy release rate requires to account only for the elastic contribution, the calculation of $W(\lambda)$ can be carried out by using the area under the un-loading curve, instead of the loading one, that represents the elastic part of the loading energy as in Equation 7-2.

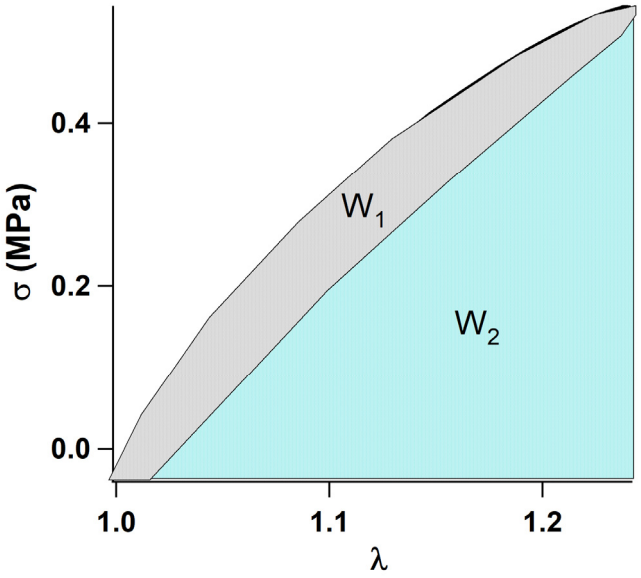

Figure 7-4 Typical stress-strain curve of filled SBR after pre-conditioning from Mzabi [18].

$$W_{unload} = -\int_{\lambda_{max}}^{\lambda_{min}} \sigma \, d\lambda \qquad \textbf{Equation 7-2}$$

Applying this method to TPUs without modification creates several challenges that are the focus of this paper. The first issue is that TPUs typically show significant residual deformation when unloaded. If cyclic loading is carried out at a constant maximum applied strain, the residual strain increases during cycles, and hence the stress-stretch curve is modified and the actual energy release rate seen by the crack is not constant. Unlike conventional rubbers the applied energy release rate G is a function of both the maximum applied strain and the number of cycles n: $G(\lambda,n)$. Moreover if the sample is allowed to unload up to $\lambda_{min} = 1$, calculated using the initial height h_0 of the pristine sample, , the residual plastic strain causes an extensive buckling of the TPU sample during unloading cycles that may induce additional undesirable damage in the sample.

Since TPUs are typically tested in cyclic fatigue at significantly larger strains than filled rubbers, a second important issue needs to be addressed. The well-established pre-conditioning procedure cannot be easily implemented to eliminate transient effects, since it would involve very large strains that are likely to damage the sample. Also if the sample is preconditioned to a stress λ_{max} that is only slightly larger than the cyclic stretch λ to be tested, the values of the energy release rate will precisely depend on this maximum stretch: $G(\lambda,\lambda_{max})$ applied during the preconditioning.

Defining in which conditions should the cyclic load be applied in TPU to obtain reliable and reproducible crack propagation data is precisely the objective of this work.

7.3 Materials and methods

7.3.1 Styrene-Butadiene Rubber

We used SBR rubber filled with carbon black. The SBR has a mass M_n of 120 kg/mol and a polydispersity of 1.94 and was provided by the Michelin research center. Its styrene content is 15 wt% and the glass transition temperature T_g measured by differential scanning calorimetry (DSC at 10°C/min) is -48°C. The detailed composition is reported in Table 7-1 as provided by Michelin:

Table 7-1 SBR composition in PHR. Filler content and crosslinking density are reported in volumetric fraction (data from[18]). Note that N347 is a type of carbon black, Sulfur is a crosslinking agent, Struktol™ and N-Cyclohexyl-2-benzothiazole sulfenamide (CBS) are accelerators to vulcanize the rubber, and N-(1,3-dimethylbutyl)-N'-phenyl-p-phenylenediamine (6PPD) is an anti-oxidant.

	20CB_19XL
SBR	100
N347	5
6PPD	1
Struktol	3
CBS	1.5
Sulfur	1.5
ϕ	0.03
ν	$8.1 \cdot 10^{-5}$

All samples were prepared, moulded and cured by Michelin. For tensile tests, samples where cut in a dog-bone shape with a cross section of 2x4 mm and loaded with a strain rate of 4 s^{-1}. For crack propagation experiments, pure shear samples were moulded with the following dimensions: length = 157 mm, height = 13 mm, thickness = 2 mm. Two edge cracks and a centre crack were cut with a fresh razor blade in the direction perpendicular to the loading. Uncracked samples were preconditioned at λ_{max}=1.27 for 1000 cycles to get rid of transient effects. Then, the same samples were used to calculate $G(\lambda) = W(\lambda)h_0$. Each preconditioned sample was then notched and strained for 50.000 cycles at values of G corresponding to $\lambda < \lambda_{max}$. All tests were performed at 10 Hz.

7.3.2 TPU

The TPU is a polyester-polyurethane block copolymer kindly provided by BASF (commercial name: EC 60 A 10 Elastollan©). The volume fraction ϕ= 0.24of hard segments and the average distance L=12-15 nm between hard domains was estimated from X-Ray diffraction of pristine samples using the lamellar model Fourier analysis[19,20]. A T_g of -50°C was obtained by Differential Scanning Calorimetry (DSC) at 10°/min (very similar to that obtained for filled SBR).

PS Samples were injection moulded BOY 50M injection moulding machine (Boy machines Inc., US) at the LRCCP using the procedure recommended by BASF. The temperature used in the injection procedure is summarized in Table 3 and schematically showed in Figure 7-5.

Table 7-2 Barrel temperature profile for the injection procedure. Zones 1 to 4 are located between the rear and the front of the barrel.

Barrel / Sample	**Zone 1 (°C)**	**Zone2(°C)**	**Zone4(°C)**	**Nozzle (°C)**	**Mold (°C)**
(TPU)	165	170	175	170	30

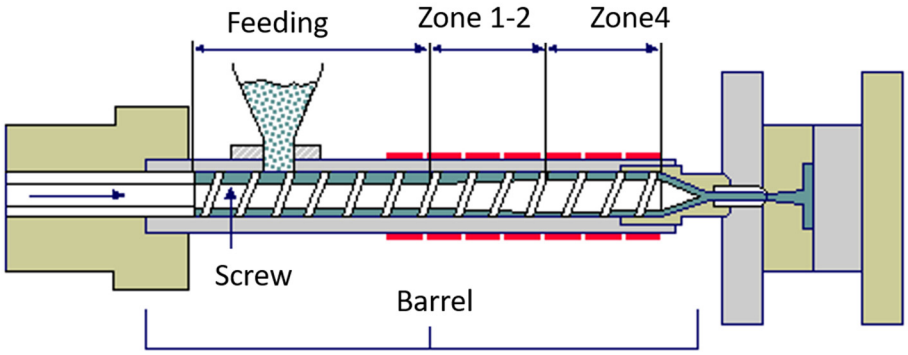

Figure 7-5 Schematic of injection process with the different zones of the barrel

7.3.3 Large strain tensile tests

Uniaxial tensile tests were performed on dog-bone samples (with a cross section of 2x4 mm cut from a square plate) using an Instron 5590 tensile machine. The samples were deformed at constant stretch rate $\dot{\lambda} = 4\ s^{-1}$ up to rupture or in cyclic conditions. In the second case, 10 cycles were performed up to maximum stretch of 20, 40 and 100% of the stretch at break λ_b.

7.3.4 Dynamic mechanical analysis (DMA)

DMA analysis was performed on circular disks of 10 mm diameter and 2 mm thickness cut from a square plate using a METRAVIB (DMA+450 series, FR). The cylinders are glue to three metallic supports placed in metallic grips. The middle support moves and generates an oscillatory displacement up and down between 0.005% and 100% of strain at temperature of 23°C and frequency of 10 Hz/s as schematically showed in Figure 7-6.

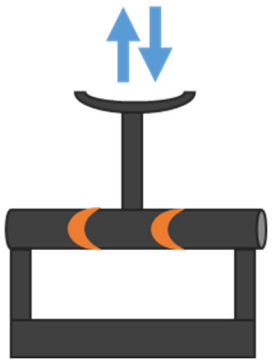

Figure 7-6 Illustration of DMA apparatus

7.3.5 Fracture toughness and cyclic fatigue

Fracture toughness and cyclic fatigue tests were carried out using pure shear samples of 65x5x1 mm with a single crack of 22 mm cut along the direction parallel to the sample's length. Each cut was made in non-relaxing conditions on the clamped sample and after the application of a small pre-stretch. For measuring the fracture toughness Γ, the material was stretched stretch rate $\dot{\lambda} = 4\ s^{-1}$ up to fracture. The minimum strain to propagate the crack λ_c is determined from the point where the stress undergoes a maximum value in the stress-stretch curve of notched samples. At the crack propagation conditions the equivalence $G = \Gamma$ holds[15] and the value of fracture toughness is defined as $\Gamma = W(\lambda_c)h_0$ where $W(\lambda_c)$ is calculated by integrating the stress-stretch loading curve of pristine PS samples between λ and λ_c[21,22]. Cyclic fatigue experiments were carried out at frequency of 10 Hz using the procedure reported below.

7.4 Materials characterization

7.4.1 Small strain properties

The filled SBR and TPU have similar values of the storage shear modulus μ' at low strain, and both materials display a decreasing modulus with applied strain as shown in Figure 7-7. This strain

softening, known as Payne effect, is common in filled rubbers[23]. The main difference between TPU and SBR is that in TPU the linear regime extends to higher strains before a drop in the modulus is observed. This reflects the limited structure modifications up to 10% strain.

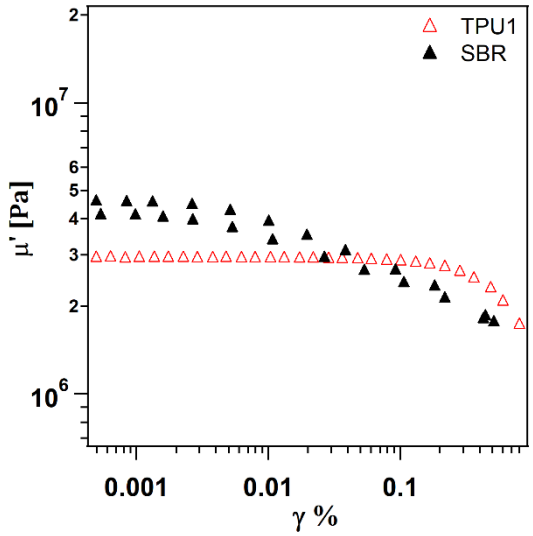

Figure 7-7 Storage modulus vs. dynamic strain amplitude for TPU and SBR at 23°C and 10Hz.

7.4.2 Uniaxial tensile tests

Figure 7-8(a) shows representative stress-strain curves for TPU and filled SBR. The linear regime is only observed for less than 20% strain and is similar for both materials as underlined by the close values of Young's moduli reported in Table 7-3 along with the values of maximum strength σ_b and extensibility λ_b for both materials. After the linear regime, both materials display stress-softening followed by strain-hardening although to a very different extent. Among all factors contributing to the mechanisms of crack growth, viscoelastic dissipation is known to play an important role in elastomers[24,25]. In Figure 7-8(b) we show uniaxial step-strain cycles of deformation for TPU and SBR. Both materials exhibit cyclic hysteresis that is more pronounced in the first cycle and then gradually decreases in the following ones. This phenomenon, knows as Mullins effect, was already observed both in filled rubbers and unfilled TPU[2627]. Although there is no generally accepted microscopic explanation, the Mullins effect is often attributed to structural modifications of the filler network or of the hard domains respectively for filled rubbers and unfilled TPUs[26,28,29]. It is important to note that despite its thermoplastic character the fraction of dissipated energy at fixed applied strain is lower for TPU than for filled SBR. This is true in the 1st cycle, characterizing damage (Figure 7-9(a)) and in the 10th cycle (Figure 7-9(b)) representing stabilized cycling conditions where an excessive hysteretic behaviour is often undesirable, since it may lead to heat build-up, reducing the material's ability to resist crack propagation.

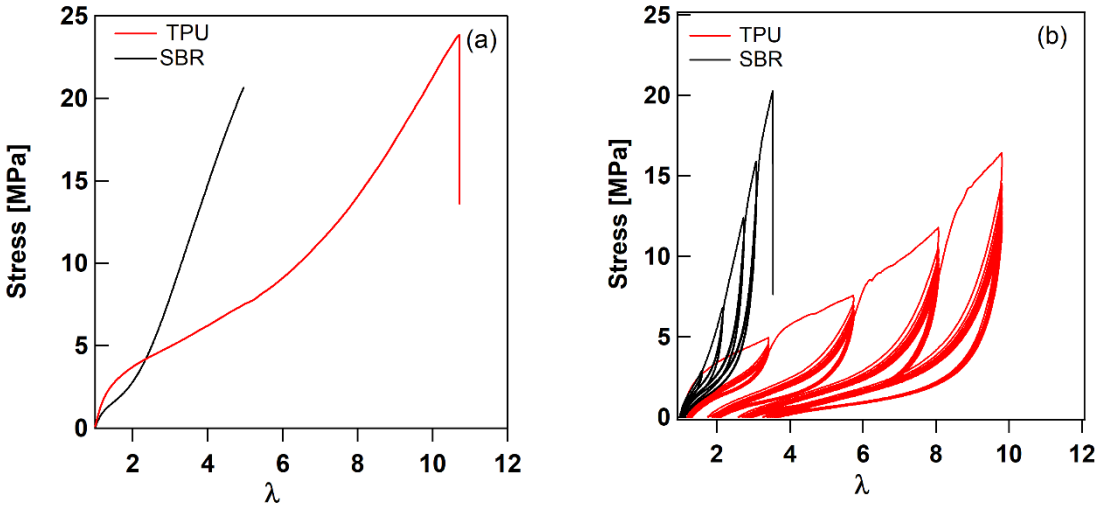

Figure 7-8 Uniaxial nominal tensile test at 23°C for TPU (red) and SBR (black) up to failure (a) and in cyclic experiments (b)

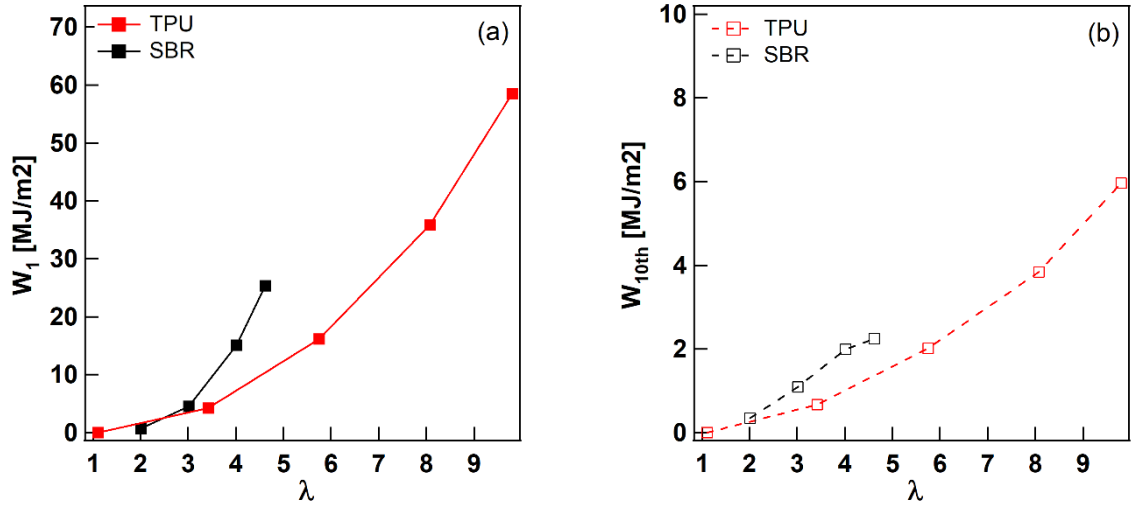

Figure 7-9 Dissipated energy during the first (a) and the 10th (b) cycle of the uniaxial cyclic experiments

Table 7-3 Linear modulus, stretch and stress at break and toughness of TPU and SBR (data from Mzabi[18])

Name	E [MPa]	λ_b	σ_b [MPa]	Γ KJ/m^2
TPU	7.3 ± 0.12	10.8 ±1.9	24.7 ±2.3	138 ±13
SBR *	8.2 ± 0.5	3.6 ± 0.1	16.6 ± 1.1	23 ±3

7.4.3 Fracture toughness

Table 7-3 reports the value of Γ calculated for notched SBR and TPU. Despite similar linear properties of the two materials, TPU is almost one order magnitude tougher than the SBR filled rubber at 23°C indicating clearly that large strain properties (that predominate around the crack tip singularity) play an important role in the toughness.

7.4.4 Results on the cyclic fatigue of TPU

7.4.4.1 Effect of the loading conditions

The fatigue resistance of TPU samples was probed with two different loading protocols as schematically shown in Figure 8: either a minimum value of stress $\sigma_{min} = 0$ was imposed at every cycle (Protocol A) or the sample was unloaded to the displacement corresponding to its initial length (Protocol B), as it is classically done for SBR.

With Protocol A the sample is strained between an imposed λ_{max} and a variable minimum stretch λ_{min}, corresponding to the imposed condition $\sigma_{min}=0$, that increases in time due to residual plastic strain experienced by the sample, as illustrated in Figure 7-10(a). Therefore, the applied value of G decreases with the number of cycles until a steady-state is reached[30,31].

With Protocol B the sample is strained between imposed nominal values of both λ_{max} and $\lambda_{min} = 1$, implying that the sample will undergo compressive stresses and buckle when the strain decreases below the residual plastic strain λ_{res}, as illustrated in Figure 7-10(b). In classical rubbers the two loading schemes A and B are substantially identical, since the residual plastic strain is generally

negligible and it stabilizes after a few cycles (Figure 7-3(b)).

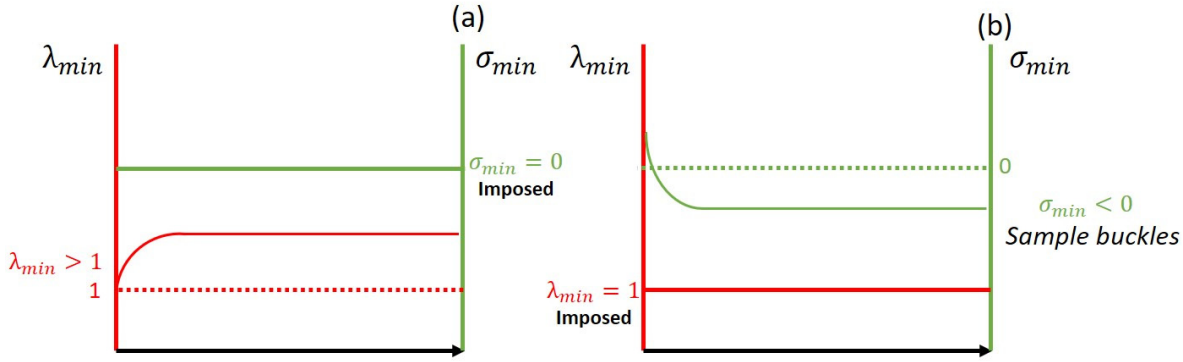

Figure 7-10 Sketch of evolution of minimum strain λ_{min} and minimum stress σ_{min} as function of the number of cycles during a fatigue experiment for Case A (a) and B (b).

7.4.4.2 Evaluation of G in TPU

As discussed in the introduction we did not use any pre-conditioning procedure in TPU, unlike what is classically done for filled chemically crosslinked rubbers.

Figure 7-11 shows the stress-stretch curve for TPU at λ=2.2 for the 1st , 200th , 5.000th and 10.000th cycle (a) and the corresponding values of G as a function of the number of cycles are reported in Figure 7-11 (b). Most of the softening and the accumulation of plastic strain occurs over the first cycles of the experiment and the stress-stretch curve eventually stabilizes between 5.000 and 10.000 cycles and the value of G is very stable during further cycles. Even after the shake-down, the stress-stretch curve of TPU shows a residual hysteresis, as it is also the case for SBR (Figure 7-4). Nevertheless, as previously indicated for uniaxial cyclic experiments, for the same value of maximum stretch the hysteresis is comparable or lower for TPU.

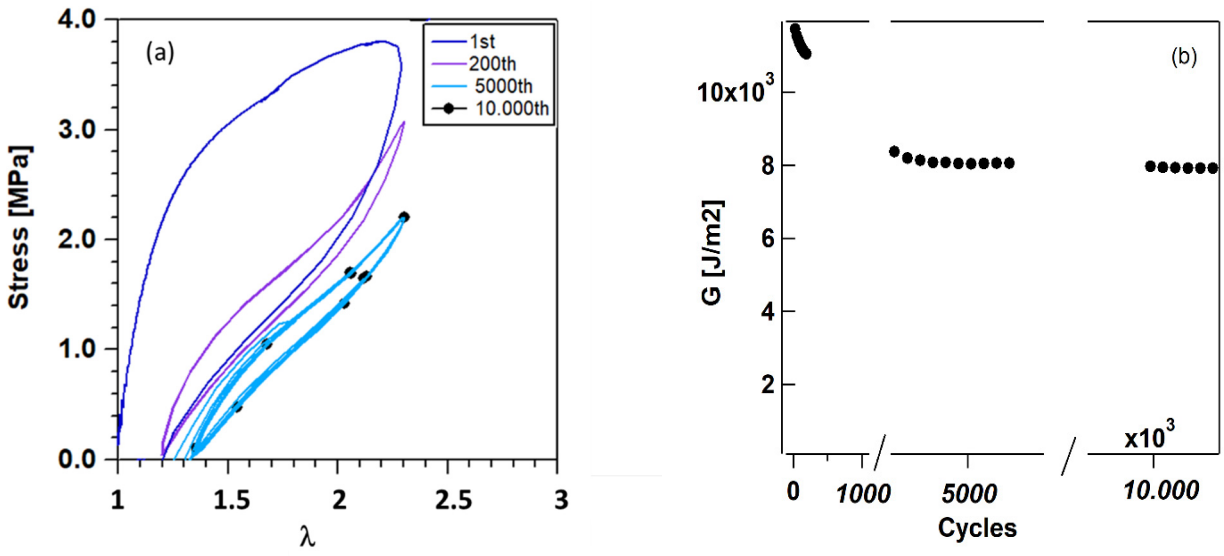

Figure 7-11 Stress-stretch curve of TPU strained atλ =2.3 and evolution of G with cycles.

Figure 7-12 shows an example of stabilized curve of TPU obtained with the methods A (a) and B (b). The value of elastic energy density per cycle (*W*) was always calculated using the positive area below the unloading curve (shaded in Figure 7-12(a) and (b)). Interestingly, for comparable values of the maximum stretch, the unloading path of the stress-stretch curve is not much affected by the methodology and the calculated values of $W(\lambda)$ overlap as it can be appreciated in Figure 7-13. Nevertheless, in case B the stress-stretch curve per cycle results in a higher hysteresis than method A.

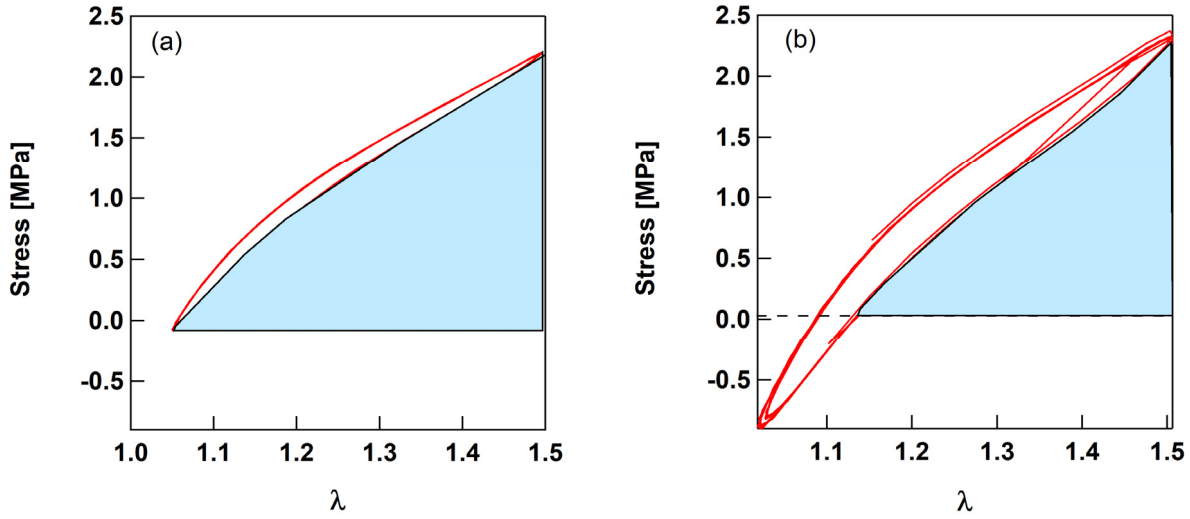

Figure 7-12 Stress-stretch curve for the stabilized cycle obtained using method A (a) and B (b). The shaded area represents the stored elastic energy density.

Figure 7-13(b) reports the values of $G(\lambda)$ obtained without any pre-conditioning but using the 10.000th unloading curve (after shake-down) for different values of increasing applied deformation for both methodologies A and B. All the data can be consistently fitted with a linear relationship for the curve $G(\lambda)$.

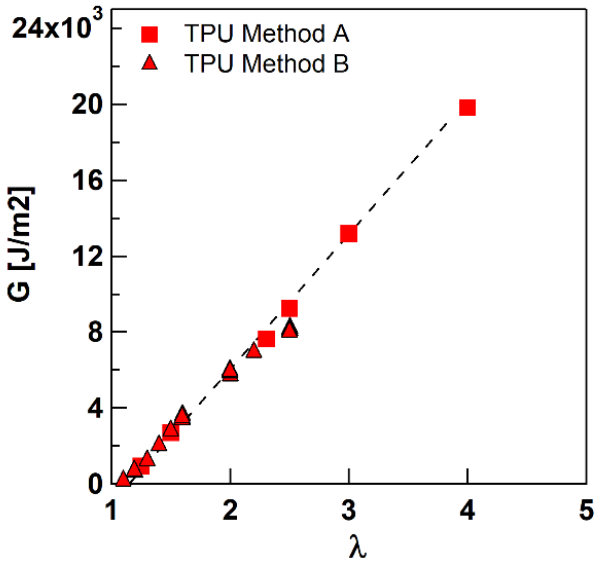

Figure 7-13 Example of calculated G vs λ for TPU without pre-conditioning using the 10.000th stress-strain curve for each value of the increasing applied stretch. The data for method A and B overlap.

7.4.5 Fatigue Failure

Once *G(λ)* has been experimentally calibrated on unnotched samples, crack propagation experiments under cyclic loading were carried out on notched samples for at least 36.000 cycles at different values of applied stretch corresponding to the selected values of G(λ). For each fatigue experiment, we evaluated the crack length *c* during the cycles by taking images of the crack tip at regular time intervals and identifying the maximum value of the x-coordinate of the contour of the crack in the open position, as shown in Figure 7-14(a). The crack profile is clearly blunted rather than sharp in TPU. To quantify the difference in crack shape between TPU and SBR we calculated the crack tip radius in the open position during cyclic experiments using a parabolic fitting (yellow line in Figure 7-14 (a)). Figure 7-14 (b) reports an example of the fitted radius for TPU and SBR strained at: G=8.000 J/m^2 and G=1.800 J/m^2 respectively, corresponding to the highest values of G used in fatigue experiment for both materials. After a first transient stage, where the crack tip changes shape, both TPU and SBR show a constant value of the fitted radius. Remarkably, TPU shows a considerably blunted profile and a higher radius than SBR according the higher value of G (and λ) required to the propagation.

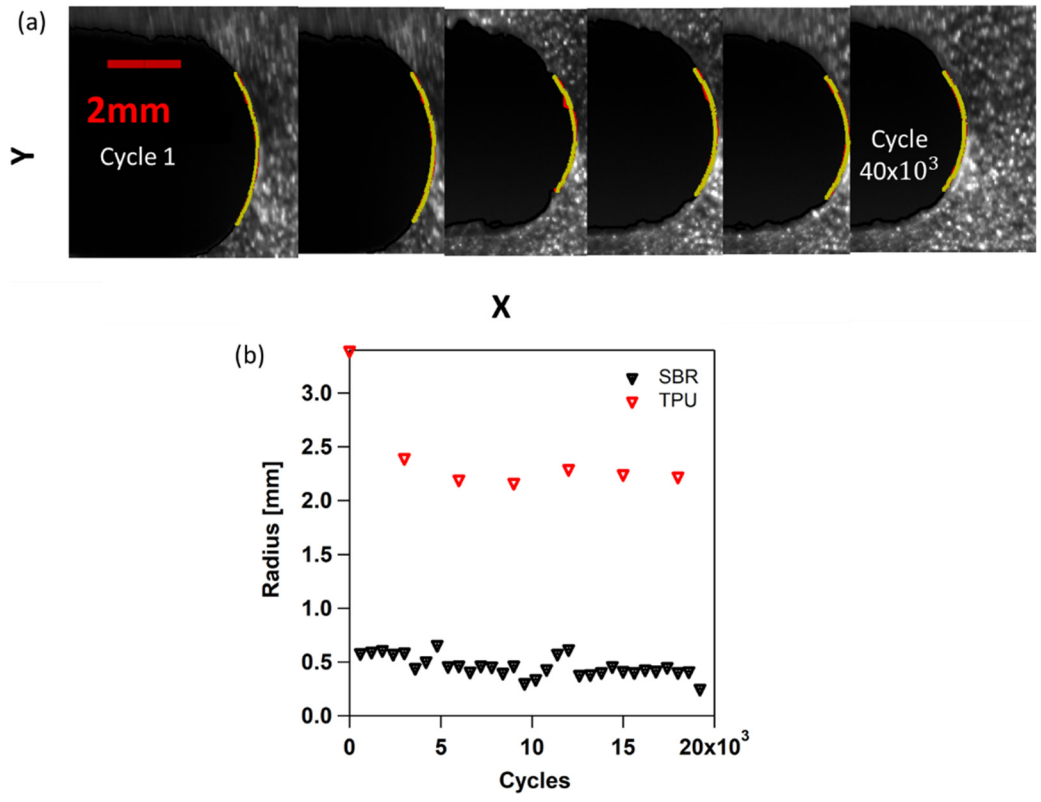

Figure 7-14 Example of crack profile and parabolic fitting during cycles (a) and calculated radius for TPU and SBR in a cyclic experiment

Figure 7-15(a,b) reports the crack length *c* as a function of the number of cycles for TPU tested either with protocol A (no buckling) and protocol (B). In the case of protocol A, at the beginning of the experiment, the crack extension per cycle is higher and gradually approaches a steady state growth rate (constant *dc/dn*). This behaviour, may be related to stress accommodation: at the beginning of the experiment, the stress singularity around the crack tip is more pronounced and the material is not "accommodated" yet. Moreover, in the case of TPU the residual plastic strain in the bulk is not stabilized yet. To evaluate the value of crack propagation per cycle expressed as *dc/dn* we only considered the data points after 10.000 cycles and we evaluated the slope of the curve *c vs*. the number of cycles. In the case of protocol B, the crack increases almost linearly with the number of cycles, and we also evaluated the slope of the curves above 10.000 cycles as is conventional. The final results for TPU tested with both protocol and for SBR, are reported in Figure 7-15(c) as *dc/dn* vs applied G. The values of dc/dn in the whole range of tested G are always higher for the protocol B than protocol A. This is probably a consequence of the continuous buckling of the specimen during unloading cycles that, in case B, is likely to damage the sample along the main fold in the centre, leading to lower fatigue resistance.

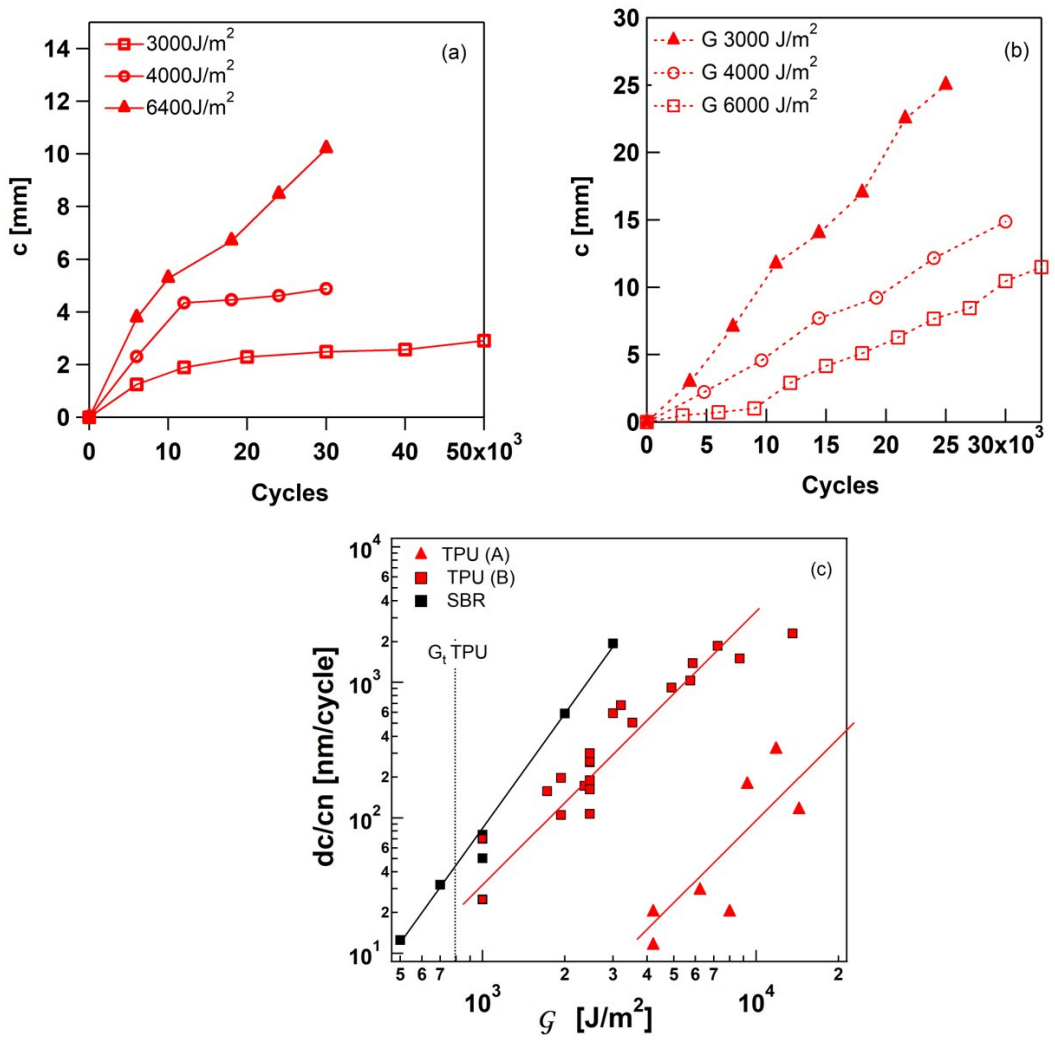

Figure 7-15 Crack length vs cycles for TPU with protocol A (a) and protocol B (b) for different values of the applied G. Crack propagation per cycle for TPU (protocol A and B) and SBR (c).

It is also interesting to discuss the "threshold" value G_t required to propagate the crack between TPU and SBR. According to Lake and Lindley[17,32], in vulcanized rubbers G_t can be estimated using the extrapolation of the linear part of the curve dc/dn VS *G*. In case of TPU, we did not see this linear regime, furthermore we observed a rapid transition between values of *G* with very low crack propagation (<0.5 nm/cy) and some 20-50 nm/cy. In order to estimate the value of G_t we carried out some longer fatigue tests at low *G*. The resolution of the optical system was ~10 µm and we completed 400.000 cycles at 10Hz. This implies that the minimum detectable crack growth is 0.025nm. Using this definition, dc/dn < 0.025 nm/cy at $G < 800 J/m^2$. At slightly higher values ($G = 1000 J/m^2$) we observed an unstable regime where dc/dn assumes values between 0.7 and 70 nm/cy (Figure 7-16). We thus can assume $G_t \sim 800\ J/m^2$. This value is surprisingly high compared to classical thermoset rubbers which generally show typical values of G_ts between 40 and 70 J/m^2 [17,33,34].

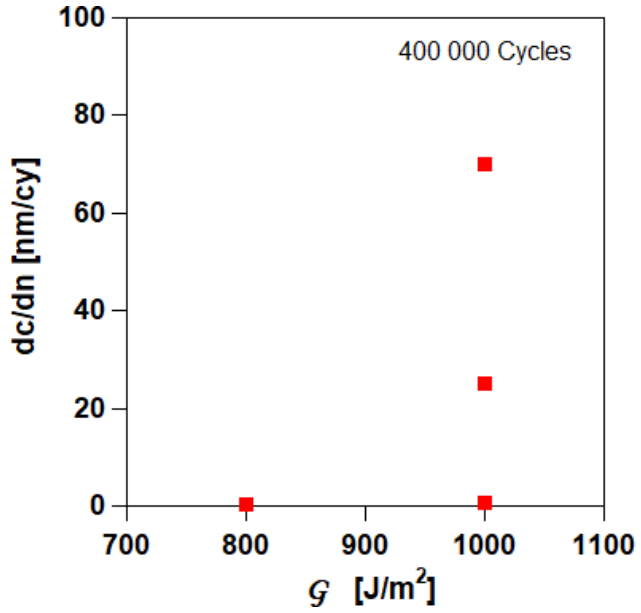

Figure 7-16 dc/dn for samples tested at lowest G for 400.000 cycles. Linear representation

7.5 Discussion

The results of this paper highlight two important elements in the cyclic crack propagation behaviour of TPU compared to crosslinked rubbers: a) TPU have higher G_t than those of common elastomers, b) the linear regime in dc/dn VS G typically found in crosslinked rubbers, is replaced by a fast transition between not propagating and fast propagating (or power law regime) crack. We also showed that the fatigue resistance of TPU is affected by the specific testing procedure, and in case of buckling of the sample during cycles (caused in principle by the residual deformation) dc/dn is significantly increased by mechanical damage on the folding line.

The high values of strain required to propagate the crack in TPU are accompanied by significant blunting developed at the crack tip (Figure 7-14) and bring additional difficulties in the evaluation of the fatigue resistance. The average crack tip radius is indicative of a zone of the sample where large deformations are involved. Although the methodology presented to evaluate G is in principle compatible with large deformations of soft materials, the fracture mechanics approach still requires that the dissipative process zone remains smaller than the sample's dimensions. In the case of TPUs, the clear blunting revealed by the large crack tip radius suggests a more extended large strain process zone region that may become comparable with the height of the sample.

The independence of the crack propagation curves *dc/dn* vs G from sample dimension should thus be carefully checked in the future. In our case we planned to stay as close as possible to the procedure adopted for SBR for better comparison. Moreover, despite the very large fracture energy of TPUs in monotonic loading, it is well known that in these materials the fatigue threshold is considerably lower than toughness and crack propagation in cyclic fatigue is generally observed for strains far below their maximum extensibility in monotonic loading[2,35,36]. Thus, such a large-strain fatigue regime of TPUs was unexpected. In order to check if such uncommon result is affected by the combination of high deformation and small sample dimension, or if it is rather an intrinsic material behaviour, larger samples than those used in this work (and conventionally adopted for rubbers) should be used for comparison. We remark that in order to preserve the aspect ratio required for a proper analysis of the pure shear sample, the whole sample should be scaled up as well as the loading fixtures. This cannot be done easily without an extensive investigation of the effects of moulding TPU at larger scale on the modification of its structure and properties.

7.6 Conclusion

We have proposed an approach to evaluate cyclic fatigue resistance in TPUs using the framework of fracture mechanics as developed for cross-linked elastomers. We showed that compared to methods used for of classical filled elastomers, a different protocol is required to account for time-dependent properties and permanent plastic strain of TPUs. This must include a control in force of the minimum of each cycle to avoid the phenomenon of buckling which can in turn damage the material inducing higher dc/dn.

Moreover, we demonstrated that TPUs possess typical values of fracture toughness and a cyclic fatigue threshold (where $dc/dn < 0.025$ nm/cy) almost one order of magnitude larger than that of filled SBR rubbers with similar values of Young modulus. This implies that TPUs may either resist for more cycles than classical rubbers when similar energy release rates are applied, or may sustain larger strains with only moderate crack growth when rubbers would fail in a single cycle. This result confirms that TPUs possess the combination of high fatigue threshold and low stiffness that is strongly desirable for practical applications and still missing in conventional elastomers as proved by the numerous attempts to develop high fatigue resistance elastomers implementing different complex techniques[37–39].

7.7 Acknowledgements

The PhD work of G. Scetta was jointly funded by the French ANRT and the LRCCP. We are indebted to Dr. Matthias Gerst, Dr. Elke Marten and Mr. Stephan Dohmen from BASF AG for kindly providing the TPU samples. We are grateful to Stephane Delaunay for injecting the samples.

7.8 References

1. Tee YL, Loo MS, Andriyana A. Recent advances on fatigue of rubber after the literature survey by Mars and Fatemi in 2002 and 2004. *Int J Fatigue*. 2018;110:115-129. doi:10.1016/j.ijfatigue.2018.01.007
2. Mars W, Fatemi a. A literature survey on fatigue analysis approaches for rubber. *Int J Fatigue*. 2002;24(9):949-961. doi:10.1016/S0142-1123(02)00008-7
3. Major Z, Miron MC, Cakmak UD. Characterization of Thermoplastic Elastomers for Design Efforts. *Adv Mater Res*. 2014;905:161-166. doi:10.4028/www.scientific.net/AMR.905.161
4. Major Z, Isasi M, Schwarz T. Characterization of the fracture and fatigue behavior of thermoplastic elastomer materials. *Key Eng Mater*. 2010;417-418:789-792. doi:10.4028/www.scientific.net/KEM.417-418.789
5. Mars W V., Ellul MD. Fatigue Characterization of a Thermoplastic Elastomer. *Rubber Chem Technol*. 2017;90(2):367-380. doi:10.5254/rct.17.83780
6. Bonart R. X-ray investigations concerning the physical structure of cross-linking in segmented urethane elastomers. *J Macromol Sci Part B*. 1968;2(1):115-138. doi:10.1080/00222346808212867
7. Toki S, Hsiao BS, Kohjiya S, Tosaka M, Tsou AH, Datta S. Synchrotron X-Ray Studies of Vulcanized Rubbers and Thermoplastic Elastomers. *Rubber Chem Technol*. 2011;79(3):460-488. doi:10.5254/1.3547946
8. J.W.C Van Bogart, A. Lilaonitkul SLC. Morphology and properties of segmented polyether poly(urethaneureas). *Am Chem Soc*. 1979. doi:10.1295/polymj.17.969
9. Yeh F, Hsiao BS, Sauer BB, Michel S, Siesler HW. In-situ studies of structure development during deformation of a segmented poly(urethane-urea) elastomer. *Macromolecules*. 2003;36(6):1940-1954. doi:10.1021/ma0214456
10. Mars, W. V., Fatemi A. Factors That Affect the Fatigue Life of Rubber. *History*. 2004;77(3):419-423. doi:10.5254/1.3547831
11. Y. Marco, I. Masquelier, V. Le Saux and PC. Fast prediction of the wöhler curve from thermal measurements for a wide range of nr and sbr compounds. *Rubber Chem Technol*. 2016.
12. Cadwell SM, Merrill RA, Sloman CM, Yost FL. Dynamic Fatigue Life of Rubber. *Ind Eng Chem - Anal Ed*. 1940;12(1):19-23. doi:10.1021/ac50141a006
13. Thomas a. G. Rupture of Rubber V Cut Growth in Natural Rubber Vulcanizates. *Rubber Chem Technol*. 1958;32(2):477-489. doi:10.5254/1.3542412
14. Lake GJ. Fatigue and Fracture of Elastomers. *Rubber Chem Technol*. 1995;68(3):435-460.

doi:10.5254/1.3538750

15. Rivlin RS, Thomas AG. Rupture of rubber. I. Characteristic energy for tearing. *J Polym Sci*. 1953;10(3):291-318. doi:10.1002/pol.1953.120100303
16. Yeoh OH. Fracture Mechanics of Bond Failure in the “Pure Shear” Test Piece. *Rubber Chem Technol*. 2003;76(2):483-494. doi:10.5254/1.3547755
17. Lake GJ, Lindley PB. Mechanical Fatigue Limit for Rubber. *J Appl Polym Sci*. 1965;9:1233-1251. doi:10.5254/1.3544847
18. Mzabi S. Caractérisation et analyse des mécanismes de fracture en fatigue des élastomères chargés. 2010:1-310.
19. Strobl GR, Schneider M. Direct Evaluation of the Electron Density Correlation Function of Partially Crystalline Polymers. *J Polym Sci Part A-2, Polym Phys*. 1980;18(6):1343-1359. doi:10.1002/pol.1980.180180614
20. Koberstein JT, Russell TP. Simultaneous SAXS-DSC Study of Multiple Endothermic Behavior in Polyether-Based Polyurethane Block Copolymers. *Macromolecules*. 1986;19(3):714-720. doi:10.1021/ma00157a039
21. Zhang E, Bai R, Morelle XP, Suo Z. Fatigue fracture of nearly elastic hydrogels. *Soft Matter*. 2018;14(18):3563-3571. doi:10.1039/c8sm00460a
22. Sun JY, Zhao X, Illeperuma WRK, et al. Highly stretchable and tough hydrogels. *Nature*. 2012;489(7414):133-136. doi:10.1038/nature11409
23. Payne AR. Hysteresis in rubber vulcanizates. *J Polym Sci Polym Symp*. 1974;48(1):169-196. doi:10.1002/polc.5070480114
24. Morishita Y, Tsunoda K, Urayama K. Velocity transition in the crack growth dynamics of filled elastomers: Contributions of nonlinear viscoelasticity. *Phys Rev E*. 2016;93(4):1-11. doi:10.1103/PhysRevE.93.043001
25. Persson BNJ, Brener EA. Crack propagation in viscoelastic solids. 2005;(June 2004):1-8. doi:10.1103/PhysRevE.71.036123
26. Sui T, Salvati E, Ying S, et al. Strain softening of nano-scale fuzzy interfaces causes Mullins effect in thermoplastic polyurethane. *Sci Rep*. 2017;7(1):1-9. doi:10.1038/s41598-017-00904-3
27. Qi HJ, Boyce MC. Stress-strain behavior of thermoplastic polyurethanes. *Mech Mater*. 2005;37(8):817-839. doi:10.1016/j.mechmat.2004.08.001
28. Mullins L. Softening of rubber by displacement. *Rubber Chem Technol*. 1969;42(1):339-362.
29. Diani J, Fayolle B, Gilormini P, Diani J, Fayolle B, Gilormini P. A review on the Mullins effect

To cite this version : HAL Id : hal-00773015. 2013:601-612.

30. Zhang W, Liu X, Wang J, et al. Fatigue of double-network hydrogels. *Eng Fract Mech*. 2018;187:74-93. doi:10.1016/j.engfracmech.2017.10.018
31. Bai R, Yang Q, Tang J, Morelle XP, Vlassak J, Suo Z. Fatigue fracture of tough hydrogels. *Extrem Mech Lett*. 2017;15:91-96. doi:10.1016/j.eml.2017.07.002
32. Lake, G. J. Lindely PB. Cut growth and fatigue of rubbers. 1964;455(2):292-300.
33. Lake GJ, Lindley PB, Natural T, Producers R. Fatigue of Rubber at Low Strains. 1966;10:343-351.
34. Bhowmick AK. Threshold Fracture of Elastomers. *J Macromol Sci Part C*. 1988;28(3-4):339-370. doi:10.1080/15583728808085379
35. Creton C, Ciccotti M. Fracture and adhesion of soft materials: A review. *Reports Prog Phys*. 2016;79(4):46601. doi:10.1088/0034-4885/79/4/046601
36. Lake GJ, Thomas AG. The Strength of Highly Elastic Materials. *Proc R Soc A Math Phys Eng Sci*. 1967;300(1460):108-119. doi:10.1098/rspa.1967.0160
37. Li C, Yang H, Suo Z, Tang J. Fatigue-Resistant elastomers. *J Mech Phys Solids*. 2020;134:1-12. doi:10.1016/j.jmps.2019.103751
38. Xiang C, Wang Z, Yang C, Yao X, Wang Y, Suo Z. Stretchable and fatigue-resistant materials. *Mater Today*. 2019;(September). doi:10.1016/j.mattod.2019.08.009
39. Wang Z, Xiang C, Yao X, Le P, Mendez J, Suo Z. Stretchable materials of high toughness and low hysteresis. 2018;116(13):5967-5972. doi:10.1073/pnas.1821420116

8 MECHANICAL PROPERTIES OF SOFT TPU AND STRAIN INDUCED STRENGTHENING

Mechanical properties of Soft Thermoplastic Polyurethanes: effect of morphology on large strain behaviour and strain-induced strengthening.

Giorgia Scetta[1], Jianzhu Ju[1], Nathan Selles[2], Patrick Heuillet[2], Matteo Ciccotti[1] and Costantino Creton*[1]*

[1]Sciences et Ingénierie de la Matière Molle, ESPCI Paris, Université PSL, CNRS, Sorbonne Université, 75005, Paris, France.

[2]Laboratoire de Recherches et de Contrôle du Caoutchouc et des Plastiques, 60, Rue Auber 94408 Vitry-sur-Seine, France

matteo.ciccotti@espci.psl.eu, Costantino.creton@espci.psl.eu

8.1 Abstract

The cyclic mechanical response of three soft TPUs (linear modulus <10MPa) was investigated. Their physical structure was analyzed with X-ray scattering (SAXS and WAXD) revealing differences in their crystallinity and the presence of Polybutylene terephthalate (PBT) in a TPU based on soft aliphatic polyester. While different large strain properties were measured for the three TPU in uniaxial strain, they all present similarities in their inelastic behavior (such as residual deformation after unloading and fraction of dissipated energy) in cyclic conditions. All TPUs present a first cycle softening that is qualitatively similar to what is commonly found in filled rubbers but is hardly related to the concept of strain-induced damage in cyclic loading as has been done in case of conventional crosslinked rubbers. In fact, the application of step-strain cycles results in a marked stiffening effect in all TPU when measured in a true stress/Hencky strain representation. The generality of the phenomenon suggests that this stiffening is probably associated to the restructuring of hard domains with applied strain and the generation of a permanent modification of the structure associated with a residual plastic deformation.

8.2 Introduction

Thermoplastic polyurethane elastomers (TPU) were first introduced to the market around 1960 and experienced a rapid diffusion since then[1]. Soft TPU are multiblock copolymers characterized by alternating soft segments (SS) and hard segments (HS) forming a two-phase microstructure where the soft phase is the majority. The microphase separation between soft and hard segments is driven by the ability of the hard segments to form inter and intra-chain

hydrogen bonds between carbonyl and amine groups developing therefore small stiff domains surrounded by the soft phase. Depending on chemical composition, molecular weight and steric hindrance, the phase separation is more or less complete. Hard domains have a typical size of 5-30 nm and are stiffer than soft domains acting both as nanoscale fillers and physical crosslinks[2,3]. Soft TPU are well known for their outstanding combination of reversible elasticity, abrasion resistance and easy processability. Additionally, the absence of chemical crosslinking allows these soft TPU to be re-shaped and re-used contrary to thermoset rubbers that are difficult to recycle. Despite the much higher material cost, the versatile processing, recyclability and comparable reversible elasticity make TPU a serious competitor to replace elastomers in a number of technical applications. It is not surprising then, that several studies on TPU mainly concentrated on the correlation between composition of TPU and mechanical properties at small and large strain [2,4–6] with the target to further explore the field of applications of this class of materials. It is generally accepted that the thermoplastic nature of TPUs, results in a higher viscoelastic dissipation, compared to thermoset rubbers, that may explain their high fracture resistance[7–9]. In particular, the presence of higher energy losses and stress softening during the first loading-unloading cycle (Mullins effect) have been observed in unfilled TPU[4,10]. The Mullins effect was first detected in filled (or crystallizing) rubbers[11] and despite its relevance for final rubber properties, its origin is still debated and may depend on the detailed structure of the material. It is generally accepted however, that the first cycle hysteresis comes in particular from structural rearrangements of filler aggregates[12].

Recently, a mechanical behavior with the same characteristics as those of the Mullins effect was observed also in other unfilled systems such as double network hydrogels[13] and semi-crystalline materials [14] that have in common the presence of inhomogeneities in their structure. In the case of unfilled TPU, this phenomenon has been often associated with changes in the hard-soft domains structure of TPU with applied strain[3,4,15,16]. The majority of the studies of cyclic dissipation in TPU mostly concentrate on the qualitative effect of composition or strain rate on the macroscopic mechanical behaviour without providing any useful tool to interpret this strain-induced damage in molecular or microscopic terms. Yet, the Mullins effect has been extensively investigated in rubbers[17] and recently, Merckel and co-workers [18] proposed an easy methodology to quantify the Mullins contribution that allows an easy comparison between different materials. They worked on filled styrene-butadiene-styrene rubber (SBR) cyclically strained at different, medium to large, strain levels and they introduced two damage parameters: one to account for the reduction in linear modulus with applied strain and the other to account

for the change in the onset of strain hardening with increasing strain, as induced by a loading at larger strain. They showed that, for filled elastomers, these two parameters have the same dependence on strain and also have very similar values. This led them to conclude that in filled elastomers, small and large strain damage are two manifestations of a single phenomenon. We used the above-mentioned methodology [18] to quantitatively evaluate the effect of repeated cycles on the inelastic characteristics of TPU. Furthermore, we proposed a comparison between TPU and filled SBR, emphasizing similarities between these two classes of materials often associated in terms of small and large strain elasticity, but with completely different structures and large strain behaviours.

8.3 Materials and methods

8.3.1 Materials

The three TPU used in this work are polyester based polyurethanes with commercial names EC 60 A 10P , LP9 277 10 and 565 A 12P respectively produced by BASF in the Elastollan© series. We labeled them TPU_HARD, TPU_SOFT and TPU_XTAL respectively, to underline the difference in their large strain behavior as will be discussed in the experimental part. Their glass transition temperature T_g measured by differential scanning calorimetry (DSC at 10°/min) is reported in Table 8-1.

Table 8-1 Glass transition temperature for all TPUs

Sample	TPU_HARD	TPU_SOFT	TPU_XTAL
Tg a 10°/min °C	-50	-48	-34

The chemical composition was not available since they are commercial products. The number average molar mass (M_n) and polydispersity index (PDI) as measured on samples after injection is reported in Table 8-2 and was obtained using gel permeation chromatography (GPC) with THF as carrier solvent. TPU_SOFT was not soluble in THF. From our previous investigation (see Annexes) TPU_SOFT seems to be a blend between a TPU and polybutylene terephthalate (PBT) with small quantity of urea that may explain the les good solubility in a solvent like THF.

Table 8-2 Average Molar mass and polydispersity index of used TPU

Name	Mn [Kg/mol]	PDI
TPU_XTAL	47.09	1.3
TPU_HARD	83.02	1.4
TPU_SOFT	Not soluble in THF	Not soluble in THF

Specimens were injected by the Laboratory of Research and Control of Caoutchouc and Plastics (LRCCP) into 2 mm thick large square-plate from which tensile dog-bone samples (cross section of 2x4 mm) were cut. The temperatures used in the injection molding procedure are summarized in Table 8-3 for all samples as recommended by BASF.

Table 8-3 Barrel temperature profile for injection procedure. Zone 1 to 4 goes from the rear to the front of the barrel

Barrel / Name	Zone 1 (°C)	Zone2(°C)	Zone4(°C)	Nozzle (°C)	Mould (°C)
TPU_XTAL	170	180	190	185	30
TPU_SOFT	190	200	205	200	30
TPU_HARD	165	170	175	170	30

The SBR rubber is filled with carbon black (CB) and all data concerning that rubber comes from the work of Mzabi et al.[19,20]. The unvulcanised SBR has a mass M_w of 120 kg/mol and a polydispersity of 1.94 and was provided by Michelin. Its styrene content is 15 wt % and the glass transition temperature T_g measured by differential scanning calorimetry (DSC at 10°/min) is -48°C. The detailed composition is reported in Table 8-4 as provided by Michelin. All samples were prepared, moulded and cured by Michelin. For tensile tests, samples where cut in a dog-bone shape and cross section of 2x4mm and loaded with a strain rate of $4s^{-1}$.

Table 8-4 SBR composition in PHR. Filler content and crosslinking density are reported in volumetric fraction. Data from [19] Note that N347 is a type of carbon black, Sulfur is a crosslinking agent, Struktol™ and N-Cyclohexyl-2-benzothiazole sulfenamide (CBS) are accelerators to vulcanize the rubber, and N-(1,3-dimethylbutyl)-N'-phenyl-p-phenylenediamine (6PPD) is an anti-oxidant.

	20CB_19XL
SBR	100
N347	5
6PPD	1
Struktol	3
CBS	1.5
Sulfur	1.5
ϕ	0.03
ν	8.1*10-5

8.3.2 Structural study

Information on the physical structure of nanodomains was obtained by X-Ray analysis using the facilities of the materials science center of DSM, Netherlands. The beam wavelength was 0.154nm. The 2D data were integrated using "FIT-2D"[21] software. All data were corrected by subtracting background scattering and circularly integrated to obtain 1D profile. SAXS data was expressed in terms of wave vector $q = \frac{4\pi sin\theta}{\nu}$ where 2θ is the scattering angle and ν is the wavelength.

The long period or inter-hard domain distance was evaluated in two ways: using the peak of scattering (Bragg's law) and using the correlation function on the SAXS intensity I(q).

For Bragg's law the long period (d) was evaluated as the position of the maximum in 1D SAXS profile q* as $d = \frac{2\pi}{q^*}$.

The correlation function has the form of Equation 8-1 and this approach is based on a two-phase, lamellar morphology[22] . The evaluation of Equation 8-1 requires the extrapolation of the data at $q \rightarrow \infty$ and $q \rightarrow 0$ and an integration. The data were extrapolated using Porod's law I $\approx q^4$ and Guinier's law: I≈A+Bq respectively.

$$K(x) = \int_0^\infty 4\pi q^2 I(q)\cos(2\pi q x)\, d \qquad \textbf{Equation 8-1}$$

This analysis of the correlation curve in Figure 8-1 was used to identify different parameters such as the long period (L) the crystalline layer thickness (C) and an estimated bulk volume crystallinity (ϕ) graphically indicated in Figure 8-1

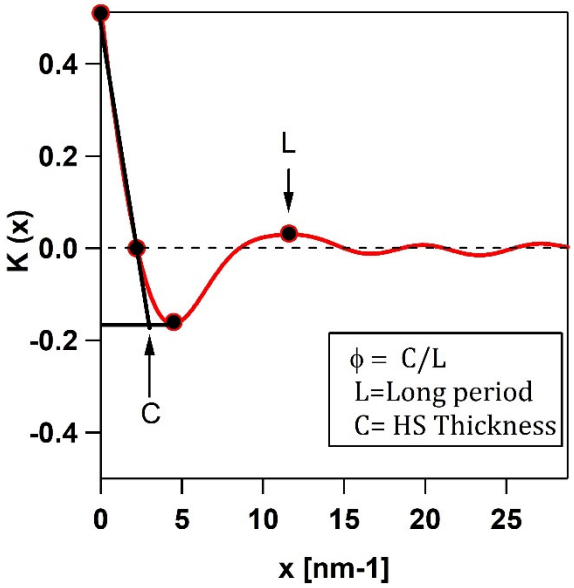

Figure 8-1 Example of correlation function and interpretation of its features for TPU_HARD based on the analysis of Strobl and Schneider [22]

8.3.3 Mechanical testing

8.3.3.1 Dynamical Mechanical Analysis

DMA analyses were performed on the instrument Metravib DMA+400, FR. The measurements were carried out at 10Hz over a temperature range from -80°C to 80°C with a heating rate of 10°C/min.

8.3.3.2 Step-Cycle Tests

The two edges of the dog-bone shaped samples were strongly fixed between mechanical clamps. An optical system was used to measure the local stretch in the gauge area of the sample and check the absence of slippage from the clamps during the test. The samples were strained in uniaxial conditions at the stretch rate of $\dot{\lambda} = 4\ s^{-1}$. The elongation was performed in a stepwise mode: 5 or 10 cycles were performed for each increasing value of maximum stretch for SBR and TPU respectively. The force was reduced to σ=0 between two successive steps. Strain (ε),

stretch (λ), Hencky strain (h), stress (σ) and true stress (T) are defined as below with l_0 and l indicating the initial length and instantaneous length respectively, A_0 the initial cross section area and F the measured force.

$$\varepsilon = \frac{l-l_0}{l_0} \quad \lambda = \frac{l}{l_0} \quad \sigma = \frac{F}{A_0}$$

$$T = \sigma * (1+\varepsilon) \quad h=\ln(\lambda)$$

In particular the Hencky strain derives from the sum of the incremental strain $\delta\varepsilon = \frac{\delta l}{l}$ and is obtained integrating this incremental strain between the initial and the final length of the sample: $\int_{l_0}^{l} d\varepsilon = \ln(\lambda)$.

8.3.4 Thermal analysis

Thermal properties of TPUs were studied by digital scanning calorimetry (DSC) (TA instrument, Q200 device, USA). The samples were heated first from ambient temperature to a maximum temperature (T1) that corresponds to 200°C and 100°C respectively for TPU and SBR and maintained at this temperature for 3 minutes. They were then cooled to -100°C and finally re-heated to the maximum temperature T_1. Both cooling and heating rates were fixed at 10°C/min. Thermal scans were performed on pristine and strained samples.

8.4 Mechanical testing and Structural Investigations

8.4.1 Mechanical characterization

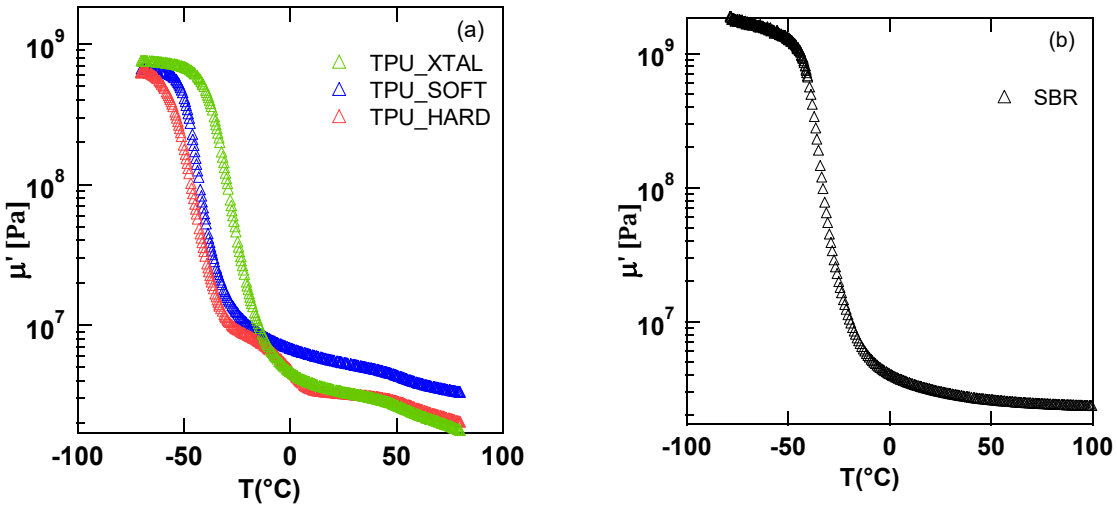

Figure 8-2 Storage modulus VS temperature for three TPUs (A) and for a SBR (B)

Figure 8-2 shows the temperature dependence of the storage modulus for all TPUs and for SBR. All materials display a drop in the modulus of almost 3 decades indicating the transition from a glassy to a rubbery state. The main difference between TPU and SBR is the variation of the low modulus in the rubbery state that decreases faster for all TPUs compared to that of filled SBR. The presence of chemical crosslinks in SBR ensures a higher temperature stability than the physical crosslinking present in TPU. An increase in temperature may induce partial debonding of inter-urethane hydrogen interactions (that ensure HD stability) leading to a faster reduction in modulus for temperatures higher than their melting temperature T_g. TPU_SOFT shows the highest and most stable plateau at high temperature indicating greater stability in hard-segment domains.

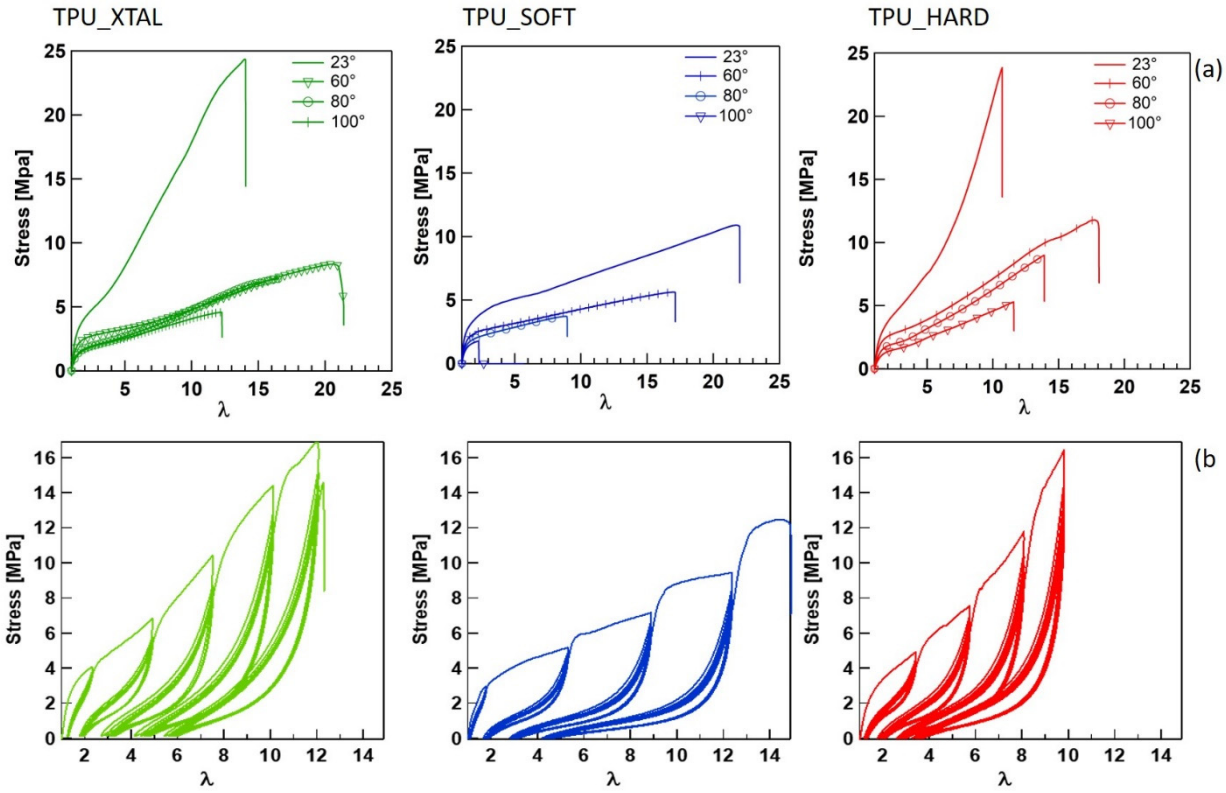

Figure 8-3 Uniaxial stress-strain curves at different temperatures (a) and cyclic stretch-stress curve at 23° (b) for three TPUs.

Figure 8-3(a) shows the uniaxial engineering stress-stretch curves for the three TPUs at different temperatures. All TPUs are characterized by a high extensibility at failure. The linear regime is only observed for a few percent of deformation. Above this limit all three materials show first a strain softening. Then TPU_XTAL and TPU_HARD show a marked strain

hardening that is less intense in TPU_SOFT. The effect of increasing the temperature is mainly that of reducing the stress at break σ_b for all materials and, in case of TPU_SOFT also to reduce its maximum extensibility. This reduction of mechanical performance with temperature was already observed in some other classes of thermoplastic elastomers as reported by Aime [23] for thermoplastic elastomer (TPE) based on PBT as hard segment that confirms the hypothesis of the blend with PBT for TPU_SOFT.

Figure 8-3 (b) reports stress-strain curves of uniaxial step-strain cyclic test for all TPUs at 23°. All curves present similar characteristics:

i) Unloading and reloading paths during the first cycle at a higher stretch significantly differ (large hysteresis).
ii) There is a very pronounced softening after the first loading, and the envelope of the monotonic test behavior is recovered only when the material is stretched to higher values than those previously applied (Mullin's effect).
iii) A marked residual deformation (λ_{res}) is visible after unloading.

This large residual deformation λ_{res} is consistent with literature data on TPU [4,5] and is probably related to the absence of chemically crosslinked points and the possible plastic deformation of the hard domains with applied strain. The Table 8-5 summarizes the principal mechanical properties for all TPUs.

Table 8-5 Young modulus, stretch and stress at break for all TPUs at 23 , 60, 80°. *At the maximum displacement allowed by the capacity of the testing machine the sample did not break.

	23°C			**60°C**			**80°C**		
Name	E [MPa]	λ_b	σ_b [MPa]	E [MPa]	λ_b	σ_b [MPa]	E [MPa]	λ_b	σ_b [MPa]
TPU_XTAL	8.7 ±0.1	15.4 ±1.2	25.1 ±1.3	5.03 ±0.7	>20*	>8*	3.8 ±0.1	>18*	>7*
TPU_SOFT	7.8 ±0.1	17.7 ±1.5	11.8 ±0.5	5.8 ±0.1	17.0 ±0.6	5.4 ±0.2	5.2 ±0.8	3.7 ±0.1	8.9 ±1.9
TPU_HARD	7.3 ± 0.1	10.8 ±1.9	24.7 ±2.3	5.7 ±0.1	19.2 ±0.7	12.6 ±2.1	4.1 ±0.3	7.1 ±3.3	16.2 ±1.2

Figure 8-4(a) summarizes the values of λ_{res} VS λ_{max} for all TPUs (at 23°C and 60°C) and for SBR. A surprisingly simple and uniquely linear relationship between residual and maximum applied strain can be observed for all three TPU with some major deviations for TPU_HARD. All values of λ_{res} in SBR, for comparable $\lambda_{max,}$ are considerably smaller since the chemical crosslinking prevents plastic deformation.

In Figure 8-4 (b) we plot the fraction of dissipated energy per cycle for the 10^{th} cycle, i.e. in nearly steady state situation, for each value of increasing strain. The fraction of the provided energy that is effectively dissipated per cycle, weakly depends on the magnitude of the strain and is only shifted at slightly lower values increasing testing temperature from 23° to 60° for all three TPUs. One interesting result is that, for comparable values of applied deformation, the fraction of dissipated energy in SBR is comparable or higher than that of TPUs at 23°. This behavior is counter-intuitive if we consider that, unlike SBR, TPUs have hard domains which can be plastically deformed under strain. The absence of an excessive mechanical dissipation in a stabilized cycle in TPU is a very important aspect especially in applications requiring repeated cycles in time. In this case in fact, an excessive energy dissipation is not only intrinsically undesirable but may lead to local heat build-up especially in weakly conductive materials such as rubbers and TPUs.

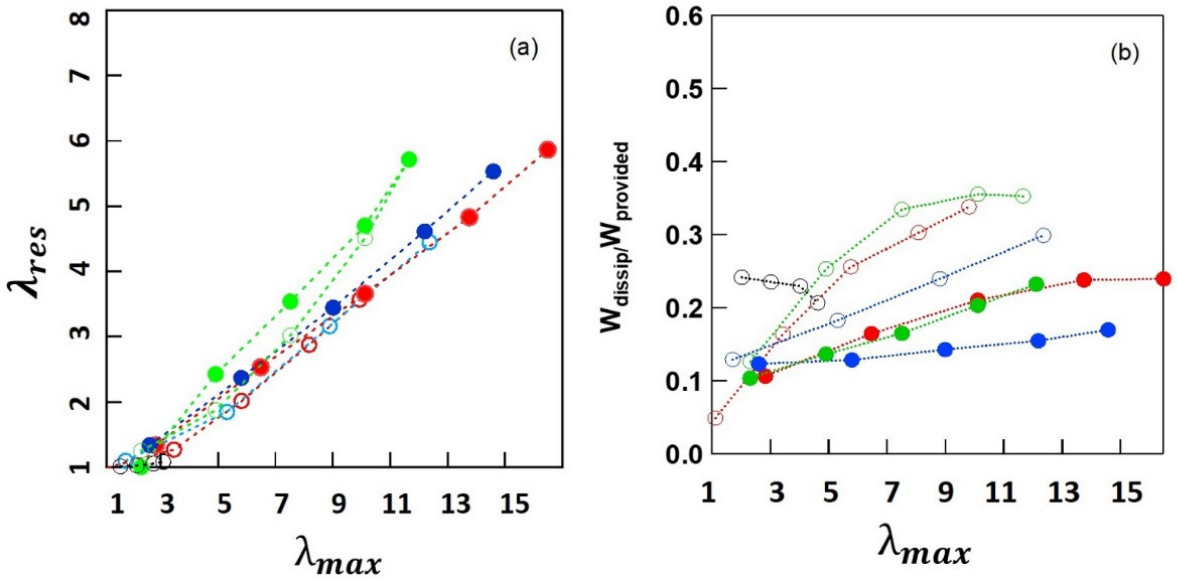

Figure 8-4: (a) Residual VS applied deformation and (b) ratio between dissipated and provided energy during the 10th cycle for all materials. At 23° for: TPU_XTAL, TPU_SOFT, TPU_HARD, SBR and at 60° for: TPU_XTAL TPU_SOFT TPU_HARD.

8.4.2 Structural investigations

WAXS 1D intensity profile are shown in Figure 8-5 for all three soft TPU (data were vertically shifted for readability). The absence of any crystalline reflection in TPU_XTAL and TPU_HARD indicate a completely amorphous hard phase. The crystalline peaks (indicated by the arrows) in TPU_SOFT are compatible with the crystalline structure of PBT as indicated by literature[24,25].

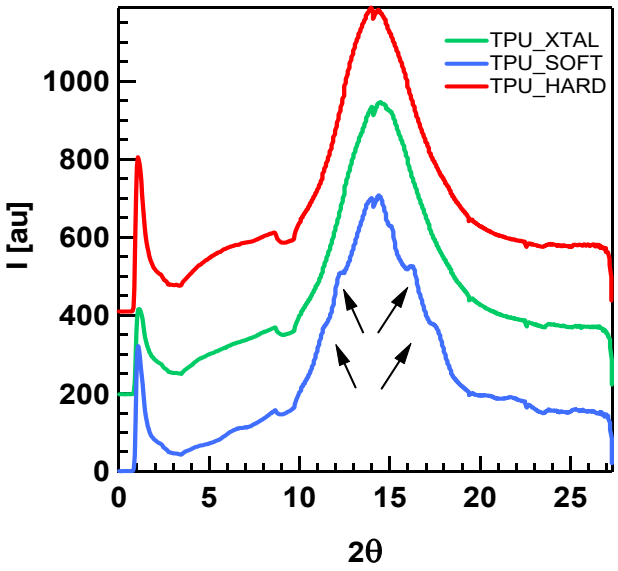

Figure 8-5 WAXS pattern for pristine TPU_XTAL, TPU_SOFT and TPU_HARD

2D SAXS images and the corresponding integrated profiles are reported in Figure 8-6. All curves are characterized by a maximum in the intensity that represents the long-range correlation of hard-domains (or long period) due to microphase separation in TPU[26] .

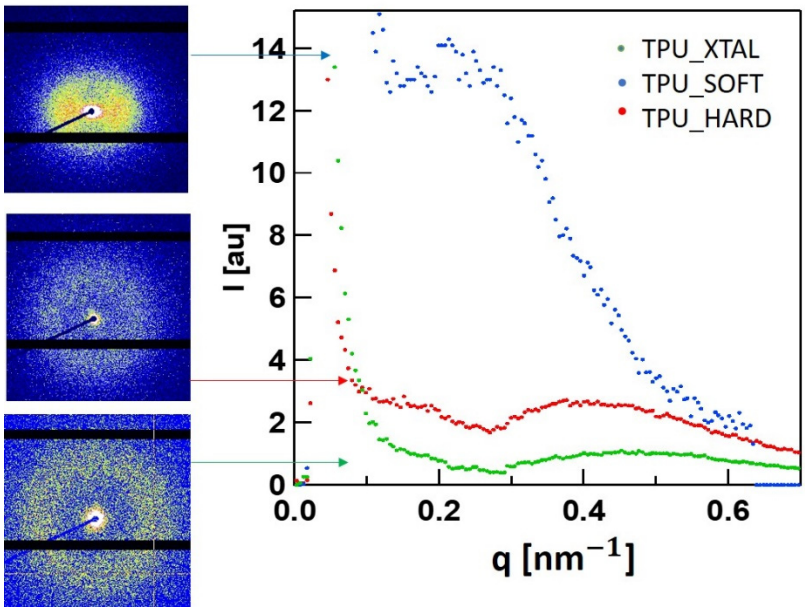

Figure 8-6 2D Pattern and 1D integrating profile for all TPUs.

The data of the long period (calculated from Bragg's law and indicated as *d* and from the analysis of the correlation function K(x), indicated as L (when possible), are reported in Table 8-6. A schematic of the polymer structure as considered for the correlation analysis is reported

in Figure 8-7.

Table 8-6 ID SAXS images and inter-domain spacing, domains thickness, hard segment volume fraction.

	L nm	***d*(Bragg's) nm**	**C nm**	**ϕ**
TPU_XTAL	11.8	13.4	2.9	0.24
TPU_SOFT	-	29.9	-	-
TPU_HARD	12.3	15	2.9	0.24

Comparable values of d (between 10-30nm) are reported in the literature for similar phase-separated TPU systems [4,27,28]. TPU_SOFT has an elliptical SAXS pattern (Figure 8-6) indicating the presence of a preferential orientation in the lamellae (probably induced by injection) that makes the lamellar model inappropriate. The analysis of the correlation function in fact, is based on the hypothesis of random orientation of lamellae. The similarity between the value of the long period evaluated with Bragg's law and with the correlation function in TPU_XTAL and TPU_HARD is indicative of the good reliability of the correlation analysis (lamellar method). The strong similarity in ϕ and C between the two TPUs (Table 8-6) confirms that they possess a similar thickness of hard domains (C) and comparable hard segment volume fraction ϕ as suggested by the similar linear modulus. The higher L for TPU_SOFT confirms the presence of some major structural difference compared to TPU_XTAL and TPU_HARD in agreement with our hypothesis of a blend of TPU-PBT.

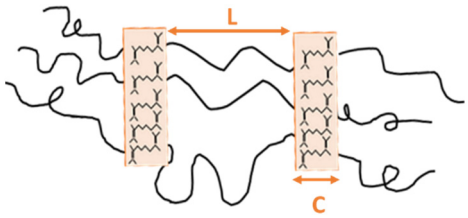

Figure 8-7 Schematic illustrating the parameter extracted from the correlation analysis L (long period between hard domain) and C (thickness of the hard phase).

8.4.3 Thermal analysis

Figure 8-8 reports the DSC thermogram carried out both on all pristine TPUs (a) and on the fractured part of samples strained up to rupture (b). Pristine TPU_HARD and TPU_XTAL are essentially amorphous as witnessed by the absence of melting peak in their thermogram. On the contrary, TPU_SOFT presents a visible melting peak around 190°C (indicated by the arrow) which is attributed to PBT crystals whose melting peak is around 200°C (higher for pure PBT and lower for blends) [29,30].

For strained TPU, Figure 8-8 (b) on the other hand, it appears a clear the endothermic peak (T_{mSIC}) in the originally amorphous TPU_XTAL. This peak is associated to the new crystalline phase generated during uniaxial tension in TPU_XTAL as consequence of the strain induced crystallization phenomenon (SIC). SIC consists in the progressive alignment of polymer chains, for an original amorphous polymer, into an ordered and crystalline structure with increase of applied strain. In case of TPU, unlike what is generally observed in crosslinked rubbers, SIC can be partially retained after the removal of strain and residual crystalline fraction can still be observed in the unloaded polymer [31–33]. The smaller endothermic peak in TPU_SOFT after strain (T_{mPBT}) may be associated to original PBT crystal that were broken in smaller dimension with applied strain.

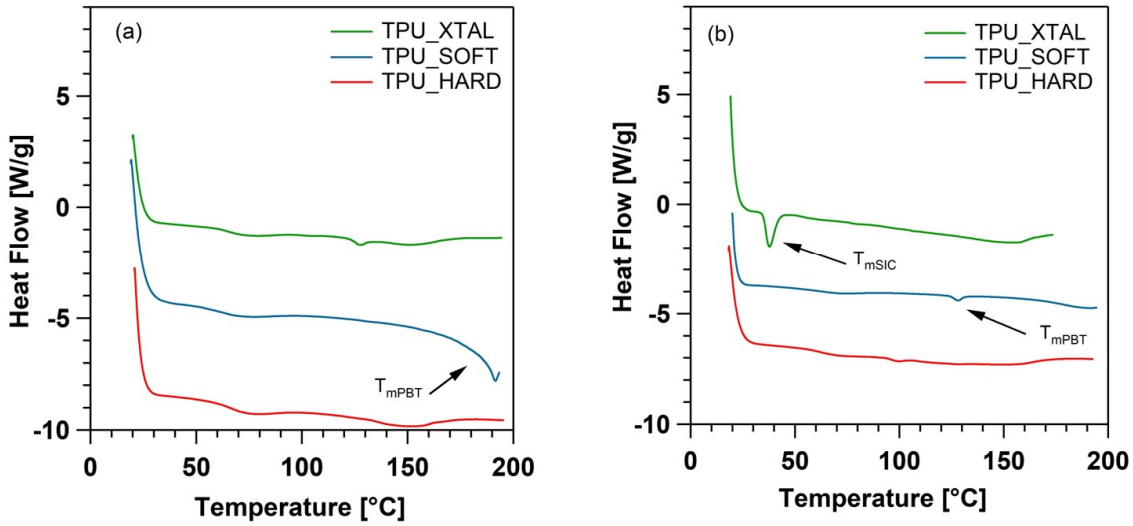

Figure 8-8 DSC thermogram for all TPU pristine (a) and after being strained to rupture (b)

8.5 Damage analysis in cyclic loading

8.5.1 Strain-Induced Damage in filled SBR

Figure 8-9 reports an example of cyclic stress-strain curve for TPU_HARD and SBR in the Hencky strain VS true stress representation.

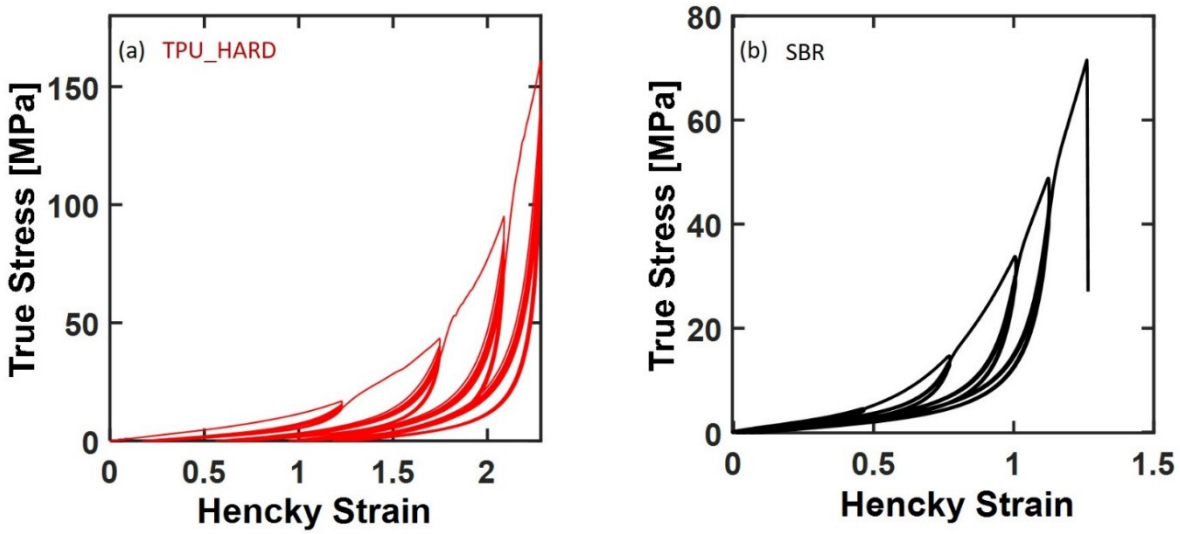

Figure 8-9 True Stress-Hencky strain representation of Cyclic experiment for TPU_XTAL (a) and SBR(b).

We used the approach proposed by Merckel et al.[18] to estimate the damage in both our unfilled TPU and filled SBR in terms of large strain damage (D_{ls}) and small strain damage (D_{ss}) as detailed in the following.

The value of D_{ss} for each increasing maximum strain (k), is obtained from the ratio between the linear modulus for the cycle (E_k) and that of the pristine material (E_0) so that:

$$D_{ss} = 1 - \frac{E_k}{E_0} \qquad \textbf{Equation 8-2}$$

Figure 8-10 (a) shows an example of linear fitting used to calculate E. The values of the fitted modulus calculated for all TPUs and SBR are shown in Figure 8-10 (b). The higher values of maximum Hencky strain at which the modulus was evaluated for TPUs are justified by their higher maximum extensibility compared to SBR. In the case of SBR, E always decreases with maximum applied strain. In all TPU, on the other hand, E initially decreases and, for Hencky strains higher than 1.5 (λ~4), E increases again reaching the pristine value or even higher in case of TPU_XTAL.

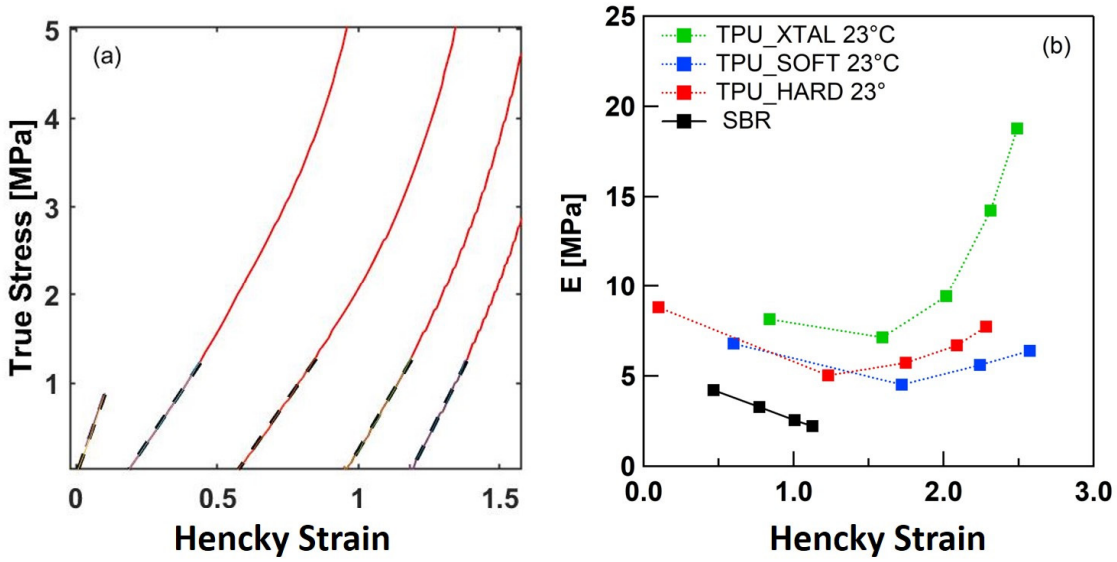

Figure 8-10 Example of linear fitting of calculated E for TPU_HARD(a). E vs Hencky strain for all TPUs and SBR (b)

The large strain damage or D_{ls} is on the other hand associated to the onset of strain hardening in cyclic loading at different maximum strain and is defined as:

$$D_{ls} = 1 - \alpha \qquad \textbf{Equation 8-3}$$

where α is a re-scaling factor on the Hencky strain obtained as follows. Each unloading curve

is first shifted to the origin to compensate for the residual strain (Figure 8-11 (a-c)). This step is considerably important especially for materials, as TPU, which present remarkable residual strain when unloaded. Shifting the stress-strain curve on the origin in fact, we obtain the same curve which a user, unaware of the previous history, would measure experimentally.

Then a master-curve is built by performing a superposition fit using a least square minimization of each unloading curve using the first loading curve as a reference (Figure 8-11 (b-d)). This is mathematically equivalent to write $h_{virgin} = \alpha * h_{shifted}$

The shifted curves reported for TPU_HARD and SBR in Figure 8-11 (a-c) demonstrate the different effect on the onset of strain hardening (approximatively indicated as λ_{hard}) between TPU_HARD and SBR. Unlike to SBR, each unloading curve in TPU_HARD for the step k+1 displays an onset of strain hardening at comparable or lower strain than step k. This has a strong influence on the described rescaling procedure as we'll be clarified by the different resulting values of the damage parameter D_{ls} between SBR and TPUs.

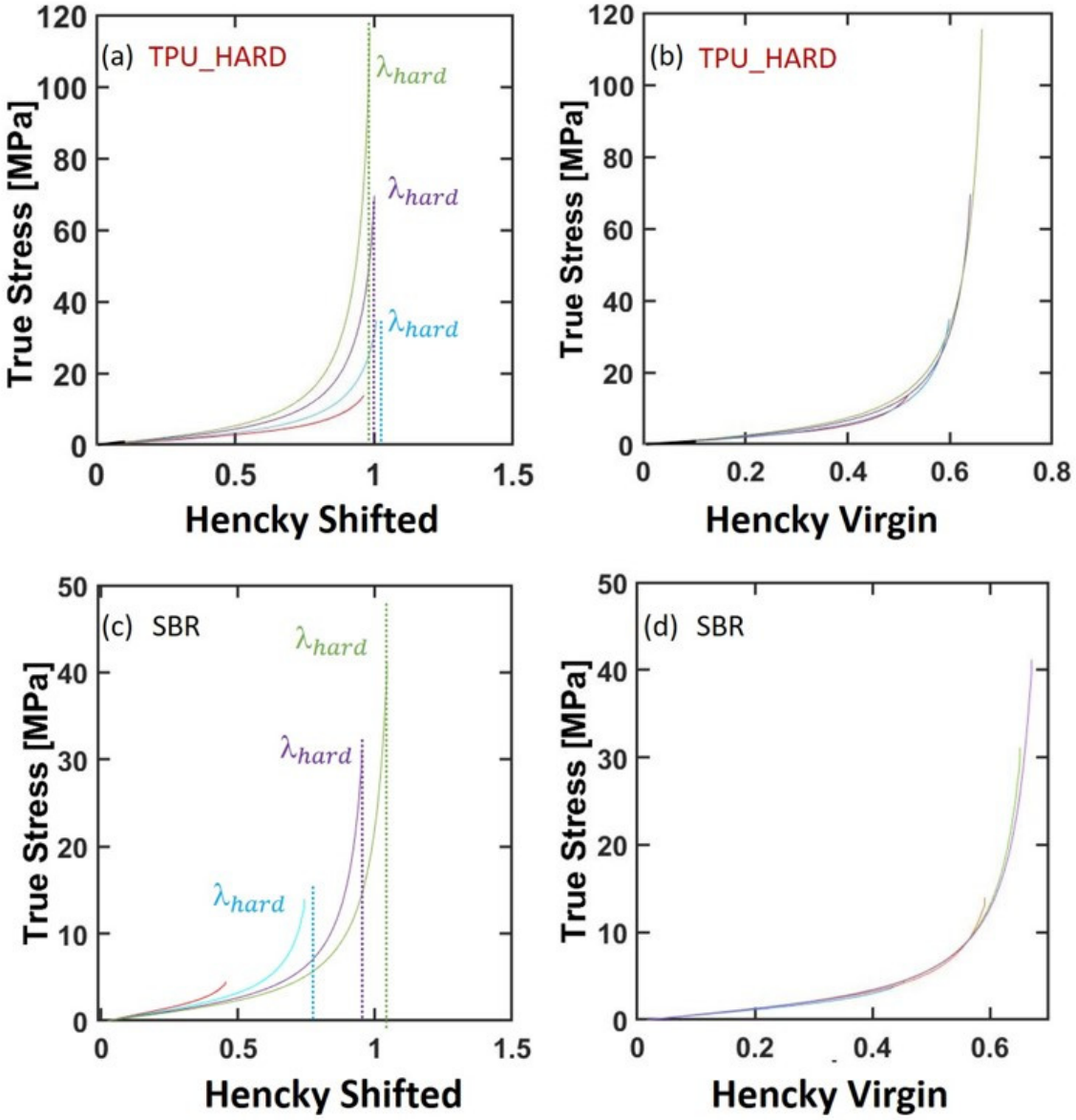

Figure 8-11 Example of True stress VS Hencky Shifted (a-c) and True Stress VS Hencky Virgin (b-d) respectively for TPU_HARD and SBR. The line represent an estimation of the onset of strain hardening and are used for guiding the eyes.

Figure 8-12a,b,c reports the calculated values of D_{ss} and D_{ls} for SBR at 23° and for all three TPUs at 23 and 60°. The trend is substantially different between SBR (where both D_{ss} and D_{sl} similarly increase with strain) and for the TPU. In all TPU D_{ss} and D_{sl} have a dependence on the maximum Hencky strain that is qualitatively similar to that we just discussed for the linear modulus. Both damage parameters first increase (softening) and then decrease (stiffening) eventually becoming negative in case of TPU_XTAL. At 60° this trend is even more evident and all values are negative. This means that the damage due to plastic deformation stiffens the

TPU and does not soften it, at least in uniaxial tension, and the damage in small and large strain are decoupled.

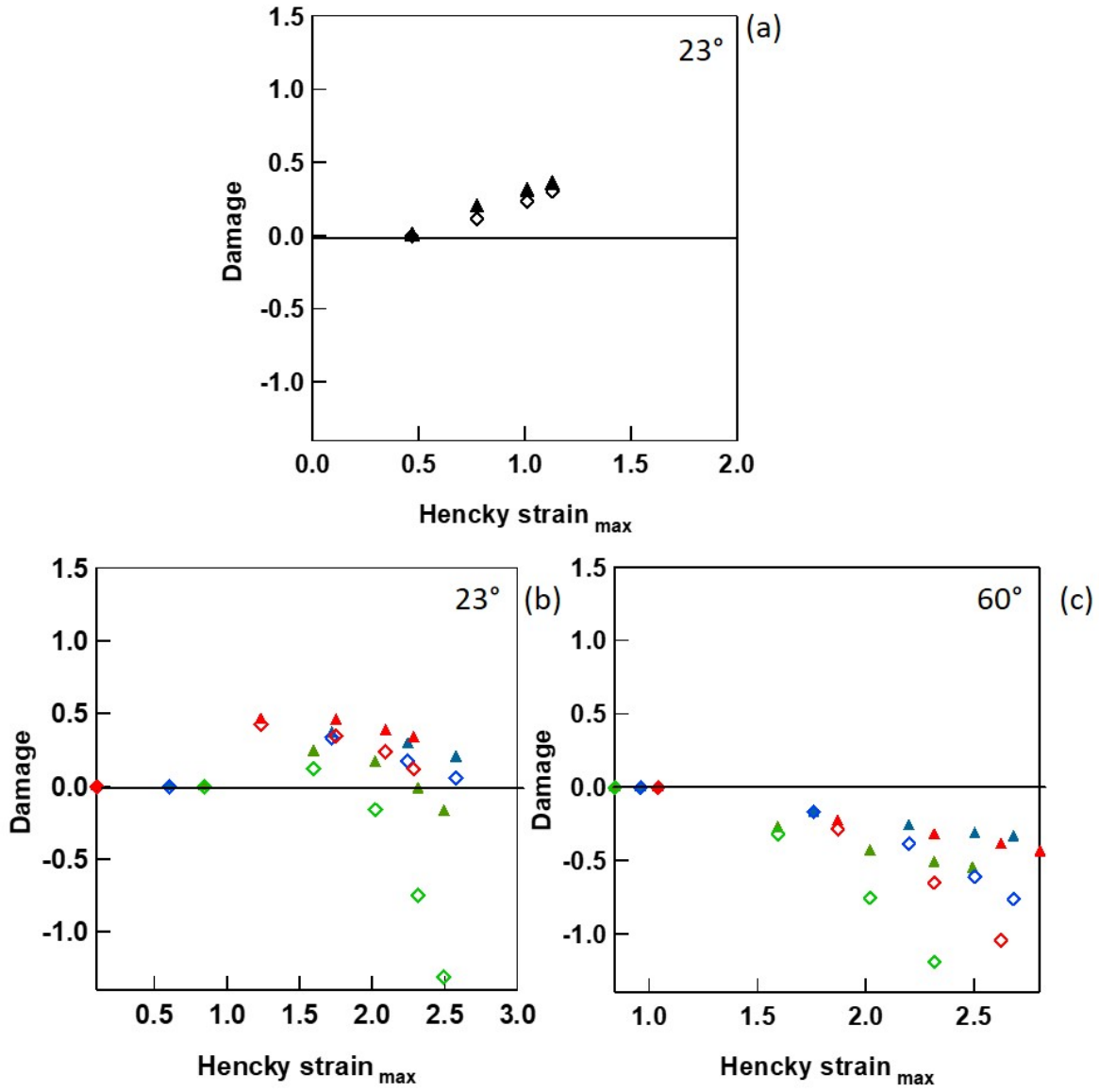

Figure 8-12 Damage VS Hencky strain calculated for SBR (a) and TPU at 23° (b) and 60° (c) . The symbols indicate Dss for: SBR: ▲, TPU_HARD: ▲, TPU_SOFT : ▲, TPU_XTAL: ▲. Dls for SBR : ◇ ,TPU_HARD: ◇ ,TPU_SOFT: ◇ ,TPU_XTAL: ◇ ..

8.6 Discussion on the differences between TPU and SBR

In the case of SBR, the analysis of damage shows that both damage parameters (D_{ls} and D_{ss}) nearly overlap and have a positive dependence on the applied strain meaning that the damage in the material increases with deformation. Merckel and coworkers[18] interpreted this as an

indication that, in filled SBR, the application of a cyclic strain generates some kind of physical damage on the polymer that affects in a similar way both the small and large strain properties of the polymer itself. Or, in other words, they speculate that in SBR the change in the small and large strain mechanical response with applied strain have the same origin. On the other hand, although in all three TPUs D_{ls} and D_{ss} have similar trends, they do not superimpose well and, above a threshold value of strain, they reduce with increasing maximum Hencky strain. In specific conditions, D_{ss} and D_{ls} even assume negative values. The main difference between TPU and SBR, which leads to a different trend in the calculated damage, is the residual deformation $\lambda_{res.}$ In the case of SBR, λ_{res} is mostly negligible while, in the case of TPU, λ_{res} accounts for almost one third of λ_{max} and has a great effect on the rescaling procedure. In cyclic deformation of TPU, the engineering stress-strain representation, that seems to suggest a cyclic softening, is misleading. The engineering representation of strain in fact, only compares the final state with the initial state and, in the case of materials with high residual strain it introduces a non-negligible error on the measure. Contrarily, the Hencky strain accounts for all the incremental steps of deformation (considering the value of the sample length just before each strain increment).

8.6.1 Interpretation of the calculated damage in TPU

The decrease of D_{ss} in TPU, is justified by the increase in E with applied deformation for all samples (Figure 8-10(b)). In particular TPU_XTAL that can crystallize under strain at 23°C, shows the highest values of E that eventually becomes higher than in the pristine material, for larges values of maximum applied deformation. It is clear that using a negative value to describe strain induced-damage does not have any physical meaning but, the increase in modulus with applied deformation, indicates that the deformation induces stiffening in TPU. This unconventional increase in modulus with applied deformation must depend on the specific multi-phase structure of each TPU that re-arranges with applied strain [26]. Additionally, the different values of D_{ls} and D_{ss} are in line with the hypothesis of Cooper and van Bogart [34]. They argued that while the Young's modulus depends on the rigidity and morphology of the hard domains, the stress softening also depends on the coupled action of hard and soft segment re-organization.

We believe that the breakdown of the original hard domains in smaller domains with applied deformation, has the same effect of increasing the physical crosslinking points causing an increase of the stiffness. In the case of TPU_XTAL, which crystallizes under strain, the

increase in physical crosslinking (attributed to the fragmentation of hard domains) is enhanced by the intrinsic stiffness of the crystallites (that act as additional hard points) explaining the enhanced trend in E(h) for TPU_XTAL.

8.7 Conclusions

The cyclic mechanical behavior at small and large strain of three TPUs has been analyzed. The three TPUs have been chosen because of their similar linear modulus (~ 7-8 MPa at 23°C) but differ in composition and large strain properties as shown by X-Ray analysis and DSC. TPU_SOFT is a blend with semi-crystalline PBT and has a large softening before fracture while TPU_XTAL and TPU_HARD have similar fractions of HD and a remarkable strain-hardening, which only for TPU_XTAL can be attributed to SIC. Despite their differences, we discovered two remarkable similarities among all materials: 1) a surprising almost unique linear relation between residual and maximum strain during cycles at different temperatures 2) a similar fraction of dissipated energy in the stabilized cycle, almost independent of the applied strain. However, the most remarkable and potentially impactful result of the present work lies in the discovery of strain induced stiffening in TPU with applied strain in cyclic loading. This finding is fundamentally different from the strain induced softening (also referred as cyclic damage) typically observed in filled rubbers. While the molecular origin of this peculiar behavior in TPU has not been clarified unambiguously, we proposed that it originates from the fragmentation of original HD in smaller but more numerous sub-units that may themselves act as additional physical crosslinking points. This strain-dependent strengthening, analogous to the strain-induced crystallization observed in stretched natural rubber, can be interesting in specific applications in which the TPU can be locally reinforced by the presence of an inhomogeneous strain for example as in the case of cyclic fatigue.

8.8 Acknowledgements

The PhD work of G. Scetta was jointly funded by the French ANRT and the LRCCP. We are grateful to Aude Belguise for her support with correlation function analysis. We are indebted to Dr. Matthias Gerst, Dr. Elke Marten and Mr. Stephan Dohmen from BASF AG for kindly providing the TPU samples. We thank Stephane Delaunay for injecting the samples and Mohamed Hanafi for his help with DSC analysis.

8.9 References

1. Holden G. *Understanding Thermoplastic Elastomer.*; 2000.
2. Z. S.Petrovic JF. POLYURETHANE ELASTOMERS. *Prog Polym Sci*. 1991;16:695-836.
3. Bonart R. Thermoplastic Elastomers. *Brydson's Plast Mater Eighth Ed*. 1979;20(July):653-703. doi:10.1016/B978-0-323-35824-8.00024-4
4. Buckley CP, Prisacariu C, Martin C. Elasticity and inelasticity of thermoplastic polyurethane elastomers: Sensitivity to chemical and physical structure. *Polymer (Guildf)*. 2010;51(14):3213-3224. doi:10.1016/j.polymer.2010.04.069
5. Prisacariu C, Scortanu E, Agapie B. Effect of the hydrogen bonding on the inelasticity of thermoplastic polyurethane elastomers. *J Ind Eng Chem*. 2013;19(1):113-119. doi:10.1016/j.jiec.2012.07.012
6. Russo R, Thomas EL. Phase Separation in Linear and Cross-Linked Polyurethanes. *J Macromol Sci Part B*. 1983;22(4):553-575. doi:10.1080/00222348308224776
7. Mueller H, Knauss WG. Fracture Energy and Some Mechanical Properties of a Polyurethane Elastomer. *Trans Soc Rheol*. 1971;15(2):217-233. doi:10.1122/1.549209
8. Smith TL. Tensile Strength of Polyurethane and Other Elastomeric Block Copolymers. *J Polym Sci Polym Phys Ed*. 1974;12:1825-1848. doi:10.5254/1.3534952
9. Creton C. 50th Anniversary Perspective: Networks and Gels: Soft but Dynamic and Tough. *Macromolecules*. 2017;50(21):8297-8316. doi:10.1021/acs.macromol.7b01698
10. Drozdov AD. Mullins' effect in thermoplastic elastomers: Experiments and modeling. *Mech Res Commun*. 2009;36(4):437-443. doi:10.1016/j.mechrescom.2008.12.007
11. Mullins L. Softening of rubber by displacement. *Rubber Chem Technol*. 1969;42(1):339-362.
12. Diani J, Fayolle B, Gilormini P. A review on the Mullins effect. *Eur Polym J*. 2009;45(3):601-612. doi:10.1016/j.eurpolymj.2008.11.017
13. Webber RE, Creton C, Brown HR, Gong JP. Large strain hysteresis and mullins effect of tough double-network hydrogels. *Macromolecules*. 2007;40(8):2919-2927. doi:10.1021/ma062924y
14. Drozdov AD, De Christiansen JC. Mullins' effect in semicrystalline polymers: Experiments and modeling. *Meccanica*. 2011;46(2):359-370. doi:10.1007/s11012-010-9314-z
15. Qi HJ, Boyce MC. Stress-strain behavior of thermoplastic polyurethanes. *Mech Mater*.

2005;37(8):817-839. doi:10.1016/j.mechmat.2004.08.001

16. Yi J, Boyce MC, Lee GF, Balizer E. Large deformation rate-dependent stress-strain behavior of polyurea and polyurethanes. *Polymer (Guildf)*. 2006;47(1):319-329. doi:10.1016/j.polymer.2005.10.107
17. Diani J, Fayolle B, Gilormini P, Diani J, Fayolle B, Gilormini P. A review on the Mullins effect To cite this version : HAL Id : hal-00773015. 2013:601-612.
18. Merckel Y, Diani J, Brieu M, Gilormini P, Caillard J. Characterization of the mullins effect of carbon-black filled rubbers. *Rubber Chem Technol*. 2011;84(3):402-414. doi:10.5254/1.3592294
19. Mzabi S. Caractérisation et analyse des mécanismes de fracture en fatigue des élastomères chargés. 2010:1-310.
20. Mzabi S, Berghezan D, Roux S, Hild F, Creton C. A critical local energy release rate criterion for fatigue fracture of elastomers. *J Polym Sci Part B Polym Phys*. 2011;49(21):1518-1524. doi:10.1002/polb.22338
21. Hammersley AP. "FIT2D." 2016. http://www.esrf.eu/computing/scientific/FIT2D/.
22. Strobl GR, Schneider M. Direct Evaluation of the Electron Density Correlation Function of Partially Crystalline Polymers. *J Polym Sci Part A-2, Polym Phys*. 1980;18(6):1343-1359. doi:10.1002/pol.1980.180180614
23. Aime S, Eisenmenger NDD, Engels TAPAP. A model for failure in thermoplastic elastomers based on Eyring kinetics and network connectivity. *J Rheol (N Y N Y)*. 2017;61(6). doi:10.1122/1.5000808
24. Li, H.L.: White J. Elastic Response of Copolyether-ester Fiber on Its Phase Morphology under Different Heat-treatment Condition. *Polym Eng Sci*. 2000;40:917-928.
25. Yokouchi M, Sakakibara Y, Chatani Y, Tadokoro H, Tanaka T, Yoda K. Structures of Two Crystalline Forms of Poly(butylene terephthalate) and Reversible Transition between Them by Mechanical Deformation. *Macromolecules*. 1976;9(2):266-273. doi:10.1021/ma60050a018
26. Bonart R. X-ray investigations concerning the physical structure of cross-linking in segmented urethane elastomers. *J Macromol Sci Part B*. 1968;2(1):115-138. doi:10.1080/00222346808212867
27. Koberstein JT, Russell TP. Simultaneous SAXS-DSC Study of Multiple Endothermic Behavior in Polyether-Based Polyurethane Block Copolymers. *Macromolecules*. 1986;19(3):714-720. doi:10.1021/ma00157a039

28. Kojio K, Matsuo K, Motokucho S, Yoshinaga K, Shimodaira Y, Kimura K. Simultaneous small-angle X-ray scattering/wide-angle X-ray diffraction study of the microdomain structure of polyurethane elastomers during mechanical deformation. *Polym J*. 2011;43(8):692-699. doi:10.1038/pj.2011.48
29. Huo PP, Cebe P. Melting Point Depression in Poly(butylene terephthalate)/Polyarylate Blends. *Macromolecules*. 1993;26(12):3127-3130. doi:10.1021/ma00064a021
30. Shen Z, Luo F, Bai H, et al. A study on mediating the crystallization behavior of PBT through intermolecular hydrogen-bonding. *RSC Adv*. 2016;6(21):17510-17518. doi:10.1039/c5ra25438h
31. Chen Y, Zhang H, Fang X, Lin Y, Xu Y, Weng W. Mechanical activation of mechanophore enhanced by strong hydrogen bonding interactions. *ACS Macro Lett*. 2014;3(2):141-145. doi:10.1021/mz400600r
32. Toki S, Hsiao BS, Kohjiya S, Tosaka M, Tsou AH, Datta S. Synchrotron X-Ray Studies of Vulcanized Rubbers and Thermoplastic Elastomers. *Rubber Chem Technol*. 2011;79(3):460-488. doi:10.5254/1.3547946
33. Zhu P, Zhou C, Dong X, Sauer BB, Lai Y, Wang D. The segmental responses to orientation and relaxation of thermoplastic poly(ether-ester) elastomer during cyclic deformation: An in-situ WAXD/SAXS study. *Polymer (Guildf)*. 2020;188:122120. doi:10.1016/j.polymer.2019.122120
34. J.W.C Van Bogart, A. Lilaonitkul SLC. Morphology and properties of segmented polyether poly(urethaneureas). *Am Chem Soc*. 1979. doi:10.1295/polymj.17.969

9 SELF-ORGANIZATION AT THE CRACK TIP AND CYCLIC FATIGUE IN TPU

Self-organization at the crack tip of fatigue-resistant thermoplastic polyurethane elastomers

Giorgia Scetta[1], Eric Euchler[2], Jianzhu Ju[1], Nathan Selles[3], Patrick Heuillet[3], Matteo Ciccotti[1] and Costantino Creton[1*].*

[1]Sciences et Ingénierie de la Matière Molle, ESPCI Paris, Université PSL, CNRS, Sorbonne Université, 75005, Paris, France.

[2]Leibniz-Institut für Polymerforschung Dresden e.V., 01069, Dresden, Germany.

[3]Laboratoire de Recherches et de Contrôle du Caoutchouc et des Plastiques , 60, Rue Auber 94408 Vitry-sur-Seine, France

matteo.ciccotti@espci.psl.eu, Costantino.creton@espci.psl.eu

9.1 Abstract

Despite its technological relevance, the resistance of soft Thermoplastic Polyurethanes (TPU) to cyclic fatigue has not been investigated in detail yet. In this work, we explore the resistance to cyclic fatigue of two TPUs with a similar linear modulus (~ 8 MPa), but a different large strain behavior. We found an extremely high fatigue threshold compared to filled elastomers with similar linear moduli. Using digital image correlation (DIC) and in situ X-Ray diffraction (SAXS and WAXD), we characterized the region of high strain ahead of the crack tip in both TPUs, before and after cyclic fatigue. The lower strain localization and anisotropic structure found at the crack tip in both TPUs after cyclic fatigue was related to the local restructuring of the hard domains that derive from a self-organization in the TPU copolymer network. This hard-domain restructuration, activated by the larger strain induced in the first loading cycles close to the crack, induces a higher stiffness in the region surrounding the crack. This spatial variation of the mechanical properties reduces the strain concentration in the following cycles, thus shielding the crack tip from high values of strain and reducing the probability of bond scission at every loading cycle, explaining therefore the remarkable cyclic fatigue resistance in TPUs. The presence of strain induced crystallization in one of the TPUs was found to further enhance this shielding mechanism based on a local stiffening in the crack tip region, but it is not a necessary condition for local reinforcement.

9.2 Introduction

TPUs are segmented multiblock copolymers characterized by alternating blocks of soft segments (SS) and hard segments (HS). The first are composed by long and flexible polyester or polyether chains that ensure high deformability, while the second consist of urethane rich hard segments. The TPUs typically self-organize in micro-hard domains (HD). The HD are generated from the lateral stacking of HS through physical interactions and hydrogen bonding. They generally have dimensions of tens of nm[1,2], comparable to that of common reinforcing fillers used in rubbers. The flexible chains represent the majority of the material and are physically crosslinked by the HD providing the material with rubber-like elasticity and preventing macroscopic flow at ambient temperature.

TPUs can be produced in different grades with Young's moduli *E* ranging from some MPa to 1.000 MPa. Among those, soft TPUs (E<10 MPa) include materials with high elasticity and excellent abrasion resistance. Soft TPUs have found many applications in several fields as sportswear and footwear and have recently gained increasing industrial attention because they are a great candidate for a recyclable alternative to replace classical filled thermoset rubbers in structural applications such as cables, dampers and belts. One of the most desirable properties in this kind of structural applications is the ability to sustain several cyclic loadings without hazardous rupture of the material. In other words, having an appreciable cyclic fatigue resistance.

In Chapter 7 , we used the classic fracture mechanics approach, originally developed for rubbers, to develop a method to probe the cyclic fatigue resistance of soft TPUs. They highlighted that during cyclic deformation TPUs experience a shake down[3] or stabilization of the cycle. Provided that the loading and unloading cycles are conveniently adapted to tackle the effects of plastic creep, the crack propagation can be robustly expressed as crack propagation per cycle *dc/dn* vs. the energy release rate (*G)*. These preliminary results confirmed the very high resistance of soft TPUs to crack propagation in cyclic fatigue conditions even for large applied strains.

Yet, a clear shortcoming in the literature for this class of materials is the lack of connection between the cyclic fatigue resistance and their peculiar large strain behavior that has a fundamental role in defining the material's resistance to crack propagation. Although the typical range of bulk strain used in fatigue experiments is generally considerably lower than the strain at break in uniaxial tests, the presence of the crack induces significantly larger local

strains at the crack tip [4,5]. This strain concentration is particularly important for TPUs since their structure evolves with applied strain [6–11]. However, previous studies on the structural evolution of HD with the applied strain, only focused on homogeneous samples and did not include the effect of singularities such as defects or pre-cracks. To our knowledge a comprehensive characterization of the local morphology induced at the crack tip during a cyclic fatigue experiment, and the discussion of its effects on the crack propagation rate for soft TPUs has never been carried out. To understand this crack tip structural change, it is useful to briefly recall some key results obtained in uniaxial extension of TPUs [7,9–16]. Bonart [6] was among the firsts to investigate the deformation behavior of TPU using small and wide angle X-Ray scattering. He proposed that, for moderate levels of stretch $\lambda<3$, the progressive alignment of the soft segments along the tensile direction exerts a torque on the HDs. As a result, the HD tend to orient in a transversal direction relative to the applied load. In TPU with a low percentage of HS, further elongation generally corresponds to a re-organization of HD and alignment along the loading direction. This process, defined as "restructuring of the cross-linking" by Ishihara [12], consists in breaking and re-forming hydrogen bonds to realign the hard segments. An excellent summary on X-ray investigations in deformed TPU with low hard segment content (<12%) was provided by Yeh and co-workers [7].

In this work, we tested the cyclic fatigue resistance of two TPUs which share very similar small strain properties, but present completely different large strain behavior especially when changing the temperature. In addition to the fatigue experiments measuring *dc/dn* as a function of the applied G and uniaxial step-cycle tests, we used two additional techniques to characterize the structural changes occurring in the bulk and at the crack tip as the sample is fatigued: digital image correlation (DIC) and in-situ X-Ray wide and small angle scattering analysis (WAXS, SAXS).

9.3 Materials and methods:

9.3.1 Materials

The used TPUs are commercial polyester based polyurethane multiblock copolymers produced by BASF with the trade names: 565A 12P and LP9277 10 of the Elastollan© series,

respectively denoted as TPU_XTAL and TPU_SOFT based on the large strain behavior. The materials were kindly provided by BASF.

Specimens were injection molded into two different shapes: rectangular pure shear samples (PS) with dimensions of 65x5x1 mm for the crack propagation experiments, and dog-bone samples with a cross section of 2x4 mm, cut within a 2 mm thick large square-plate. The PS geometry is generally used in cyclic fatigue experiments because the energy release rate G is easily calculated and is independent of the crack length [17]. The temperatures used in the injection molding procedure are summarized in Table 9-1 for both samples. All PS samples were pre-notched with a 20 mm cut.

Table 9-1 Barrel temperature profile for the injection procedure

Barrel / Sample	**Zone 1 (°C)**	**Zone2(°C)**	**Zone4(°C)**	**Nozzle (°C)**	**Mould (°C)**
TPU_XTAL	170	180	190	185	30
TPU_SOFT	190	200	205	200	30

The chemical composition of both TPUs is not available since they are commercial products. The M_n of TPU_XTAL after injection is 47kg/mol and was obtained by gel permeation chromatography (GPC) using THF as carrier solvent. TPU_SOFT was not soluble in THF or in other common polar solvents. Fourier transform infrared spectroscopy (FTIR) was used for structural analysis of the polymer, revealing an absorbance peak around 1640 cm^{-1} consistent with the presence of bidentate urea (that is generally associated with stronger interactions than simple hydrogen bonding in HD) [18] and may explain the poor solubility of TPU_SOFT suggesting a stronger inter-domain stability.

9.3.2 Step-strain cyclic Tests

The dog-bone shaped samples were mechanically clamped in order to withstand large strains. An optical system was used to measure the local strain in the gauge region. The samples were strained in uniaxial tension at the stretch rate $\dot{\lambda} = 4\ s^{-1}$. The elongation was performed in a stepwise mode: 10 cycles were performed at progressively larger maximum applied stretches

λ. The force was unloaded to σ = 0 between two successive steps in order to prevent buckling. Strain ε, stretch λ, Hencky strain h, stress σ and true stress T are defined as below with l_0 and l indicating the initial and instantaneous gauge length respectively, A_0 the initial cross section area and F the measured force.

$$\varepsilon = \frac{l-l_0}{l_0} \quad \lambda = \frac{l}{l_0} \quad \sigma = \frac{F}{A_0}$$

$$T = \sigma \cdot (1+\varepsilon) \quad h = \ln(\lambda)$$

9.3.3 WAXD and SAXS Characterization

In situ WAXD and SAXS experiments on strained samples were carried out at the PETRA III beamline P03 at Deutsches Elektronen-Synchrotron (DESY) in Hamburg. The technical details of the scattering experiments are summarized in Table 9-2.

Table 9-2 Parameters of X-Ray experiments

Facility	DESY, Petra III
Energy	13 KeV
Wave length (ν)	0.096 nm
Beam size	22x16 μm
Step width	100 μm
Distance from detector (SAXS)	4050 mm
Distance from detector (WAXD)	171 mm
Image resolution	172x172 pixel

2D scattering data were integrated using FIT-2D [19]. All data were corrected by subtracting background scattering. We indicated as meridional and equatorial directions those parallel and perpendicular to the applied load.

WAXD analysis:

The 2D diffraction pattern was circularly integrated. Peaks in the 2θ range between 260° and 280° were deconvoluted using Gaussian/Lorentzian peak fitting routines. The crystalline fraction χ_c was evaluated classically as the ratio between the total area of crystal peaks I_{cr} and the total area (amorphous and crystalline: $I_{cr} + I_{am}$) underneath the diffraction profile as: $\chi_c = \int_{2\theta} \frac{I_{cr}}{I_{cr}+I_{am}}$

Azimuthal integration was performed on the most prominent peak as indicated in Figure 9-1(a). The obtained peak was then fitted with a Gaussian function to calculate the Full Width at Half Maximum (FWHM) Figure 9-1(b). The value of FWHM is indicative of the variability of the lattice parameter around its average value and is an indication of the level of disorder of the structure. A high value of FWHM indicates less ordering in the crystal phase.

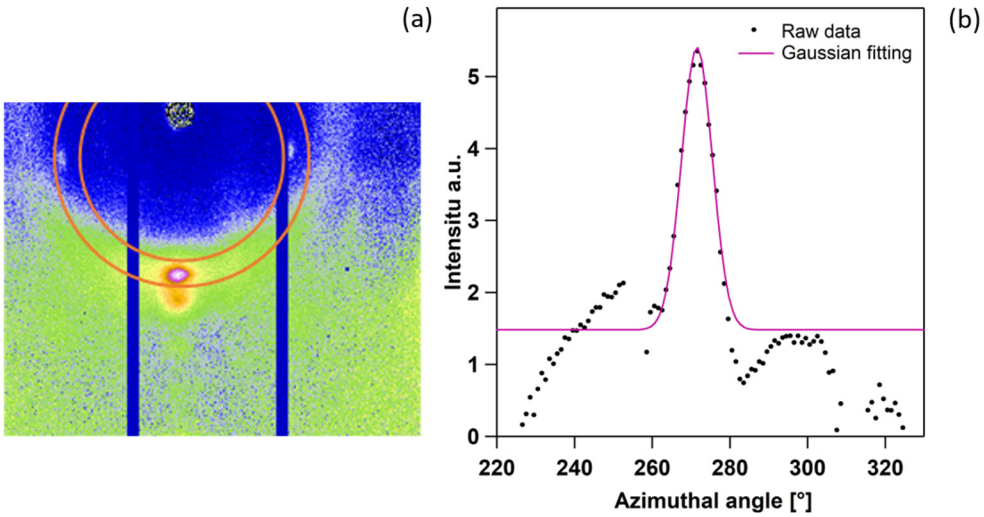

Figure 9-1 Example of azimuthal integration to evaluate the orientation factor (a). Example of Gaussian fitting of Azimuthal 1D profile to evaluate the FWHM (b).

SAXS analysis:

SAXS data are expressed in terms of intensity as a function of wave vector $q = \frac{4\pi sin\theta}{\nu}$ where 2θ is the scattering angle and ν is the wavelength. The long period L represents the recurrent spacing periodicity between hard domains [6] and it was calculated as $L = \frac{2\pi}{q^*}$ where q^* represents the center of the Gaussian fitting of the peak in the 1D SAXS profile.

9.3.4 Cyclic fatigue experiments

Fatigue results are generally expressed in terms of crack propagation per cycle *dc/dn* vs. applied energy release rate G. All the experiments were carried out on PS samples following the procedure developed in Chapter 7 for TPUs. We applied sinusoidal cycles between σ_{min}=0 and an increasing value of the maximum stretch λ_{max} at the frequency of 10 Hz on an un-notched sample. Under cyclic conditions the stress-stretch curve of TPU shows a very marked stress softening and some residual strain that eventually stabilizes between 5.000 and 10.000 cycles (shake down[3]). We used the stress-stretch curve at 10.000 cycles to evaluate $G(\lambda_{max})$ as $G = HW_{PS}(\lambda_{max})$ where H is the unstrained height of the PS sample [17]. To evaluate the crack propagation per cycle, a single long notch of 22 mm was cut and the sample was strained between σ_{min}=0 and $\lambda_{max}$for a minimum of 36.000 cycles. During the test, the extension of the crack, was monitored using a digital BAUMER VCXU-32M camera with resolution of 3.1 Megapixel equipped with a macro objective resulting in a pixel size of 38 μm. The crack propagation rate stabilizes after 5.000-10.000 cycles and then we evaluate *dc/dn*.

9.3.5 Digital Image Correlation (DIC)

DIC is a technique which allows one to measure displacement fields by matching a reference with a deformed image. We used CorreliLMT software[20] which represents the displacement field by the same kind of mesh as in finite element methods. The final displacement is evaluated using an algorithm that minimizes the difference in the gray levels between the matched images, while imposing some level of regularity to the solutions. Images were taken with a BAUMER VCXU-32M camera with a resolution of 3.1 Megapixel equipped with an objective resulting in a pixel size of 7 μm. The spatial resolution of the DIC analysis (minimum distance between two adjacent estimates of displacement) was 112 μm (corresponding to 16 pixels). Since the datapoint associated by convention to a distance of 0 mm from the crack tip is indeed the closest available point, this spatial resolution should also be considered as an uncertainty on the distance of such point from the crack tip. The samples were uniformly backlighted. A random speckle texture was obtained by black ink spraying, which provides the best contrast with the sample surface (either white or transparent). For each DIC characterization, a set of 40-60 images was acquired between σ_{min}=0 and λ_{max}. In order to minimize the alteration of the gray levels by the large applied strains during DIC, we first performed the correlation procedure between each couple of subsequent images from the unloaded condition to the maximum strain. Then we evaluated the total displacement for each λ by progressively adding

the differential displacement fields of each step. The total displacement field was then used to evaluate the local strain field following the same procedure as in Mzabi[21]

9.4 Results

9.4.1 Tensile tests

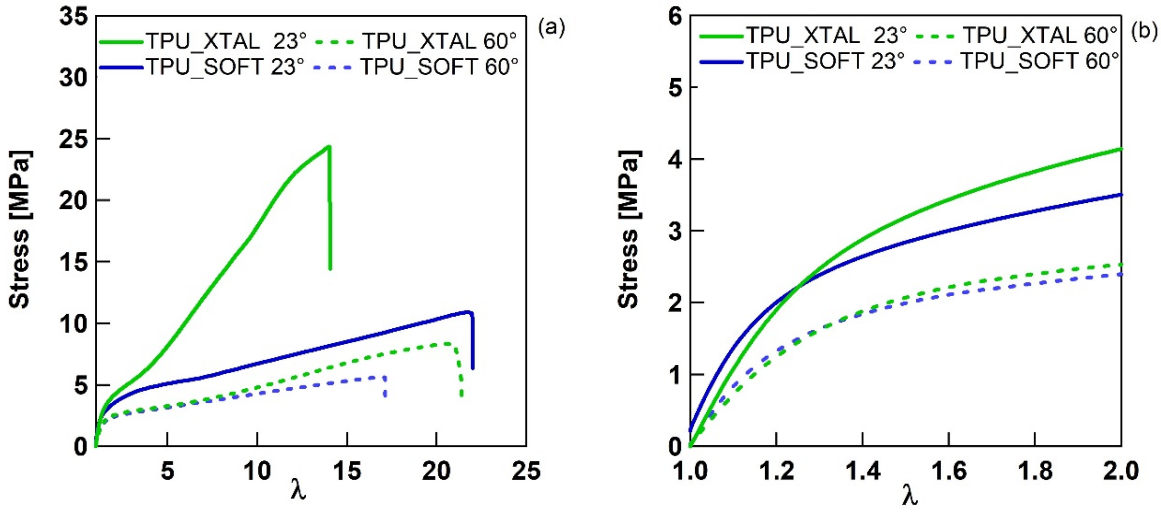

Figure 9-2 Uniaxial nominal stress-stretch curve of TPU_XTAL and TPU_SOFT at 23°C and 60°C (a). Zoom on the small stretch region (b).

Figure 9-2(a) reports the stress-stretch curve in uniaxial tension at 23 and 60°C and highlights the main differences in large strain behavior between TPU_XTAL and TPU_SOFT. At ambient temperature, both TPUs are characterized by a high extensibility at failure (more than 1000%). After an initial linear elastic regime that only lasts a few percent strain, both TPUs soften as displayed in Figure 9-2(b). In the case of TPU_XTAL this is rapidly followed by a marked strain hardening, which is much less pronounced in TPU_SOFT. At 60°C the TPU_XTAL has a significant drop in its stress curve up to failure, but not in the maximum extensibility that is found to slightly increase. The TPU_SOFT has a less pronounced drop in the stress curve, but

becomes less extensible than at 23°C. Table 9-3 reports the elastic moduli as well as the stress and stretch at break for both TPUs at 23 and 60°C.

Table 9-3 Young modulus (E), maximum stretch at break (λ_b) and maximum stress (σ_b) for TPU_XTAL and TPU_SOFT at 23 and 60°C. *At the maximum displacement allowed by the capacity of the testing machine the sample did not break.

	23°C			60°C		
Name	**E [MPa]**	**λ_b**	**σ_b [MPa]**	**E [MPa]**	**λ_b**	**σ_b [MPa]**
TPU_XTAL	*8.7 ±0.1*	*15.4 ±1.2*	*25.1 ±1.3*	*5.0 ±0.7*	*>20**	*>8**
TPU_SOFT	*7.8 ±0.1*	*17.7 ±1.5*	*11.8 ±0.5*	*5.8 ±0.1*	*17.0 ±0.6*	*5.4 ±0.2*

9.4.2 Cyclic fatigue

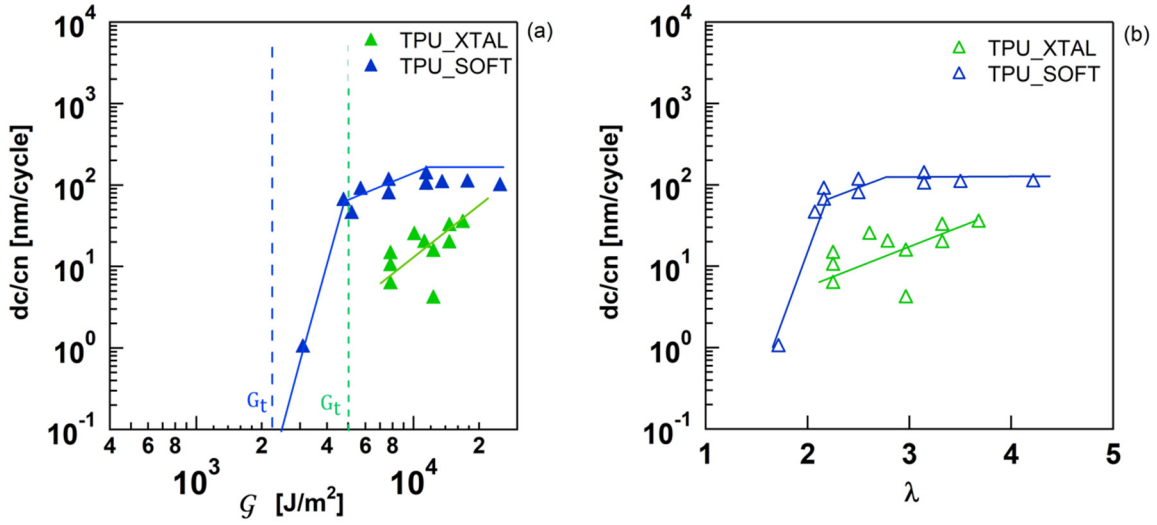

Figure 9-3 Crack growth rate per cycle as function of the applied release rate G (a) and of applied stretch λ (b) for TPU_XTAL and TPU_SOFT at 23°C.

Figure 9-3 (a) shows the values of *dc/dn* in the steady state regime as a function of G for both TPUs. The threshold value G_t, indicated in the picture for each TPU, corresponds to the minimum value of G below which we could not detect any crack propagation. Our optical system has a resolution of 38 μm and the experiments last for 36.000 Cycles, this means that the minimum detectable crack growth was ~1nm. Using this definition, the value of G_t was found to be ~2.000 J/m^2 and ~5.000 J/m^2, respectively for TPU_SOFT and TPU_XTAL. As already remarked in Chapter 7, this is not a physical value of G_t but it does depend on the system and we cannot exclude that, higher resolution and/or longer test may lead to lower value of G. Nevertheless, in classical rubbers average G_t was found between 40-100 J/m^2 [22,23], well below those obtained for TPUs which present a fatigue threshold (and corresponding λ_{max}) almost 1 order magnitude larger. Above the threshold, *dc/dn* of TPU_XTAL increases as a power law $\approx G^{2.7}$. This behavior is similar to that found in several elastomeric systems, which generally present a value of *n* varying between 1 and4 [24]. On the other hand, TPU_SOFT has a rapid transition between a very slow or almost not propagating regime to a fast propagating regime where the values of *dc/dn* only weakly depends on G and are higher than for TPU_XTAL at comparable G. The toughness, generally defined as a critical G_c above which the crack propagates so fast that the sample breaks in a few cycles [25], must be above 20.000 J/m^2 in both TPUs since this unstable regime was not observed. For comparison, for a typical filled natural rubber with similar linear modulus the average value is generally below 10.000 J/m^2 [25]. Figure 9-3(b) reports an equivalent representation in terms of *dc/dn* vs. the maximum stretch λ, which demonstrates the extremely large strain required to propagate a crack in cyclic fatigue for TPUs. Interestingly, comparable value of dc/dn, for similarly high value of λ were reported by other Li et al.[26] in another multi-phase system. They showed that highly fatigue resistance hydrogel containing a reinforcing hard phase at the 100nm scale, larger than the polymer network (10nm), can be deformed at comparable maximum stretch for thousands of cycles without initiating a catastrophic propagation of the crack.

A very visible crack tip blunting is associated to the propagating crack in cyclic fatigue experiments in both TPUs, a typical example is shown in Figure 9-4(a). The crack tip radius *R,* plotted Figure 9-4*(b)* as a function of G, was obtained using a parabolic fitting of the crack profile as indicated by the green line. The fitted crack radius increases with applied G and for

the highest tested values of G its dimension becomes comparable with the height of the sample (Figure 9-8 (b)).

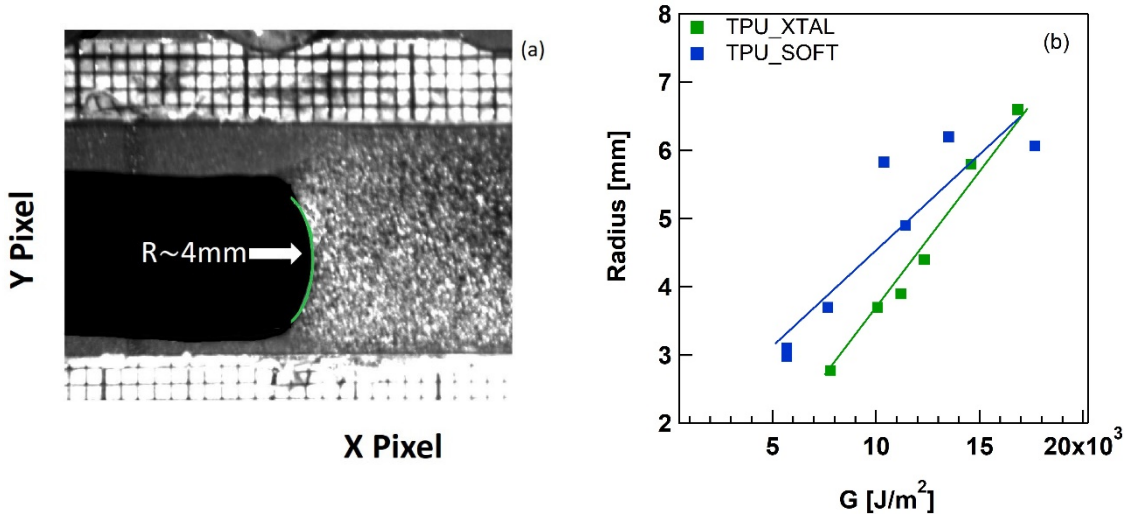

Figure 9-4 Example of crack opening profile in TPU_XTAL at G = 12.000 J/m² (a) and fitted radius as a function of the energy release rate for both TPUs (b)

Fatigue experiments were also performed at 60°C for both TPUs using the same procedure described above. The results in terms of *dc/dn* as a function of applied G and maximum applied λ are reported in Figure 9-5. In both materials, increasing the testing temperature causes a reduction in fatigue resistance, i.e. a higher crack propagation rate for the same G. TPU_XTAL maintains a lower *dc/dn* than TPU_SOFT in the whole range of G, but the gap is greatly reduced compared to 23°C and *dc/dn* is still in a power law regime. Again, the crack propagation per cycle in TPU_SOFT is almost constant in a large range of applied G. Three different propagating regimes can be distinguished in TPU_SOFT. In the ranges 2.000-3.000 J/m^2 and 5.000-13.000 J/m^2, *dc/dn* is independent from G and it is equal to ≈ 10 nm/cy and ≈ 1000 nm/cy respectively. Then above 14.000 J/m^2 the value of the crack propagation per cycle drastically increases and the sample breaks in a few cycles, which corresponds to the toughness or G_c. Overall, both TPUs have a higher fatigue resistance than classical filled elastomers at the same applied G and require a much higher strain to propagate the crack during cyclic fatigue. In

particular, increasing the testing temperature does not affect the value of G_t which is very similar to those calculated at 23° for both TPUs .

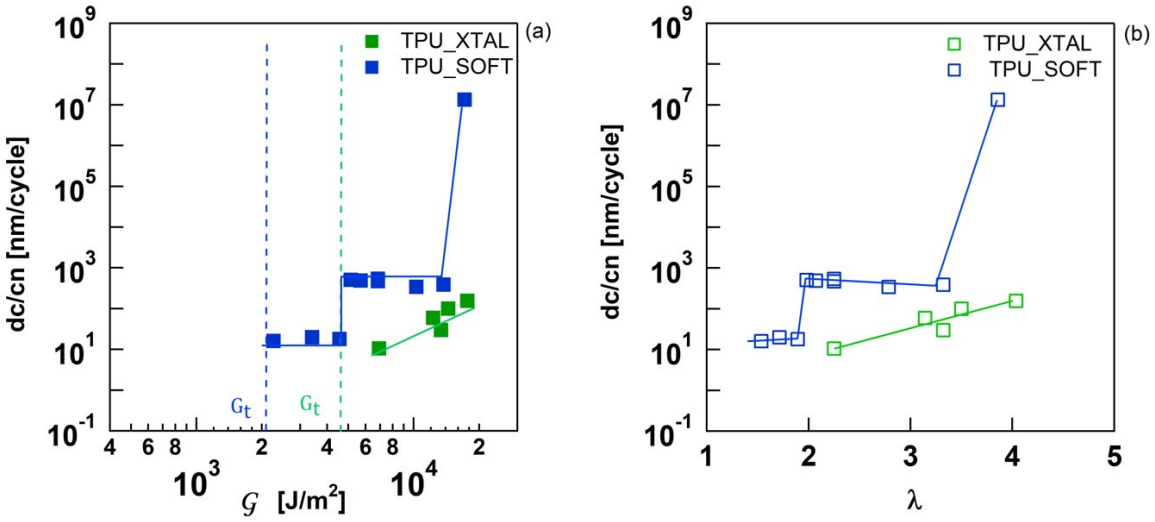

Figure 9-5 Crack growth rate per cycle as function of applied release rate G (a) and applied stretch λ (b) for TPU_XTAL and TPU_SOFT at 60°

9.4.3 Change in Structure due to Uniaxial Cycles of Deformation

Characterizing the large strain cyclic behavior is fundamental to better understand the fatigue resistance of TPUs. In cyclic fatigue, the crack propagates at levels of bulk applied stretch considerably lower than the strain at break in static extension. Despite that, close to the crack tip, the local strain is higher than in the bulk because of the stress and strain concentration induced by the notch. The history of a material point near the crack plane during cyclic fatigue can be simplistically represented by step-strain cyclic experiments up to rupture. When the crack propagates, the fresh material near the crack plane will experience a progressively increasing strain. Figure 9-6 (a) shows the stress-strain curve for a uniaxial cyclic step-strain experiment for TPU_XTAL and TPU_SOFT at 23°C. After the unloading TPUs retain a permanent stretch λ_{res}. Moreover, the first loading pattern is substantially different from the unloading characterized by a visible stress softening. This hysteresis behavior is usually referred as Mullins effect and is commonly found in several filled rubbers [27,28] and TPUs [29,30]. The dissipative behavior in uniaxial extension of TPU_SOFT and TPU_XTAL are qualitatively very similar (Chapter 8) and cannot thus explain in any obvious way the considerably higher fatigue resistance of TPU_XTAL, especially at 23°C.

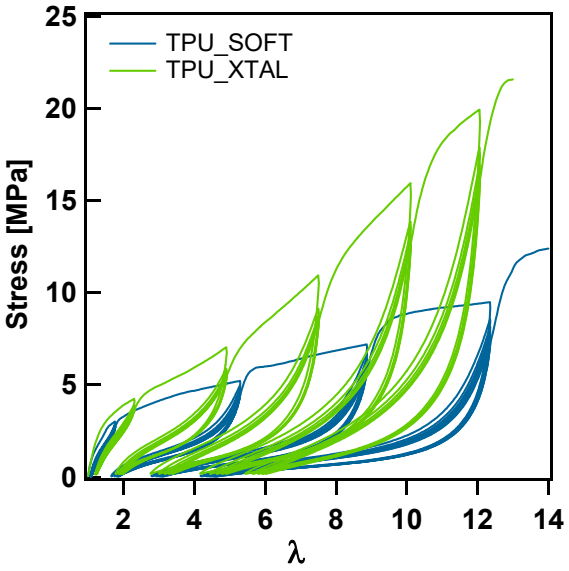

Figure 9-6 Cyclic stress-stretch curve for TPU_XTAL and TPU_SOFT at 23°C and 60°C.

During the cyclic experiments the stress-strain response of the material is permanently affected by the maximum applied strain. One way to characterize this effect is to evaluate the evolution of the tangent modulus at low strain E with the maximum applied λ. We adopt the Hencky-strain, true-stress representation as already done in our previous work (Chapter 8). The linear modulus E was calculated with a linear fitting of the initial part of each unloading curve plotted in terms of true stress vs. Hencky strain as reported in Figure 9-7(a). Cyclic relaxation experiments carried out on filled SBR demonstrated that the viscoelastic effect is more evident in the loading path than in the unloading [31]. Therefore, we decided to use the unloading curve to calculate E in order to minimize viscoelastic effects in the calculation of the modulus. Figure 9-7(b) shows the values of E obtained for TPU_XTAL and TPU_SOFT at 23°C. Compared to the behavior of filled rubbers, where E linearly decreases with applied strain and the material softens [31], in both TPUs E first decreases with maximum applied strain (for $\lambda < 4$) and then increases. At 60°C for values of Hencky strain corresponding to $\lambda > 3$ the modulus linearly increases with the applied deformation in both TPUs. Overall, these results indicate a stiffening effect combined with a residual deformation, that is soundly related to the observed permanent strain-induced modification in the TPU microstructure as will be detailed in the following section. The stiffening effect in TPU_XTAL is considerably larger than in TPU_SOFT for all values of applied maximum stretch, in particular at 23°C.

These differences in strain-induced stiffening between TPU_XTAL and TPU_SOFT should play an important role at the crack tip. As proved by Mzabi et al. [4]in filled SBR, the presence of a loaded crack generates a local strain gradient at the crack tip that depends on the external loading and on the material's characteristics. In order to understand the role of the increase of the elastic modulus with applied strain in TPUs we need to better investigate the crack tip microstructure in both TPUs.

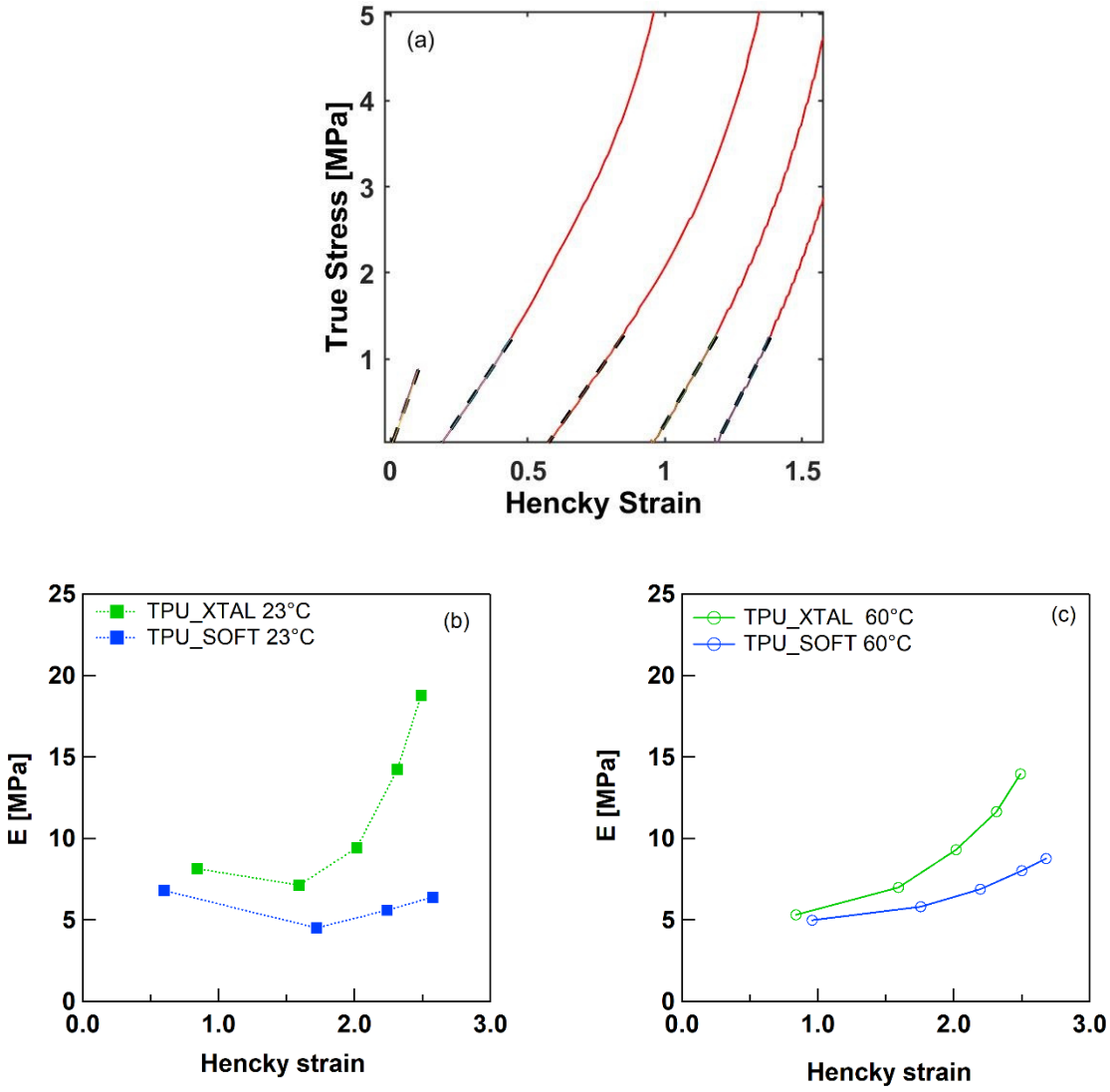

Figure 9-7 Representative true-stress VS Hencky strain unloading curve in cyclic experiment for TPU_XTAL, the inset shows the linear approximation used to calculate E (a). E vs maximum Hencky strain for both TPUs at 23°C (b) and 60°C (c)

9.5 Differences between microstructure at bulk and crack tip

9.5.1 Crack tip characterization in pristine samples

In situ WAXD and SAXS experiments were carried out for two sets of samples: samples that were pre-fatigued and pristine samples. All of them contained a notch. The notched PS specimens were stretched in a displacement-controlled mode up to λ=2.25, then 2D WAXD and SAXS scans were performed along the entire sample's length parallel to the crack and in front of it. The position of the first point (the actual crack tip) is not very precise and it has an uncertainty of $\pm$ 100 µm, i.e. the step width between each successive scan. Figure 9-8 (a) illustrates the set-up of the in-situ scattering experiment. The meridional and equatorial directions are represented by the arrows. Figure 9-8 (b) is an example of the crack profile of the loaded sample and show the deformed mesh used to evaluate the local strain at the crack tip. The axis X_1 and X_2 correspond to the direction parallel and perpendicular to the applied load respectively. Note that in the sketch of X-Ray experiment in Figure 9-8 (a) the sample is turned of 90° compared to the picture of the sample in Figure 9-8 (b).

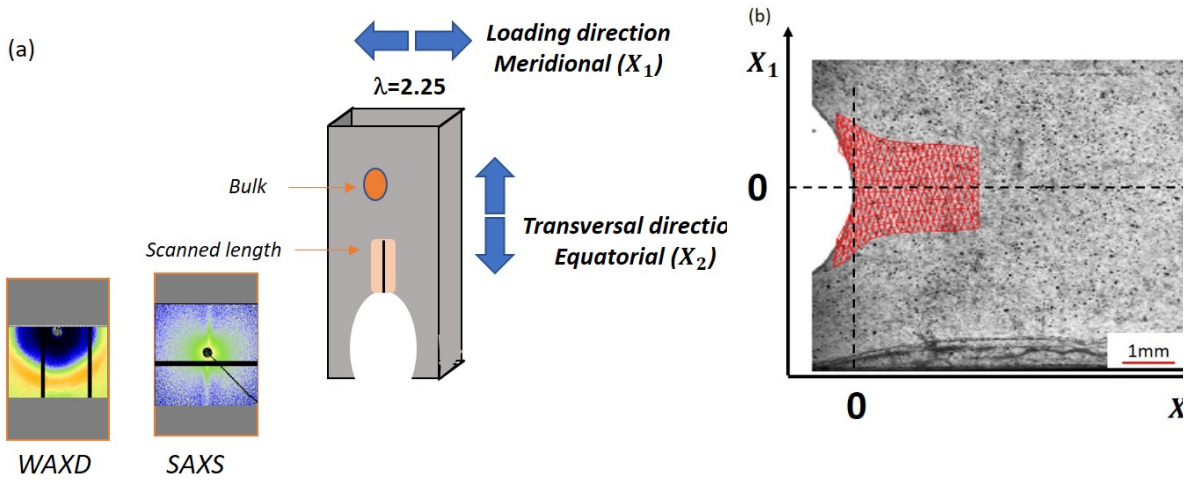

Figure 9-8 Sketch of experimental set-up for WAXD and SAXS experiments (a). Example of open crack profile and deformed mesh obtained from DIC analysis. X_1 indicates the direction parallel direction (meridional) and X_2 the perpendicular direction (equatorial) to the applied load (b).

Figure 9-9(a-b) shows an overview of the crack tip characterization in terms of DIC and X-Ray analysis. Figure 9-9(a) reports the local stretch λ_1 in the loading direction calculated at different distances from the crack tip for both TPUs. The grey shadowed area corresponds to the bulk of the sample where the effect of the crack tip is negligible. The purple shadowed area indicates the area of the material affected by the strain gradient induced by the loaded crack. The maximum local increase of stretch is slightly higher in TPU_SOFT than in TPU_XTAL. Figure 9-9(b) shows the WAXD and SAXS 2D patterns far away and close to the crack tip obtained for TPU_XTAL strained at $\lambda_{max}\approx 2.25$.

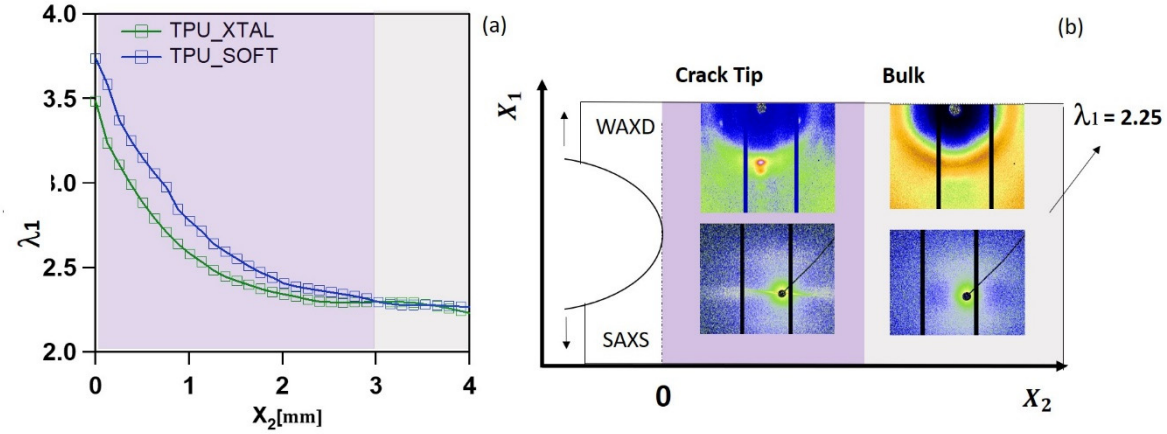

Figure 9-9 Maximum stretch in the vertical direction (λ_1) at increasing distance from the open crack tip (a) In situ WAXD and SAXS 2D representative pattern for TPU_XTAL close and far from the open crack (b) for pristine sample monotonically strained at λ_{max}=2.25. The scattering vector varies between q_{min}= 0.2 (corresponding to the beam stop) and q_{max} = 0.9 nm^{-1}.

Both SAXS and WAXD 2D patterns in the bulk are substantially different from the crack tip region, revealing that the structure in the material changes as the local strain gradient develops. In particular, the WAXD pattern at the crack tip for TPU_XTAL reveals 4 spots (two along the equator and two along the meridional direction) that are characteristic of the presence of well oriented strain induced crystallization (SIC) [32,33], while only an amorphous halo is visible in the bulk. The darker area of the halo in the equatorial direction is indicative of the sample anisotropy developed at $\lambda_{max}\approx 2.25$. SAXS images, both in the bulk and close to the crack in Figure 9-9 (b) confirm the anisotropic character at $\lambda_{max}\approx 2.25$ as evidenced by the appearance of two meridional sharp reflections (or lobes) that were absent in the amorphous SAXS pattern for the pristine unstrained TPU_XTAL (as reported in Figure S 9-1). According to different

authors [7,9,10,33], this indicates the preferential tilting of the HD along the meridional (loading direction) axis. At the crack tip the two meridional lobes become barely visible, while a new equatorial sharp streak appears. The appearance of the streak can be associated either to voids [34] or to a fibrillar morphology [35] and it is frequently found in TPU deformed at large strains [7–10,14,33]. This feature stems from the destruction of HD in favor of rod-like soft domains composed of both elongated SS and HS. The appearance of the streak is then connected to the increased density difference between fibrillar rod-like structure and HD morphology. Yet, the inter-domain distance *L* revealed by the maximum of position in the SAXS 1D profile remains almost unchanged between the bulk and the crack tip (Figure S 9-3). Figure 9-10 reports the 1D WAXD profile for TPU_SOFT in comparison with TPU_XTAL. In this case the crystalline peaks visible in the bulk are associated to the crystalline structure of PBT as indicated in the literature [36]. In principle, PBT and strain-induced crystalline peaks can overlap [33].

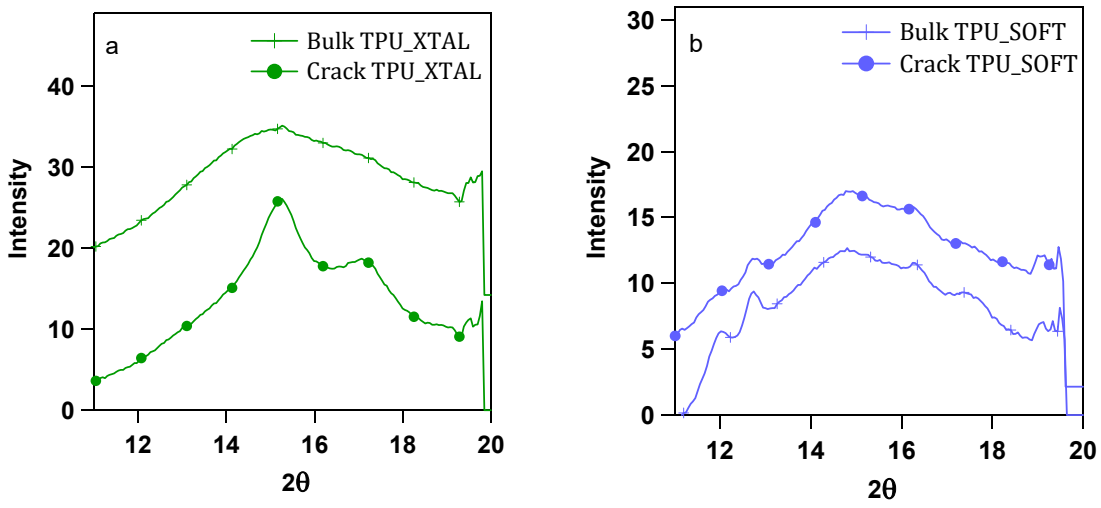

Figure 9-10 Integrated 1D profile of WAXD crystalline peak in TPU_XTAL (a) and TPU_SOFT (b) representative of the crack tip and bulk area.

9.5.2 Effect of loading cycles on the crack tip structure

In the previous section, we explored the effect of the strain concentration on the modification of the local morphology at the crack tip compared to the bulk, proving therefore that, during the firsts loading cycles, the structural organization developed at the crack tip may evolve and eventually stabilize to a position dependent structure near the crack tip. In other word the

presence of the crack induces not only a stress and a strain concentration but a gradient in structure.

We also performed DIC and X-Ray analysis on both TPU samples that were previously notched and fatigued for 40.000 cycles at 10 Hz at $\lambda_{max}\approx2.25$. In this case we did not impose the fully relaxed condition ($\sigma_{min}=0$) and the sample was free to return to the displacement corresponding to the initial length of the undeformed state. This procedure is described in Chapter 7 as "method B". Unlike the method used to obtain the values of *dc/dn* vs. *G* shown in Figure 9-3, in this case the sample was allowed to buckle during the unloading cycle producing higher *dc/dn* compared to Figure 9-3 as described in the supplementary information (Section 9.4). We believe however that the results are also representative of the case reported in Figure 3. Results of the DIC analysis on fatigued samples at increasing distance from the crack tip are reported in Figure 9-11 for both materials, with the same color code previously used for pristine materials in Figure 9-9(a). For comparable distances from the crack tip, the value of vertical strain λ_1 is lower than the pristine counterpart in both TPUs. Remarkably, in the case of TPU_XTAL the strain localization is much weaker after fatigue and only involves a smaller area around the crack (≈1000 μm) than for the TPU_SOFT (≈3000 μm).

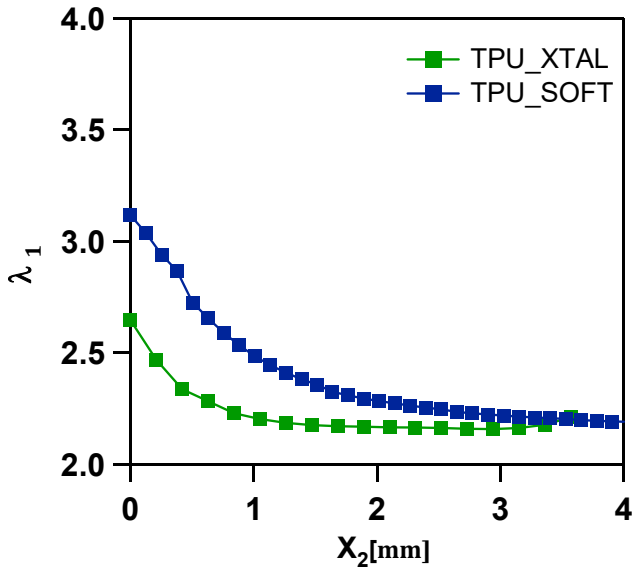

Figure 9-11 Maximum stretch in the vertical direction λ_1 as a function of the distance from the open crack tip for samples fatigued at $\lambda_{max}=2.25$

Figure 9-12(a) compares the representative WAXD 2D images, taken close to the open crack, between the pristine and the fatigued sample monotonically strained at $\lambda_{max}\approx2.25$. For both

TPUs, the images of the pristine samples are different from those of their fatigued counterpart as witnessed by the larger width of the crystalline peaks (corresponding to SIC for TPU_XTAL and PBT planes for TPU_SOFT). In Figure 9-12(b) we compare the SAXS 2D pattern at the closest distance from the crack tip between a pristine and a fatigued sample. The equatorial streak, that is generally observed for large values of strain in homogeneous TPU [7–9,14], is less intense in the fatigued samples. This phenomenon is extremely pronounced in TPU_XTAL.

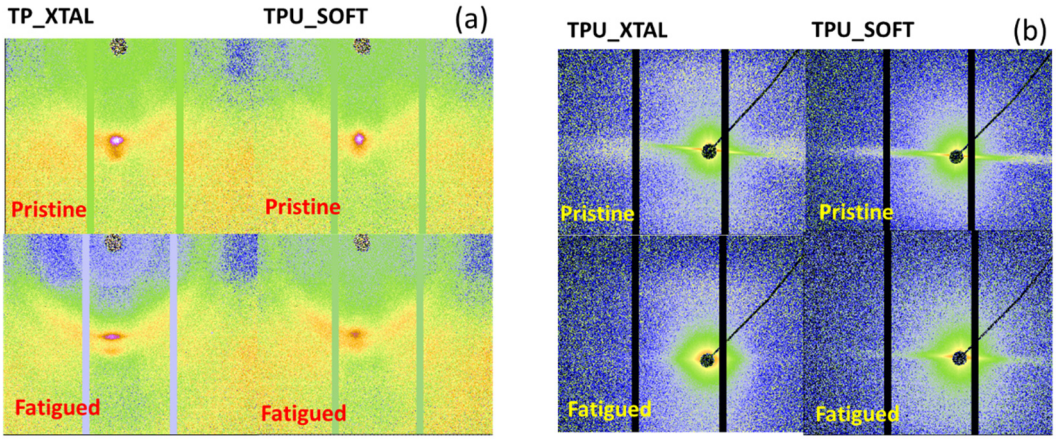

Figure 9-12 WAXD (a) and SAXS (b) representative 2D patterns taken close to the crack tip for pristine and fatigued TPU monotonically strained at λ_{max}=2.25

We evaluated the FWHM of the peak integrated along the azimuthal direction (as indicated in the methods section) for the pristine and the damaged samples at different distances from the crack tip in an area of about 500 μm close to the crack tip. Figure 9-13(a) represents the ratio FWHM_p/FWHM_f obtained from the average FWHM calculated from the single values at different distances from the crack tip, where p and f indicate the pristine and fatigued sample respectively. As the dotted line indicates equal values between pristine and fatigued sample, values lower than unity indicate that the quality of the crystal orientation in the pristine sample is higher than for the fatigued sample, at comparable distance from the crack tip. Therefore, in the case of TPU_XTAL, the strain induced crystallization of the soft segments occurs at the crack tip, but with smaller crystallites, while in TPU_SOFT the original crystallites (of the hard domains) are partially fragmented into smaller units. Figure 9-13(b) reports the crystalline fraction χ, obtained at different distances from the crack tip for TPU_XTAL both pristine and fatigued. χ gradually increases when approaching the crack tip, following the same trend as that of the maximum strain (Figure 9-11).

However the fatigued samples present a lower degree of orientation and in the case of TPU_XTAL, also a lower fraction of crystalline phase when stretched again after being fatigued. This reduced ability of the damaged sample to orient and crystallize under stretch is somewhat unexpected, considering the remarkable fatigue resistance showed by both TPU, and especially by TPU_XTAL.

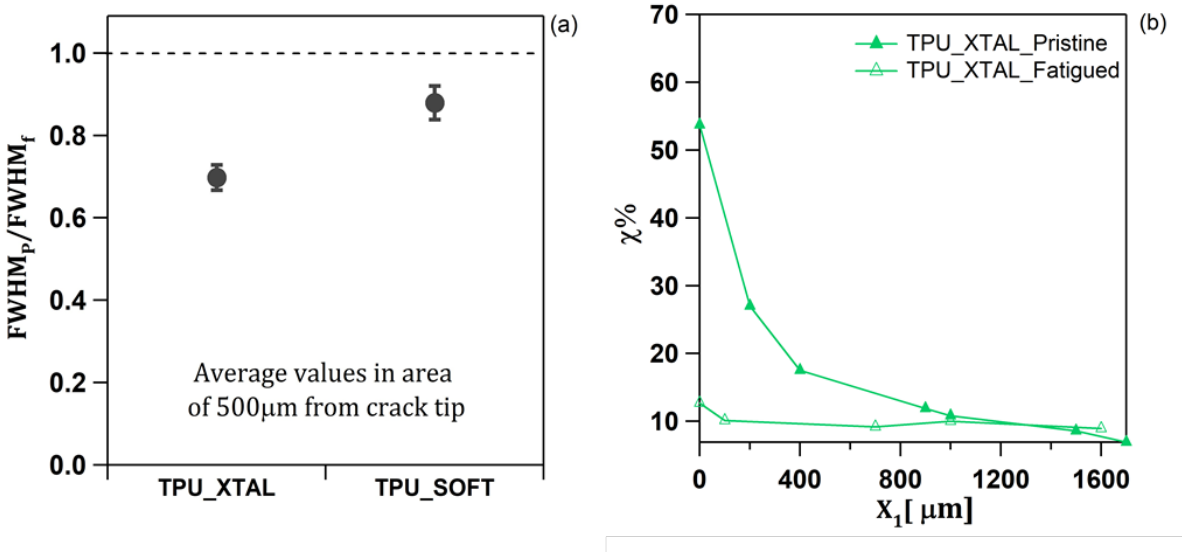

Figure 9-13 Values of FWHM ratio between pristine and fatigued sample(a) and crystalline fraction in TPU_XTAL at increasing distance from the crack for pristine and damaged sample (b) monotonically strained at λ_{max}=2.25 .

9.6 Discussion

9.6.1 A model to explain the strain-induced reinforcement in TPU

The changes in local microstructure with applied strain in TPU have been investigated in depth in the past for homogeneously strained samples[7,10,11,13,14,32,33,37]. Several authors showed that some of those changes are permanent and that the unloaded material does not completely come back to its original state. Depending on the maximum experienced strain, the polymer retains a certain degree of anisotropy or strain induced crystallites as shown by DSC analysis in Figure S 9-4. In particular, for TPU made from SS able to crystallize under strain, the fragmentation of the original amorphous hard domains and the formation of new crystalline domains, that are

persistent after the unloading, is generally considered responsible for the strengthening of the material with strain [10,16,33].

In our case the linear modulus of both TPUs increases with applied strain, but only TPU_XTAL crystallizes under strain. This indicates that the strengthening effect induced by the strain is not uniquely related to the formation of a crystalline phase, but is a general property of the self-organization of TPU in soft and hard domains. We believe that the permanent re-organization of the two-phase microstructures in TPU induces self-strengthening of the material through two main mechanisms:

1) Above a certain value of λ, the original HD are fragmented into smaller units and this new structure partially persists after the removal of the strain (as suggested by the decrease of the long period *L* length for strained TPU (Figure S 9-3). In a homogeneously stretched sample, these smaller and probably well dispersed HD, act as new physical crosslink points for the SS. The re-loaded sample results to have a higher physical crosslink density compared to the original one, leading to both an increase in the modulus and a reduction of the limiting extensibility with applied strain as schematically shown in Figure 9-14.

2) In this new configuration of HD some soft chains, which were highly elongated during the deformation of the sample, may be prevented from recovering their original configuration, thus remaining partially elongated in the unloaded sample explaining the presence of residual crystallinity in TPU_XTAL. This residual crystalline phase, acts as additional hard domains as suggested by the larger increase of *E* (and reduction ofλ_1) in TPU_XTAL. This leads to increasing the fatigue resistance, but it is not a necessary condition for strain-induced reinforcement of TPU.

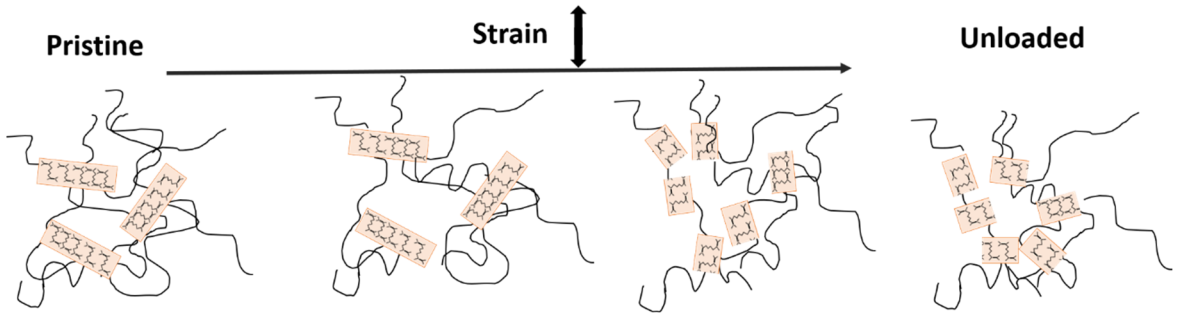

Figure 9-14 Sketch of the effect of elongation on HD restructuration

9.6.2 The effects related to the presence of a crack in cyclic deformation

Previous investigations on the structural evolution of soft TPUs with the applied strain mainly focused on homogeneously strained materials, and showed a remarkable strain stiffening after elongation [10]. To the best of our knowledge, the effect of the presence of a crack and its associated strain localization has never been investigated. In this work, we show that the presence of a strain gradient at the crack tip generates a spatial gradient in the structural reorganization within the TPU, thus affecting the local mechanical response to the applied strain.

Intriguingly, we observed that the repetition of several cycles (at the same bulk λ_{max}) leads to a decrease of the strain-induced anisotropy and crystallinity fraction (in TPU_XTAL) in the crack tip region and in general to a decrease in the sharpness of the structural gradient. This raises the question: how is the local decrease of crystallinity and alignment related to the stable and low *dc/dn* at high values of *G* ?

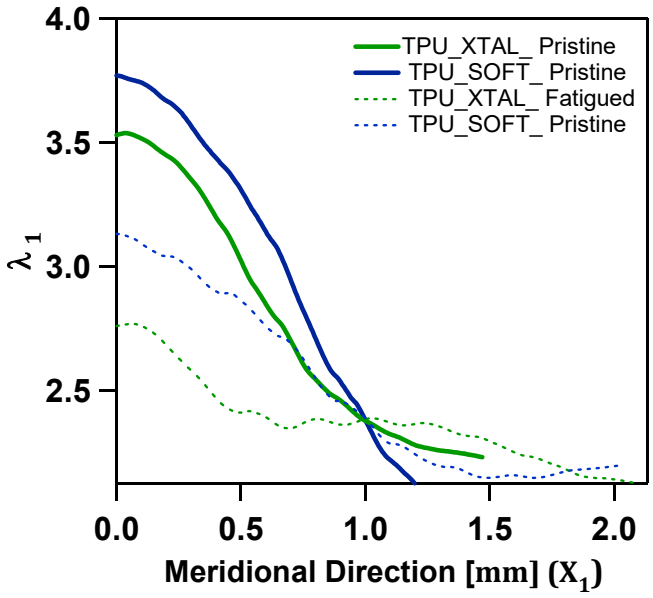

Figure 9-15 Distribution of the maximum λ_1 at the crack tip along the loading direction X_1 for pristine and fatigued samples.

We infer that the less oriented structure created by cyclic fatigue at the crack tip, compared to their pristine counterpart, is associated to the reduction of the strain concentration at the crack tip induced by the non-homogeneous spatial strengthening of the material during the first

loading cycles. In fact, in cyclic fatigue the strain experienced in the bulk is lower than close to the crack tip, where the strengthening mechanisms are active. This generates a spatially non-homogeneous reinforced structure consisting of a stiffer core in the crack tip region with local large strain, embedded in a softer bulk material in the zone where the loading condition are less severe as schematically shown in Figure 9-16. This implies that when a macroscopic strain is applied to a notched sample, the material far from the crack must deform more to compensate the low deformability of the area around the crack tip (as an incompressible filler into a deformable matrix). This results in a reduction of the strain concentration effect at the crack tip as visible in Figure 9-15 that shows the strain distribution of λ_1 along the direction X_1, parallel to the applied load, in the close vicinity of the crack tip. We can observe that the fatigued samples have a more uniform distribution of λ_1 along the vertical direction X_1.

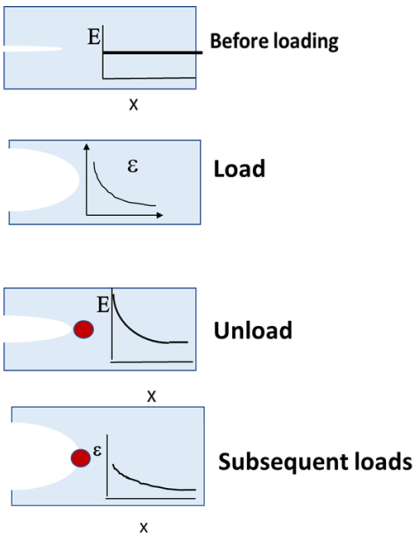

Figure 9-16 Sketch of the spatial evolution of the Young modulus in a TPU containing a crack during cyclic deformation.

The latter would explain both the lower crystallinity observed in TPU_XTAL and the less evident equatorial streaks in TPUs after fatigue. In particular, the appearance of an equatorial streak in the large strain region (λ_{max}>52.2) is characteristic of several TPUs [6–8,10] and was associated to the presence of voids and fibrillar structures. Therefore, as far as the macroscopic strain remains moderate and does not induce the nucleation of voids, only the local strengthening mechanism is activated in the crack tip regime. However, when the whole sample is strained above this strain threshold, some structural damage can take place at the bulk scale causing a ruin of the sample. In other words, the TPU_XTAL is able to reduce the strain concentration to a level such that the crack tip only experiences a mildly

enhanced mechanical stress than the bulk. As explained in Chapter 6, the probability that the crack advances in cyclic fatigue is linked to two main aspects: the maximum stretch experienced by the material at the crack tip (which depends on the effect of the strain concentration induced by the crack) and the average maximum chain extensibility (which depends on the polymer network). It is thus reasonable to suppose that this low strain concentration reduces significantly the probability of breaking bonds at the crack tip at each loading cycle and hence reduces *dc/dn*, making the material highly fatigue resistant. The peculiar feature of the TPU is the ability to maintain an excellent reversible elasticity in the bulk (necessary for applications), while using its ability to plastically deform at high strain to reduce the severity of the strain concentration at the crack tip. In turn this less severe localization is essential in fatigue since it reduces the probability of bond scission at every loading cycle and hence reduces greatly *dc/dn*. A similar mechanism has been recently shown for polyampholyte hydrogels where a strain dependent structural change is also active[26]

9.7 Conclusion

The cyclic fatigue behavior and structural evolution of two soft TPUs with different large strain behavior has been investigated using a strategy defined in our previous work (Chapter 7), and reported as *dc/dn* vs. G. We found that the presence of strain induced crystallization improves the cyclic fatigue resistance by reinforcing the crack tip in a similar way to what happens in stretched natural rubbers. However, SIC does not represent the unique source of local strengthening in fatigue. The presence of a strain gradient in an area close to the loaded crack was shown to generate a self-adapting non-uniform spatial organization of the TPU microstructure, which produces a selective reinforcement above a threshold value of strain. The more strained region at the crack tip becomes stiffer than the bulk, leading to a reduction of the strain localization and thus reducing the probability of bond scission at every loading cycle that is necessary to propagate the crack. As a result of this weak strain concentration the crack propagation rate by cyclic fatigue *dc/dn* is markedly reduced. Some open questions remain regarding the behavior of this selective reinforcement in more severe conditions when the whole sample is highly strained, so that the permanent change in the microstructure can also affect the whole bulk region away from the crack. However, this study clearly shows on commercial materials the effectiveness of a strain-dependent structural change that is responsible for enhanced fatigue resistance and for high strain plasticity in TPUs.

9.8 Acknowledgments

The PhD work of G. Scetta was jointly funded by the French ANRT and the LRCCP. We thank Dario Cavallo for the helpful discussion on X-Ray data interpretation. We are indebted to Dr. Matthias Gerst, Dr. Elke Marten and Mr. Stephan Dohmen from BASF AG for kindly providing the TPU samples. We are grateful to DSM for the availability of the facilities and specially to Junyu Li for the help with X-Ray analysis.

9.9 References

1. Bonart R. Thermoplastic Elastomers. *Brydson's Plast Mater Eighth Ed*. 1979;20(July):653-703. doi:10.1016/B978-0-323-35824-8.00024-4

2. Z. S.Petrovic JF. POLYURETHANE ELASTOMERS. *Prog Polym Sci*. 1991;16:695-836.

3. Bai R, Yang J, Suo Z. Fatigue of hydrogels. *Eur J Mech A/Solids*. 2019;74:337-370. doi:10.1016/j.euromechsol.2018.12.001

4. Mzabi S, Berghezan D, Roux S, Hild F, Creton C. A critical local energy release rate criterion for fatigue fracture of elastomers. *J Polym Sci Part B Polym Phys*. 2011;49(21):1518-1524. doi:10.1002/polb.22338

5. Martinez JRS, Toussaint E, Balandraud X, et al. Heat and strain measurements at the crack tip of filled rubber under cyclic loadings using full-field techniques To cite this version : HAL Id : hal-01148252 Heat and strain measurements at the crack tip of filled rubber under cyclic loadings using full-f. 2015.

6. Bonart R. X-ray investigations concerning the physical structure of cross-linking in segmented urethane elastomers. *J Macromol Sci Part B*. 1968;2(1):115-138. doi:10.1080/00222346808212867

7. Yeh F, Hsiao BS, Sauer BB, Michel S, Siesler HW. In-situ studies of structure development during deformation of a segmented poly(urethane-urea) elastomer. *Macromolecules*. 2003;36(6):1940-1954. doi:10.1021/ma0214456

8. Rahmawati R, Masuda S, Cheng CH, et al. Investigation of Deformation Behavior of Thiourethane Elastomers Using in Situ X-ray Scattering, Diffraction, and Absorption Methods. *Macromolecules*. 2019;52(18):6825-6833. doi:10.1021/acs.macromol.9b00982

9. Kojio K, Matsuo K, Motokucho S, Yoshinaga K, Shimodaira Y, Kimura K. Simultaneous small-angle X-ray scattering/wide-angle X-ray diffraction study of the microdomain structure of polyurethane elastomers during mechanical deformation.

Polym J. 2011;43(8):692-699. doi:10.1038/pj.2011.48

10. Koerner H, Kelley JJ, Vaia RA. Transient microstructure of low hard segment thermoplastic polyurethane under uniaxial deformation. *Macromolecules*. 2008;41(13):4709-4716. doi:10.1021/ma800306z

11. Blundell DJ, Eeckhaut G, Fuller W, Mahendrasingam A, Martin C. Real time SAXS / stress – strain studies of thermoplastic polyurethanes at large strains. *Polymer (Guildf)*. 2002;43:5197-5207.

12. Ishihara H, Kimura I, Yoshihara N. Studies on Segmented Polyurethane-Urea Elastomers: Structure of Segmented Polyurethane-Urea Based on Poly(tetramethylene glycol), 4,4′-Diphenylmethane Diisocyanate, and 4,4′-Diaminodiphenylmethane. *J Macromol Sci Part B*. 1983;22(5-6):713-733. doi:10.1080/00222348308245751

13. J.W.C Van Bogart, A. Lilaonitkul SLC. Morphology and properties of segmented polyether poly(urethaneureas). *Am Chem Soc*. 1979. doi:10.1295/polymj.17.969

14. Waletzko RS, James Korley LST, Pate BD, Thomas EL, Hammond PT. Role of increased crystallinity in deformation-induced structure of segmented thermoplastic polyurethane elastomers with PEO and PEO-PPO-PEO soft segments and HDI hard segments. *Macromolecules*. 2009;42(6):2041-2053. doi:10.1021/ma8022052

15. Zhu P, Dong X, Wang D. Strain-Induced Crystallization of Segmented Copolymers: Deviation from the Classic Deformation Mechanism. *Macromolecules*. 2017;50(10):3911-3921. doi:10.1021/acs.macromol.6b02747

16. Toki S, Hsiao BS, Kohjiya S, Tosaka M, Tsou AH, Datta S. Synchrotron X-Ray Studies of Vulcanized Rubbers and Thermoplastic Elastomers. *Rubber Chem Technol*. 2011;79(3):460-488. doi:10.5254/1.3547946

17. Rivlin RS, Thomas AG. Rupture of rubber. I. Characteristic energy for tearing. *J Polym Sci*. 1953;10(3):291-318. doi:10.1002/pol.1953.120100303

18. Mattia J, Painter P. A comparison of hydrogen bonding and order in a polyurethane and poly(urethane-urea) and their blends with poly(ethylene glycol). *Macromolecules*. 2007;40(5):1546-1554. doi:10.1021/ma0626362

19. Hammersley AP. “FIT2D.” 2016. http://www.esrf.eu/computing/scientific/FIT2D/.

20. Laboratory of mechanics and technology of ENS C. CORRELI.

21. Mzabi S. Caractérisation et analyse des mécanismes de fracture en fatigue des élastomères chargés. 2010:1-310.

22. Bhowmick AK. Threshold Fracture of Elastomers. *J Macromol Sci Part C*. 1988;28(3-4):339-370. doi:10.1080/15583728808085379

23. Lake GJ, Lindley PB. Mechanical Fatigue Limit for Rubber. *J Appl Polym Sci*. 1965;9:1233-1251. doi:10.5254/1.3544847

24. Mars W, Fatemi a. A literature survey on fatigue analysis approaches for rubber. *Int J Fatigue*. 2002;24(9):949-961. doi:10.1016/S0142-1123(02)00008-7

25. Lake, G. J. Lindely PB. Cut growth and fatigue of rubbers. 1964;455(2):292-300.

26. Li X, Cui K, Lin T, et al. Mesoscale bicontinuous networks in self-healing hydrogels delay fatigue fracture. *Proc Natl Acad Sci*. 2020;117(14). doi:10.1073/pnas.2000189117

27. Diani J, Fayolle B, Gilormini P. A review on the Mullins effect. *Eur Polym J*. 2009;45(3):601-612. doi:10.1016/j.eurpolymj.2008.11.017

28. Mullins L. Softening of rubber by displacement. *Rubber Chem Technol*. 1969;42(1):339-362.

29. Qi HJ, Boyce MC. Stress-Strain Behavior of Thermoplastic Polyurethane. *Mech Mater*. 2004;37(December 2003):1-51. doi:10.1016/j.mechmat.2004.08.001

30. Sui T, Salvati E, Ying S, et al. Strain softening of nano-scale fuzzy interfaces causes Mullins effect in thermoplastic polyurethane. *Sci Rep*. 2017;7(1):1-9. doi:10.1038/s41598-017-00904-3

31. Merckel Y, Diani J, Brieu M, Gilormini P, Caillard J. Characterization of the mullins effect of carbon-black filled rubbers. *Rubber Chem Technol*. 2011;84(3):402-414. doi:10.5254/1.3592294

32. Toki S, Sics I, Hsiao BS, et al. Structural Developments in Synthetic Rubbers during Uniaxial Deformation by In Situ Synchrotron X-Ray Diffraction. *J Polym Sci Part B Polym Phys*. 2004;42(6):956-964. doi:10.1002/polb.10679

33. Zhu P, Zhou C, Dong X, Sauer BB, Lai Y, Wang D. The segmental responses to orientation and relaxation of thermoplastic poly(ether-ester) elastomer during cyclic deformation: An in-situ WAXD/SAXS study. *Polymer (Guildf)*. 2020;188:122120. doi:10.1016/j.polymer.2019.122120

34. Statton WO. Microvoids in fibers as studied by small-angle scattering of x-rays. *J Polym Sci*. 1962;58(166):205-220. doi:10.1002/pol.1962.1205816611

35. Stribeck N, Sapoundjieva D, Denchev Z, et al. Deformation behavior of poly(ether ester) copolymer as revealed by small- and wide-angle scattering of X-ray radiation from synchrotron. *Macromolecules*. 1997;30(5):1329-1339. doi:10.1021/ma9612079

36. Li, H.L.: White J. Elastic Response of Copolyether-ester Fiber on Its Phase Morphology under Different Heat-treatment Condition. *Polym Eng Sci*. 2000;40:917-928.

37. Kimura I, Ishihara H, Ono H, Yoshihara N, Nomura S, Kawai H. Morphology and Deformation Mechanism of Segmented Poly(urethaneureas) in Relation to Spherulitic Crystalline Textures. 1974;7(3):355-363. doi:10.1021/ma60039a018

9 EXTENDED SUPPLEMENTARY INFORMATION

9.1 X-Ray analysis

Static WAXD and SAXS characterization was performed on pure shear (PS) samples in two conditions: pristine and unloaded after being fatigued at $\lambda_{max} \approx 2.25$ for 40.000 cycles as described in 9.4 Cyclic fatigue method B. The technical details of the scattering experiment are summarized in Table S 9-1. The 2D SAXS images for TPU_XTAL for pristine and fatigued sample are showed in Figure S 9-1 (a-b). The similar circular pattern in both images indicates that the TPU_XTAL recovers the original isotropic character when the strain is removed. On the other side, TPU_SOFT has an elliptical shape in the pristine configuration, induced by the injection procedure, Figure S 9-1(c) that persists after fatigue Figure S 9-1 (d).

Facility	DSM, Netherlands
Energy	8.04 KeV
Wave length (λ)	0.154 nm
Beam size (SAXS)	300 μm
Beam size (WAXD)	700μm
Distance from detector (SAXS)	1465.45mm
Distance from detector (WAXD)	120.45 mm
Image resolution	172x172 pixel

Table S 9-1 Parameters of X-Ray experiment

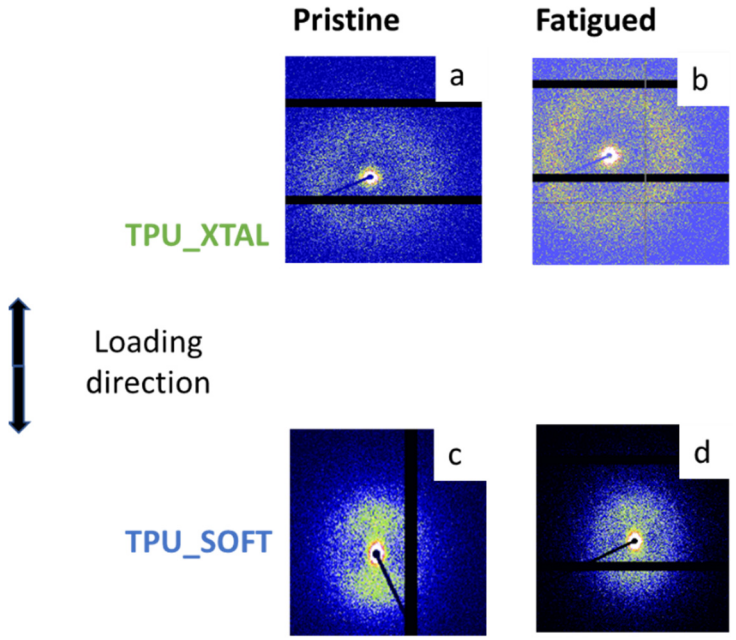

Figure S 9-1 2D SAXS Pattern for both TPU pristine (a-c) and after fatigue (b-d).

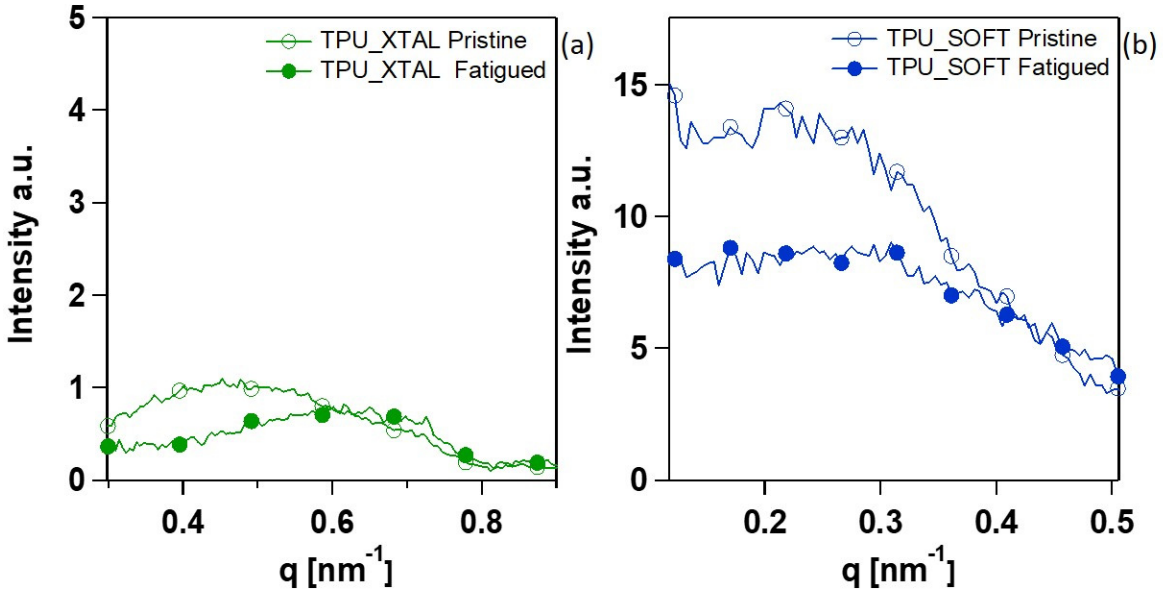

Figure S 9-2 1D integrated SAXS profile for TPU_XTAL (a) and TPU_SOFT (b) both in pristine and fatigued conditions.

The 1D integrated profiles for all samples are reported inFigure S 9-2. The profile for TPU_SOFT is obtained integrating along the vertical direction. For TPU_XTAL, because of the symmetric pattern, we performed a circular integration. The long period L , evaluated as the center of a Gaussian fitting of the maximum in each intensity curve, is reported in Table S 9-2. In both materials the value of L is smaller after fatigue compared to pristine samples. The reduction of L along the tensile direction with strain has been previously observed in similar TPU systems[2,5,6,20] and it was associated to the partial disruption of the original HD in smaller fragments reducing therefore their average inter-distance. Overall, this suggests that the strained sample has different HD size and organization compared to the pristine one and the original state is not recovered after the removal of the load.

Name	Pristine L [nm]	Fatigued L [nm]
TPU_XTAL	13.4	9.9
TPU_SOFT	29.9	26.1

Table S 9-2 Long period for TPU_XTAL and TPU_SOFT for pristine and fatigued samples.

9.2 Strain-induced structural changes during tensile deformation of TPU

The application of external strain induces anisotropy on original isotropic TPU_XTAL as indicated by the ellipsoidal 2D SAXS with two prominent lobes along the straining direction (Figure 9-9 (b)). We calculated the value of long period L along both meridional (Me) and equatorial (Eq) direction in strained samples at increasing distance from the crack tip. (Figure S 9-3(a) shows an example of 1D-SAXS intensity profile, integrated along the meridional direction for TPU_XTAL). The calculated values of long period L at λ_{max}=2.25 are reported in Figure S 9-3 (b). The dotted line indicates approximatively the original value of L calculated in the pristine sample. The lower values along the equatorial direction compared to the meridional one, are related to the shrinking lamellae within the aligned domains in the direction perpendicular to the stress as consequence of the Poisson effect. Additionally, the value of L remains almost constant, in both direction, at different distance from the crack suggesting the lack of spatial correlation (or affine deformation) in this new formed high-strain configuration. Similar results were obtained for TPU_SOFT.

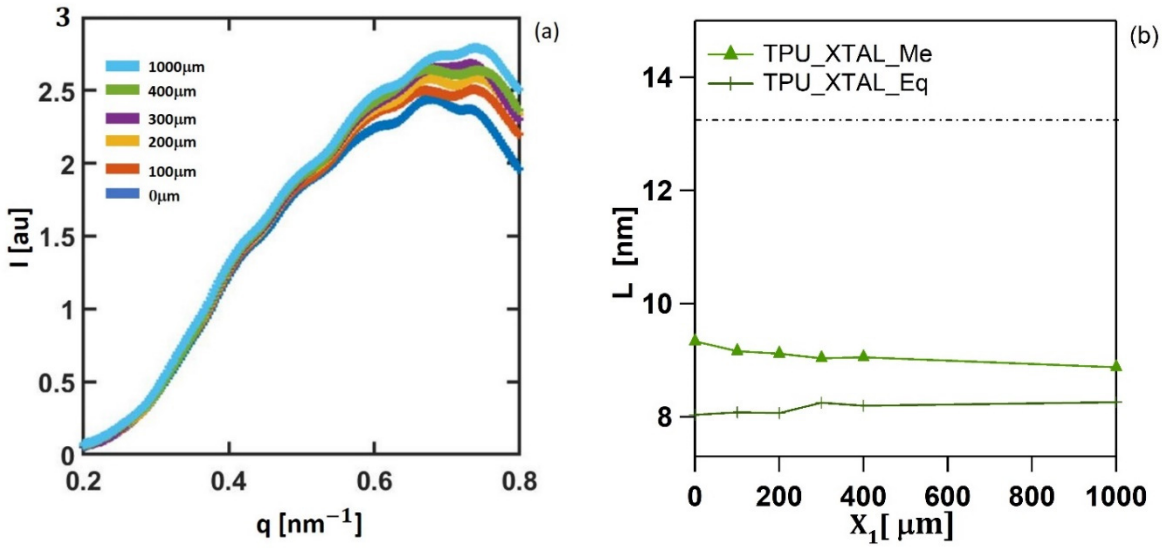

Figure S 9-3 1D SAXS profile for strained TPU1 at selected distances from the crack tip (a). Evolution of inter-distance L for pristine TPU1 (dotted line)and as function of the distance from the crack tip in strained sample (b) at λ_{max}=2.25.

9.3 Residual crystallinity in uniaxial strained TPU_XTAL

Thermal properties of TPUs were studied by differential scanning calorimetry (DSC) (TA instrument, Q200 device, USA). The samples were heated first from ambient temperature to 200°C and maintained at this temperature for 3 minutes. They were then cooled to -100°C and finally re-heated to 200°C. Both cooling and heating rates were fixed at 10°C/min. Thermal scan were performed on pristine and strained samples.

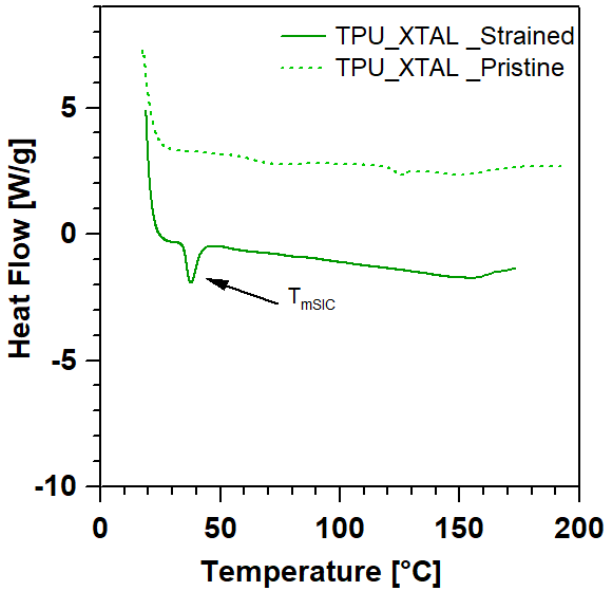

Figure S 9-4 DSC thermogram for all TPU pristine and after being strained to rupture

Figure S 9-4 reports the DSC thermogram carried out pristine TPU_XTAL and on the fractured part of a sample strained up to rupture. The endothermic peak (T_{mSIC}) in strained TPU_XTAL , that was absent in the pristine material, is associated to the new crystalline phase generated during uniaxial tension that persists after the removal of the load (SIC).

9.4 Cyclic fatigue method B

The fatigued sample TPU_XTAL and TPU_SOFT used in in situ X-Ray experiments, were notched and strained for 40.000 cycles between $\lambda_{max} = 2.25$ and $\lambda_{min} = 1$. An accurate description of the fatigue method is reported in Chapter 7 (Method B). Both samples present un-negligible residual deformation ($\lambda_{res} > 1$) when cyclically deformed. This implies that the sample buckles during each cycle as showed in Figure S 9-5. The crack extension during cycle was monitored with the optical system described in the present paper and the value of crack propagation are

expressed as dc/dn VS G. Figure S 9-6 shows the values of dc/dn in the steady state regime as function of G for both TPU at different values of G . The two fatigued samples used for X-Ray characterization are indicated by a red circle. TPU_SOFT propagates almost 2 order magnitudes faster than TPU_XTAL confirming the strong reinforcing effect of SIC in crack propagation resistance for TPU_XTAL. Both TPU propagate faster compared to the values reported in the paper (obtained with fully relaxed cyclic conditions preventing buckling). This suggests that the continuous buckling of the sample induces some mechanical damage on the sample lowering the overall fatigue resistance.

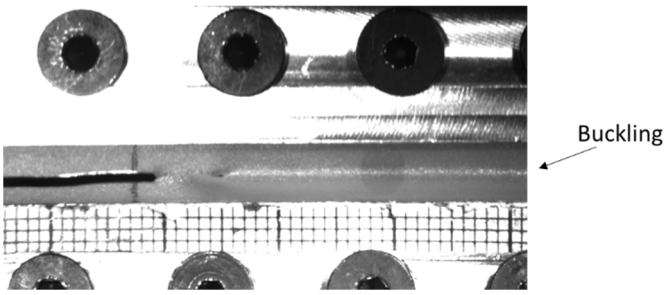

Figure S 9-5 Example of buckling during cyclic fatigue.

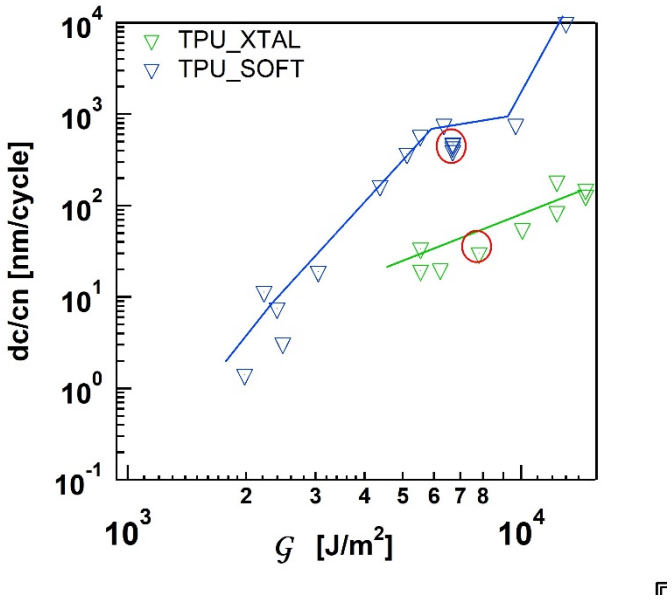

Figure S 9-6 Crack propagation per cycle as function of applied G, method B (allows buckling) for both TPU. The red circles indicate the sample used in X-Ray in situ experiment.

10 GENERAL CONCLUSION AND PROSPECTS

This thesis has been motivated by two different but complementary purposes which, together, explain the merging of the industrial and the academic interest into the subject of fatigue fracture in TPU. On the one hand, there is the industrial need to fulfil: the lack of suitable testing procedures to evaluate the fatigue resistance and durability of TPU. On the other hand, the scientific interest towards this class of polymers that, in the absence of any filler or permanent covalent crosslinking, demonstrates a remarkable fracture resistance comparable or superior to that of classical filled thermoset rubbers.

TPU are experiencing a fast diffusion and gradually replacing thermoset rubbers in specialty applications. Nevertheless, the fatigue and fracture behaviour of TPU has not obtained yet the attention devoted to thermoset rubbers, in part because TPU are relatively new compared to rubbers. In 1960 actually, while TPU saw their first commercialization, almost all the conventional rubbers that we know today were already widespread and commercialized[1].In part because it's not trivial to deal with a class of polymer, such as TPU, which can sustain considerably large strain ($\lambda \sim 10$), present high inelastic phenomena such as tendency to creep and have strain-dependent morphology.

Connecting the dots: cyclic fatigue from thermoset rubber to thermoplastic elastomers.

Cyclic fatigue has been deeply investigated in filled rubber and one of the most diffused method is the fracture mechanic approach. This includes the introduction of pre-crack into the sample and the evaluation of the crack propagation rate per cycle (dc/dn) as function of energy release rate G. A complete understanding of the mechanisms involved in cyclic fatigue fracture for elastomers is still missing but it has been showed that the highly strained region at the crack tip (process zone) plays a significant role in determining cyclic fracture resistance[2].

An accurate investigation of the process zone in SBR during cyclic fatigue was provided by Mzabi et al[3]. They showed that SBRs differing for chemical crosslinking density and filler content, have different values of dc/dn vs. G but all the curves collapse if the crack propagation per cycle is plotted against a new energy parameter: g_{loc} which only considers the fraction of G locally available in the process zone at the crack tip.

In Chapter 6, we re-analyzed the data reported in the work of thesis of Mzabi[2] to propose a fracture criterion for cyclic fatigue in thermoset elastomers. We introduced the concept of bond scission events as a necessary condition for crack propagation in cyclic fatigue. We argued in fact that, the probability of chain breakage in cyclic fatigue, must be related to the ratio between the maximum strain experienced at the crack tip (λ_{max}) and the distribution of maximal chain extensibility of the polymer strands between crosslinks (λ_b). Within this context the fraction of energy release rate that is effectively available at the crack tip, named g_{loc}, determines the average rate in nm/cycle at which the fracture propagates.

In Chapter 7, we approached one of the the core topic of this work: the cyclic fatigue in TPU. We proposed an optimized testing procedure to evaluate fatigue resistance in TPU. We introduced a value of λ_{min} defined by a zero applied force, to avoid the phenomenon of buckling related to the development of residual plastic deformation. Furthermore, we highlighted the presence of a shake down (steady-state regime), where we evaluated a stable value of the energy release rate *G*. Additionally, we pointed out that values of stretch well above λ=2 are required to propagate the crack in cyclic fatigue for TPU, well above those conventionally used in cyclic fatigue of filled rubbers.

In Chapter 8, we analyzed the large strain properties of TPUs and we re-interpreted the concept of Mullin's effect and cyclic damage typically adopted in thermoset elastomers, for TPUs.

We used three TPUs strongly different in terms of large strain behavior: TPU_HARD and TPU_XTAL are completely amorphous in pristine state and present strong strain hardening effect when loaded in uniaxial conditions. Moreover, the phenomenon of SIC was only detected in

TPU_XTAL. TPU_SOFT on the other hand, presents traces of semicrystalline polymer (PBT) and shows very weak strain hardening compared to the other two. Despite their differences, all TPUs present a common behavior: they became stiffer when deformed above a certain stretch threshold (around $\lambda \sim 4$). This stiffening effect is maintained when the strain is removed and it is different from the strain-softening generally observed in filled rubbers (Mullins' effect). The fact that similar behavior is observed for all three TPUs suggests that is does depend on the two-phase structure of TPUs but not on the specific composition of the polymer (neither on the large strain behavior and presence of SIC). We associated the strain-stiffening effect to fragmentation of HD with applied strain and we argued that this effect may have important consequences in determining the fracture resistance when the material is subjected to a homogeneous strain as in the case of cyclic fatigue.

In Chapter 9, we applied the cyclic fatigue protocol developed in Chapter 6 on TPU_SOFT and TPU_XTAL. In particular, we analyzed the crack tip area using in situ X-Ray analysis and DIC to study:

- The effect on structure modification and strain gradient induced by the strain singularity within the first cycle.
- The effect on structure modification and strain gradient induced by the strain singularity after thousands of cycles.
- The possibility that some structural modifications remain after the removal of the load.

We showed that the presence of large strain at the crack tip locally alters the original morphology in TPU reducing the inter-distance between HD and inducing an anisotropic character. This modified structure is partially retained after the removal of the load and it affects the mechanical behavior under the following cycles for same value of maximum applied strain. Using DIC in fact, we demonstrated that the strain gradient at the crack tip in TPU in the 36.000th cycle is strongly reduced compared to what observed in the 1st cycle of for notched sample in both TPUs.

We concluded our analysis proposing a general fracture mechanism in TPU which is can be summarized as follows:

- Before loading the TPU presents a multiphase structure composed by HD and SD homogeneously dispersed.
- After the first load the high strain generated by the singularity at the crack tip promotes the fragmentation of HD and, when possible, strain induced crystallites. Both events

- After the removal of the load the modified structure around the crack tip is partially retained (while this is not the case in NR where crystallites melt during unload) forming a harder core at the crack tip which is less deformable than the bulk.
- Under the action of the following cycles, the less deformable core protects the crack tip partially shielding the large strain and retarding crack propagation explaining the remarkable fatigue resistance of TPUs.

10.1 Final remarks and future perspectives

The fatigue fracture mechanism proposed for TPU in Chapter 9 is clearly aligned with the hypothesis presented for SBR in Chapter 6 that the maximum strain experienced by the highest stretched polymers chains at the crack tip, $\lambda_{max,}$ is one of the main factors contributing to propagation of the crack. In case of SBR, we proposed that the maximum chain extensibility λ_b , which depends on the composition, was a complementary condition to fracture. The closest the two values the higher the probability of crack propagation. In our view, also in case of TPU, a major role is played by the highest local strain locally experienced by the polymer within the process zone (λ_{max}) . TPUs remarkable fatigue fracture resistance was indeed associated to the strain shielding effect of the hard core at the crack tip which reduces λ_{max} but we couldn't discuss the effect of maximum chain extensibility as done for SBR. In this work in fact, we used commercial materials whose composition was partially unknown therefore, we couldn't approach deeply the molecular aspects. Nevertheless, we think that in TPU, also creep and excessive fragmentation of HD have a key role in determining crack propagation in cyclic fatigue condition and they should be carefully investigated in the future. A final remark must be done concerning the proposed cyclic fracture mechanism in TPU and the effect of harder core at the crack tip. We could not fully verify the validity of this hypothesis because the stiffening effect was observed above λ=4 while in both TPU_XTAL and TPU_SOFT the maximum stretch detectable at the crack tip, within the spatial resolution of the DIC analysis, was < $\lambda\sim4$ in our experimental condition.

To conclude, with this work we opened the route towards a better understanding of cyclic fatigue mechanisms operating in TPU: we proposed a possible explanation to understand the high fatigue resistance of TPU and we validated the importance of tracking the evolution of the microstructure in the process zone of TPU under cyclic experiments using in situ X-Ray analysis.

A more exhaustive characterization should include mapping the entire region at the crack tip for pristine and fatigued samples at different λ_{max}. This would allow a systematic evaluation of the

evolution in HD orientation and fragmentation, and in case of SIC the evolution of the crystalline morphology with the number of cycles.

10.2 References

1. Holden G. Thermoplastic Elastomers. *Appl Plast Eng Handb*. January 2011:77-91. doi:10.1016/B978-1-4377-3514-7.10006-6

2. Mzabi S. Caractérisation et analyse des mécanismes de fracture en fatigue des élastomères chargés. 2010:1-310.

3. Mzabi S, Berghezan D, Roux S, Hild F, Creton C. A critical local energy release rate criterion for fatigue fracture of elastomers. *J Polym Sci Part B Polym Phys*. 2011;49(21):1518-1524. doi:10.1002/polb.22338

ANNEXES

1. FTIR analysis

Fourier transform infrared analysis (FTIR) was used to identify the principal functional groups in all TPUs. Figure 1 shows the FTIR spectrum obtained from pristine samples. The absorption peak around 1157 cm^{-1} is the footprint of the polyester C-O-C vibration present in all TPUs. Additionally, all samples present: two absorption bands at 1540 cm^{-1} and 3300 cm^{-1} corresponding to the NH in plane bending vibrations and stretching respectively, and the double peak at 2860 and 2930 cm^{-1} associated with -CH_2 stretching. Finally, the absorption peak of carbonyl is shifted at different wavelength when the group is either free or bonded[1] (inset of Figure 1). The peak at 1726 cm^{-1} represents the stretch of the non-hydrogen bonded carbonyl and is predominantly associated with carbonyl groups in the polyester soft blocks. The peak at 1700 cm^{-1} indicates the carbonyl stretch resonance for hydrogen-bonded urethane groups. This corresponds to the intra-hard segments hydrogen bonding cooperating in the gathering of hard segment to form hard domain structures[2–4].

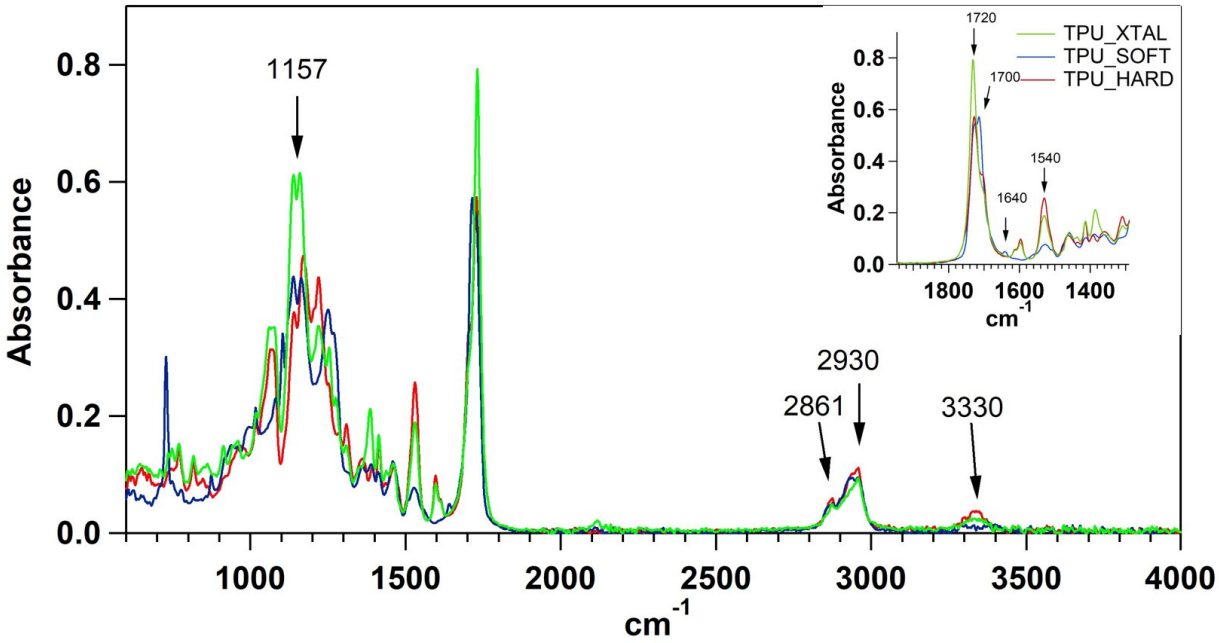

Figure 1 Complete FTIR spectra for all TPUs and expansion of Carbonyl Stretch/N-H Bend Region (inset)

Overall, the FTIR spectra for all three TPUs are qualitatively very similar as expected. The main relevant difference concerns the presence of two absorption peaks in TPU_SOFT at 727 and 1640 cm^{-1} that are absent in the other materials.

The first peak at 727 cm^{-1} is indicative of an aromatic component and is compatible to the aromatic ring of PBT. According to literature[2,5] the second peak (~1640 cm^{-1}) is compatible with the presence of strong hydrogen bonds between urea and carbonyl groups in a bidentate configuration. The presence of small quantity of urea offers more stable bonding than the single H-H bonds of polyurethane. If our hypothesis is correct, this would suggest high stability of hard domains in TPU_SOFT in agreement with the higher plateau modulus of TPU_SOFT in Figure 8-2 (Chapter 8). Hydrogen bonding plays an important role in defining the morphology and mechanical properties of TPU[6,7]. A schematical representation of different hydrogen bonds in polyurethane and polyurea TPU is presented in Figure 2 from [5].

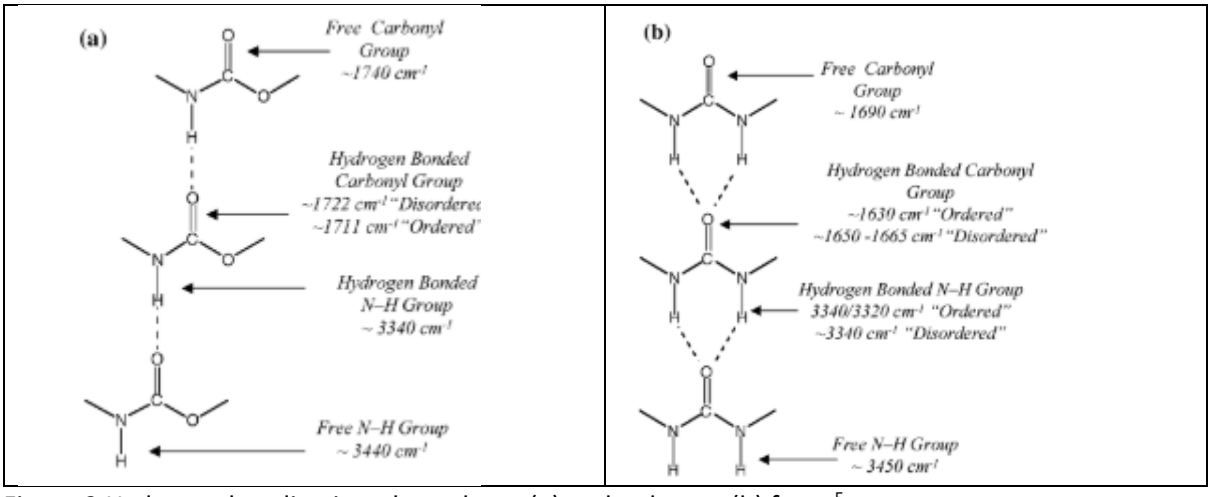

Figure 2 Hydrogen bonding in polyurethane (a) and polyurea (b) from [5]

2. Toughness: effect of temperature and strain rate

In Chapter 7 we reported the value of fracture toughness Γ for TPU_HARD at 23°C. Here we provide a more extended investigation on the fracture resistance of all TPUs at different temperatures and stretch rates.

Experimental conditions

We prepared two sets of samples with same PS geometry. One set is pristine the other is notched with a pre-crack of 10 mm. The uncut sample was clamped between the grips and a monotonic load was applied.

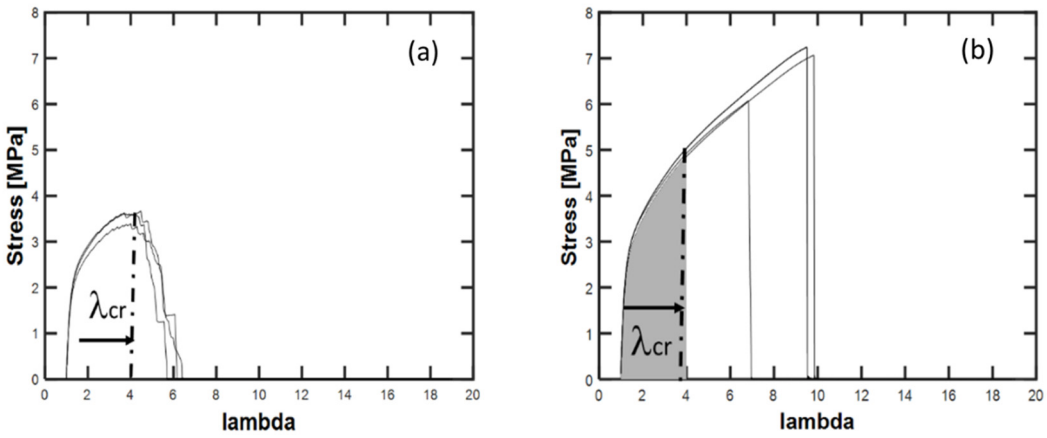

Figure 3 Example of stress-stretch curve for the a) notched and b) un-notched sample. The fracture energy is evaluated as the integral under the curve between 1 and λ_{cr}.

First, the test was performed on pre-notch samples to evaluate λ_c , that is the critical length required to propagate the crack at the imposed strain rate. The critical stretch was evaluated at the maximum of the notched stress-stretch curve (Figure 3) following the procedure already adopted by other authors [8–10]. As reported in Chapter 5, in PS samples the toughness is evaluated as:

$$\Gamma = h_0 W(\lambda_c) \qquad \textbf{Equation 1}$$

where h_0 is the initial height of the sample and $W(\lambda_c)$ is the energy per volume of the uncut sample. $W(\lambda_c)$ is evaluated from the un-notched sample (black area in Figure 3 b) integrating the stress-stretch curve up to the λ_c measured on the notched sample.

Figure 4 shows the effect of temperature on Γ for all TPUs at stretch rate $\dot{\lambda}$ of 4 sec^{-1}. At 23°C the samples present different values of Γ varying between 60 and 140 kJ/m^2 with TPU_HARD being the toughest. Increasing temperature has two main effects: reducing the differences among all samples and reducing the average value of Γ.

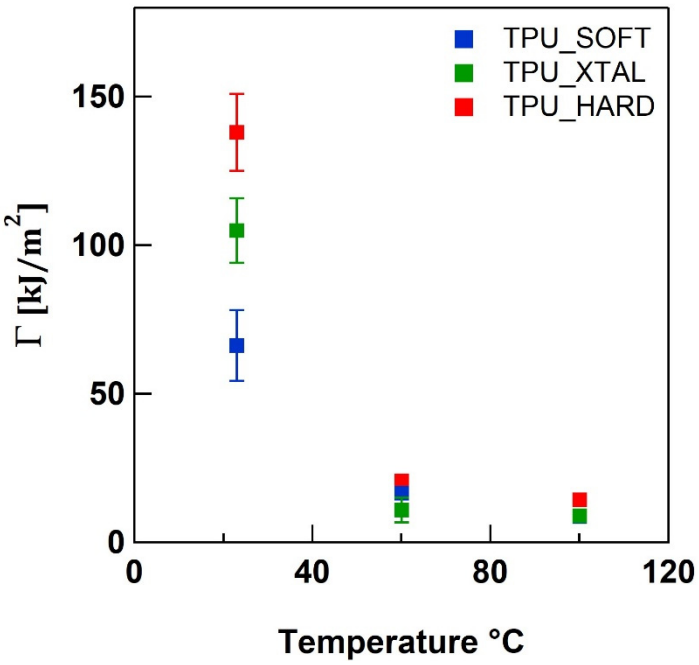

Figure 4 Monotonic toughness for all three TPUs as a function of temperature at 4 s^{-1}.

3. Crack extension and blunting at high stretch rate

In cyclic fatigue experiments we used a constant frequency of 10 Hz that, for the used values of maximum applied stretch λ, corresponds to a strain rate $\dot{\lambda}$ between 20 and 40 s^{-1}. In order to evaluate whether Γ strongly depends on the strain rate, we decided to carry out monotonic fracture experiments at $\dot{\lambda}$ =20 s^{-1}, which is one order of magnitude higher than that used in the previous chapter and comparable to the value experienced by the material in cyclic fatigue. We did the experiments on TPU_SOFT and TPU_HARD at 23° and 60°C, monitoring with a fast camera the extension of the pre-cut. The calculated values of toughness at 20 sec^{-1} and 4 sec^{-1} are summarized in Table 1. There are no significant differences between those obtained at the same temperature and different $\dot{\lambda}$ indicating that, despite their inelastic behavior, fracture toughness in TPU has only a weak dependence on stretch rate in the used testing conditions.

Table 1 Fracture toughness for TPU_HARD and TPU_SOFT at 20 s^{-1} (23 and 60°C) and 2 s^{-1}(23, 60 and 100 °C)

	Stretch rate 20 s^{-1}		**Stretch rate 4 s^{-1}**	
Temp. °C	**TPU_HARD** kJ/m^2	**TPU_SOFT** kJ/m^2	**TPU_HARD** kJ/m^2	**TPU_SOFT** kJ/m^2
23	156±37	45±31	138±13	66±12
60	27±2.6	18±1	20.7±0.2	16.5±1.8
100			14.3±0.1	8.6±0.4

Interestingly, we evidenced that in some cases the crack does not always propagates straight to rupture. Figure 5 reports the value of crack length and crack radius (obtained by a parabolic fitting of the crack opening profile) vs. the applied λ during a typical fracture experiment for TPU_SOFT (a) and TPU_HARD (b) at 23°C. In the case of TPU_HARD we observe a sharp increase in both crack extension and crack radius at λ_c~5.8 (Figure 5(b)), which almost corresponds to the maximum in the stress-stretch curve for the cut sample in Figure 5(d). For TPU_SOFT the crack length increases quasi-monotonically with the applied λ up to the complete rupture of the sample. Some tiny jumps in the crack length for TPU_SOFT, indicated by black arrows in Figure 5(b), correspond to relative maxima in the stress-stretch curve in Figure 5(c). In this case we decided to conventionally adopt the value of the first maximum (or the first jump) to evaluate Γ as already found in other works[8]. Overall, if we compare the increase in crack extension and the crack radius with the applied λ during the whole experiment for both TPUs, we can distinguish a different trend. In case of TPU_HARD the achievement of a plateau in the radius anticipates the final rupture of the sample. In the case of TPU_SOFT the radius keeps increasing with applied λ, similarly to the crack extension. This indicates that the ability of the material to blunt plays an important role in defining the critical extensibility

before breaking the sample. In TPU_SOFT as far as the crack can keep blunting the crack propagation is controlled. Nevertheless, the value of Γ is higher in TPU_HARD than TPU_SOFT because of the large-strain softening in the stress strain curve of TPU_SOFT.

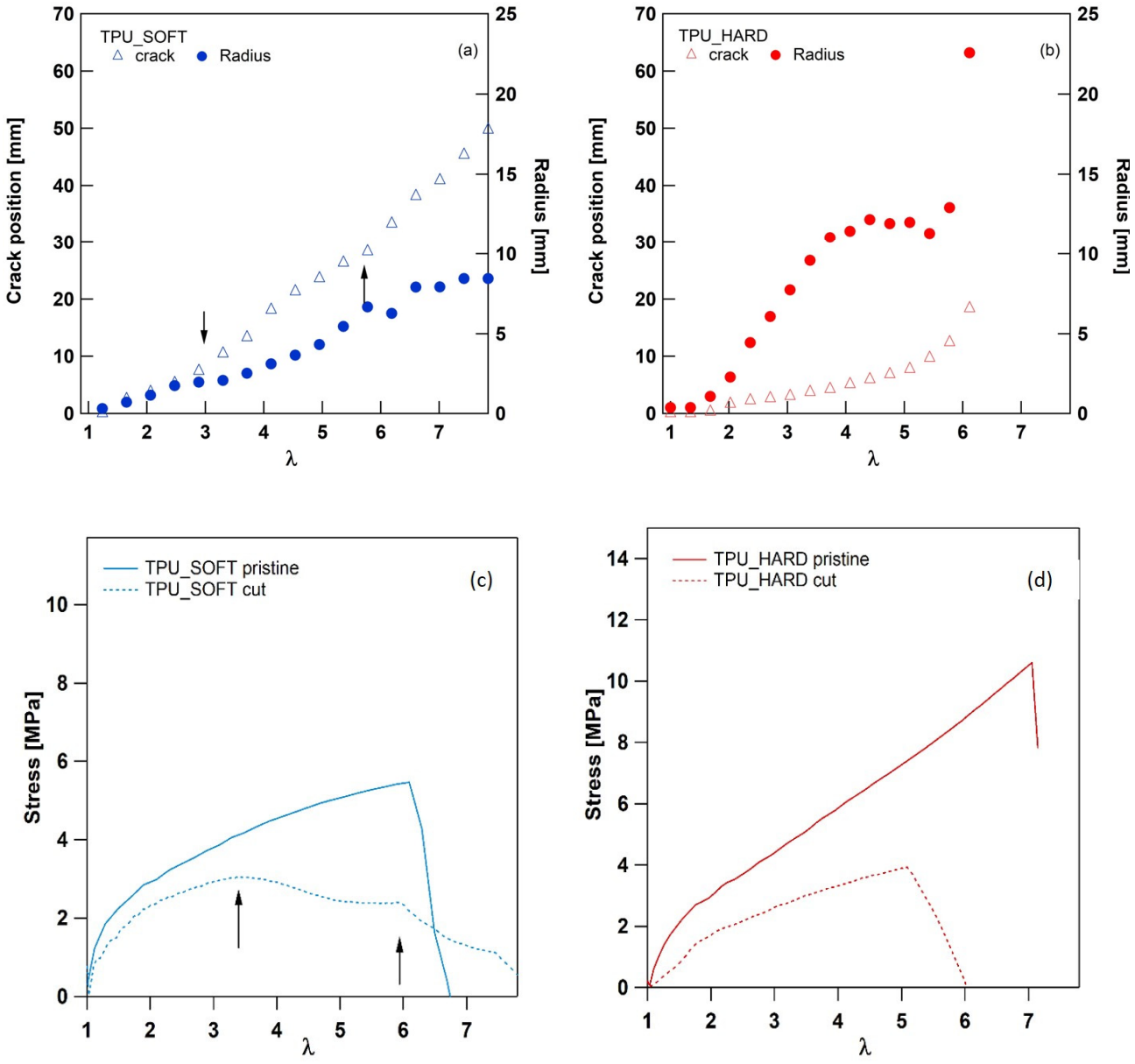

Figure 5 Evolution of crack length with applied stretch for TPU_HARD (a) and TPU_SOFT (b) at 23°C. Example of stress-stretch curve for notched and un-notched TPU_SOFT (c) and TPU_HARD (d) used to evaluate Γ.

4. Creep and stress relaxation

Creep is when a material, held at constant load, shows an elongation increasing with time. Stress relaxation occurs when a material, held under constant displacement, shows stress decreasing with time. In Figure 6 are represented the characteristic curves for stress relaxation and creep experiments. Both behaviors were investigated by Gent in vulcanized rubbers[11,12]. Gent shown that both creep and relaxation behavior exhibit a linear dependence on the logarithm of time. But while stress relaxation rate is independent on the applied strain (for moderate value of deformation)[13] the creep rate is not. We decided to adopt the approach proposed by Gent for thermoset rubbers to compare the amount of these viscoelastic phenomena between vulcanized rubbers and soft TPU.

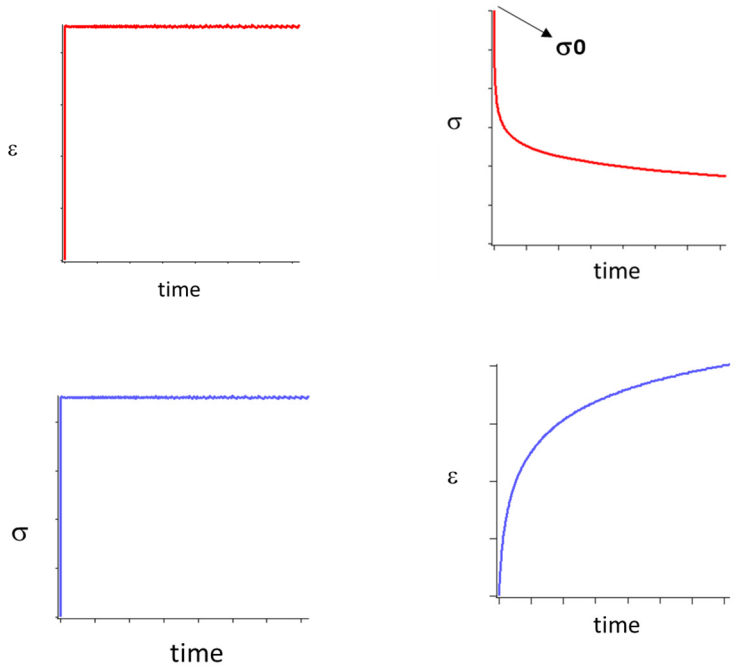

Figure 6 Characteristic curves of an experiment of stress relaxation (top) and creep (bottom).

Definition of the method

The creep compliance of elastomers is often found to have an approximately linear dependence upon the logarithm of time described by the following equation[13]:

$$J(t) = J_0\left(1 + A\ \log\frac{t}{t_0}\right)$$ **Equation 2**

where J_0 is the creep compliance at a reference time t_0 and A is a parameter indicative of the rate of increase of $J(t)$. A similar equation can be written for stress relaxation where A is a parameter indicative of the rate of decrease of $\sigma(t)$.

$$\sigma(t) = \sigma_0\left(1 + A\ \log(t/t_0)\right)$$ **Equation 3**

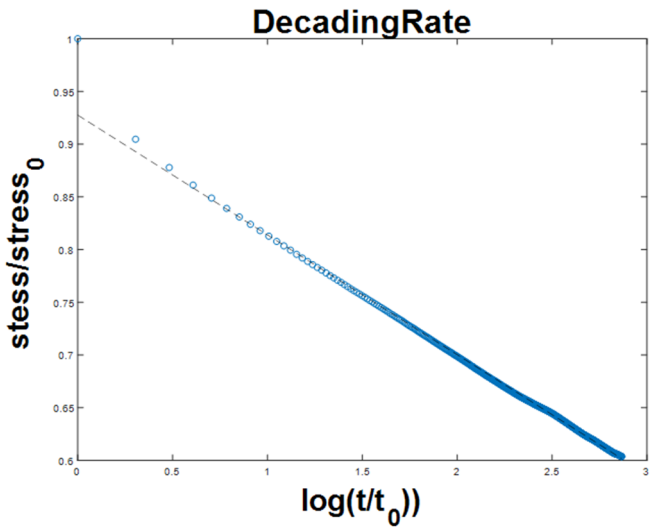

Figure 7 Semi logarithmic plot for the stress decay data

Following the previous equation, we can evaluate A (indicative of the rate of decrease) as the slope of the stress vs. time curve in a semi-log plot as shown in Figure 7.

Experimental section

The stress relaxation was determined by measuring the residual force in the sample at time intervals of 5 sec after imposing a constant deformation. The creep was measured by applying the same

procedure to a sample held under constant applied load. The values of stress relaxation and creep rates are reported in Figure 8(a and b) for two selected temperatures: 60° and 23°C.

For both tested TPUs, TPU_HARD and TPU_SOFT, the stress relaxation per decade was very similar and almost independent from the applied strain similarly to what reported for unfilled vulcanized rubbers[11,13]. The average values of stress relaxation per decade in both TPUs at 23°C is ~5.2%, only slightly higher than the 4.6% value reported by Yamaguchi et al.[13] in unfilled vulcanized NR. Furthermore, increasing the temperature only slightly increases this value, and in a similar way for both TPUs.

On the other hand, creep follows a very different trend. The value of creep rate was found to be different among the two materials and increasing with the applied stress. The dependence of creep on stress was also found in unfilled vulcanized rubbers, but it is hard to compare the value of creep per decade obtained for TPU with those reported by other authors[12,13] for vulcanized rubbers, because of the very different range of applied stress. The value of creep rate found by Gent was between 5 and 20% per decade for maximum imposed stress <0.2 MPa. TPU_SOFT at 23°C shows a creep rate per decade between 2 and 30% up to 2.5 MPa, while higher values were obtained for TPU_HARD at 23°C. A similar trend is confirmed also at 60°C with TPU_HARD having a higher creep rate per decade. The overall lower tendency to creep in TPU_SOFT confirms our previous hypothesis of bidentate urea in this TPU as suggested by FTIR analysis.

As a final remark, these values of creep were obtained for samples kept under static load for 1 hour. This condition is probably more severe for creep than that experienced by the sample in cyclic experiments and it can not be directly associated to the cyclic fatigue resistance. Further experiments of cyclic creep would be required to understand its role in cyclic fatigue for TPU.

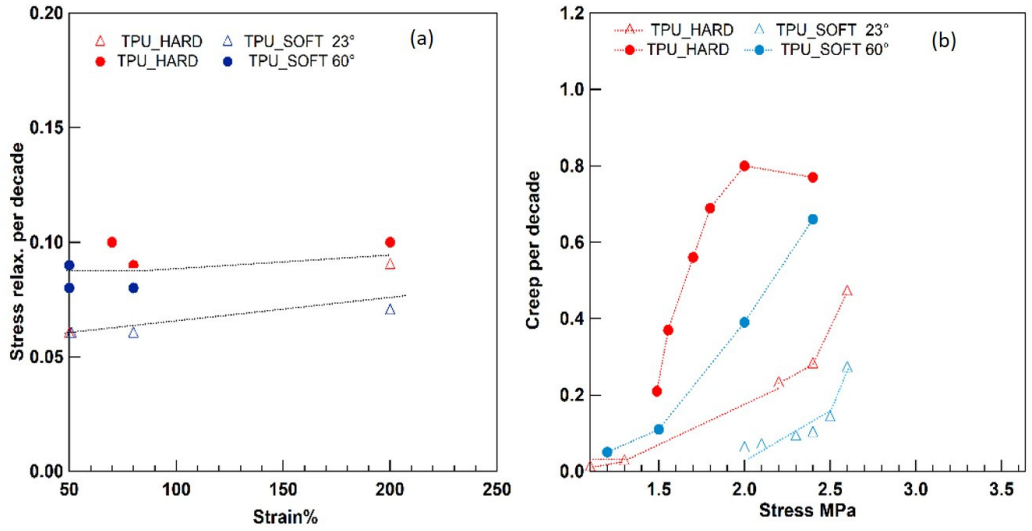

Figure 8 Plot of stress relaxation rate per decade (a) and creep rate (b).

5. References

1. Z. S.Petrovic JF. POLYURETHANE ELASTOMERS. *Prog Polym Sci*. 1991;16:695-836.

2. Lindsay CI, Woutters S, Norval S. A New Family of Soft Elastic TPUs. *Polyurethanes Tech Conf*. 2007;(Figure 2):1-15.

3. Tereshatov V V., Makarova MA, Senichev VY, Slobodinyuk AI. Interrelationship between ultimate mechanical properties of variously structured polyurethanes and poly(urethane urea)s and stretching rate thereof. *Colloid Polym Sci*. 2012;290(7):641-651. doi:10.1007/s00396-011-2585-7

4. Zhao P, Wang Y, Zhu J, Hua X, Wen Q. Characterization of graded polyurethane elastomer by FTIR. *Sci China, Ser B Chem*. 2008;51(1):58-61. doi:10.1007/s11426-007-0093-x

5. Mattia J, Painter P. A comparison of hydrogen bonding and order in a polyurethane and poly(urethane-urea) and their blends with poly(ethylene glycol). *Macromolecules*. 2007;40(5):1546-1554. doi:10.1021/ma0626362

6. He Y, Xie D, Zhang X. The structure, microphase-separated morphology, and property of polyurethanes and polyureas. *J Mater Sci*. 2014;49(21):7339-7352. doi:10.1007/s10853-014-8458-y

7. Prisacariu C, Scortanu E, Agapie B. Effect of the hydrogen bonding on the inelasticity of thermoplastic polyurethane elastomers. *J Ind Eng Chem*. 2013;19(1):113-119. doi:10.1016/j.jiec.2012.07.012

8. Sun JY, Zhao X, Illeperuma WRK, et al. Highly stretchable and tough hydrogels. *Nature*. 2012;489(7414):133-136. doi:10.1038/nature11409

9. Bai R, Yang J, Suo Z. Fatigue of hydrogels. *Eur J Mech A/Solids*. 2019;74:337-370. doi:10.1016/j.euromechsol.2018.12.001

10. Bai R, Yang Q, Tang J, Morelle XP, Vlassak J, Suo Z. Fatigue fracture of tough hydrogels. *Extrem Mech Lett*. 2017;15:91-96. doi:10.1016/j.eml.2017.07.002

11. Gent AN. Relaxation processes in vulcanized rubber. I Secondary relaxation due to network breakdown. *J Appl Polym Sci*. 1962;6(22):442-448. doi:10.1002/app.1962.070062208

12. Gent AN. Relaxation processes in vulcanized rubber. II. Secondary relaxation due to network

breakdown. *J Appl Polym Sci*. 1962;6(22):442-448. doi:10.1002/app.1962.070062208

13. Yamaguchi K, Thomas AG, Busfield JJC. Stress relaxation, creep and set recovery of elastomers. *Int J Non Linear Mech*. 2015;68:66-70. doi:10.1016/j.ijnonlinmec.2014.07.004

Datemi un punto di appoggio e vi solleverò il Mondo.

[Archimede]

RÉSUMÉ

Les élastomères thermoplastiques de polyuréthane (TPU) sont une classe de copolymères à blocs caractérisés par une élasticité réversible et une excellente résistance à l'abrasion. Ils sont déjà utilisés dans un certain nombre d'applications de type caoutchouc telles que semelles, roues, câbles flexibles, etc. Pourtant, le comportement en fatigue du TPU sous chargement cyclique n'a pas été étudié en détail, et plusieurs questions restent ouvertes sur la meilleure façon de prédire la durabilité à long terme des TPU. En l'absence de procédure établie pour évaluer la résistance à la fatigue dans les TPU, nous avons proposé une méthode basée sur la propagation de fissure qui permet des comparer la résistance a fatigue des TPU avec les élastomères vulcanisés. On a caractérisé les propriétés mécaniques en petites et grandes déformations de trois TPU avec modules linéaires similaires mais des comportements différents en grandes déformations : adoucissement, rhéodurcissement et cristallisation sous contrainte. Contrairement aux élastomères vulcanisés, tous ces TPU se rigidifient avec la déformation. La diffusion des rayons X a été utilisée pour caractériser les changements de structure à des échelles microscopique induits au fond de fissure pendant le chargement cyclique. La remarquable résistance à la fatigue cyclique du TPU a été expliquée comme une conséquence de la modification de la structure locale des TPU qui génère un durcissement en fond de fissure empêchant le transfert des contraintes pendant le chargement cyclique. On á enfin proposé que ce rhéodurcissement vient de la fragmentation des domaines rigides en domaines plus petits mais plus nombreux qui agissent comme des points de réticulation physiques additionnels.

MOTS CLÉS

Fissuration- Fatigue- Elastomères thermoplastiques

ABSTRACT

Soft thermoplastic polyurethane elastomers (TPU) are a class of block copolymers characterised by a low linear modulus (<10MPa), reversible elasticity and excellent abrasion resistance already used in several rubber-like applications such as soles, wheels, flexible cables, etc. Yet, their fatigue behaviour under cyclic loading has not been fully investigated so far, leaving several open questions about how predicting long-term durability of TPUs for a safe design. In this work we proposed a reproducible experimental protocol to assess and compare the resistance to crack propagation in cyclic conditions of TPU, with that of classical filled rubbers by using a fracture mechanics approach. Furthermore, we characterized the mechanical response under cyclic loading at large and small strain of three commercial TPUs with similar linear moduli and rheology but different large strain behaviours: extended softening, strain hardening and strain hardening enhanced by SIC. Irrespectively of their composition, all TPUs presented an unconventional strain induced stiffening in step-cyclic experiment. Using DIC and X-Ray in situ experiments we showed that, the strain gradient at the crack tip generates a spatial re-organization of the TPU microstructure consistent with a volume locally stiffer than the bulk. This heterogeneity in the deformability reduces the strain intensification at the crack tip explaining the high fatigue resistance in TPU. The local stiffening was ultimately associated to the fragmentation of original hard domains in smaller but more numerous units increasing the degree of physical crosslinking.

KEYWORDS

Fatigue-Thermoplastic elastomers- Fracture